VOLUME 77 APRIL 12, 1973 NUMBER 8

JPCHAx

THE JOURNAL OF PHYSICAL CHEMISTRY

PUBLISHED BIWEEKLY BY THE AMERICAN CHEMICAL SOCIETY

THE JOURNAL OF

PHYSICAL CHEMISTRY

AMERICAN CHEMICAL SOCIETY, *1155 Sixteenth St., N.W., Washington, D. C. 20036*

Books and Journals Division

JOHN K CRUM *Director*
RUTH REYNARD *Assistant to the Director*

CHARLES R. BERTSCH *Head, Editorial Processing Department*
D. H. MICHAEL BOWEN *Head, Journals Department*
BACIL GUILEY *Head, Graphics and Production Department*
SELDON W. TERRANT *Head, Research and Development Department*

 Published biweekly by the American Chemical Society at 20th and Northampton Sts., Easton, Pa. 18042. Second-class postage paid at Washington, D. C., and at additional mailing offices.

All manuscripts should be sent to *The Journal of Physical Chemistry*, Department of Chemistry, University of Minnesota, Minneapolis, Minn. 55455.

Additions and Corrections are published once yearly in the final issue. See Volume 76, Number 26 for the proper form.

Extensive or unusual alterations in an article after it has been set in type are made at the author's expense, and it is understood that by requesting such alterations the author agrees to defray the cost thereof.

The American Chemical Society and the Editor of *The Journal of Physical Chemistry* assume no responsibility for the statements and opinions advanced by contributors.

Correspondence regarding accepted copy, proofs, and reprints should be directed to Editorial Processing Department, American Chemical Society, 20th and Northampton Sts., Easton, Pa. 18042. Head: CHARLES R. BERTSCH. Assistant Editor: EDWARD A. BORGER. Editorial Assistant: JOSEPH E. YURVATI.

Advertising Office: Centcom, Ltd., 142 East Avenue, Norwalk, Conn. 06851.

Business and Subscription Information

Remittances and orders for subscriptions and for single copies, notices of changes of address and new professional connections, and claims for missing numbers should be sent to the Subscription Service Department, American Chemical Society, 1155 Sixteenth St., N.W., Washington, D. C. 20036. Allow 4 weeks for change of address. Please include an old address label with the notification.

Claims for missing numbers will not be allowed (1) if received more than sixty days from date of issue, (2) if loss was due to failure of notice of change of address to be received before the date specified in the preceding paragraph, or (3) if the reason for the claim is "missing from files."

Subscription rates (1973): members of the American Chemical Society, $20.00 for 1 year; to nonmembers, $60.00 for 1 year. Those interested in becoming members should write to the Admissions Department, American Chemical Society, 1155 Sixteenth St., N.W., Washington, D. C. 20036. Postage to Canada and countries in the Pan-American Union, $5.00; all other countries, $6.00. Single copies for current year: $3.00. Rates for back issues from Volume 56 to date are available from the Special Issues Sales Department, 1155 Sixteenth St., N.W., Washington, D. C. 20036.

This publication and the other ACS periodical publications are now available on microfilm. For information write to MICROFILM, Special Issues Sales Department, 1155 Sixteenth St., N.W., Washington, D. C. 20036.

Notice to Authors last printed in the issue of November 23, 1972

THE JOURNAL OF
PHYSICAL CHEMISTRY

Volume 77, Number 8 April 12, 1973

JPCHAx 77(8) 973–1082 (1973)

AUTHOR INDEX

In papers with more than one author the name of the author to whom inquiries about the paper should be addressed is marked with an asterisk in the by-line.

THE JOURNAL OF
PHYSICAL CHEMISTRY

VOLUME 77, NUMBER 8 APRIL 12, 1973

Kinetics and Mechanism of the Reaction between Chlorine and Phenol in Acidic Aqueous Solution

Eugene Grimley and Gilbert Gordon*

The Department of Chemistry, University of Iowa, Iowa City, Iowa 52242 *(Received April 17 1972)*

In aqueous solution below pH 2, the reaction between chlorine and phenol proceeds stepwise by means of consecutive reactions. The first reaction corresponds to the second-order formation of a $[Cl_2 \cdot C_6H_5OH]$ intermediate with an observed rate constant equal to $(2.3 \pm 0.5) \times 10^4\ M^{-1}\ sec^{-1}$ at 5.0°. This phenol-chlorine intermediate has an apparent molar absorptivity of $18 \pm 3\ M^{-1}\ cm^{-1}$ at 325 nm. The second reaction is a first-order decomposition of the intermediate which occurs *via* three parallel pathways: a hydrogen ion and chloride ion dependent path; a hydrogen ion dependent path; and a hydrogen ion and chloride ion independent path.

Introduction

The reaction between uranium(IV) and chlorine(III) in acidic aqueous solution in the presence of phenol[1-3] and the various interactions between chlorine-containing intermediates[4] formed in this reaction have been studied in this laboratory as part of an overall investigation[5] of metal ion oxidation by chlorine oxidants in aqueous solution.[3,6] Potentially, chlorine could react with phenol in order to account for the scavenger effect of phenol in the uranium(IV)-chlorine(III) reaction.[2] The appropriate rate is unknown.

The major chlorine species in aqueous solution are governed by the three interdependent equilibria

$$Cl_2(aq) + H_2O \overset{K_{hyd}}{\rightleftharpoons} H^+ + Cl^- + HOCl \quad (1)$$

$$HOCl \overset{K_a}{\rightleftharpoons} H^+ + OCl^- \quad (2)$$

and

$$Cl_2(aq) + Cl^- \overset{K_1}{\rightleftharpoons} Cl_3^- \quad (3)$$

The equilibrium constant[7] for chlorine hydrolysis is $3.9_4 \times 10^{-4}\ M$ at zero ionic strength and the acid dissociation[10] constant for hypochlorous acid is $2.91 \times 10^{-8}\ M^{-1}$. The equilibrium constant for the chloride-trichloride equilibrium is reported[8] as $0.18\ M^{-1}$.

The reaction of phenol with solutions of aqueous chlorine in the pH range of 5 to 12 has been studied by Lee.[11] The predominant chlorine species in this pH range are hypochlorous acid and hypochlorite ion. The data from the investigation by Lee agree in part with the earlier work reported by Soper and Smith.[12] The reaction between hypochlorous acid and phenol was part of a detailed study of the kinetics and mechanisms of aromatic halogen substitution reactions by de la Mare, Ketley, and Ver-

(1) G. Gordon and F. Feldman, *Inorg. Chem.*, 3, 1728 (1964).
(2) E. B. Grimley, R. Buchacek, and G. Gordon, *Inorg. Chem.*, **10**, 873 (1971).
(3) R. Buchacek and G. Gordon, *Inorg. Chem.*, **11**, 2154 (1972).
(4) (a) F. Emmenegger and G. Gordon, *Inorg. Chem.*, **6**, 633 (1967); (b) R. G. Kieffer and G. Gordon, *Inorg. Chem.*, **7**, 235, 239 (1968); (c) G. Gordon, R. G. Kieffer, and D. Rosenblatt, *Progr. Inorg. Chem.*, **15**, 201 (1972); H. Taube and H. Dodgen, *J. Amer. Chem. Soc.*, **71**, 3330 (1949).
(5) (a) D. M. A. Kern and G. Gordon in "Theory and Structure of Complex Compounds," B. Jezowska-Trzebiatowska, Ed., Pergamon Press, New York, N. Y., 1964, p 655; (b) G. Gordon, *Proc. XIII Int. Conf. Coord. Chem.*, 11 (1970).
(6) (a) B. Z. Shakhashiri and G. Gordon, *Inorg. Chem.*, **7**, 2454 (1968); (b) B. Z. Shakhashiri and G. Gordon, *J. Amer. Chem. Soc.*, **91**, 1103 (1969); (c) M. Ondrus and G. Gordon, *Inorg. Chem.*, **10**, 474 (1971); (d) M. Ondrus and G. Gordon, *Inorg. Chem.*, **11**, 985 (1972); (e) W. Melvin and G. Gordon, *Inorg. Chem.*, **11**, 1912 (1972).
(7) A conductometric value of $3.9_4 \times 10^{-4}$ is reported for the equilibrium constant extrapolated to zero ionic strength by Connick and Chia.[8a] Silverman[9] reports a spectrophotometric value of $(5.1 \pm 0.3) \times 10^{-4}\ M^2$ in 1 *M* $HClO_4$ and $(6.2 \pm 0.3) \times 10^{-4}\ M^2$ in 1 *M* $NaClO_4$ or 1 *M* NaCl. The difference is due to the changes in activity coefficients for HCl in differing media and changes in the ratio of the activity coefficients for Cl_2 and HOCl from unity.
(8) (a) R. E. Connick and Y. Chia, *J. Amer. Chem. Soc.*, **81**, 1280 (1959); (b) G. Zimmerman and F. C. Strong, *J. Amer. Chem. Soc.*, **79**, 2063 (1957).
(9) R. A. Silverman, Ph.D. Thesis, University of Iowa, to be published, 1973.
(10) J. C. Morris, *J. Phys. Chem.*, **70**, 3798 (1966).
(11) C. F. Lee, "Principles and Applications of Water Chemistry," Faust and Hunter, Ed., Wiley, 1967, p 55.
(12) F. G. Soper and G. F. Smith, *J. Chem. Soc. (London)*, 1582 (1926).

non.[13] They studied the reaction in the presence of added silver perchlorate in order to reduce the concentration of chloride ion in solution such that reaction between phenol and molecular chlorine would be negligible. Thus, no details are available with respect to the rate or mechanism of the reaction in acidic solution. In this paper we report the results of a detailed kinetic investigation of the reaction between chlorine and phenol below pH 2.

Experimental Section

Reagents. Phenol was obtained from Mallinckrodt in the 88% liquified form with no added preservatives. Phenol used in all of the kinetic measurements was purified by vacuum distillation and the product was stored in an amber jar under an atmosphere of nitrogen. Stock solutions of phenol were prepared by weighing out the appropriate amount of purified phenol into a volumetric flask and adding other solutions as desired. *o*-, *m*-, and *p*-chlorophenol and 2,4-dichlorophenol were used as obtained from commercial sources. An ionic strength of 1 *M* was maintained for all reactant solutions with twice recrystallized sodium perchlorate.[14]

Hypochlorous acid was prepared using the procedure described by Cady.[15] The optical absorption spectrum was measured and was found to be in agreement with that published by Morris.[10] Aqueous solutions of chlorine were prepared by bubbling reagent grade chlorine gas obtained from Matheson into solutions containing appropriate amounts of perchloric acid, hydrochloric acid, sodium chloride, and sodium perchlorate. The chlorine gas was first passed through two washing towers which contained water in order to remove hydrogen chloride gas and iron-containing impurities.

Analytical Methods. Solutions of aqueous chlorine were carefully analyzed to determine species concentrations because of their potential effect on the kinetic studies. A typical aqueous chlorine solution was analyzed in the following manner: the aqueous stock solution was drawn into a storage syringe[4b,9] and considerable care was taken to avoid air bubbles in the vessel containing the aqueous chlorine stock solution because of the volatility of chlorine. Aliquots were removed for titrimetric analysis by a second smaller calibrated glass syringe[9] in a manner such that air bubbles were again excluded. Each aliquot was ejected below the surface of a solution which contained sodium iodide and perchloric acid and was immediately titrated with standardized sodium thiosulfate solution. In addition, a clean, dry 1.00-cm cylindrical quartz cell was rapidly filled to overflowing with the chlorine solution. The cell was stoppered quickly with a glass stopper. Care was taken to prevent the presence of air bubbles or an air space in the cell. The spectrum of the solution was recorded from 350 to 250 nm with a Cary 14 spectrophotometer. Replicate spectra and titrations for individual chlorine solutions gave excellent agreement. The total chlorine concentration was calculated from the averaged titration data. The hydrogen ion and chloride ion concentration were varied, while the ionic strength was maintained at a constant value of 1.00 *M* with sodium perchlorate.

Beer's Law behavior was verified for aqueous chlorine solutions by comparing the absorbance measured at 325 nm to the absorbance calculated from the total chlorine concentration. A detailed comparison of the molar absorptivities of hypochlorous acid, chlorine, and trichloride ion[8b,16] and the appropriate ionic strength dependent equilibrium constants will be published elsewhere.[9]

Stoichiometry and Product Analysis. The products and stoichiometry of the reaction of phenol with aqueous chlorine were determined by extracting the products with ether and by separating the major products by gas chromatography. An F & M Model 500 gas chromatograph was equipped with a Carbowax column and there was no evidence for the presence of low molecular weight oxidation products of phenol when the reaction products were separated at a column temperature of 75°. The separated products at a column temperature of 150° were characterized by their infrared and ultraviolet spectra as well as their gas chromatographic retention times. All of the products were found to be transparent at 325 nm.

The major products recovered in addition to unreacted phenol were o-chlorophenol and *p*-chlorophenol, while only a small amount of 2,4-dichlorophenol was formed. Of the total phenol in the reaction, 86% was recovered as chlorinated products plus unreacted phenol. Of the total phenol recovered, 18% was *o*-chlorophenol and 16% was *p*-chlorophenol. The predicted percentage of total chlorophenols produced was 35%. This prediction is based on the assumption that for every chlorine molecule that disappears, one chlorophenol molecule is produced. These results indicate that the stoichiometry can be written as

$$Cl_2 + C_6H_5OH = ClC_6H_5OH + Cl^- + H^+ \quad (4)$$

Kinetic Measurements. A Durrum-Gibson stopped-flow spectrophotometer was used to follow the reaction between phenol and aqueous solutions of chlorine and the reaction of hypochlorous acid with chloride ion at 5.0°. Constant temperature was maintained to ±0.1° and solutions were allowed to equilibrate at least 15 min before the reaction was initiated. The transmittance at 325 nm was recorded on a Textronix 564 storage oscilloscope with a type 2A63 differential amplifier and a type 3B3 time base. Three overlapping replicate runs were triggered before the oscilloscope was photographed for each set of reaction conditions. Transparency film was used and photographic enlargements were prepared. The data were read manually from the enlarged photographs and the transmittance voltages were converted directly to absorbance units.

Results and Discussion

In order to determine the effect of chlorophenolic products on the stoichiometry of the phenol–aqueous chlorine reaction, it was necessary to measure the rates of reaction between aqueous chlorine solutions and various chlorophenols. Kinetic experiments were performed at 5.0° with 0.569 *M* perchloric acid and 0.0195 *M* sodium chloride while 1.00 *M* ionic strength was maintained with sodium perchlorate. The loss of chlorine was followed at 325 nm and Table I gives a comparison of the apparent second-order rate constants for the reaction of phenol with chlorine under the same experimental conditions.

Of the various chlorophenols, *m*-chlorophenol has the largest second-order rate constant but even it reacts only ¼ as fast as does phenol. Thus, under conditions of the phenol reaction with aqueous chlorine in which phenol is in tenfold or greater excess, additional oxidation of the

(13) P. B. D. de la Mare, A. D. Ketley, and C. A. Vernon, *J. Chem. Soc.*, 1290 (1954); C. G. Swain and D. R. Christ, *J. Amer. Chem. Soc.*, **94**, 3195 (1972).
(14) G. Gordon and P. H. Tewari, *J. Phys. Chem.*, **70**, 200 (1966).
(15) G. H. Cady, *Inorg. Syn.*, **5**, 157 (1957).
(16) The molar absorptivity for the trichloride ion is 193 ± 5 M^{-1} cm^{-1}.

TABLE I: Comparison of Second-Order Rate Constants[a] between the Reaction of Phenol and Some Chlorophenols with Aqueous Chlorine at 5.0°

Phenolic reactant	Apparent second-order rate constant, M^{-1} sec^{-1}
Phenol[b]	2.3×10^4
o-Chlorophenol	0.11×10^4
m-Chlorophenol	0.56×10^4
p-Chlorophenol	$0.05_5 \times 10^4$
2,4-Dichlorophenol	Very slow

[a] Reaction conditions were 0.569 *M* hydrogen ion, 0.0195 *M* chloride ion, 1.00 *M* ionic strength, 5.0×10^{-4} *M* total chlorine, and 5.0×10^{-3} *M* phenolic compound. [b] Average apparent second-order rate constant from Table III.

chlorophenols produced will not contribute significantly to the loss of chlorine.

Eigen and Kustin[17] report a forward rate constant for the process

$$HOCl + Cl^- + H^+ \underset{k_r}{\overset{k_f}{\rightleftharpoons}} Cl_2 + H_2O \qquad (5)$$

to be 1.8×10^4 M^{-2} sec^{-1} at 20° as measured by the temperature-jump method. In view of the fact that chlorine solutions may contain appreciable concentrations of hypochlorous acid, particularly under conditions of low hydrogen ion and chloride ion concentrations, it was necessary to determine the forward rate constant for the HOCl-Cl$^-$ reaction at 5°.

At 325 nm, hypochlorous acid has a molar absorptivity[8b] of 11.0 ± 0.2 M^{-1} cm^{-1}, whereas that of chlorine is 75.3 ± 0.3 M^{-1} cm^{-1} at the same wavelength. For acidic aqueous chlorine solutions of low chloride and hydrogen ion concentrations, the predominant chlorine species is hypochlorous acid. By rapidly changing the chloride and/or the hydrogen ion concentrations *via* a concentration-jump experiment in the stopped-flow spectrophotometer, the formation of chlorine can be followed under pseudo-first-order conditions.

Two kinetic runs were made with both reactant solutions containing 0.0230 *M* hydrogen ion and at an ionic strength of 1.00 *M*. Upon mixing, the chloride ion concentration was 0.50 *M* and the hypochlorous acid concentration was 4×10^{-3} *M*. Computer analysis[18] of the pseudo-first-order data at 5° yielded an average value of the rate constant for the overall third-order process of (1.1 ± 0.1) $\times 10^4$ M^{-2} sec^{-1}. From the values of forward rate constants at 20 and 5°, rough estimates of ΔH_f^* equal to 4.7 kcal mol^{-1} and ΔS_f^* equal to −23 eu are obtained. From the reported value of the temperature-dependent equilibrium constant,[8] the reverse rate constant for reaction 5 is estimated to be about 5 sec^{-1} at 5°.

For the actual kinetic experiments between aqueous chlorine solutions and phenol, the initial concentrations of chlorine, hypochlorous acid, trichloride ion, and phenol were calculated for each kinetic run from the appropriate equilibrium data. Reactant concentrations were such that the phenol concentration was in at least a tenfold excess over the total chlorine concentration, thus giving rise to pseudo-first-order conditions.

After a series of initial experiments at high hydrogen ion concentrations, a series of runs at low hydrogen ion concentrations revealed the fact that there were clearly two consecutive processes observable at 325 nm. The first process corresponds to the dissappearance of chlorine in a very rapid bimolecular reaction with phenol in which an intermediate is formed. The pseudo-first-order rate constant for the formation of the intermediate is defined as k_a. This intermediate has a finite absorbance at 325 nm which is a direct function of the concentration of each of the initial reactants. Thus, we propose that this first process could correspond to either the formation of a hypochlorous acid-phenol complex or to a chlorine-phenol complex. However, solutions of hypochlorous acid and phenol do not give evidence for complex formation at 325 nm. Thus, the consecutive reactions observed in the phenol-aqueous chlorine reaction can be represented as

$$Cl_2 + C_6H_5OH \xrightarrow{k_a} [Cl_2 \cdot C_6H_5OH] \xrightarrow{k_b} ClC_6H_5OH + H^+ + Cl^- \qquad (6)$$

In order to test this model, the sum of the squares of the differences between the observed absorbance data and the best fit calculated absorbance data were minimized[18] for the integrated equation for consecutive first-order reactions

$$\text{abs} = p\epsilon_a A_0 \exp(-k_a(t + \Delta t)) + \frac{p\epsilon_b A_0 k_a}{k_b - k_a}[\exp(-k_a(t + \Delta t)) - \exp(-k_b(t + \Delta t))] \qquad (7)$$

where abs = absorbance at time t, k_a = observed first-order rate constant shown in eq 6 under conditions of excess phenol, k_b = observed first-order rate constant shown in eq 6 for the dissappearance of the intermediate, ϵ_a = effective molar absorptivity of the chlorine solution, ϵ_b = molar absorptivity of the $[Cl_2 \cdot C_6H_5OH]$ intermediate complex, A_0 = initial concentration of total chlorine, Δt = incremental zero time error, and p = cell path length.

Due to the high speed of the initial reaction, a small error in placement of zero time on the time axis could result in substantial errors in the individual values of k_a. Thus, all of the absorbance-time data for the aqueous chlorine-phenol reaction were analyzed by evaluation[18] of the parameters ϵ_b, Δt, k_a, and k_b in eq 7. In general the zero time correction was less than 1 msec which is on the order of the actual mixing time. Absorbance-time data for a typical chlorine-phenol reaction are given in Table II. The molar absorptivity of the intermediate is significantly less than the apparent molar absorptivities of the various solutions of aqueous chlorine. The absorbance due to the intermediate decreases to zero by a first-order process at a rate slower than that observed for the first reaction.

Also due to the high speed of the initial reaction, some difficulty was encountered in obtaining reproducible second-order rate constants and a wide range of values was obtained with different initial concentrations. Conditions were adjusted such that the optimum pseudo-first-order rate constant determination would be most accurate. At best, even at low concentrations of excess phenol and a temperature of 5°, not more than 75% of the first reaction could be studied in that the stopped-flow spectrophotom-

(17) M. Eigen and K. Kustin, *J. Amer. Chem. Soc.*, **84**, 1355 (1962).
(18) A description of the algorithm of the computer program is given in the Los Alamos publication No. LA-2367 and addenda. In this nonlinear least-squares program which uses the method developed by Gauss, the square of the differences between the observed and calculated dependent variable is minimized. Normally, each individual data point is given unit weights. A modified Fortran(IV) version of this program is presently available from G. Gordon at the University of Iowa.

TABLE II: Typical Absorbance vs. Time Data for an Aqueous Chlorine–Phenol Reaction[a]

Time, msec	Measured absorbance	Calculated absorbance[b]
1.4	0.171_3	0.171_9
1.6	0.161_3	0.160_6
1.8	0.151_5	0.150_8
2.0	0.141_9	0.142_3
2.2	0.134_3	0.135_0
2.4	0.128_7	0.128_6
2.6	0.122_6	0.123_1
2.8	0.118_3	0.118_3
3.0	0.114_7	0.114_1
3.4	0.107_6	0.107_4
3.8	0.102_3	0.102_3
4.4	0.096_5	0.096_8
5.0	0.093_1	0.093_1
6.0	0.089_1	0.089_3
20.0	0.076_2	0.076_2
40.0	0.063_7	0.063_6
60.0	0.052_6	0.053_0
80.0	0.044_2	0.044_2
100.0	0.038_1	0.037_0
120.0	0.031_0	0.030_8
140.0	0.025_5	0.025_7
160.0	0.021_1	0.021_4
180.0	0.017_2	0.017_9

[a] Conditions: 0.0230 M H^+, 0.0228 M Cl^-, 2.7×10^{-3} M Cl_2, 0.0235 M phenol, and an ionic strength of 1.00 M. Absorbance measured at 325 nm and 5° in 2.00-cm cells. [b] Calculated using the non-linear least-squares computer program.[18] The following parameter values were evaluated by computer: $\epsilon_b = 16.7 \pm 0.1$, $\Delta t = (2.2 \pm 0.1) \times 10^{-5}$ sec, $k_a = (7.38 \pm 0.06) \times 10^2$ sec^{-1}, and $k_b = 9.05 \pm 0.05$ sec^{-1}. The value of ϵ_a used was 59.84 appropriate to the initial absorbance of the Cl_2 solution.

eter was at its upper limit in terms of rate of the reaction being studied. The fit of the data for the initial first-order process was very good and 80-fold variation in the initial phenol concentration demonstrated that the first reaction was also first order in phenol. These data are shown in Table III where k_c corresponds to $k_a/[\text{phenol}]$.

The observed rate law for the disappearance of chlorine, resulting in formation of the intermediate by means of the first reaction, is given as

$$\frac{-d[Cl_2]_{aq}}{dt} = k_c[C_6H_5OH][Cl_2]_{aq} \qquad (8)$$

At 1.00 M ionic strength, maintained with sodium perchlorate, and 5°, the average value of k_c is $(2.3 \pm 0.5) \times 10^4$ M^{-1} sec^{-1}. The apparent second-order rate constant is independent of chloride ion in the range 0.0021 to 1.00 M and independent of hydrogen ion in the range of 0.023 to 1.00 M within experimental error as can be seen from the data in Table III.

The average from all of the kinetic experiments for the apparent molar absorptivity for the intermediate was found to be 18 ± 3 M^{-1} cm^{-1}. The molar absorptivity for the intermediate was independent of chloride and hydrogen ion concentrations under the conditions studied.

Variation in the hydrogen ion and chloride ion concentrations affect the value of the first-order rate constant for the disappearance of the intermediate, whereas the initial phenol and chlorine concentrations have no effect on the decomposition reaction. The observed rate law for the disappearance of the intermediate which appears to have the composition $[Cl_2 \cdot C_6H_5OH]$ corresponds to

$$-\frac{d[Cl_2 \cdot C_6H_5OH]}{dt} = k_b[Cl_2 \cdot C_6H_5OH] \qquad (9)$$

A plot of the observed first-order rate constant, k_b, for the disappearance of complex as a function of the hydrogen ion concentration is linear at 0.230 M chloride ion. This is shown in Figure 1 for the average rate constants given in Table IV. The slope, 99 M^{-1} sec^{-1}, and the intercept, 9 sec^{-1}, correspond to the rate constants for the parallel hydrogen ion dependent and independent pathways, respectively.

As is shown in Figure 2, a plot of the apparent first-order rate constant as a function of the chloride ion concentration, at 0.0232 M hydrogen ion, is also linear within experimental error for the average of rate constants shown in Table IV. This plot has a slope of 6.5 M^{-1} sec^{-1} and an intercept of 8 sec^{-1}.

Additional support for the formation of the intermediate from chlorine and phenol rather than from hypochlorous acid comes from the experiment with 0.0064 M chloride ion and 0.023 M hydrogen ion where the apparent first-order rate constant for the decomposition of intermediate is considerably less than that predicted on the basis of the proposed rate law. Initially, chlorine and hypochlo-

TABLE III: Effect of Initial Concentrations of Phenol, Hydrogen Ion, and Chloride Ion in the Apparent Second-Order Rate Constant[a] for the Initial Chlorine–Phenol Reaction at 5.0°

$[\text{Phenol}]_0$, M	$[H^+]$, M	$[Cl^-]$, M	$10^{-4}k_c$, M^{-1} sec^{-1}
0.0693	1.00	0.230	1.5
0.0392	1.00	0.230	2.2
0.0300	1.00	0.230	2.2
0.0254	1.00	0.230	2.6
0.0092	1.00	0.0021	1.5
0.0076	1.00	0.0021	3.0
0.0747	0.300	0.230	1.8
0.0638	0.300	0.230	1.8
0.0441	0.300	0.230	2.2
0.0307	0.300	0.230	2.0
0.0216	0.300	0.230	3.0
0.0243	0.100	0.100	1.9
0.0219	0.100	0.100	1.8
0.0144	0.100	0.100	1.9
0.0073	0.100	0.100	2.1
0.0670	0.0800	0.230	2.9
0.0460	0.0800	0.230	3.3
0.0363	0.0800	0.230	2.7
0.0238	0.0800	0.230	2.5
0.0398	0.0232	0.232	2.2
0.0256	0.0232	0.232	2.4
0.0197	0.0232	0.232	2.8
0.0156	0.0232	0.232	2.6
0.0139	0.0232	0.232	2.6
0.0516	0.0230	0.0228	2.4
0.0397	0.0230	0.0228	3.0
0.0235	0.0230	0.0228	3.1
0.0468	0.0230	1.00	1.7
0.0302	0.0230	1.00	1.8
0.0201	0.0230	1.00	1.8
0.0206	0.0230	0.0064	2.3
0.0111	0.0230	0.0064	2.2
			Av 2.3 ± 0.5

[a] Each k_c value is the average of three individual kinetic runs. The value of k_c is calculated directly from the ratio of the observed first-order rate constant to that of phenol (*i.e.*, $k_c = k_a/[\text{phencl}]$).

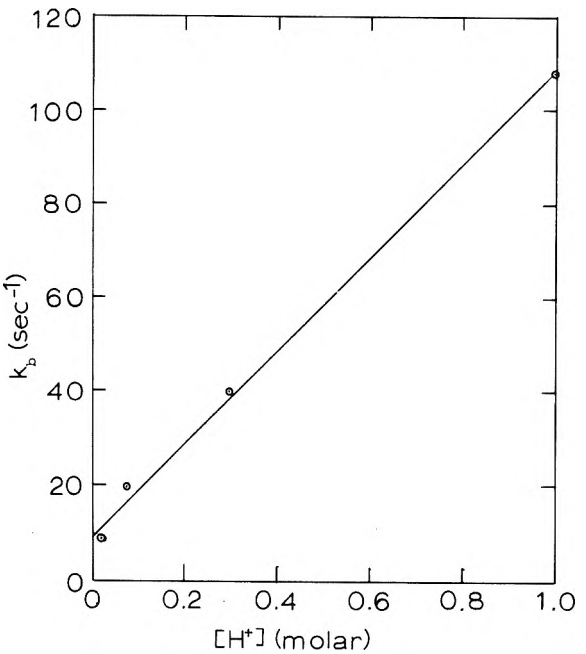

Figure 1. A plot of k_b as a function of the hydrogen ion concentration for the disappearance of the [Cl_2·C_6H_5OH] intermediate at 5.0°, 0.230 *M* chloride ion concentration, and 1.00 *M* ionic strength.

TABLE IV: Variation in the First-Order Rate Constant[a] for Disappearance of Intermediate with Variations in Initial Hydrogen Ion and Chloride Ion Concentrations

[H$^+$], *M*	[Cl$^-$], *M*	k_b, sec^{-1} (exptl)	k_b, sec^{-1} (calcd)
1.00	0.230	108 ± 13	106
0.300	0.230	40 ± 10	37
0.0800[b]	0.230	20 ± 1	16
0.0232	0.230	9 ± 1	10
0.023	1.00	15 ± 2	14
0.023	0.232	9.8 ± 0.6	10
0.023	0.0228	9.0 ± 0.6	9
0.023	0.0064	(3.7 ± 0.1)[c]	9

[a] Reaction conditions: 1.00 *M* ionic strength at 5°. The uncertainties represent one standard deviation from the mean for the average of at least four replicate experiments. [b] Three replicate experiments. [c] Low due to the very slow formation of Cl_2 from HOCl at very low chloride ion concentrations.

rous acid are in equilibrium prior to the dilution which occurs upon mixing in the stopped-flow spectrometer but the solution contains primarily hypochlorous acid and only small amounts of intermediate are formed initially. As the intermediate decomposes at the characteristic first-order rate, hypochlorous acid slowly reacts with chloride ion to form more chlorine which in turn forms more intermediate. Since the rate of formation of chlorine from hypochlorous acid and the rate of decomposition of the intermediate are competitive in the solutions containing low hydrogen ion and low chloride ion concentrations, a pseudo-steady-state situation occurs,[19] and the apparent rate of decomposition of the intermediate decreases.

By increasing the chloride ion concentration to 2.28×10^{-2} *M*, the hypochlorous acid forms chlorine almost ten times faster than the intermediate decomposes. Under these conditions normal first-order rate constants are observed for the decomposition process as can be seen from the data in Table IV.

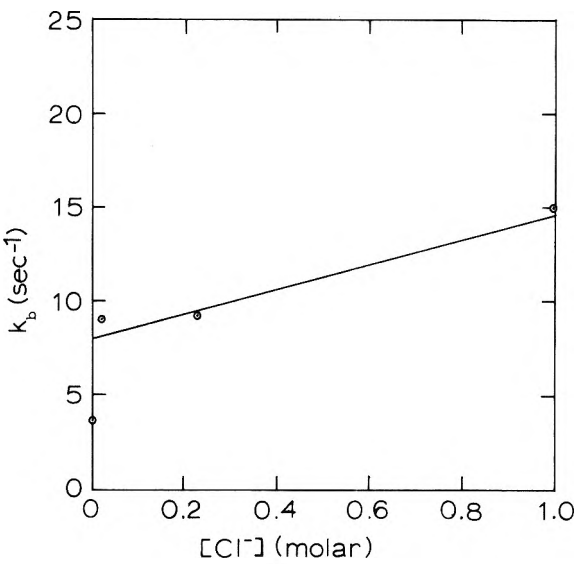

Figure 2. A plot of k_b as a function of the chloride ion concentration for the disappearance of the [Cl_2·C_6H_5OH] Intermediate at 5.0°, 0.0230 *M* hydrogen ion concentration, and 1.00 *M* ionic strength.

The observed first-order rate constants for the decomposition of intermediate increase with increases of either the hydrogen ion or the chloride ion concentrations. Since both Figures 1 and 2 show similar finite intercepts, the final rate law must contain at least three terms. A variety of different types of rate laws were fitted by means of our non-linear least-squares fitting program.[18] In this case, the data were weighted by the square of the inverse of the observed rate constant for the decomposition in order to minimize the per cent deviation. The best fit of the data is given by the equation

$$-\frac{d[Cl_2{\cdot}C_6H_5OH]}{dt} = \{k_1[H^+][Cl^-] + k_2[H^+] + k_3\} \times [Cl_2{\cdot}C_6H_5OH] \quad (10)$$

where $k_1 = 244 \pm 35\ M^{-2}\ sec^{-1}$, $k_2 = 42 \pm 6\ M^{-1}\ sec^{-1}$, and $k_3 = 7.9 \pm 0.6\ sec^{-1}$. The average rate constant under each set of conditions is reproduced to better than ±3% which is less than the average deviation from the mean for each individual measurement.

Conclusions

The initial reaction that occurs is first order each in phenol and chlorine. The second-order rate constant is $(2.3 \pm 0.5) \times 10^4\ M^{-1}\ sec^{-1}$ and corresponds to the formation of a phenol–chlorine intermediate. The net activation process[20] of the first step is

$$Cl_2 + C_6H_5OH = [Cl_2{\cdot}C_6H_5OH]^* \rightarrow [Cl_2{\cdot}C_6H_5OH] \quad (11)$$

The most significant path for decomposition of this phenol–chlorine intermediate at low hydrogen and chloride ion concentration has a net activation process corresponding to

$$[Cl_2{\cdot}C_6H_5OH] = [Cl_2{\cdot}C_6H_5OH]^{\ddagger} \quad (12)$$

At high hydrogen ion concentrations the predominant net

(19) Simulation of these data by means of a forward integration technique by using the Runge–Kutta procedure results in data in excellent agreement with the qualitative arguments presented here.
(20) T. W. Newton and S. W. Rabideau, *J. Phys. Chem.*, **63**, 365 (1959).

activation process becomes

$$[Cl_2 \cdot C_6H_5OH] + H^+ = [Cl_2 \cdot C_6H_5OH \cdot H^+]^\ddagger \quad (13)$$

In addition, the predominant net activation process in solutions which contain both high hydrogen ion and chloride ion concentrations is

$$[Cl_2 \cdot C_6H_5OH] + H^+ + Cl^- = [Cl_2 \cdot C_6H_5OH \cdot HCl]^\ddagger \quad (14)$$

The phenol-chlorine intermediate has an apparent molar absorptivity of $18 \pm 3\ M^{-1}\ sec^{-1}$. Formation of this complex and its physical properties are very similar to reported charge transfer compounds of halogens,[21] particularly the benzene-chlorine complex where the halogen lies along the axis perpendicular to the center of the benzene ring.[22]

Acknowledgments. The authors wish to express their appreciation to the Atomic Energy Commission for financial support of this research.

(21) L. J. Andrews and R. M. Keefer, *Advan. Inorg. Chem. Radiochem.*, **3**, 91 (1961).
(22) F. A. Cotton and G. W. Wilkinson, *Advan. Inorg. Chem.*, **2**, 564 (1966); E. M. Kosoner, *Progr. Phys. Org. Chem.*, **3**, 81 (1965); O. Hassel and Chr. Romming, *Quart. Rev., Chem. Soc.*, **16**, 1 (1962).

Competitive Electron Scavenging Experiments in the Radiolysis of Hydrocarbons. Results at Low Solute Concentrations[1]

George W. Klein and Robert H. Schuler*

Radiation Research Laboratories, Center for Special Studies and Department of Chemistry, Mellon Institute of Science, Carnegie-Mellon University, Pittsburgh, Pennsylvania 15213 *(Received January 2, 1973)*

Publication costs assisted by The U.S. Atomic Energy Commission and Carnegie-Mellon University

The competitive effect of adding various second solutes (CH_3Br, CH_3I, C_2H_5Cl, C_2H_5Br, N_2O, SF_6, CCl_4, $(C_6H_5)_2$, c-C_4F_8 or c-C_6F_{12}) to 10^{-3} M solutions of methyl chloride in cyclohexane has been examined in experiments designed to determine the reactivity of each of these solutes toward the electrons produced in the radiolysis of the solvent. It is shown that the dependence on the concentration of added solute is of the form expected from simple competitive considerations and that all data are superimposable by proper adjustment of the reactivity parameter α used in the empirical description of the concentration dependence for electron scavenging in single solute systems. Most of the values of α determined in this way are in the range 10–20 M^{-1} with the most efficient electron scavengers being CH_3I and c-C_6F_{12}. Values of this magnitude indicate that the electrons react in diffusion-controlled processes which are several orders of magnitude more rapid than for reactions involving molecular anions. A relatively slow rate is observed in the case of ethyl chloride where $\alpha(C_2H_5Cl) = 0.24\ M^{-1}$. A difference of a factor of 20 between the reactivities of methyl and ethyl chloride illustrates the very profound effect that can be made by a relatively small change in the molecule. Measurement of the parameter α by a competitive method, such as is done here, allows one to describe electron scavenging in systems where it is frequently not possible to make direct measurements readily.

The competition between two solutes for scavenging the electrons produced in the radiolysis of liquid hydrocarbons has previously been discussed in detail.[2] It has been commented on that the experimental results on certain mixed systems indicate that secondary ionic processes are important at high (*i.e.*, $>10^{-2}$ M) solute concentrations.[2,3] Where they occur these secondary processes interfere in attempts to use the results from competitive studies to measure the relative reactivity of an electron scavenger by measuring its effect on the yield of product from a reference reaction. It, however, should be possible to determine the reactivity of a solute toward electrons from competitive measurements at low concentrations where the secondary reactions are less important. Appropriate expressions on which such a determination can be based have previously been given.[2] These expressions are derived from the empirical description of the dependence for ion scavenging on solute concentration noted in earlier studies by Warman, Asmus, and Schuler.[3] It has recently been shown that the competition between two solutes can be considered in a quite general way in terms of a phenomenological model involving the description of the distribution of ionic lifetimes in the pure hydrocarbon as manifested by the functional dependence of scavenging on solute concentration and that an explicit concentration dependence needs to be introduced only as a convenience

(1) Supported in part by the U. S. Atomic Energy Commission.
(2) P. P. Infelta and R. H. Schuler, *J. Phys. Chem.*, **76**, 987 (1972).
(3) J. M. Warman, K.-D. Asmus, and R. H. Schuler, *J. Phys. Chem.*, **73**, 931 (1969).

in handling the data by numerical methods.[4] Because charge recombination limits the lifetime of the majority of the ions[5] these general considerations also show that at solute concentrations $\sim 10^{-3}$ M the secondary processes should indeed be of negligible importance and that the expressions describing the simple competition should apply very well. We have carried out studies of the effect of various solutes in reducing the methyl radical yield from CH_3Cl in the region of 10^{-3} M for purposes of intercomparing a number of solutes commonly used as electron scavengers in hydrocarbon systems and report the results here. The methyl radicals produced by reaction of electrons with the methyl chloride are easily determined either

$$CH_3Cl + e^- \xrightarrow{k > 10^{11}\ M^{-1}\ sec^{-1}} [CH_3Cl^-] \xrightarrow{\tau < 3 \times 10^{-8}\ sec} CH_3\cdot + Cl^- \quad (1)$$

in terms of the methane which results from abstraction of hydrogen from the solvent[6] or by iodine scavenging methods.[3] The methyl chloride, itself, does not seem to be susceptible to attack by other reactive intermediates present in the radiolysis system.[2] Because the yields are low at the concentrations of CH_3Cl present in these studies, a radiochemical method of the type described by Warman and Rzad[6] was used to provide the necessary sensitivity and to distinguish between the methyl radicals produced from the solute and from other sources. Cyclohexane solutions have been studied because of the availability of a large amount of detailed ion-scavenging information in this solvent.

Experimental Section

$^{14}CH_3Cl$ of specific activity 6.5 Ci/mol was obtained from New England Nuclear Co., purified gas chromatographically, diluted by a factor of ~ 30 with inactive material in order to give a volume with which it was practical to work, and stored on a vacuum line. Certain preliminary experiments were carried out with $^{14}CH_3Br$ of specific activity ~ 0.05 Ci/mol. Samples were prepared by adding a known (PV measurement) amount of the halide to 1 ml of outgassed cyclohexane. The cyclohexane (Phillips Research Grade) had been purified by passing it through a silica gel column after which it was pumped on the vacuum line at room temperature to remove dissolved CO_2 and the first fourth of the sample discarded. A middle fraction was then transferred to a storage flask provided with a metal stopcock. The competing solutes (CH_3Br, CH_3I, N_2O, SF_6, C_2H_5Br, C_2H_5Cl, CCl_4, c-C_4F_8, c-C_6F_{12}, and $(C_6H_5)_2$) were used as obtained from the various suppliers. Except for biphenyl, a known amount of the solute was determined by a PV measurement and added to the outgassed sample containing the reference solute. Biphenyl could not be quantitatively transferred on the vacuum line so that in this case a cyclohexane solution containing the desired concentration was first outgassed and the radioactive material then added. In certain experiments iodine was also added to scavenge the radicals. In these cases a weighed amount was added to the irradiation cell prior to transfer of the solvent. The sealed ampoules contained less than $\sim 10\%$ vapor volume so that the solutes were essentially completely in the solution phase.

Irradiations were carried out in a ^{60}Co source at an absorbed dose rate of 3.3×10^{17} eV g^{-1} min^{-1} in the cyclohexane. The volume of cyclohexane was measured in a calibrated volume on the vacuum line and was known to $\sim 1\%$. Total doses were, in general, in the region of 3×10^{18}–10^{19} eV/g. These doses are 1–2 orders of magnitude greater than those used in the previous studies with iodine scavenger.[2,3] At these doses only $\sim 2\%$ of the methyl chloride is consumed but other products from the radiolysis of the solvent build up to concentrations $\sim 5 \times 10^{-4}$ M and may possibly interfere to a small extent in the determinations. Where iodine was added as a radical scavenger it was necessary to add at least 10^{-3} M I_2 to assure that the iodine would not be depleted during the course of the irradiation.

After irradiation the sample was transferred to the chromatographic column in total by breaking the ampoule in the eluting gas stream (see ref 6). Transfer of the methane thus was quantitative. The chromatographic columns and detection were as described by Warman and Rzad.[6] After passing through a thermal conductivity detector the effluent was burned, the water trapped in Dehydrite absorber, and the activity of the CO_2 determined in a proportional counter. The sensitivity of the radiochemical detector was determined by measuring the activity of a known amount (PV measurement) of the starting material under conditions identical with those used in the chromatographic analysis. In the experiments where the $^{14}CH_3\cdot$ radicals were trapped with iodine, $^{14}CH_3I$ was determined in addition to $^{14}CH_4$. The combustion served to convert the CH_3I, which otherwise would act as a quencher in the counter, to CO_2 and the iodine was removed by reaction with the copper oxide or in the Dehydrite train. Methane was observed as a narrow well-defined chromatographic peak, which, for $G(^{14}CH_4) = 0.2$, contained ~ 5000 counts on a background ~ 100 counts. The yields are known with an accuracy of a few per cent. Methyl iodide was eluted after the methyl chloride and the peaks were fairly broad so that the accuracy here was only $\sim 10\%$. In the studies with inactive methyl iodide this fraction did not contain any significant amount of activity.

Results and Discussion

In the absence of complicating secondary reactions $G(P_1)$s, the yield of product from the reaction of electrons with a given solute S_1 as affected by the presence of a second solute S_2, should be given[2,3] very closely by

$$G(P_1)_{S_2} = \frac{\alpha_1[S_1]}{\alpha_1[S_1] + \alpha_2[S_2]}\left[G_{fi} + G_{gi}\frac{\sqrt{\alpha_1[S_1] + \alpha_2[S_2]}}{1 + \sqrt{\alpha_1[S_1] + \alpha_2[S_2]}}\right]\epsilon \quad (1)$$

where α_1 and α_2 are parameters describing the reactivities of the solutes present at concentrations $[S_1]$ and $[S_2]$, G_{fi} and G_{gi} are the yields of free and geminate ions, and ϵ is the overall efficiency with which product P_1 is produced from S_1 as the result of the electron scavenging reaction.[7] The quantities α_1, $G_{fi}\epsilon$, and $G_{gi}\epsilon$ can be evaluated from a

(4) R. H. Schuler and P. P. Infelta, *J. Phys. Chem.*, **76**, 3812 (1972).
(5) S. J. Rzad, P. P. Infelta, J. M. Warman, and R. H. Schuler, *J. Chem. Phys.*, **52**, 3971 (1970).
(6) J. M. Warman and S. J. Rzad, *J. Chem. Phys.*, **52**, 485 (1970).
(7) Equation I is derivable (see ref **2**) from the dependence of product yield on scavenger concentration which for the methyl radical yields from methyl bromide and chloride solutions in cyclohexane has been found experimentally to be given very closely by the relationship

$$G(R) = G_{fi} + G_{gi}\frac{(\alpha[S])^{1/2}}{1 + (\alpha[S])^{1/2}}$$

(see ref 3). In systems containing two electron scavengers eq 1 should be an equally good description of the partition of the initial reactions between the two solutes and should also describe the experimental results provided complicating secondary reactions do not occur.

study of the dependence of the yield of product P_1 on the concentration of S_1 in the absence of the second solute. For methyl chloride α has been reported to be 5.4 M^{-1} from a study of the concentration dependence of scavengeable methyl radicals. The low concentration limit was found to be 0.12 ($= G_{fi}\epsilon$) and the high concentration limit 3.9 ($= \epsilon(G_{fi} + G_{gi})$).[3] The studies reported below show that a small yield (~5% of the methyl radicals) of methane is produced in the presence of 10^{-3}–10^{-2} M iodine. If this methane is also attributable to electron capture the value of ϵ appropriate to the previous studies would be slightly less than unity and a value of G_{gi} of 4.2 would be more in accord with the various results than the value of 3.8 previously given.[8] Since the absolute measurements do not give α directly but only the quantity $\epsilon G_{gi}\alpha^{1/2}$ the experimental results are describable only by choosing α to be consistent with the other parameters. The parameters G_{gi} = 4.2, $\alpha(CH_3Cl)$ = 5.0 M^{-1}, and ϵ = 1 are used to describe the methane production in the following treatment.[8]

Previously it has been shown that the $CH_3\cdot$ yields from mixed systems containing 10^{-2} M CH_3Cl and C_2H_5Br, SF_6, N_2O, or CO_2 can be interpreted reasonably well in terms of eq 1 with α_2 chosen as appropriate to the second solute. Consistent results were obtained from similar competitive studies between CH_3Br and C_2H_5Br, SF_6, or N_2O but studies with CO_2 showed unexpectedly large yields of methyl radicals which appeared to result from secondary attack on the CH_3Br. Although CH_3Br undergoes dissociative electron capture more readily than does CH_3Cl, and in many ways would appear to be the preferable reference solute, competitive studies are necessarily suspect because of the possibility of secondary effects similar to those observed in the CH_3Br–CO_2 system. At high solute concentrations mixed systems containing CH_3Cl are also complicated since the lifetime of the intermediate methyl chloride anion produced in the radiolysis of methyl chloride solutions appears to be sufficiently great that appreciable electron transfer to the other solutes can occur. The effects in this latter case are, however, relatively minor. Equation 1 can be appropriately modified to take into account secondary transfer (see eq XIII in ref 2) and it can be shown, from parameters measured in the region of 0.1 M, that at solute concentrations ~10^{-3} M, the effect should be the reduction of $G(CH_3\cdot)$ by only ~0.002. This effect is negligible with respect to the experimental error involved in the yield measurement.

While most of the studies carried out in the present investigation were on CH_3Cl solutions preliminary measurements were made on mixtures of 0.01 M $^{14}CH_3Br$ and varying concentrations of CH_3Cl. In the absence of iodine the $^{14}CH_4$ yields were 0.1–0.2 units higher than expected.[9] These studies did, however, show that the addition of CH_3Cl to 10^{-2} M solutions of $^{14}CH_3Br$ results in the reduction of $G(^{14}CH_4)$. For example, the $^{14}CH_4$ yield from a mixture containing 0.01 M CH_3Br and 1.5 M CH_3Cl was only 0.15. This result shows that the methyl bromide is "protected" by a competing electron scavenger. By adding iodine it was shown that the nonscavengeable methyl radicals amounted to only ~10% of the total so that the high methane yields must result from experimental difficulties and/or difficulties in the application of eq 1 with the parameters determined from the iodine scavenging studies. Table I contains a summary of results from $^{14}CH_3Br$–CH_3Cl–I_2 solution where the thermal methyl radicals were trapped with I_2 and measured as $^{14}CH_3I$. The experimental yields agree reasonably well with the total yields calculated from eq XVI of ref 2 (which takes into account electron transfer from the methyl chloride anion). Slightly lower values are predicted by eq 1. In addition a nonscavengeable $^{14}CH_4$ yield ~10% of that of the $^{14}CH_3I$ was observed for all mixed solutes. The fact that the addition of CH_3Cl causes a reduction in the $^{14}CH_4$ yield parallel to that of the $^{14}CH_3I$ indicates very strongly that this methane results from the reaction of hot methyl radicals produced in the electron scavenging process.

TABLE I: $^{14}CH_4$ and $^{14}CH_3I$ Yields from $^{14}CH_3Br$–CH_3Cl–I_2 Solutions in Cyclohexane[a]

$[^{14}CH_3Br]$ $\times 10^3$ M	$[CH_3Cl]$ $\times 10^3$ M	$[I_2]$ $\times 10^3$ M	$G(^{14}CH_4)$	$G(^{14}CH_3I)$	$G(^{14}CH_3)_{calcd}$[b]
9.6	0	0	1.45		1.31
9.0	0	1.5	0.12	1.05	1.28
9.5	0	20	0.08	1.02[c]	1.30
8.7	4.8	27	0.07	0.96[c]	1.15
9.6	25.8	4.0	0.09	0.80	0.91
9.7	108	5.5	0.05	0.51	0.53
9.4	492	5.1	0.03	0.22	0.25

[a] Measured at doses of 10^{19} eV/g. [b] Calculated from eq XVI of ref 2 with $\alpha(CH_3Br)$ = 16.2 M^{-1}, $\alpha(CH_3Cl)$ = 5.0 M^{-1}, G_{fi} = 0.12, G_{gi} = 4.2 (with ϵ = 1) and the exchange parameters β = 0.5 M^{-1} and $\delta(CH_3Cl)$ = 0.03. Values lower by 0–0.1 units are predicted by eq 1 of the present discussion. [c] These yields are expected to be somewhat low because of the very high iodine concentration present.

In addition to the studies on CH_3Cl solutions, the $^{14}CH_4$ and $^{14}CH_3I$ yields observed from $^{14}CH_3Cl$ and $^{14}CH_3Cl$–I_2 solutions are given in Table II. It is seen that in this case the nonscavengeable $^{14}CH_4$ amounts to only ~5% of the CH_3 yield.[10] Because of the low yields these experiments required relatively high doses. In order to ensure that iodine would not be depleted during the irradiation it was added in high concentra-

(8) In the previous study (ref 3) an empirical extrapolation of the CH_3I or C_2H_5I yields to infinite electron scavenger concentration gave geminate ion yields of 3.76, 3.84, and 4.01, respectively, for CH_3Br, C_2H_5Br, and CH_3Cl based on ϵ as unity. The value of $\alpha(CH_3Cl)$ = 5.4 was obtained from a best fit of the data on the assumption that a common limit corresponding to a geminate ion yield of 3.8 applied to all three sets of data. If one assumes that the nonscavengeable CH_4 observed here also results from electron scavenging processes and corrects for the slightly different efficiencies of 0.90 and 0.95 implied by the present results, geminate ion yields of 4.18 and 4.22 are obtained. A yield of 4.22 has recently been suggested for G_{gi} from the simplest interpretation of the secondary processes producing N_2 in the cyclohexane–N_2O system (P. P. Infelta and R. H. Schuler, *Int. J. Radiat. Phys. Chem.*, ref 12. The exact values of the individual parameters in eq 1 are subject to some uncertainty but the model is generally applicable (ref 4) and not dependent on knowledge of these values. Experimentally one measures the quantity $\epsilon G_{gi}\alpha^{1/2}$ from the slope of a plot of $1/G$ *vs.* $1/[S]^{1/2}$ (see ref 2) and in dilute solutions it is this quantity that mainly controls the functional dependence of yield on solute concentration. If the geminate ion yield is taken as 4.2 and ϵ as 0.95 then $\alpha(CH_3Cl)$ = 5.0 M^{-1} must be used to describe the scavengeable methyl radical yields reported in ref 3.

(9) Warman and Rzad (ref 6) studied CH_3Br solutions in the absence of I_2 and reported CH_4 yields which agreed with the yields of CH_3 radicals determined by iodine scavenging methods. More recent studies show somewhat higher yields which seem to be critically dependent on the methods used to purify the solvent (S. J. Rzad, private communication). The differences are small (<20%) and it is not clear at this moment whether they result from difficulties in carrying out the experiments, from as yet not completely understood secondary effects, or are fundamental to the ion scavenging process. Methyl chloride solutions appear to be free of similar difficulties.

(10) R. H. Schuler, *J. Phys. Chem.*, 61, 1472 (1957), reported a methane yield of 0.6 from iodine scavenged cyclohexane solutions 0.1 M in CH_3I. This methane amounts to ~20% of the yield estimated for the electron scavenging process. An increase in the yield of nonscavengeable methane with increase in the electron affinity of the halogen atom and decrease in C–X bond strength in going from CH_3Cl to CH_3Br to CH_3I is therefore indicated.

TABLE II: Methane and Methyl Iodide Yields from $^{14}CH_3Cl$–I_2 Solutions in Cyclohexane

$[CH_3Cl]$ × 10^3 M	$[I_2]$ × 10^3 M	Dose × 10^{-18}, eV/g	$G(CH_4)$	$G(CH_3I)$	$G(CH_3)_{calcd}$[a]
1.4		20.6	0.40		0.44
1.44		10	0.43		0.45
8.6		3.2	0.79		0.84
9.9		3.2	0.85		0.88
14	19	10	0.04	0.84[b]	1.00
15	16	32	0.05	0.80[b]	1.02
15	18[c]	32	0.03[c]	0.88[c]	1.02

[a] Calculated from eq 1 ([S_2] = 0) with $\alpha(CH_3Cl)$ = 5.0 M^{-1}, G_{fi} = 0.12, G_{gi} = 4.2, and ϵ = 1. [b] These yields are expected to be somewhat low because of the very high iodine concentrations present. [c] Sample also contained 0.14 M cyclopropane. Within experimental error the presence of this positive ion scavenger does not influence the yield of either CH_4 or CH_3I.

TABLE III: $^{14}CH_4$ Yields from $^{14}CH_3Cl$–CH_3Br Solutions

$[^{14}CH_3Cl]$ × 10^3 M	$[CH_3Br]$ × 10^3 M	$G(^{14}CH_4)$	$G(^{14}CH_3)_{calcd}$[a]	$G(CH_3)_{calcd}$[b]
1.44	0	0.42[c]	0.45	0.45
1.42	0.168	0.35	0.36	0.50
1.41	1.33	0.20	0.18	0.73
1.39	11.9	0.059	0.049	1.42

[a] Calculated from eq 1 with $\alpha(CH_3Cl)$ = 5.0 M^{-1}, $\alpha(CH_3Br)$ = 16.2 M^{-1}, G_{fi} = 0.12, G_{gi} = 4.2, and ϵ = 1. [b] Total methyl radical yield calculated from $G(CH_3) = G_{fi} + G_{gi}\{(\alpha(CH_3Cl)[CH_3Cl] + \alpha(CH_3Br)[CH_3Br])^{1/2}/[1 + (\alpha(CH_3Cl)[CH_3Cl] + \alpha(CH_3Br)[CH_3Br])^{1/2}]\}$ (see eq II in ref 2). [c] The yields observed in the absence of added solute are lower than calculated by 0.02–0.03 units. This difference may be caused by the relatively large doses used which results in the buildup of product to concentrations ~5 × 10^{-4} M (see Experimental Section).

tion so that the methyl iodide yields are, as a result, somewhat lower than calculated from eq 1. The results, however, indicate that the nonscavengeable methane is small and that the chemical complications are at a minimum.

Results of the production of $^{14}CH_4$ from $^{14}CH_3Cl$–CH_3Br solutions are given in Table III and are compared with the yields calculated from eq 1 based on $\alpha(CH_3Br)$ = 16.2 M^{-1}.[3] The agreement is seen to be very satisfactory. The observed yield of $^{14}CH_4$ can also be compared with the total yield of CH_4 given in the last column of Table III which is calculated to be produced from both solutes (eq 2 in ref 2).

The dependence of $G(P_1)_S$ on the concentration of S_2 for 0.0014 M solutions of CH_3Cl, calculated from eq 1, is plotted as the solid curve in Figure 1. It is seen in this equation that at a given $[S_1]$ the yield $G(P_1)_S$ is a function only of the quantity $\alpha_2[S_2]$. It should be possible, therefore, to superimpose the data on this curve by appropriate choice of α_2. The fit of the data for CH_3Br was optimized (minimum RMS deviation between calculated and observed yields) with $\alpha(CH_3Br)$ = 15.6 M^{-1}. Such a treatment tends to weight the measurements in the region where the dependence is steepest (*i.e.*, where $\alpha_2S_2 \sim 2\alpha_1S_1$ and the yield is reduced by a factor ~2). Because small variations in the experimental yields are reflected by very large changes in the calculated values of α, an uncertainty of ~20% must be assigned to values of α_2 determined in this way. The dotted curve given in Figure 1 takes into account secondary transfer as represented by eq XIII of ref 2 (with β = 0.5 M^{-1} and δ = 0.03 as required

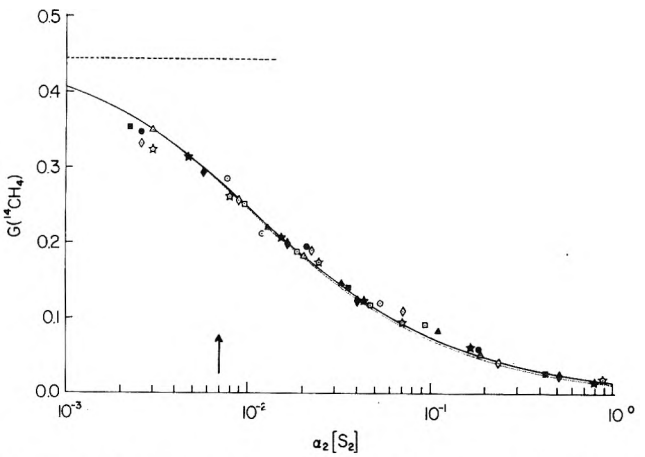

Figure 1. Dependence of the yield of $^{14}CH_4$ from a 0.0014 M $^{14}CH_3Cl$ solution on the concentration of added solute. Concentrations are expressed in units of the dimensionless quantity $\alpha_2[S_2]$ where the values of α_2 (in units of M^{-1}) are for CH_3Br (●) 16, CH_3I (▲) 22, C_2H_5Cl (◊) 0.24, C_2H_5Br (■) 10, N_2O (△) 8, SF_6 (○) 16, CCl_4 (♦) 12, $(C_6H_5)_2$ (□) 15, c-C_4F_8 (★) 14, and c-C_6F_{12} (☆) 21. Solid curve represents eq 1 with $\alpha(CH_3Cl)$ = 5.0 M^{-1}, G_{fi} = 0.12, and G_{gi} = 4.2. Dotted curve illustrates the slightly lower yields calculated if electron exchange from the methyl chloride anion occurs as indicated in the CH_3Cl–C_2H_5Br system (see eq XIII in ref 2). The dashed line in the upper left is the yield calculated in the absence of added solute. The arrow indicates the value of αS for the methyl chloride.

to describe the competition between CH_3Cl and C_2H_5Br).[2] It is seen that at the concentration of CH_3Cl used here this latter effect is small compared to the errors in the experimental measurements and, for all practical purposes, can be neglected.

Considerations of the phenomenological model[4] show that the data for all solutes should be superimposable on a common curve irrespective of the exact form of the curve or the scavenging function from which it can be derived (see eq VI–IX in ref 4). One can therefore regard the $^{14}CH_3Cl$ simply as providing an indicator system which allows relative values of k_2 for various solutes to be determined from a comparison of their effects with that of a reference second solute such as CH_3Br. However since the empirical description of the scavenging function given by Warman, Asmus, and Schuler[3] can be incorporated analytically into the phenomenological model[4] (as is done in eq 1 with the parameters α_1 and α_2 proportional to k_1 and k_2) one can, in fact, make absolute comparisons of each of the solutes directly with CH_3Cl. That the data for each of the solutes studied are, in fact, superimposable on each other is illustrated in Figure 1. The $^{14}CH_4$ yields in the presence of the various solutes are plotted as a logarithmic function of $\alpha_2[S_2]$ with the values of α_2 for each solute adjusted for best fit with eq 1 (minimum RMS deviation between calculated and observed yields). For purposes of plotting the data corrections to the yield for small variations of the CH_3Cl concentration from 1.4 × 10^{-3} M were calculated from eq 1. The agreement with the absolute dependence predicted by eq 1 is good in all cases (RMS deviation ~0.01) and particularly excellent for the five measurements on perfluorocyclobutane and four on CCl_4 (RMS deviations of only 0.003 and 0.004). In each case these measurements were made over a concentration range of two orders of magnitude. The values of α_2 used in Figure 1 are summarized in Table IV.

TABLE IV: Electron Reactivity Parameter α as Determined by Competition with CH_3Cl

Compd	Electron scavenging reactivity, α, M^{-1}		
	This work	Previous competitive study[a]	Absolute measurements
CH_3Cl	(5.0)[b]		5.4[c]
CH_3Br	16		16.2[c]
CH_3I	22		
C_2H_5Cl	0.24		0.5[c]
C_2H_5Br	10	8	7.8[c]
N_2O	8	10	~10[d]
SF_6	16	17	
CCl_4	12		
$(C_6H_5)_2$	15		
c-C_4F_8	14		
c-C_6F_{12}	21		30[e]
CO_2		13	

[a] Determined in ref 2 from CH_3 radical measurements at CH_3Cl concentrations of 0.01–0.2 M. Similar values were applicable to the decrease in the CH_3 radical yield from CH_3Br solutions resulting from the addition of C_2H_5Br, N_2O, and SF_6. Anomalously high CH_3 radical yields were obtained from CH_3Br–CO_2 solutions because of secondary reactions involving the CH_3Br. [b] Assumed. Determined as 5.4 in ref 3 from the concentration dependence for methyl radical formation but corrected here for $\epsilon = 0.95$ (see footnote 8). [c] Reference 3. [d] The N_2O system appears to be complicated by secondary reactions which contribute to nitrogen formation. The simplest mechanistic assumption which involves a doubling of the nitrogen yield as the result of a secondary ionic process allows the yields to be interpreted in terms of $\alpha(N_2O) = 10\ M^{-1}$ (ref 12). [e] Reference 11.

Methyl chloride and bromide have previously been compared with ethyl bromide in competitive experiments where the methyl and ethyl radical yields could both be measured.[2,3] The ratios $\alpha(CH_3Cl)/\alpha(C_2H_5Br)$ and $\alpha(C_2H_5Br)/\alpha(CH_3Br)$ were determined to be 0.67 and 0.55.[2] The present intercomparison of CH_3Br and CH_3Cl closes the circle and gives a value of $\alpha(CH_3Br)/\alpha(CH_3Cl)$ of 3.1. The product of these three ratios is 1.14 which is equal to unity well within experimental error. The results of the competitive experiments are, therefore, internally consistent. The ratios of the reactivities measured in the competitive experiments agree very well with the ratios of the absolute values of α determined directly from the dependence of product yield on solute concentration (0.69, 0.48, and 3.0, respectively, for $\alpha(CH_3Cl)/\alpha(C_2H_5Br)$, $\alpha(C_2H_5Br/\alpha(CH_3Br)$, and $\alpha(CH_3Br/\alpha(CH_3Cl)$. The value of 10 M^{-1} for $\alpha(C_2H_5Br)$ from the present study is ~20% higher than indicated either by the absolute measurements or by the previous competitive studies against methyl chloride and bromide. Since the ethyl radical yields were also measured in the latter experiments they must be given more weight than the present results and the difference appears to reflect the relatively large error possible in studies where only one component is examined. The ratio $\alpha(C_2H_5Br)/\alpha(CH_3Br) = 0.62$ determined by the comparison of the effects of both CH_3Br and C_2H_5Br on the scavenging by CH_3Cl is somewhat higher than the same ratio determined from the individual product yields (0.55, see above).[3] Previous results on mixture of methyl and ethyl bromide appeared to indicate a very slight bias (*i.e.*, 5–10%) toward high ethyl and low methyl radical yields and it was tentatively suggested that electron transfer might have a slight importance in this system. This apparent bias is largely negated by the present results and one must conclude that for all intents and purposes in the methyl bromide–ethyl bromide system electron transfer does not contribute within the experimental errors involved in the measurements.

Of the other compounds included in Table IV, information on the values of α from direct measurements on the concentration dependence of product formation exists only for perfluorocyclohexane, ethyl chloride, and N_2O. In the first instance Sagert, Reid, and Robinson[11] derived a value of α of 30 M^{-1} from measurements of the production of c-C_6HF_{11} in cyclohexane solutions. In the second, preliminary results on the formation of ethyl radicals showed yields considerably lower than those expected from the results on the other halides with yields of 0.68, 1.06, and 1.40 being measured at 0.1, 0.2, and 0.5 M C_2H_5Cl.[3] It was not clear at the time of these earlier experiments whether the yields were low as the result of a low efficiency for production of radicals in the scavenging process or whether the reactivity parameter for C_2H_5Cl is, in fact, considerably lower than those for the other halides. It is now obvious that the latter is the case. Using the value for $\alpha(C_2H_5Cl)$ determined here the ethyl radical yields predicted (assuming $\epsilon = 1$ with the other parameters as for CH_3Cl) are 0.68, 0.87, and 1.20. The agreement between the predicted and experimental is somewhat better if $\alpha(C_2H_5Cl)$ is taken as 0.4 M^{-1}. The N_2O system is complicated by secondary reactions but can be interpreted if $\alpha(N_2O)$ is taken as ~10 M^{-1}.[12] Values of α for other solutes are indirectly available from studies of their effect on H_2 production from cyclohexane. Values of 18 and 16 were required to superimpose the data for SF_6 and N_2O on the curve obtained for CH_3Br.[13] It is seen that these different approaches give values of α which vary by a factor of about 1.5. Since small inconsistencies in the interpretation of the data (either in the actual experimental results or in the application of the model to the specific type of measurement) are magnified considerably in the resultant value of α this agreement must, for the moment, be regarded as satisfactory. Yield calculations are fairly insensitive to the exact values used for α. It is pointed out, for example, that the difference between the value of 30 M^{-1} given by Sagert, Reid, and Robinson in their direct observations on the perfluorocyclohexane–cyclohexane system and that of 21 M^{-1} obtained here from the competitive studies corresponds to a difference of only 7% in the yield of c-C_6HF_{11} at 0.1 M c-C_6F_{12}.

It is seen in Table IV that most solutes have values of α in the range of 10–20 M^{-1}. The rate constant for the reaction is given by $\alpha\lambda$ where λ is a frequency which describes the recombination of the ion pairs in the pure hydrocarbon.[5] A lower limit to λ has been estimated[5] as 2×10^{10} sec^{-1} and a recent treatment[14] based on the assumption that the positive ions which enter into the recombination have mobilities as high as $\sim 2 \times 10^{-2}$ $cm^2\ V^{-1}\ sec^{-1}$ indicates that λ may be as high as 7×10^{11} sec^{-1}. The rate constants for most of these electron scavenging reactions are, therefore, in the region 2×10^{11}–10^{13} $M^{-1}\ sec^{-1}$. These rate constants are two to three orders of magnitude higher than those of conventional diffusion-controlled chemical processes and appear to reflect the high mobility of the electron in cyclohexane. A recent measurement has

(11) N. H. Sagert, J. A. Reid, and R. W. Robinson, *Can. J. Chem.*, **47**, 2655 (1969).
(12) P. P. Infelta and R. H. Schuler, *Int. J. Radiat. Phys. Chem.*, **5**, 41 (1973).
(13) K.-D. Asmus, J. M. Warman, and R. H. Schuler, *J. Phys. Chem.*, **74**, 264 (1970).
(14) P. P. Infelta and S. J. Rzad, *J. Chem. Phys.*, in press.

given this mobility as 0.35 $cm^2\ V^{-1}\ sec^{-1}$ [15] or about three orders of magnitude greater than the mobilities of molecular anions. The diffusion coefficient appropriate to the scavenging process should be similarly higher. Values of α in the range of 10–20 M^{-1} would, therefore, seem to indicate that the electrons react with most of the solutes studied here in diffusion-controlled processes with the value of $\sim 20\ M^{-1}$ observed for both methyl iodide and perfluorocyclohexane representing an approximate upper limit for this type of process. Certain electron scavenging reactions proceed at a rate considerably less than this limit (*i.e.*, CH_3Cl and C_2H_5Cl with α values of 5.0 and 0.24 M^{-1}). The profound difference that can be caused by a relatively small change in the molecule is exemplified by the comparison of CH_3Cl and C_2H_5Cl where the rate constant for reaction of electrons with the latter is 20-fold lower. Reactions which occur with rate constants less than $\sim 10^8\ M^{-1}\ sec^{-1}$ (*i.e.*, $\alpha < 10^{-3}$) will produce products with yields from the geminate ion component which are less than 0.1 at concentrations of 0.1 M and for the most purposes are of negligible importance. For compounds which have higher electron scavenging rate constants appropriate equations derivable from application of the empirical expression of Warman, Asmus, and Schuler[3] to the phenomenological model[4] allow calculation of yields to be made based on an assumed reaction scheme. Values of the parameter α determined by competitive measurements, such as those presented here, permit these calculations to be carried out in cases where this parameter is not available from direct measurements.

(15) W. F. Schmidt and A. O. Allen, *J. Chem. Phys.*, **52**, 4788 (1970).

Formation of Benzyl Radicals by Pulse Radiolysis of Toluene in Aqueous Solutions

H. C. Christensen,*

AB Atomenergi, Studsvik, Fack, S-611 01 Nyköping, Sweden

K. Sehested,

Danish Atomic Energy Commission Research Establishment, Riso, DK-4000 Roskilde, Denmark

and E. J. Hart

Argonne National Laboratory, Argonne, Illinois 60439 *(Received December 11, 1972)*

Publication costs assisted by AB Atomenergi

Benzyl radicals are formed by reaction of e_{aq}^- with benzyl compounds in aqueous solutions (benzyl chloride, bromide, thiocyanate, formate, and acetate). The observed spectrum of the benzyl radical is similar to the spectrum in organic solvents including the recently observed absorption band at 258 nm. The extinction coefficients at the maxima 258, 307, and 317.5 nm are 14,000, 3200, and 5500 $M^{-1}\ cm^{-1}$, respectively. OH reacts with toluene in aqueous solutions to form the hydroxymethylcyclohexadienyl radical, which in acid solutions eliminates H_2O to form the benzyl radical. The rate of this reaction is proportional to the proton concentration and the rate constant is $(1.11 \pm 0.04) \times 10^6\ M^{-1}\ sec^{-1}$. In strongly alkaline solutions O^- reacts with toluene to form benzyl radicals by abstraction of an H atom from the side group with $k = (2.1 \pm 0.3) \times 10^9\ M^{-1}\ sec^{-1}$.

Introduction

The reactions of OH radicals and H atoms with toluene in aqueous solutions have been shown by Dorfman, *et al.*,[1,2] and Sauer and Ward[3] to yield cyclohexadienyl radicals. An appreciable contribution from benzyl radicals to the absorption spectra was ruled out.

Recently Christensen and Gustafsson[4] have shown that bibenzyl is the major product ($G = 1.6$) in γ-radiolysis of aqueous, N_2O-, and toluene-saturated solutions at pH 3. As the benzyl radical had not been seen in pulse radiolysis studies[1-3] and was not seen in γ-radiolysis of unbuffered solutions it was postulated that this radical was formed indirectly in an acid-catalyzed water elimination reaction from the primarily formed hydroxymethylcyclohexadienyl radical. The reaction is easier to detect in γ-radiolysis studies because of the much lower dose rate compared with pulse radiolysis studies. First-order reactions are, therefore, favored in competition with second-order reactions. The purpose of the present investigation is to study the elimination reaction in more detail.

(1) L. M. Dorfman, I. A. Taub, and R. E. Buhler, *J. Chem. Phys.*, 36, 3051 (1962).
(2) L. M. Dorfman, I. A. Taub, and D. A. Harter, *J. Chem. Phys.*, 41, 2954 (1964).
(3) M. C. Sauer, Jr., and B. Ward, *J. Phys. Chem.*, 71, 3971 (1967).
(4) H. C. Christensen and R. Gustafsson, *Acta Chem. Scand.*, 26, 937 (1972).

Preliminary results including the absorption spectrum of the benzyl radical in aqueous solutions down to 263 nm have been reported previously.[5]

Experimental Section

Materials. Toluene (Merck p.a.) was purified either by recrystallization twice or by the method given in ref 6. The results were independent of the purification method. Other chemicals were of p.a. quality and used without further purification. The water was triply distilled.

Irradiations. The pulse radiolysis experiments were carried out at the Risö Linac using an optical detection system similar to that described previously[7] but modified by Fenger and Sehested by moving the detection system outside the radiation field. The essential features of the setup are a Linac delivering 0.2-4-μsec single pulses of 11-MeV electrons with a peak current of 250 mA as a maximum, an Osram XBO 450-W xenon lamp used in pulsed operation, a Zeiss MM 12 double quartz prism monochromator, an EMI 9558Q photomultiplier tube, and a Tektronix 555 double beam oscilloscope.

The time profile of the electron pulse, recorded in every experiment by monitoring the current induced in a coil surrounding the electron beam, was used for relative dosimetry. The absolute dose was measured with the hexacyanoferrate(II) dosimeter[8] using $g(e_{aq}^- + OH) = 5.25$ and $\epsilon(420\text{ nm})$ 1000 M^{-1} cm^{-1}. Due to the slow hydrolysis of some of the benzyl compounds in water the solutions were always irradiated immediately after the preparation.

The intensity of the light was increased by a factor of 30 by pulsing the 450-W xenon lamp. This allowed the double monochromator to be used with a small slit above 280 nm even when doses down to 200 rads were applied. The bandwidth of the monochromator above 280 nm was thus only 1.5 nm.

Analysis. Chemical analysis of bibenzyl was carried out as described previously.[4]

Corrections. The absorption spectra were corrected for depletion of solute (S) in the wavelength range where the solute absorbs light ($\lambda \leq 270$ nm). $G(-S)$ was assumed to be 5.8 [$= g(e_{aq}^-) + g(H) + g(OH)$] in N_2O-saturated unbuffered toluene solutions and 3.2 [$= g(e_{aq}^-) + g(H)$] in argon-saturated solutions of benzyl compounds. In the latter case corrections were also made for the contribution to the absorption of methanol or t-BuOH radicals (R) assuming $G(R) = 2.65$ [$= g(OH)$].

Results and Discussion

Benzyl Compounds. The benzyl radical and the methylcyclohexadienyl radical both absorb light in the wavelength range 300–330 nm. The benzyl radical was therefore produced and studied in aqueous solutions without interference from methylcyclohexadienyl radicals by pulse radiolysis of various benzyl compounds in argon-saturated aqueous solutions. The spectrum obtained for benzyl formate solutions containing 0.1 M *tert*-butyl alcohol after a dose of 2.500 rads is shown in Figure 1. The spectrum above 290 nm is similar to the benzyl radical spectrum obtained by radiolysis or photolysis of benzyl compounds or toluene in organic solutions and glasses.[9-12] The recently[13] reported new absorption band with λ_{max} at 258 nm in solutions of 3MP is also observed in aqueous solutions (Figure 1). The extinction coefficients are 14,000, 5500, and 50 M^{-1} cm^{-1} at 258, 317.5, and 450 nm (not shown in Figure 1), respectively. The benzyl radical decay

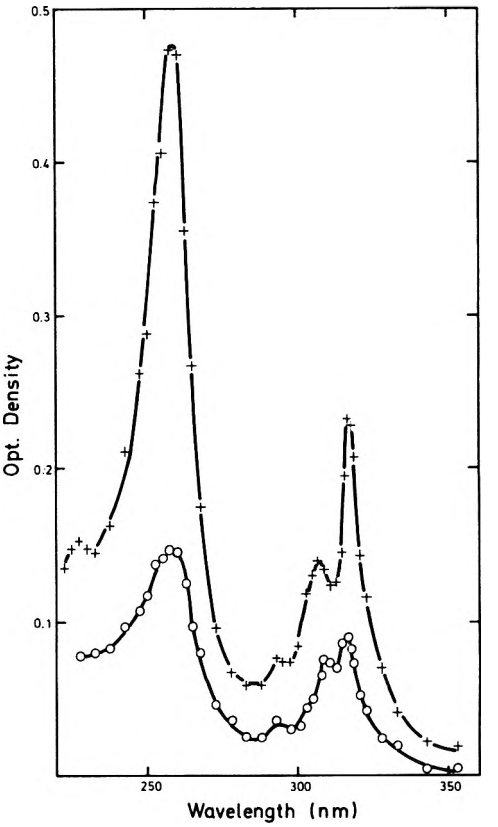

Figure 1. Absorption spectrum of the benzyl radical in aqueous solution obtained by pulse radiolysis of argon-saturated, aqueous 10^{-3} M benzyl formate solutions containing 0.1 M *tert*-butyl alcohol: dose 2.500 rads, (+) 2 and (O) 75 μsec after the pulse. The spectrum is not corrected for the small contribution of the H adduct.

follows second-order kinetics and has a rate constant $2k = (3.1 \pm 0.3) \times 10^9$ M^{-1} sec^{-1} determined both at 258 and 317.5 nm. The same absorption spectrum is obtained when methanol is used instead of *tert*-butyl alcohol and also from pulse radiolysis of aqueous solutions of benzyl chloride, bromide, thiocyanate, formate, and acetate. The rate constants for the reaction of e_{aq}^- with these compounds are (in units of 10^9 M^{-1} sec^{-1}) 1.6, 1.5, 2.0, 1.5, and 1.1, respectively. The rate constants were determined from the kinetics of the formation of the benzyl radical.

Mittal and Hayon[14] have recently reported the absorption spectrum of the benzyl radical in aqueous solutions down to 235 nm. The radical was produced and studied by a method similar to that reported previously by Christensen and Sehested,[5] who gave the spectrum down to 263 nm. Our values for the extinction coefficients and rate of decay given above is about a factor of 2 lower than the

(5) H. Christensen and K. Sehested, Kjeller Report No. KR-146, Kjeller, Norway, Feb 1972, p 43; AB Atomenergi Report No. AE-453, Studsvik, Sweden, May 1972, p 6.
(6) A. I. Vogel, "A Textbook of Practical Organic Chemistry," Longmans, London, 1961, p 173.
(7) H. C. Christensen, G. Nilsson, P. Pagsberg, and S. O. Nielsen, *Rev. Sci. Instrum.*, **40**, 786 (1969).
(8) R. Rabani and M. S. Matheson, *J. Phys. Chem.*, **70**, 761 (1966).
(9) G. Porter and M. W. Windsor, *Nature (London)*, **180**, 187 (1957).
(10) B. Brocklehurst, G. Porter, and M. I. Savadatti, *Trans. Faraday Soc.*, **60**, 1187 (1960).
(11) R. L. McCarthy and A. MacLachlan, *Trans. Faraday Soc.*, **56**, 1187 (1960).
(12) R. J. Hagemann and H. A. Schwartz, *J. Phys. Chem.*, **71**, 2694 (1967).
(13) G. Porter and M. I. Savadatti, *Spectrochim. Acta*, **22**, 803 (1966).
(14) J. P. Mittal and E. Hayon, *Nature (London), Phys. Sci.*, **240**, 21 (1972).

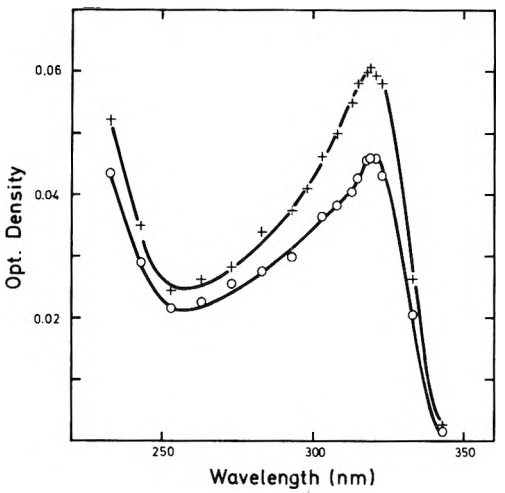

Figure 2. Transient absorption spectrum obtained by pulse radiolysis of N_2O-saturated, aqueous 10^{-3} *M* benzyl chloride solutions: dose 440 rads, (+) 2 and (O) 75 μsec after the pulse.

values of Mittal and Hayon[14] and the ratio of intensities of the bands at 258 and 317.5 nm also differs from their value (2.5 *vs.* 2.8). We have found that this ratio varies with the solvent and is higher in alcohols than in water (3.3 *vs.* 2.5). Some of the difference from Mittal and Hayon's value may be explained from this fact since they used 1.5 *M* *tert*-butyl alcohol solutions. In cyclohexane we have determined the ratio to be 4.5, the same value as found by Porter and Savadatti[13] in 3MP and close to the value of Johnson and Albrecht,[15] who also studied the benzyl radical in 3MP solutions.

Benzyl radicals are also formed by reaction of H atoms with benzyl chloride but not with formate. This was seen by pulse radiolysis of argon-saturated, 2×10^{-4} *M* benzyl compound in aqueous solutions containing 0.1 *M* *tert*-butyl alcohol and 10^{-3} *M* $HClO_4$. Also experiments with N_2O-saturated 10^{-4} *M* benzyl formate in aqueous solution at a hydrogen pressure of 35 atm [$C(H_2) = 0.027$ *M*] showed that the cyclohexadienyl and not the benzyl radical was formed by reaction with H atoms.

The reaction of OH radicals with benzyl chloride produces a transient with the absorption spectrum shown in Figure 2. The rather broad spectrum with λ_{max} 319 nm and ϵ 4500 M^{-1} cm^{-1} is similar to the hydroxycyclohexadienyl radical spectra of benzene[1] and benzyl alcohol[16] and is consequently assigned to the hydroxychlorocyclohexadienyl radical. The radical disappears in a bimolecular reaction with $2k = (1.6 \pm 0.2) \times 10^9\ M^{-1}\ \text{sec}^{-1}$.

Toluene Solutions. The transient absorption spectrum obtained by pulse radiolysis of N_2O-saturated, aqueous toluene solutions is shown in Figure 3 for unbuffered solutions (pH $\approx$6) and acid solutions (pH 0.3 $\sim$0.5 *M* $HClO_4$). The formation of benzyl radicals in the acid solution is easily seen from the spectrum between 300 and 320 nm which has the absorption maxima characteristic for benzyl and also from the maximum at 258 nm. In the wavelength range 245–265 nm, where the toluene itself absorbs, it was necessary to dilute the toluene solutions to 20% saturation.

The use of a narrow slit of the monochromator above 280 nm may explain why we observe the fine structure of the 300–320-nm band in unbuffered solutions. This double band was not observed previously[1,3] but it may be caused by benzyl radicals formed primarily in low yield together with cyclohexadienyl radicals. The transient spectrum is

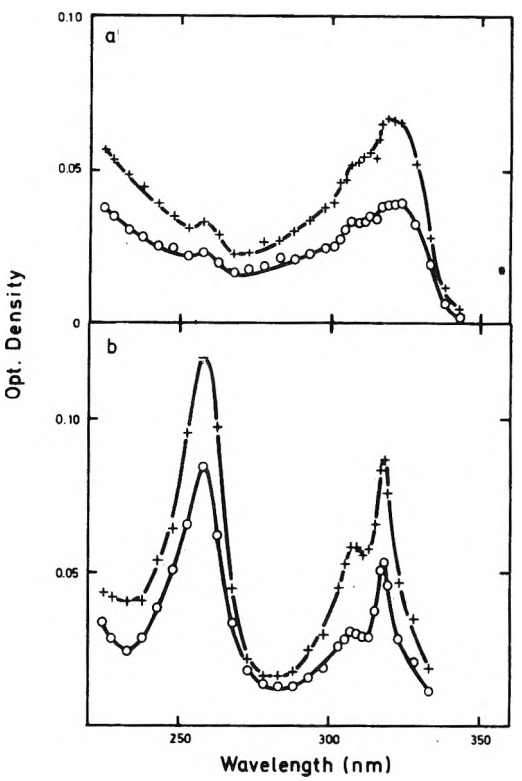

Figure 3. Transient absorption spectrum obtained by pulse radiolysis of N_2O-saturated, aqueous toluene solutions: (a) unbuffered (pH $\sim$6); (b) acid (pH 0.3); dose 440 rads (+) 2 and (O) 155 μsec after the pulse.

the same even at higher doses (3.400 rads). Another possible explanation is that the hydroxymethylcyclohexadienyl radical has an inherent fine structure similar to that of the hydroxycyclohexadienyl spectrum reported by Stein and coworkers.[17] This fine structure was taken as an indication of the possibility that the absorption spectrum was composed of two components.[17] The first explanation is the more likely since we have (1) found a small absorption even at 258 nm where the cyclohexadienyl radical is not expected to have a maximum and (2) found a small yield of radiolysis products containing the $C_6H_5CH_2$ group (phenyltolylmethanes) in unbuffered solutions, both by accelerator irradiation and previously by γ-irradiation.[4]

From the spectrum around 258 nm a ratio of the direct benzyl to cyclohexadienyl formation rate (*i.e.*, of OH abstraction to addition) of 0.033 was calculated. With a rate constant for OH addition to toluene of $3.0 \times 10^9\ M^{-1}$ sec^{-1} (ref 2) the rate constant for the abstraction reaction is $1.0 \times 10^8\ M^{-1}\ \text{sec}^{-1}$.

Benzyl radicals are not produced by direct abstraction from the methyl group by H atoms either in unbuffered or in acid solutions. This was proved by measurement of the $G(H_2)$ yield, which in both cases was equal to the primary hydrogen yield.

No significant amounts of benzyl radicals are formed from H atoms by indirect reaction (*e.g.*, in a reaction between toluene and the cyclohexadienyl radical). This is seen from Figure 4, where the transient spectra obtained by pulse radiolysis of N_2O-saturated toluene solution at pH 1 in the presence or absence of *tert*-butyl alcohol (0.5

(15) P. M. Johnson and A. C. Albrecht, *J. Chem. Phys.*, **48**, 851 (1968).
(16) P. Neta and L. M. Dorfman, *Advan. Chem. Ser.*, **No. 81**, 222 (1968).
(17) A. Mantaka, D. G. Marketos, and G. Stein, *J. Phys. Chem.*, **75**, 3886 (1971).

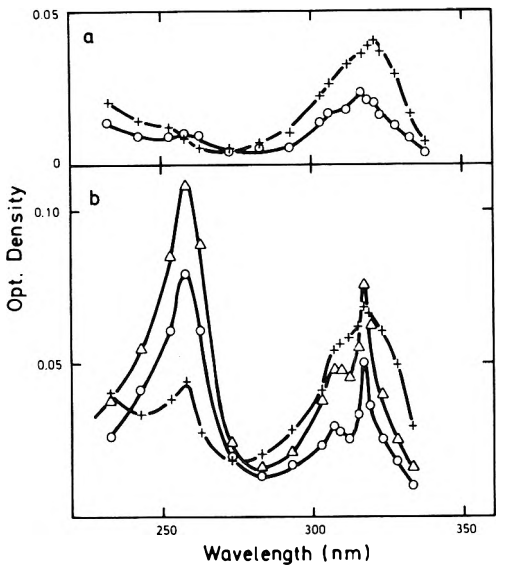

Figure 4. Pulse radiolysis of N_2O-saturated aqueous toluene solutions at pH 1 in the presence (a) and in the absence (b) of 0.5 *M* *tert*-butyl alcohol: dose 440 rads, (+) 2, (△) 30, and (○) 115 μsec after the pulse.

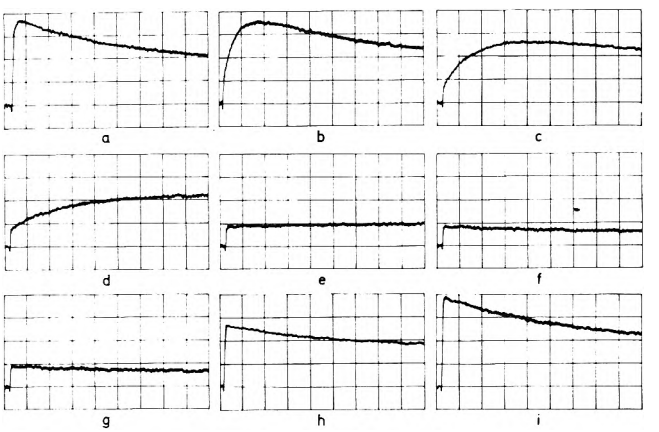

Figure 5. The formation of benzyl radicals in aqueous toluene solutions measured at 258 nm at various acid concentrations: 0.48 (a), 0.1 (b), 3.2×10^{-2} (c), 10^{-2} (d), 10^{-3} (e), and 0 (f) *M* $HClO_4$, and various alkali (NaOH) concentrations: 3.2×10^{-3} (g), 10^{-2} (h), and 10^{-1} (i): dose 440 rads, time scale 20 μsec per division.

M) are shown. The *tert*-butyl alcohol (B) reduces the OH concentration to a few per cent without significantly decreasing the H concentration (k(OH + B) = 2.7×10^8 M^{-1} sec^{-1}, C(B) = 0.5 *M* whereas k(OH + toluene) = 3.0×10^9 M^{-1} sec^{-1}, $C = 10^{-3}$ *M*, k(H + B) = 1×10^5 M^{-1} sec^{-1}, k(H + toluene) = 2.6×10^9 M^{-1} sec^{-1}). The peak at 258 nm is greatly suppressed by 0.1 *M* *tert*-butyl alcohol and is almost eliminated by 0.5 *M* *tert*-butyl alcohol (Figure 4).

From this we conclude that in acid solutions the benzyl radical is produced in an acid-catalyzed secondary water elimination reaction from primarily formed hydroxymethylcyclohexadienyl radicals according to the reactions

$$C_6H_5CH_3 + OH \longrightarrow OHC_6H_5CH_3 \quad (1)$$

$$OHC_6H_5CH_3 \xrightarrow{H^+} C_6H_5CH_2 + H_2O \quad (2)$$

The kinetics of reaction 2 were studied at 317.5 nm and in more detail at 258 nm by varying pH and the toluene concentration (Figure 5). From this figure the rate constants for the pseudo-first-order formation of the benzyl radical shown in Table I were calculated. The results obtained at 317.5 nm, where the kinetics are more complicated, agree with the values of Table I within a factor of 2. Benzyl radical formation follows first-order kinetics. By using a small dose (130 rads) the correction for the concurrent decay according to the method of Sauer[18] was minimized, and was necessary only in 10^{-2} *M* acid solutions.

TABLE I: Rate Constants for the Pseudo-First-Order Formation of the Benzyl Radical in Acid Toluene Solutions Measured at 258 nm

$C(HClO_4)$, *M*	$k_2 \times H^+ \times 10^{-4}$, sec^{-1}	$k_2 \times 10^{-6}$, M^{-1} sec^{-1}
0.48	50.0	1.04
0.100	11.5	1.15
3.2×10^{-2}	3.75	1.17
1.00×10^{-2}	1.06	1.06
		Av 1.11 ± 0.04[a]

[a] Standard deviation of the mean.

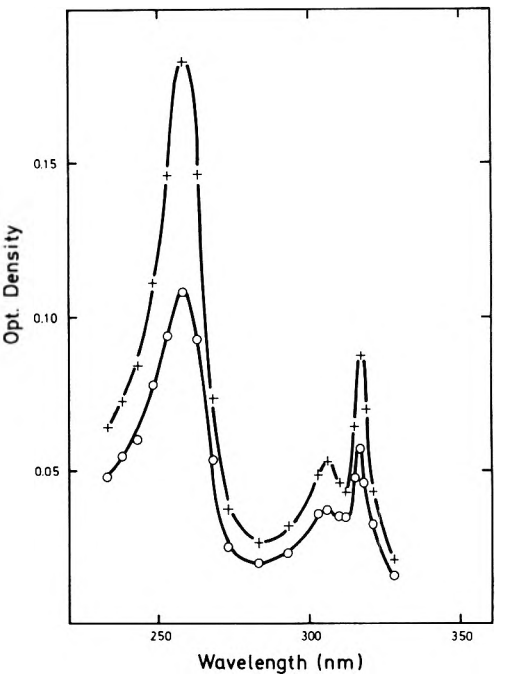

Figure 6. Transient absorption spectrum obtained by pulse radiolysis of N_2O-saturated aqueous toluene solutions at pH 13 (0.1 *M* NaOH): dose 440 rads, (+) 2 and (○) 115 μsec after the pulse.

In acid solutions the H adduct contributes to the absorption spectrum. If correction for this absorption is made the extinction coefficients at 317.5 and 258 nm are the same as those of the benzyl radical determined in aqueous solutions of benzyl compounds.

We have determined the extinction coefficient and wavelength of maximum absorption of the OH and H adducts to be 4300 M^{-1} cm^{-1} at 320 nm and 4800 M^{-1} cm^{-1} at 319 nm, respectively. These values were determined assuming that all OH radicals (respectively all H atoms) react with toluene by addition to the ring. The extinction coefficient for the H adduct was determined both

(18) M. C. Sauer, Jr., AEC Report No. ANL-7146, Argonne, Ill., Jan 1966.

in acid (pH 1) and in unbuffered solutions in the presence of *tert*-butyl alcohol or methanol. The OH and H adducts disappear in bimolecular reactions with $2k = (1.6 \pm 0.2) \times 10^9\ M^{-1}\ \text{sec}^{-1}$ (at pH 3 and in unbuffered solutions) and $2k = (2.7 \pm 0.3 \times 10^9\ M^{-1}\ \text{sec}^{-1}$, respectively. The rate of adduct formation was determined to be of the same order as the values given in the literature.[2,3]

The transient spectra obtained in N_2O-saturated toluene solutions at pH 9.3, 10.6, and 11.1 are identical with the spectrum found in unbuffered solutions. The spectrum obtained at pH 13, however, is totally different (Figure 6) and resembles the spectrum in acid solutions. Since the reaction

$$\dot{O}H + OH^- \longrightarrow O^- + H_2O \qquad (3)$$

is fast ($k \sim 3 \times 10^9\ M^{-1}\ \text{sec}^{-1}$, ref 19) and the p$K$ of OH is 11.9 (ref 20) e_{aq}^-, H, and OH appear as O^-($G(O^-) \simeq 6.5$, ref 21) within 0.1 μsec after the pulse. O^- reacts with toluene to form benzyl radicals.

$$C_6H_5CH_3 + O^- \longrightarrow C_6H_5\dot{C}H_2 + OH^- \qquad (4)$$

The rate of the reaction is independent of the OH^- concentration (0.05–0.5 M NaOH) and dose (60–600 rads) but is proportional to the toluene concentration ((6–30) $\times 10^{-5}\ M$). The rate constant $k(O^- + C_6H_5CH_3) = (2.1 \pm 0.3) \times 10^9\ M^{-1}\ \text{sec}^{-1}$. Benzyl radicals form directly by reaction (4) between O^- and toluene in strongly alkaline solutions, contrary to the situation in acid solutions where the formation is indirect. The benzyl radical disappears in a bimolecular reaction with $2k = (2.4 \pm 0.3) \times 10^9\ M^{-1}\ \text{sec}^{-1}$. This is lower than the value obtained in unbuffered solutions of benzyl compounds but is the same as that obtained in solutions of benzyl formate at pH 13. Our results agree with previous observations[22,23] that O^- reacts with aromatic compounds containing side chains preferentially by abstraction of an H atom from the side chain.

Spectra similar to those of toluene in unbuffered and acid solutions have been obtained in aqueous solutions of the various xylene isomers and mesitylene. In acid solutions methylbenzyl radicals are formed with absorption maxima displaced somewhat (by 5–10 nm) to higher wavelengths (bathochromic shifts) and with considerably higher rates than for benzyl radicals. Details of this study will be published elsewhere.

Acknowledgment. We thank the operator staff of the accelerator at Risö for their assistance and K. Nilsson for determination of the wavelength correction of the Zeiss monochromator. We are indepted to J. Eriksen and H. Corfitzen for preparation of solutions. The financial support of the Swedish Atomic Research Council obtained by one of us (H. C. C.) is gratefully acknowledged.

(19) G. E. Adams, J. W. Boag, and B. D. Michael, *Trans. Faraday Soc.*, **61**, 492 (1965).
(20) J. Rabani and M. S. Matheson, *J. Phys. Chem.*, **70**, 761 (1966).
(21) E. M. Fielden and E. J. Hart, *Radiat. Res.*, **32**, 564 (1967).
(22) P. Neta, M. Z. Hoffman, and M. Simic, *J. Phys. Chem.*, **76**, 847 (1972).
(23) H. Christensen, *Int. J. Radiat. Phys. Chem.*, **4**, 311 (1972).

Photoreduction of Dinaphtho[2,1:2′,3′]furan-8,13-dione and Dinaphtho[1,2:2′,3′]furan-7,12-dione

M. S. Walker,* M. A. Abkowitz, R. W. Bigelow, and J. H. Sharp

Research Laboratories, Xerox Corporation, Rochester, New York 14603 *(Received June 12, 1972)*

Publication costs assisted by Xerox Corporation

Photoreduction of dinaphtho[2,1:2′,3′]furan-8,13-dione (I) and dinaphtho[1,2:2′,3′]furan-7,12-dione (II) has been observed in basic alcohol solution. Quantum yields for semiquinone radical anion formation are typically 10^{-3}–10^{-2} consistent with the π–π^* nature of the low-lying electronic states of these furanquinones. A concentration dependence of the quantum yield is attributed to anion formation *via* the reaction $Q^* + Q \rightarrow Q\cdot^- + Q\cdot^+$.

Introduction

The mechanism for the photoreduction of polycyclic quinones in alcoholic solvents has received considerable experimental attention.[1] Quantum yields for reduction of 0.5 to 1[2,3] and even higher[4] have been reported for quinones with low-lying n–π^* electronic states.[5] In general the n–π^* triplet state is the reactive species in solution, though Bridge and Porter[6] have shown that duroquinone reacts *via* its singlet rather than triplet state. Substitution of the quinone with electron-donating groups gives rise to low-lying intramolecular charge-transfer (CT) states in these molecules with a concomitant decrease in photoactivity.[5,7] We have recently observed the photoreduction of

(1) J. M. Bruce, *Quart. Rev., Chem. Soc.*, **21**, 405 (1967).
(2) K. Tickle and F. Wilkinson, *Trans. Faraday Soc.*, **61**, 1981 (1965).
(3) F. Wilkinson, *J. Phys. Chem.*, **66**, 2569 (1962).
(4) P. Walker, *J. Chem. Soc.*, 5545 (1963).
(5) D. Schulte-Frohlinde and C. V. Sonntag, *Z. Phys. Chem. (Frankfurt am Main)*, **44**, 314 (1965).
(6) N. K. Bridge and G. Porter, *Proc. Roy. Soc., Ser. A*, **244**, 259, 276 (1958).
(7) H. H. Dearman and A. Chan, *J. Chem. Phys.*, **44**, 416 (1966).

the isomeric furanquinones dinaphtho[2,1:2′3′]furan-8,13-dione (I) and dinaphtho[1,2:2′,3′]furan-7,12-dione (II). Molecular structures of I and II are shown in Figures 2a and 2b, respectively. The order and nature of the low-lying electronic states of these quinones in polar media are S_0, $T_1^{\pi-\pi*}$, $S_1^{\pi-\pi*}$, $T_2^{n-\pi*}$, $S_2^{n-\pi*}$ . . . .[8,9] The S_0–S_1 transition ($\epsilon \sim 6 \times 10^3$) involves significant intramolecular charge-transfer character and as a consequence the relative energies of the singlet and triplet $\pi-\pi^*$ and $n-\pi^*$ states are solvent dependent.[9]

Experimental Section

The synthesis and purification of these compounds was reported earlier.[8] Photoreduction of quinones I and II was carried out in basic (0.01 *N* KOH) methanol solution in the concentration range 10^{-5}–3×10^{-4} *M*. Solvents were Matheson Coleman and Bell Spectroquality reagent. Solutions were subjected to a minimum of four freeze–pump–thaw cycles at a pressure of 10^{-6} mm and sealed off in 0.5-cm quartz cells for yield determinations or low loss aqueous cells for esr measurements. Monochromatic radiation (10-nm bandwidth), from a 200-W tungsten arc passed through a Bausch and Lomb grating monochromator, was used to irradiate the solutions. Light intensities were measured using a calibrated thermopile and were typically $1–5 \times 10^{15}$ photons/sec/cm^2.

Quantum yields for semiquinone radical anion formation were determined from the initial slopes of plots of radical ion concentration *vs.* irradiation time. The radical concentration was followed by monitoring its absorption in the region of 600 nm, using a Cary 14 recording spectrophotometer. The anion molecular extinction coefficient was calculated from the optical density of a solution of known initial quinone concentration, assuming quantitative conversion to anion after irradiation until no further change in optical density was noted. Any error in the above assumption would give rise to too low a value for the extinction coefficient and subsequently too high a value for the quantum yield of anion formation. However, relative quantum yield values and subsequent arguments would remain unchanged.

Electron spin resonance data were collected using a 3-cm balanced bridge homodyne instrument. The Klystron frequency was dc phase locked to the experimental cavity. Magnetic field homogeniety over the sample cell was better than 50 mG. Audio frequency modulation at 6 Hz was used to preclude side band broadening.

All measurements were carried out at 21°.

Results and Discussion

The visible absorption spectra of II in deoxygenated basic methanol solution before and after irradiation at 430 nm for several hours are shown in Figure 1. Similar spectral changes were observed on irradiating I under the same conditions. The long wavelength absorption maxima of the photoproducts are at 610 and 590 nm for I and II, respectively. In both cases the irradiated solution gave an electron spin resonance signal, which exhibited a partially resolved complex hyerfine pattern (Figure 2). In this study no subsequent attempt was made to fit hyperfine coupling constants to these incompletely resolved esr spectra which nevertheless served to distinguish the two unique photogenerated radical species. On allowing oxygen to re-enter the cell the radical products were oxidized quantitatively back to the respective quinone, otherwise they remained

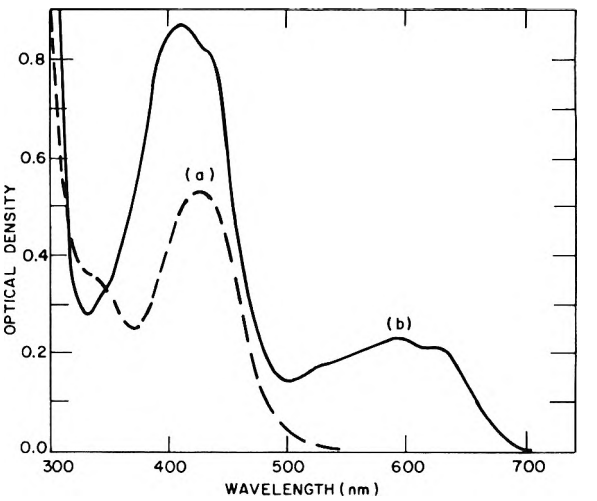

Figure 1. Visible absorption spectra of dinaphtho[1,2:2′,3′]-furan-7,12-dione in deoxygenated basic methanol solution (a) before and (b) after irradiation at 430 nm.

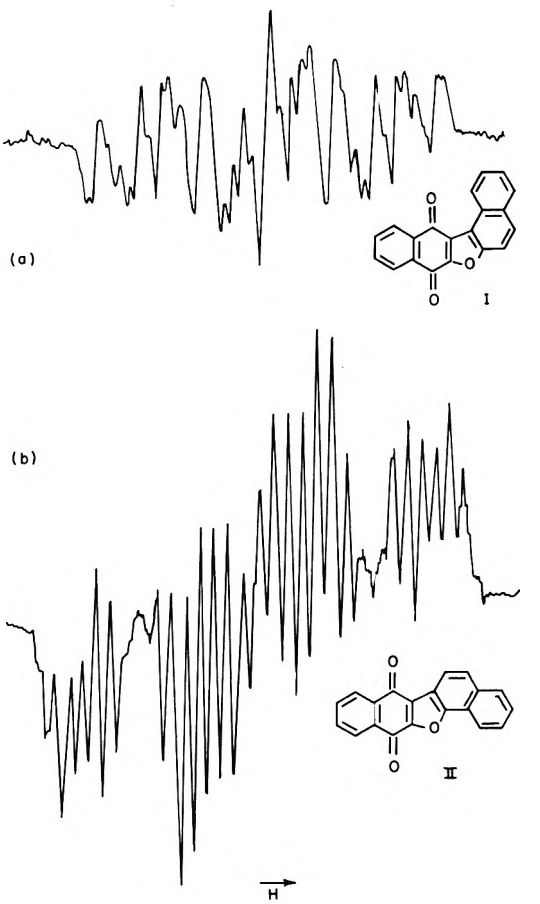

Figure 2. Electron spin resonance spectra of the semiquinone radical anions of (a) dinaphtho[2,1:2′,3′]furan-8,13-dione and (b) dinaphtho[1,2:2′,3′]furan-7,12-dione.

stable for several days. Irradiation of I and II in deoxygenated methanol solution in the absence of base resulted in an extremely slow bleaching of the originally yellow solution. No esr signal was observed under these conditions. Again on allowing oxygen to re-enter the cell the products

(8) M. S. Walker, J. E. Kuder, and R. L. Miller, *J. Phys. Chem.*, **75**, 3257 (1971).
(9) M. S. Walker, R. L. Miller, and J. E. Kuder, *J. Phys. Chem.*, **76**, 2240 (1972).

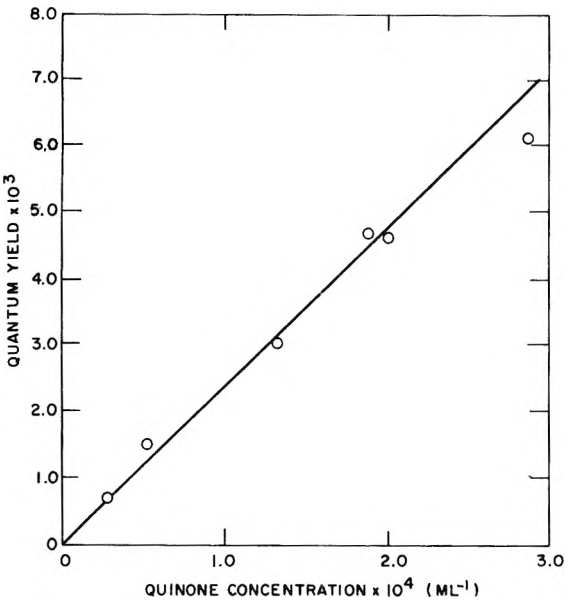

Figure 3. Concentration dependence of the quantum yield of radical anion formation for dinaphtho[1,2:2′,3′]furan-7,12-dione. Excitation wavelength is 430 nm.

TABLE I: Quantum Yields for I and II Semiquinone Radical Anion Formation in Basic Methanol Solution

Quinone	Concn, *M*	Light intensity, photons sec^{-1} cm^{-2} (λ 430 nm)	Quantum yield
I	2.9×10^{-5}	5.1×10^{15}	4.3×10^{-4}
II	3.0×10^{-5}	4.6×10^{15}	6.7×10^{-4}

were oxidized back to the respective quinone. In view of these observations the photoproducts observed in basic and nonbasic methanol solutions are attributed to the semiquinone ($Q\cdot^-$) and dihydroquinone (QH_2), respectively.

Quantum yields for the formation of the radical anions of I and II, given in Table I, were determined from the optical spectra. However, the increase in intensity of the product absorption bands, with irradiation time, was concomitant with an increase in the esr signal intensity, as expected.

The low yields for radical anion formation are consistent with these molecules having low-lying unreactive π–π^* or CT rather than n–π^* states.[9] Further, no change in the radical anion yield was observed in the presence of 10^{-3} M^{-1} anthracene as a quinone triplet state quencher. The triplet state energies of I, II, and anthracene are approximately 16,000, 16,800, and 14,900 cm^{-1}, respectively. This observation is consistent with radical anion formation in these systems *via* the quinone singlet rather than the triplet state. A linear dependence of the radical anion yield on quinone concentration was observed for II as shown in Figure 3. The low solubility of I in methanol prevented such a study for this quinone. In view of the low yields for radical anion formation it is possible that trace quantities of impurities in the quinone might be responsible for this concentration dependence. However, this is unlikely since the calculated concentration of such an impurity, assuming a quinone singlet state reaction and diffusion kinetics, would necessarily need to be of the same order as the concentration of the quinone itself.

Photoreduction in basic alcoholic media, in general, involves hydrogen abstraction from the solvent by either singlet or triplet state quinone, *i.e.*

$$^{(1,3)}Q^* + R_2CHOH \rightarrow QH\cdot + R_2\dot{C}OH \quad (1)$$

followed by dissociation of the semiquinone radical ($QH\cdot$) to the semiquinone radical anion

$$QH\cdot \rightarrow Q\cdot^- + H^+ \quad (2)$$

In the absence of base the following disproportionation reaction results in the formation of the dihydroquinone (QH_2)

$$2QH\cdot \rightarrow QH_2 + Q \quad (3)$$

Concentration dependent yields of photoreduction, resulting from a secondary attack of solvent radical ($R_2\dot{C}OH$) on a ground-state quinone molecule, have been reported.[2]

$$Q + R_2\dot{C}OH \rightarrow QH\cdot + R_2CO \quad (4)$$

However, in this case the concentration dependence of the quantum yield is nonlinear and extrapolates to a finite value at zero quinone concentration. The latter behavior is not observed in the present work.

More recently Phillips, *et al.*,[10] have identified the process

$$Q^* + Q \rightarrow Q\cdot^+ + Q\cdot^- \quad (5)$$

for sodium 9,10-anthraquinone-2-sulphonate in basic solution. $Q\cdot^+$ and $Q\cdot^-$ are the quinone radical cation and anion, respectively. This latter process involving the quinone excited singlet state ($^1Q^*$) could adequately account for the concentration dependent radical anion yields observed here. In highly basic media it is expected that $Q\cdot^+$ would disappear rapidly *via* the process

$$Q\cdot^+ + OH^- \rightarrow Q + OH\cdot \quad (6)$$

In this case only the radical anion would be observed under the steady-state photolysis conditions used in this work. Further, as pointed out by one of the referees, the subsequent reactions involving the OH· radical could also give rise to anion formation

$$OH\cdot + R_2CHOH \rightarrow HOH + R_2\dot{C}OH \quad (7)$$

$$Q + R_2\dot{C}OH \rightarrow QH\cdot + R_2CO \quad (8)$$

$$QH\cdot \rightarrow Q\cdot^- + H^+ \quad (9)$$

$$H^+ + OH^- \rightarrow HOH \quad (10)$$

For a reaction mechanism involving processes 5–10 the quantum yield for radical anion formation (QY), assuming steady-state kinetics, is given by

$$QY = 2K_5\tau_M[Q] \quad (11)$$

where τ_M is the measured lifetime of the excited state $^1Q^*$. The results reported here are consistent with this simple reaction scheme, *i.e.*, the quantum yield of anion formation is a linear function of quinone concentration. Further, the estimated yield (eq 11) for radical formation for a quinone concentration of 10^{-4} *M*, assuming diffusion-controlled kinetics for reaction 5 with $K_5 = 1.1 \times 10^{10}$ M^{-1} sec[11] and $\tau_M = 5 \times 10^{-9}$ sec,[12] is 11×10^{-3}. This value is in reasonable agreement with the interpolat-

(10) G. O. Phillips, N. W. Worthington, J. F. McKellar, and R. R. Sharpe, *J. Chem. Soc. A*, 767 (1969).

ed value (Figure 3), of approximately 2.5×10^{-3}, at this concentration. In the absence of base $Q\cdot^-$ and $Q\cdot^+$ will undergo recombination and, as observed, no esr signal would be detected. This latter process could account for the extremely slow bleaching of the quinone observed in nonbasic media.

Acknowledgment. We are grateful to Anita VanLaeken and Roger Miller for the synthesis of I and II, and to Mark Bailey for assistance in esr measurements.

(11) J. G. Calvert and J. N. Pitts, "Photochemistry," Wiley, New York, N. Y., 1966, p 627.
(12) Value estimated from Stern-Volmer quenching data.

Pulse Radiolysis Study of Sulfhydryl Compounds in Aqueous Solution

Morton Z. Hoffman[1] and E. Hayon*

Pioneering Research Laboratory, U. S. Army Natick Laboratories, Natick, Massachusetts *(Received October 10, 1972)*

Publication costs assisted by Natick Laboratories

The interactions of hydrated electrons and hydroxyl radicals with a number of sulfhydryl compounds have been studied using the technique of pulse radiolysis. Thioglycolic acid, β-mercaptopropionic acid, cysteamine, *N*-acetylcysteamine, cysteine, *N*-acetylcysteine, *S*-methylcysteine, penicillamine, glutathione, benzyl mercaptan, and thiodiacetic and thiodipropionic acids are among the compounds examined. The reaction rate constants of e_{aq}^- with these compounds were found to be strongly dependent on the acid-base properties of the sulfhydryl compounds, with the rate decreasing upon deprotonation of both the amino and the mercapto groups. The e_{aq}^- were shown to react with RSH to produce quantitatively the R· radical, $e_{aq}^- + RSH \rightarrow R\cdot + HS^-$. The reaction rate constants of OH radicals were found to be $\sim 1\text{-}3 \times 10^{10}\ M^{-1}\ sec^{-1}$ and essentially independent of the ionization constants of the sulfhydryl compounds. The OH radicals form the thiyl radicals, $OH + RSH \rightarrow RS\cdot + H_2O$. The absorption spectra, extinction coefficients, and decay kinetics of these thiyl radicals have been determined for a number of RSH compounds. The rate constants of the reactions of RS· radicals with RSH and RS^- have been measured, and the equilibrium constants for $RS\cdot + RS^- \rightleftarrows RSSR^-$ have been calculated for a few systems. The high electrophilicity of the thiyl radical is indicated.

Introduction

The role of sulfhydryl (RSH) compounds, thiyl radicals (RS·), and disulfides (RSSR) in radiation protection is well known.[2,3] The protective effect of RSH compounds (*e.g.*, cysteamine, $HSCH_2CH_2NH_2$) on irradiation of DNA, enzymes, and bacteriophage was suggested[4] many years ago to occur *via* a free-radical mechanism. Consequently, the understanding of the mechanism of the reaction of free radicals and ions with sulfur compounds became of considerable importance in radiation and photobiochemistry.

The steady-state radiation chemistry of cysteine and related compounds has been studied (see, *e.g.*, ref 5-9 and references cited therein), and a number of the products formed in the presence and absence of oxygen were determined. The formation and reactivity of some of the free radicals produced have been studied by pulse radiolysis (see ref 10-13 and references cited therein). The formation of a characteristic transient optical absorption with a maximum at ~410 nm due to the $RSSR^-$ radical anion was shown[10,11] to occur *via* reactions 1 to 4. Esr studies of these radicals have also been carried out in aqueous solutions[14-17] and in the solid state.[18]

$$RSH + OH \rightarrow RS\cdot + H_2O \quad (1)$$

$$RSH + OH^- \rightleftarrows RS^- + H_2O \quad (2)$$

$$RS^- + OH \rightarrow RS\cdot + OH^- \quad (3)$$

$$RS\cdot + RS^- \rightleftarrows RSSR^- \quad (4)$$

Most of these studies have focussed on the formation (*e.g.*, by reaction with OH radicals) and the reaction of

(1) Visiting scientist from the Chemistry Department, Boston University, Boston, Mass., 02215.
(2) Z. M. Bacq, "Chemical Protection against Ionizing Radiation," C. C. Thomas Publisher, Springfield, Ill., 1965.
(3) A. Hollaender and D. G. Doherty, "Radiation Damage and Sulfhydryl Compounds," International Atomic Energy Agency, Vienna, 1969, p 1.
(4) P. Howard-Flanders, *Nature (London)*, **186**, 485 (1960); F. Hutchinson, *Radiat. Res.*, **14**, 721 (1961); K. G. Zimmer and A. Muller, *Curr. Top. Radiat. Res.* 1 (1965).
(5) V. G. Wilkening, M. Lal, M. Arends, and D. A. Armstrong, *Can. J. Chem.*, **45**, 1209 (1967).
(6) A. Al-Thannon, R. M. Peterson, and C. N. Trumbore, *J. Phys. Chem.*, **72**, 2395 (1968).
(7) J. A. Packer and R. V. Winchester, *Can. J. Chem.*, **48**, 417 (1970).
(8) G. G. Jayson, D. A. Stirling, and A. J. Swallow, *Int. J. Radiat. Biol.*, **19**, 143 (1971).
(9) J. W. Purdie, *Can. J. Chem.*, **49**, 725 (1971).
(10) W. Karmann and A. Henglein, *Ber. Bunsenges. Phys. Chem.*, **71**, 421 (1967); W. Karmann, A. Granzow, G. Meissner, and A. Henglein, *Int. J. Radiat. Phys. Chem.*, **1**, 395 (1969).
(11) (a) G. E. Adams, G. S. McNaughton, and B. D. Michael in "Chemistry of Ionization and Excitation," G. R. A. Johnson and G. Scholes, Ed., Taylor and Francis, London, 1967, p 281; (b) *Trans. Faraday Soc.*, **64**, 902 (1968).
(12) J. P. Barton and J. E. Packer, *Int. J. Radiat. Phys. Chem.*, **2**, 159 (1970).

thiyl radicals, RS·. The predominant mechanisms of protection have been suggested to be due either (a) to hydrogen transfer from sulfhydryl compounds to organic free radicals R^1· (known as the "repair" mechanism)

$$R^1\cdot + RSH \rightarrow R^1H + RS\cdot \quad (5)$$

and/or (b) to a competition between sulfhydryl compounds and organic molecules for the oxidizing OH radicals

$$OH + R^1H \rightarrow R^{\cdot} + H_2O \quad (6)$$

i.e., competition among reactions 1, 3, and 6. The rates of reaction 5 are not high,[11b] $\leq 10^8\ M^{-1}\ sec^{-1}$. A third possibility which has apparently not been seriously considered hitherto is that sulfhydryl compounds may compete for hydrated electrons and/or be a good acceptors[19] in electron transfer processes, $k(R^1H\cdot^- + RSH \rightarrow R^1H + R\cdot HS^-) \sim 10^8\ M^{-1}\ sec^{-1}$. It is interesting to note that inactivation (in dilute solutions) of enzymes containing -SH groups were found[20] to be considerably less than for enzymes without -SH groups.

Very little kinetic information is available on the reactivity of e_{aq}^- and of OH radicals with sulfhydryl compounds. The effects of substituents and ionic forms on these reaction rates constants have not been studied. This work deals with a systematic examination of these rate constants, the intermediates produced, and the dependence of the rates of reactions 4 and 7 on the nature of the sulfhydryl compounds. A similar study with disulfide compounds, RSSR, has recently been carried out.[21]

$$RS\cdot + RSH \rightleftharpoons RSSR^- + H^+ \quad (7)$$

Experimental Section

Experimental details of the pulse radiolysis set-up used have been described elsewhere.[22]

All solutions were prepared just prior to use and buffered, and the pH was adjusted in the absence of oxygen to minimize the oxidation of the sulfhydryl compounds. In order to avoid photolysis of these solutions by the monitoring light from a boosted 450-W xenon lamp, a synchronized shutter (open for ~1–4 msec) was used. Perchloric acid, phosphate (1–3 m*M*), tetraborate (1–2 m*M*), and potassium hydroxide were used as buffers. A fresh solution was used for each pulse. Quartz cells with 2-cm optical paths were used.

Dosimetry was carried out using a KCNS solution, and the extinction coefficients were derived based on $G(e_{aq}^-) = G(OH) = 2.8$ and $G(H) = 0.55$.

The chemicals used were obtained from Calbiochem (cysteamine, cysteine, penicillamine, glutathione), Sigma (thioglycollate, Na^+ salt), Cyclochemicals (*N*-acetylcystamine, cysteine methyl ester, *S*-methylcysteine, *N*-acetylcysteine), Eastman (β-thiopropionic acid was redistilled, methionine), Aldrich (thiodiacetic acid was recrystallized, β-thiodipropionic acid, methyl thioglycollate, thiolactic acid), and Evans (benzyl mercaptan).

Results and Discussion

Reactions with e_{aq}^-. The reaction rate constants of e_{aq}^- with sulfhydryl compounds were determined (in presence of ~0.1 *M tert*-butyl alcohol in order to scavenge the OH radicals) from the pseudo-first-order decay of the hydrated electron at 700 nm. From the dependence of these rates upon the substrate concentration, the values of $k(e_{aq}^- + S)$ were calculated. These results are shown in Table I.

Sulfhydryl compounds and sulfur amino acids are present in various ionic forms depending upon the pH of the solution. A systematic examination of the dependence of $k(e_{aq}^- + S)$ upon the ionization constants of these compounds was carried out, and the values are shown in Table I and Figure 1. These results reveal that the rates are markedly dependent upon the state of protonation of the various functional groups in the molecule. In all cases, the rates decrease with increase in pH. It is evident from the "titration curves" in Figure 1 that the rate constants can be directly related to the pK_a values of the -SH groups and, in the case of amino acids or amines, to the $-NH_3^+$ groups. Previously,[23] the lowering of the rate of reaction of e_{aq}^- with cysteine (the only sulfhydryl compound hitherto studied) in alkaline solution was attributed only to the deprotonation of the -SH group. It is clear from Figure 1, that for *S*-methylcysteine (pK_a = 8.75), deprotonation of the $-NH_3^+$ group reduces the e_{aq}^- rate from 7.2×10^8 to $1.5 \times 10^8\ M^{-1}\ sec^{-1}$ at pH 12.2. It is to be noted that the values of $k(e_{aq}^- + penicillamine)$ as a function of pH are the same as those shown for cysteine.

The absolute values of $k(e_{aq}^- + S)$ generally follow the overall charge on the mercaptan. Cysteamine, with a +1 overall charge in neutral solution, exhibits a high rate, as does similarly charged cysteine methyl ester. The neutral (overall charge 0) molecules, methyl thioglycolate, cysteine, penicillamine, and *N*-acetylcysteamine, show rates which are close to the diffusion-controlled region, $\sim 1 \times 10^{10}\ M^{-1}\ sec^{-1}$. As the charge on the molecule becomes more negative (but with the -SH group remaining protonated) the rate constant decreases. Note the near identity of the values in neutral solution for thioglycolate, thiolactate, β-mercaptopropionate, *N*-acetylcysteine, and glutathione, all have a −1 charge.

The effect of deprotonation of the -SH group to $-S^-$ leads to a marked reduction in the rate of reaction with e_{aq}^- (Table I). This can be seen most clearly with thioglycolate, thiolactate, methyl thioglycolate, β-mercaptopropionate, *N*-acetylcysteamine, and *N*-acetylcysteine. The overall charge again appears to affect the rate, *e.g.*, $k(e_{aq}^- + {}^-SCH_2CH_2NHCOCH_3) = 1.9 \times 10^9\ M^{-1}\ sec^{-1}$ while $k[e_{aq}^- + {}^-SCH_2CH(NHCOCH_3)COO^-] = 3.3 \times 10^8\ M^{-1}\ sec^{-1}$.

The effect of deprotonation of the $-NH_3^+$ group in the absence of an $-S^-$ group can be seen only in the case of *S*-methylcysteine, where the loss of the positive charge (and of an electron-withdrawing group $-NH_3^+$) diminishes the rate. In contrast, deprotonation of -SH in the absence of the amino group causes an extremely large reduction of the rate, often by a factor of 10 or more. When deprotona-

(13) J. W. Purdie, H. A. Gillis, and N. V. Klassen, *Chem. Commun.*, 1163 (1971).
(14) W. W. Wolf, J. C. Kertesz, and W. C. Landgraf, *J. Magn. Resonance*, **1**, 618 (1969).
(15) W. A. Armstrong and W. C. Humphreys, *Can. J. Chem.*, **45**, 2589 (1967).
(16) P. Neta and R. W. Fessenden, *J. Phys. Chem.*, **75**, 2277 (1971).
(17) G. Nucifora, B. Smaller, R. Remko, and E. C. Avery, *Radiat. Res.*, **49**, 96 (1972).
(18) See, e. g., T. Henriksen, *Radiat. Res.*, **27**, 694 (1966).
(19) E. Hayon and M. Simic, *J. Amer. Chem. Soc.*, **93**, 6781 (1971).
(20) R. Lange, A. Pihl, and L. Eldjarn, *Int. J. Radiat. Biol.*, **1**, 73 (1959).
(21) M. Z. Hoffman and E. Hayon, *J. Amer. Chem. Soc.*, **94**, 7950 (1972). See also A. Shafferman, *Isr. J. Chem.*, **10**, 725 (1972), dealing with the kinetics of the decay of the $RSSR^-$ radical from glutathione disulfide.
(22) M. Simic, P. Neta, and E. Hayon, *J. Phys. Chem.*, **73**, 3794 (1969); J. P. Keene, E. D. Black, and E. Hayon, *Rev. Sci. Instrum.*, **40**, 1199 (1969).
(23) R. Braams, *Radiat. Res.*, **27**, 319 (1966).

TABLE I: Rate Constants for the Reaction of e_{aq}^- with Various Sulfhydryl Compounds in Aqueous Solution[a]

Compound	Structure	pK_a[b]	pH	$k(e_{aq}^- + S)$, M^{-1} sec^{-1}[c]
Thioglycolic acid	$HSCH_2CO_2H$	3.7, 10.3	6.5	5.5×10^9
			12.0	5.6×10^8
Methyl thioglycolate	$HSCH_2CO_2CH_3$	7.8	5.2	1.4×10^{10}
			10.3	1.4×10^9
Thiolactic acid	$HSCH(CH_3)CO_2H$	~4, ~10.7	7.2	5.0×10^9
			12.2	7.7×10^8
β-Mercapto-propionic acid	$HSCH_2CH_2CO_2H$	4.3, 10.3	7.4	5.0×10^9
			13.0	$\sim 2.5 \times 10^8$
Cysteamine	$HSCH_2CH_2NH_3^+$	8.6, 10.7	5.5	3.0×10^{10}
			12.5	1.5×10^9
N-Acetyl-cysteamine	$HSCH_2CH_2NHCOCH_3$	~9.5	7.1	9.1×10^9
			12.6	1.9×10^9
Cysteine	$HSCH_2CH(NH_3^+)CO_2H$	1.8, 8.3, 10.8	5.8	1.3×10^{10}
			12.5	2.0×10^8
Cysteine methyl ester	$HSCH_2CH(NH_3^+)CO_2CH_3$	6.5, 9.0	5.1	1.8×10^{10}
			10.1	6.9×10^9
S-Methyl-cysteine	$CH_3SCH_2CH(NH_3^+)CO_2H$	~2, 8.8	5.4	7.2×10^8
			12.2	1.5×10^8
N-Acetyl-cysteine	$HSCH_2CH(NHCOCH_3)CO_2H$	~2, 9.5	7.1	5.6×10^9
			12.5	3.3×10^8
Penicillamine	$HSC(CH_3)_2CH(NH_3^+)CO_2H$	~2, 7.9, 10.4	5.3	1.0×10^{10}
			12.0	5.6×10^8
Glutathione	*d*	2.1, 3.6, 8.8, 9.7	7.2	4.5×10^9
			12.7	4.7×10^8
Benzyl mercaptan	$C_6H_5CH_2SH$	9.4	7.0	8.7×10^9
Methionine	$CH_3SCH_2CH_2CH(NH_3^+)CO_2H$	2.3, 9.2	7.3	4.5×10^7
Thiodiacetic acid	$S(CH_2CO_2H)_2$	3.3, 4.5	10.8	8.3×10^7
β-Thiodi-propionic acid	$S(CH_2CH_2CO_2H)_2$	~4	10.8	5.8×10^7

[a] Measured in the presence of ~0.1 *M tert*-butyl alcohol as an OH scavenger. [b] Values taken from the "Handbook of Biochemistry," 2nd ed, Chemical Rubber Publishing Co., Cleveland, Ohio, 1970. The pK_a values of the acidic functional groups are in the order $-CO_2H < -SH < -NH_3^+$. [c] Estimated error in the values ± 10%. [d] $HO_2CCH(NH_3^+)CH_2CH_2CONHC(CH_2SH)HCONHCH_2CO_2H$.

tion of both -SH and $-NH_3^+$ occurs (*e.g.*, cysteine) the effect appears to be additive.

The effect of the sulfur atom, in compounds that exhibit the -S- thio ether linkage, on the rate of reaction with e_{aq}^- can be demonstrated for thiodiacetic acid, β-thiodipropionic acid, methionine, and *S*-methylcysteine. These compounds all give relatively low rate constants. The presence of an amino group β to the CH_3S- group, in the case of *S*-methylcysteine, allows the rate to be considerably faster than for methionine (where the $-NH_3^+$ group is γ to the $-SCH_3$ group). Whether the source of this effect is inductive or steric is not known.

It is interesting to note that the reactivity toward e_{aq}^- of RSH and R_1SR_2 compounds is considerably higher than that of ROH and R_1OR_2 compounds. The covalent radius of the sulfur atom is appreciably larger than that of the oxygen (or carbon) atom,[24] making the C–S bond more sterically accessible. Furthermore, and perhaps most important is the fact that the sulfur atom can use d orbitals to accommodate a negative charge, while this is impossible for the oxygen atom. It is more difficult to explain the difference between the rates of RSH and R_1SR_2 compounds with e_{aq}^-. It may be due to the much faster dissociative electron capture reactions of RSH (see more below) and to the higher electron affinity of the HS· radical (~53 kcal[25]) compared to that of the RS· radical.

Intermediates Produced from the Reaction with e_{aq}^-. The transient species produced from the reaction with e_{aq}^- were observed in solutions containing ~1.5 *M t*-BuOH (to scavenge the OH radicals) and argon (1 atm). Figure 2 shows the transient absorptions obtained with thioglycolic acid at pH 4.1 and 7.4. These spectra are very similar to the spectra of the $\cdot CH_2COOH$ and $\cdot CH_2COO^-$ radicals previously obtained,[26] and are formed *via* reactions 8 and 9.

$$e_{aq}^- + HSCH_2COOH \rightarrow \cdot CH_2COOH + HS^- \quad (8)$$

$$e_{aq}^- + HSCH_2COO^- \rightarrow \cdot CH_2COO^- + HS^- \quad (9)$$

The extinction coefficient ϵ_{320} 670 M^{-1} cm^{-1} for the $\cdot CH_2COOH$ radical and ϵ_{350} 880 M^{-1} cm^{-1} for the $\cdot CH_2COO^-$ radical are in good agreement with earlier[26] values. The decay rates were $2k = 3.6 \times 10^9$ M^{-1} and $2k = 9.8 \times 10^8$ M^{-1} sec^{-1} at pH 4.1 and 7.2, respectively. The insert in Figure 2 shows that the two radicals exist in an acid–base equilibrium with p$K_a \sim 4.9 \pm 0.1$, compared to p$K_a \sim 4.5$.[26]

$$\cdot CH_2COOH \underset{pK_a \sim 4.9}{\rightleftharpoons} \cdot CH_2COO^- + H^+ \quad (10)$$

The reaction of free radicals with the sulfur atom has been suggested[27] to occur *via* an addition–elimination process. The interaction of e_{aq}^- with RSH compounds undergoes a rapid ($\tau \ll 10^7$ sec) dissociative electron cap-

(24) E. C. Kooyman, *Pure Appl. Chem.*, **15**, 81 (1967).
(25) R. S. Neale, *J. Phys. Chem.*, **68**, 143 (1964).
(26) P. Neta, M. Simic, and E. Hayon, *J. Phys. Chem.*, **73**, 4207 (1969).
(27) W. A. Pryor and K. Smith, *J. Amer. Chem. Soc.*, **92**, 2731 (1970).

ture reaction, producing quantitatively the corresponding R· radical.

A similar result was obtained with 1×10^{-2} *M* $CH_3CH(SH)COOH$, where reaction with e_{aq}^- generates a transient with λ_{max} ~300 nm at pH 3.2 and ~340 nm at pH 10.6, with ϵ values consistent[26] with the assignment of the radical to $CH_3\dot{C}HCOOH$ and $CH_3\dot{C}HCOO^-$, respectively. On pulse radiolysis of 1×10^{-2} *M* $HSCH_2COOCH_3$, an intermediate with λ_{max} ~320 nm was observed at pH 5.0, consistent[28] with the formation of the $\cdot CH_2COOCH_3$ radical

$$e_{aq}^- + HSCH_2COOCH_3 \rightarrow \cdot CH_2COOCH_3 + HS^- \quad (11)$$

The reaction of e_{aq}^- with $HSCH_2CH_2COOH$ produced a dull spectrum with no absorption maximum above 250 nm, resembling that of the $\cdot CH_2CH_2COOH$ radical produced independently.[26] Inasmuch as radicals β or γ to the carboxyl group are known[26] to show similar unstructured tail absorptions, further examination of the reaction of e_{aq}^- with other sulfhydryl compounds was not undertaken.

Further confirmation that e_{aq}^- reacts with aromatic mercaptans to generate R· radicals was obtained from the reaction with benzyl mercaptan, see Figure 3. The characteristic absorption spectrum of the benzyl radical was obtained with ϵ_{318} 8520 M^{-1} cm^{-1}, as well as the new intense band ϵ 28,300 M^{-1} cm^{-1} which has recently been reported.[29] The extinction coefficients for both bands shows 100% stoichiometry for reaction 12.

$$e_{aq}^- + C_6H_5CH_2SH \rightarrow C_6H_5CH_2\cdot + HS^- \quad (12)$$

When the sulfhydryl compounds react with e_{aq}^- in alkaline solutions under conditions where $[RSH]/[RS^-] \sim 1.0$, the formation of an intense absorption maximum in the 410-nm region is observed. Such absorptions are characteristic of the $RSSR^-$ radical anion produced *via* secondary reactions involving the R· and RS· radicals, reactions 13 followed by 5, 4, and 7

$$e_{aq}^- + R^1SH \rightarrow R^1\cdot + HS^- \quad (13)$$

As will be shown in a later section, the reaction of RS· radicals with RS^- to form $RSSR^-$ is quite fast with $k \sim 10^9$ M^{-1} sec^{-1}. The rate of reaction 5 can be determined by following the formation kinetics of $RSSR^-$ at ~410 nm. Values for k_5 (where R· radicals examined where $\cdot CH_2COO^-$ and $\cdot CH_2CH_2COO^-$) were $\sim 10^8$ M^{-1} sec^{-1}, in agreement with values for some other radicals.[11b]

Reactions with OH Radicals. The reaction rate constants of OH radicals with sulfhydryl compounds present in various ionic forms was determined using the thiocyanate methods. From the decrease in the absorption at 500 nm of the $(CNS)_2^-$ radical at various $[CNS^-]/[S]$ ratios, k_1 and k_3 were obtained taking $k(OH + CNS^-) = 1.1 \times 10^{10}$ $M^{-1}\cdot sec^{-1}$. The results in Table II show that $k(OH + S)$ is quite high and appears to be fairly independent of the state of protonation of the -SH group, the presence of an amino group, or the overall charge on the molecule. Substitution of $-CH_3$ on the sulfur atom apparently lowers the rate slightly; a similar low rate for thioglycolic acid is not readily explainable.

Intermediates Produced from the Reaction with OH Radicals. The reaction of OH radicals with RSH generates a weak transient absorption in the 300-400-nm region, with a rising absorption below ~300 nm. Figure 4a shows the results for cysteine and $HSCH_2CH_2COOH$. A similar

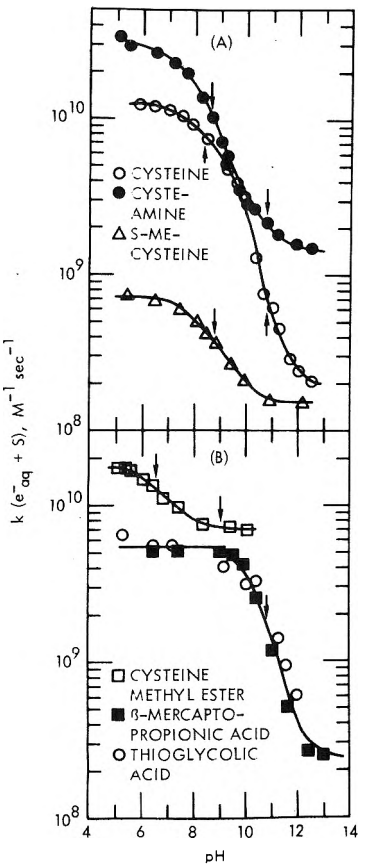

Figure 1. Rate constants for the reaction of e_{aq}^- with sulfhydryl compounds as a function of pH. The arrows indicate the pK_a values of the compounds.

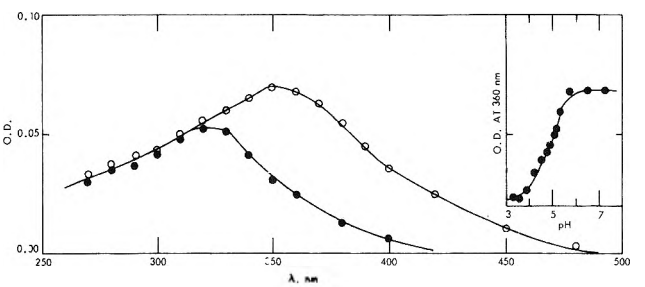

Figure 2. Transient spectra produced from the reaction of e_{aq}^- with thioglycolic acid (5 m*M*, in presence of 1.5 *M* *t*-BuOH, Ar) at pH 7.4 (O) and 4.1 (●). Insert shows change in absorbance at 360 nm with pH: total dose ~10 krads/pulse.

transient spectrum was obtained from the reaction of OH with glutathione. In all cases an absorption maximum at ~330 nm is evident. With penicillamine, the reaction with OH likewise produces an absorption with λ_{max} ~330 nm (Figure 4b), except that the intensity of the band is substantially increased. These absorptions are produced *via* reaction 1 and are assigned to the thiyl RS· radicals. The assignment is substantiated by the observation that the same spectra are obtained from the reaction of H atoms with glutathione[27] and H atoms with RSSR compounds.[21] The increasing transient absorption below 230 nm may correspond to the diffuse and featureless absorp-

(28) M. Simic and E. Hayon, *Radiat. Res.*, **48**, **244** (1971).
(29) J. P. Mittal and E. Hayon, *Nature (London)*, **240**, 20 (1972).

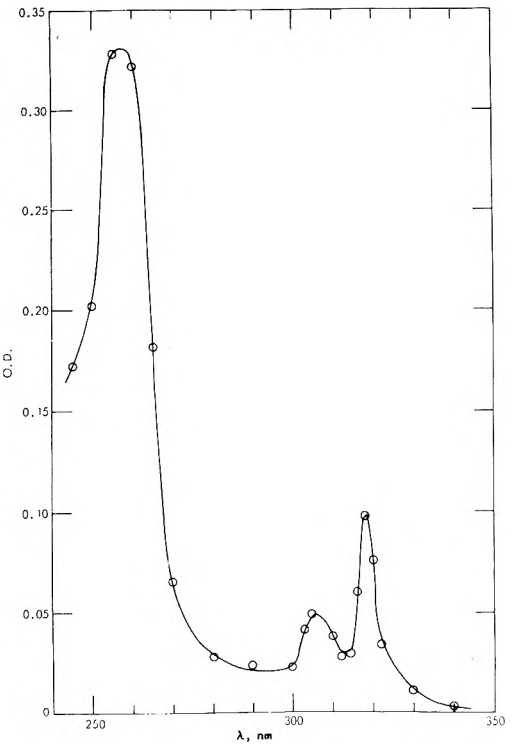

Figure 3. Transient spectra produced from the reaction of e_{aq}^- with benzyl mercaptan (2 m*M*, 1.5 *M* *t*-BuOH, Ar) at pH 7.1: dose per pulse ~2.4 krads.

TABLE II: Rate Constants for the Reaction of OH Radicals with Sulfhydryl Compounds in Aqueous Solution[a]

Compound	pH	k(OH + S), M^{-1} sec^{-1} [b]
Thioglycolic acid	6.6	5.9×10^9
	11.1	5.5×10^9
Methyl thioglycolate	5.1	2.1×10^{10}
	10.6	1.8×10^{10}
Thiolactic acid	7.2	1.7×10^{10}
	10.8	1.6×10^{10}
β-Mercaptopropionic acid	6.0	3.0×10^{10}
	10.7	2.1×10^{10}
Cysteine	0.4	1.7×10^{10}
	5.8	1.9×10^{10}
	9.8	1.8×10^{10}
	10.8	1.8×10^{10}
S-Methylcysteine	5.4	8.0×10^9
	11.0	7.9×10^9

[a] Rates determined using the thiocyanate method taking k(OH + CNS$^-$) = 1.1×10^{10} M^{-1} sec^{-1}; calculations made ignoring ionization processes. [b] Estimated error in the values ±15%.

tion band of the thiyl radical (λ_{max} 218.5 nm) observed[30] in the gas-phase flash photolysis of CH_3SH.

The RS· radicals decay *via* second-order kinetics under conditions of relatively high [RS·] (~5×10^{-5} *M*) and relatively low (~5×10^{-4} *M*) RSH concentrations. Table III summarizes some of the characteristics of the RS· radicals generated from the OH + RSH reaction. It is to be noted that the 2k values reported here at pH ~5–6 are somewhat lower than those obtained[21] at pH 1.0 from the H + RSSR reaction. The change in the overall charge, due to the protonation of the carboxyl groups, could be the source of these differences. The thiyl radicals decay

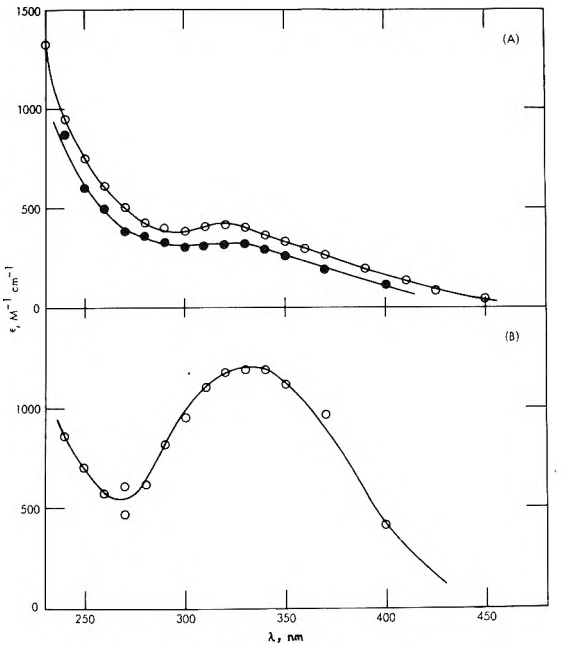

Figure 4. Transient spectra produced from the reaction of OH radicals with 0.5 m*M* sulfhydryl compounds in presence of N_2O (1 atm): (A) $HSCH_2CH_2COOH$, pH 6.0 (O) and cysteine, pH 6.4 (●); (B) penicillamine, pH 5.1, (O); total dose ~8.0 krads/pulse. Spectra corrected for depletion of the substrates.

TABLE III: Absorption Maxima and Decay Kinetics of the Thiyl Radicals RS· Produced from the Reaction of OH Radicals with RSH Compounds

RSH	pH	ϵ_{330}, M^{-1} cm^{-1}	2k, M^{-1} sec^{-1}
$HSCH_2CH_2CO_2H$	6.0	430	*a*
Cysteine	6.4	320	3.4×10^9
Penicillamine	5.1	1,220	2.3×10^9
		(1,220)[b]	(2.6×10^9)[b]
Glutathione	4.3	580	1.5×10^9

[a] Not determined. [b] From ref 13.

relatively fast to give presumably RSSR

$$RS\cdot + RS\cdot \rightarrow RSSR \quad (14)$$

Reaction with H Atoms. Steady-state radiation chemistry of RSH compounds indicates that two modes of attack are exhibited by H atoms

$$H + RSH \rightarrow RS\cdot + H_2 \quad (15)$$

$$H + RSH \rightarrow R\cdot + H_2S \quad (16)$$

For aliphatic R· radicals other than $\cdot CH_2COOH$, the transient optical absorption spectra exhibit a dull tail descending from the ultraviolet region. The RS· radicals show a weak absorption with λ_{max} ~330 nm. In an attempt to establish the relative contribution of reactions 15 and 16, penicillamine was chosen since its RS· radical has a more intense absorption at 330 nm (Figure 4b). Figure 5 shows the result of this experiment. Clearly, only a very weak absorption is observed at 330 nm which is superimposed on the dull tail of the R· radical. From a knowledge of the ϵ_{330} for RS·, one can estimate that <10% of the H atoms react with penicillamine *via* reaction 15.

(30) A. B. Callear and D. R. Dickson, *Trans. Faraday Soc.*, **66**, 1987 (1970).

TABLE IV: Rate Constants and K_{equil} for the Reaction of RS· Radicals with RS^- Compounds

Compound	$k(RS\cdot + RS^-)$, M^{-1} sec^{-1} [a]	$k(RSSR^-)$, sec^{-1} [b]	K_{equil} [c]
$HSCH_2CH_2COOH$	3.6×10^9 (11.9)	2.7×10^6 (7.3)[d]	1.3×10^3
Cysteine	1.9×10^9 (9.2)		
N-Acetylcysteine	1.1×10^9 (11.2)		
Penicillamine	2.8×10^9 (12.0)	2.9×10^6 (11.8)	1.0×10^3
			2.5×10^2 (8.0)[e]
Cysteamine	8.0×10^9 (12.0)	1.3×10^6 (11.8)	6.1×10^3
	4.9×10^9 (8.45)[f]	8.0×10^5 (8.45)[f]	6.0×10^3 [f]
Glutathione	6.2×10^8 (11.7)	1.6×10^5 (11.7)	3.9×10^3

[a] Determined from the pseudo-first-order formation of $RSSR^-$ as monitored at 420 nm. Numbers in parentheses are the pH values of the experiment. [b] Taken from ref 21. [c] K_{equil} for the reaction $RS\cdot + RS^- = RSSR^-$, determined from $k(RS\cdot + RS^-)/k(RSSR^-)$. [d] This rate is independent of pH. [e] Taken from ref 13. [f] Taken from ref 11a.

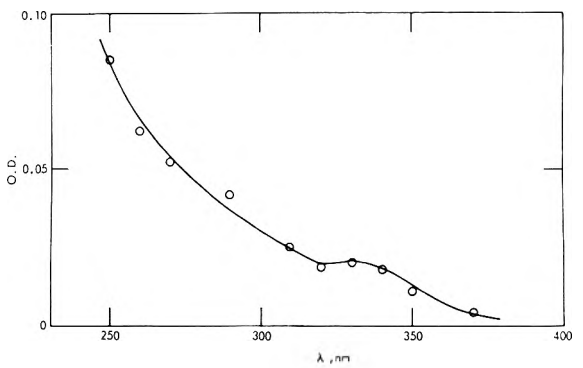

Figure 5. Transient spectrum produced from the reaction of H atoms with 1 m*M* penicillamine at pH 1.0 in presence of 1.0 *M* *t*-BuOH, Ar. Spectrum corrected for absorption of the *t*-BuOH radical below ~280 nm and for depletion of the substrate.

Reaction of Thiyl Radicals with RSH and RS^-. As mentioned above, the thiyl radicals produced *via* reactions 1 and 3 react with RS^- to produce $RSSR^-$ by reactions 4 and 7. The $RSSR^-$ produced[21] from the reaction of e_{aq}^- with RSSR (in absence of RSH)

$$e_{aq}^- + RSSR \rightarrow RSSR^- \qquad (17)$$

undergoes a unimolecular reaction to generate RS· and RS^- with a rate constant k which is markedly dependent[21] on the nature of the environment around the -S-S- linkage and the state of protonation of the adjacent $-NH_3^+$ groups. It is interesting to note that the relaxation times for intramolecular proton transfer, *e.g.*

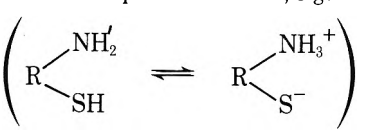

of sulfhydryl compounds in water have recently been measured[31] and times of 2.8×10^{-9} and 3.3×10^{-8} sec for cysteine and cysteamine, respectively, have been obtained. Thus, because of the equilibrium nature of reactions 4 and 7, the lifetime of $RSSR^-$ is dependent upon RS^- concentration as well as upon its inherent structural factors. The kinetics[21] of the decay of $RSSR^-$, normally first order and fast, can be rendered slow and of mixed kinetics, by the presence of RS^-, which introduces the bimolecular component to the disappearance of the RS· radical. Even at pH values where insignificant amounts of RS^- are formed, some of the sulfhydryl compounds studied showed the characteristic 410-nm band, indicating that reaction 7 must also occur. The intermediacy of the sulfenium radical RSS(H)R, the protonated form of $RSSR^-$, cannot be ruled out. Such a species has a lifetime[21] $<10^{-7}$ sec, and dissociates to give RS· and RS^-. However, if deprotonation of the sulfenium radical in neutral solution is faster than its dissociative rate, the stabilization of $RSSR^-$ can be achieved.

By monitoring the formation of the 410-nm band under pH conditions where either RSH or RS^- is the predominant species, the rate constant for the reaction of thiyl radicals with sulfhydryl compounds can be evaluated. Table IV shows the results obtained with some representative compounds. In alkaline solution where >90% of the sulfhydryl compound is present as RS^-, $k(RS\cdot + RS^-) > 10^9$ M^{-1} sec^{-1}, except in the case of glutathione. The range of values obtained (Table IV) can be rationalized in part on the basis of the overall charges of the RS· and RS^- species. Thus, cysteamine, for which the RS· and RS^- charges are 0 and −1, respectively, exhibits the highest rate while glutathione, for which the corresponding charges are −2 and −3, is more than an order of magnitude slower.

The dependence of the rate of formation of $RSSR^-$, *via* reactions 4 and 7, upon the state of protonation of the sulfhydryl group can be seen in Figure 6. The observed pseudo-first-order rate constant for the formation of $RSSR^-$ exhibits an increase at different pH values for cysteine and *N*-acetylcysteine, corresponding to the pK_a for dissociation of the RSH groups. In the case of cysteine a further increase in the rate appears at higher pH values (but the rate constants show some scatter in the values), presumably due to the deprotonation of the $-NH_3^+$ group. No such increase was observed (or would be expected) with *N*-acetylcysteine. We have already shown[21] that the β-NH_3^+ group has a retarding influence on the rate of unimolecular decay of the $RSSR^-$ radical by interacting with the electron in the expanded disulfide orbital of the radical anion. The formation of $RSSR^-$ from the RS· + RS^- reaction is the reverse process, and consideration of microscopic reversibility requires that the formation of $RSSR^-$ be affected by the presence of the $-NH_3^+$ group.

The unusually high reactivity of the thiyl radicals must be noted. The electron-demanding properties of the RS· radicals can also be seen in their chemical properties,[24] displacement reactions on sulfur atoms as well as addition to double bonds. The electrophilicity of the thiyl radicals can also be accounted for by the fact that the sulfur atom can use d orbitals to accommodate a negative charge.

Table IV also gives the equilibrium constant for reaction 4 under conditions where the mercapto and amino

(31) G. Moass and F. Peters, *Angew. Chem., Int. Ed. Engl.*, **11**, 428 (1972).

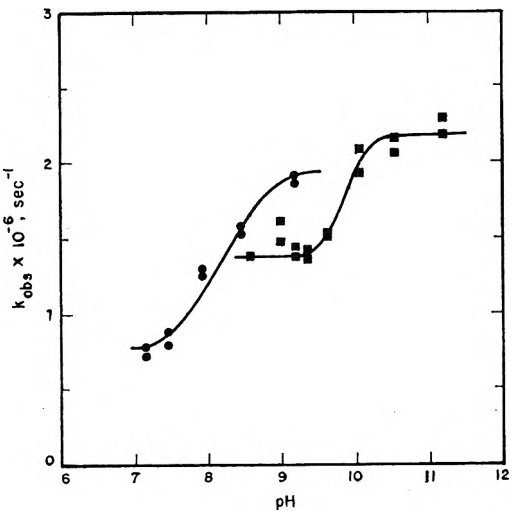

Figure 6. Dependence upon pH of the observed pseudo-first-order rate constant for the formation of RSSR$^-$ from the reaction of thiyl radicals with sulfhydryl compounds: (a) from cysteine (1 m*M*, N_2O saturated, •) and (b) from *N*-acetylcysteine (2 m*M*, N_2O saturated, ■).

groups are deprotonated. Because of the pH dependence of the dissociation of RSSR$^-$, K_{eq} values were calculated only under the limiting conditions of high pH. The values are of the same magnitude and are compared with the results for cysteamine and penicillamine reported by others.[11b,13]

Finally, because of the importance of the reactions of RS· radicals in the continuous radiolysis of sulfhydryl and disulfide compounds, an attempt was made to estimate the rate constants for some metathesis reactions involving RS·. Due to the relatively intense absorption of RS· from penicillamine, that radical was chosen for the experiments. Specifically, using 5×10^{-3} *M* penicillamine and 2×10^{-4} to 1×10^{-3} *M* cystamine (R^1SSR^1) at pH 5.0 in N_2O-saturated solution, no effect on the decay kinetics or the spectrum of the RS· radical could be seen implying that $k_{18} \leq 1 \times 10^7\ M^{-1}\ sec^{-1}$.

$$RS\cdot + R^1SSR^1 \rightarrow R^1S\cdot + RSSR^1 \qquad (18)$$

A 5×10^{-3} *M* cystamine (R^1SSR^1) solution containing $2\text{–}5 \times 10^{-4}$ *M* penicillamine (RSH) and 1.5 *M* *tert*-butyl alcohol at pH 0.8 generates the cysteamine $R^1S\cdot$ radical

$$H + R^1SSR^1 \rightarrow [R^1SS(H)R^1] \rightarrow R^1S\cdot + R^1SH \qquad (19)$$

which showed no indication of reaction with RSH within the time resolution of the instrument (~0.1 μsec) upon the monitoring of the RS· radical from penicillamine at 330 nm, indicating that $k_{20} \leq 1 \times 10^7\ M^{-1}\ sec^{-1}$.

$$R^1S\cdot + RSH \rightarrow R^1SH + RS\cdot \qquad (20)$$

The absence of any observation in support of reactions 18 and 20, under the experimental conditions used, could be due to a sterically hindering effect by the methyl groups in penicillamine.

Interaction of Solvated Electrons with the Amide and Imide Groups. Acid–Base Properties of $R\dot{C}(OH)NH_2$ Radicals

M. Simic[1a] and E. Hayon*[1b]

Pioneering Research Laboratory, U. S. Army Natick Laboratories, Natick, Massachusetts, and Zoology Department, University of Texas, Austin, Texas *(Received December 7, 1972)*

Publication costs assisted by Natick Laboratories

The technique of pulse radiolysis has been used to study the interaction of solvated electrons with various amides and imides in aqueous solutions. The reactivity of e_{aq}^- with acetamide, malonamide, succinamide, oxamide, oxamate ion, biuret, diacetamide, succinimide, and *N*-methylsuccinimide has been determined. It is found that the reactivity of the diamide oxamide is $k = 3.3 \times 10^{10}\ M^{-1}\ sec^{-1}$, and that the rate decreases with the number of methylene groups in between the $-CONH_2$ groups. Thus $k = 1.1 \times 10^9\ M^{-1}\ sec^{-1}$ for malonamide and $2.0 \times 10^8\ M^{-1}\ sec^{-1}$ for succinamide. Insertion of an $-NH-$ group instead of a $-CH_2-$ group in between two amide groups, as in biuret, also decreases the reactivity toward e_{aq}^-. The rate of e_{aq}^- with the cyclic imide succinimide is almost diffusion controlled, $k = 1.1 \times 10^{10}\ M^{-1}\ sec^{-1}$, and is the same as that of the corresponding open molecule diacetamide. The transient spectra, extinction coefficients, decay kinetics, and ionization constants of the radicals produced from the addition of e_{aq}^- to these amides and imides have been determined and correlated. Ionization constants ranging from 3.7, 8.4, and 9.8 to ≥13.5 for oxamide, succinimide, malonamide, and acetamide, respectively, have been obtained. These and other results are discussed.

Introduction

The reactivities of some amides and imides with hydrated electrons have been measured and reviewed briefly (see ref 2 and 3–5). The reactivities of simple amides $RCONH_2$ (where R = H or CH_3) toward e_{aq}^- have been

(1) (a) University of Texas. (b) Natick Laboratories.

attributed[2] to the mesomeric effect of the substituent R and correlated to the Taft's σ^* function. Other amides were found to be much less reactive (*e.g.*, urea, R = NH_2) or much more reactive (*e.g.*, oxamate ion, R = COO^-) than expected according to the log k *vs.* σ^* relation, where k is the rate constant of e_{aq}^- with the amide. Furthermore, it was anticipated[2] that the lifetimes of $(RCONH_2)^-$ radical anions would be extremely short.

Recent studies[3-5] on the reactivity of e_{aq}^- with various substituted amides (*e.g.*, amides of amino acids and peptides, *N*-ethylmaleimide, *N*-ethylmaleamic acid) and the intermediates produced from this reaction have indicated a relatively long lifetime for these transient species. We have further investigated the relationship between the reactivity of various amides with e_{aq}^-, and the effect of structure and various functional groups. In addition, the acid-base properties and the transient optical absorption spectra of the radicals produced from this reaction have been determined using the technique of pulse radiolysis.

Experimental Section

The pulse radiolysis set-up and the kinetic spectrophotometric system have already been described.[6,7] The light path of the quartz optical cells was 2 cm. Triply distilled water was radiolyzed and photolyzed previous to use. Solutions were prepared just previous to use and the pH adjusted at the last moment in oxygen-free solutions. The chemicals were of the highest purity available commercially and were usually used as received: oxamide, malonamide, succinimide, *N*-methylsuccinimide, and succinamide were from Eastman; oxamic acid was from Sigma; acetamide from Matheson Coleman and Bell; biuret from NBC; *tert*-butyl alcohol from Mallinckrodt; the buffers were from Baker and Adamson.

The pH of the solution was adjusted with perchloric acid, potassium hydroxide, phosphates (~1 mM), and tetraborate (~1 mM).

Dosimetry was done using ~5 × 10^{-2} M KCNS solutions, and the extinction coefficients calculated based on $G(e_{aq}^-) = G(OH) = 2.8$, and $\epsilon((CNS)_2^-) = 7.6 \times 10^3\ M^{-1}\ cm^{-1}$ at 500 nm.

Results and Discussion

The intermediates produced from the reaction of solvated electrons with amides and imides in aqueous solution were observed using the technique of pulse radiolysis and kinetic absorption spectrophotometry. The hydroxyl radicals formed in the radiolysis of water were scavenged by ~1.0 M *tert*-butyl alcohol. The *t*-BuOH radical produced[6] absorb relatively weakly below ~280 nm and is relatively inert. The transient spectra observed were not associated with this alcohol radical since they were not produced in presence of N_2O (1 atm), an effective scavenger of e_{aq}^-. In all cases, the absorption due to the *t*-BuOH radicals was corrected for in the spectra presented below.

In order to ascertain complete reaction of the amides and imides with e_{aq}^-, and derive exact extinctions for the intermediates produced, the reaction rate constants, k, were determined by following the pseudo-first-order decay kinetics of e_{aq}^- at 700 nm. The values obtained and the previously reported rate constants are presented in Table I.

Based on the reactivity of the substrates toward e_{aq}^-, the concentration of the amides and imides was chosen to ensure fast formation of the transient species. Some of the compounds used are not too stable at high pH and hydrolyze. The extent of hydrolysis was checked spectrophotometrically whenever possible. The experiments were performed under conditions where the bulk of the solute did not hydrolyze. However, a small percentage of hydrolysis is permissible for the recording of transient spectra since, in most cases, the products of hydrolysis have a much lower reactivity toward e_{aq}^-.

Most of the amides studied are weak bases and protonate at very low pH values (around 0 and below); they are also weak acids and deprotonate at very high pH values (*e.g.*, pK_a = 15.1 for acetamide). In the pH region studied most of the solutes were, therefore, mainly in their neutral form. Hydrolysis of the electron adducts $RC(OH)NH_2$ to $R\dot{C}O$ and NH_3 would seem to be ruled out since the resulting transient would not be expected to show any acid-base properties.

Acetamide. The reaction of e_{aq}^- with CH_3CONH_2 at pH 7.0 produced a transient spectrum with a maximum below 250 nm, Figure 1. Due to the absorption of ground-state acetamide, it was not possible to determine the transient spectrum at lower wavelengths. At pH 14.0 a more intense and red-shifted absorption was observed, Figure 1, somewhat similar to the changes observed in α-hydroxy alkyl radicals.[6,8] On monitoring the change in absorbance at 280 nm with pH, a titration-type curve is obtained from which a midpoint value of ≥13.5 can be derived. Reactions 1-3 are suggested.

$$e_{aq}^- + CH_3CONH_2 \longrightarrow CH_3\dot{C}(O^-)NH_2 \quad (1)$$

$$CH_3\dot{C}(O^-)NH_2 + H_2O \longrightarrow CH_3\dot{C}(OH)NH_2 + OH^- \quad (2)$$

$$CH_3\dot{C}(OH)NH_2 \underset{pK_a \geq 13.5}{\rightleftharpoons} CH_3\dot{C}(O^-)NH_2 + H^+ \quad (3)$$

In acetamide, the carbonyl group is the only functional group with an affinity for electrons. The rate k_1 = 3.5 × $10^7\ M^{-1}\ sec^{-1}$ is relatively small. The second-order decay kinetics of the $CH_3\dot{C}(OH)NH_2$ and $CH_3\dot{C}(O^-)NH_2$ radicals are 1.5 × 10^9 and 8.7 × $10^8\ M^{-1}\ sec^{-1}$, respectively, see Table II. These values are in agreement with the expected decrease for the bimolecular decay of two negatively charged species.

It is interesting to compare acetamide with benzamide. The $k(e_{aq}^- + PhCONH_2)$ = 1.9 × $10^{10}\ M^{-1}\ sec^{-1}$ and the pK of the $Ph\dot{C}(OH)NH_2$ radical[9] is 7.7 ± 0.2. Calculations have indicated[9] a large net positive charge at the carbonyl carbon of benzamide, due to extensive delocalization brought about by the benzene ring.

Oxamide and Oxamic Acid. The linking of two amide groups together as in oxamide, $H_2NCOCONH_2$, produces an α diketone. Semidione radicals are known[10] to exhibit some double bond character in the bond joining the two carbonyl groups. The strong resonance is demonstrated in

(2) E. J. Hart and M. Anbar, "The Hydrated Electron," Wiley-Interscience, New York, N. Y., 1970, pp 130-138.
(3) E. Hayon, T. Ibata, N. N. Lichtin, and M. Simic, *J. Amer. Chem. Soc.*, **93**, 5388 (1971).
(4) (a) M. Simic and E. Hayon, *Radiat. Res.*, **48**, 244 (1971); (b) E. Hayon and M. Simic, *ibid.*, **50**, 464 (1972).
(5) E. Hayon and M. Simic, *J. Amer. Chem. Soc.*, **93**, 6781 (1971); P. S. Rao and E. Hayon, manuscript in preparation.
(6) M. Simic, P. Neta, and E. Hayon, *J. Phys. Chem.*, **73**, 3794 (1969).
(7) J. P. Keene, E. D. Black, and E. Hayon, *Rev. Sci. Instrum.*, **40**, 1199 (1969); E. Hayon, *J. Chem. Phys.*, **51**, 488 (1969).
(8) K. D. Asmus, A. Henglein, A. Wigger, and G. Beck, *Ber. Bunsenges. Phys. Chem.*, **70**, 756 (1966).
(9) E. Hayon, T. Ibata, N. N. Lichtin, and M. Simic, *J. Phys. Chem.*, **76**, 2072 (1972).
(10) G. A. Russell and R. D. Stephens, *J. Phys. Chem.*, **70**, 1320 (1966).

TABLE I: Reaction Rate Constants of e_{aq}^- with Amides and Imides in Solution[a]

Compound	Structure	pH	$k(e_{aq}^- + S)$, M^{-1} sec^{-1}
Urea	H_2NCONH_2	9.2	3.0×10^5 [b]
Biuret	$H_2NCONHCONH_2$	10.3	2.5×10^8
Acetamide	CH_3CONH_2	9.2	3.5×10^7,[c] 1.7×10^7 [b]
Diacetamide	$CH_3CONHCOCH_3$	6.5	1.1×10^{10}
Oxamic acid	$H_2NCOCOO^-$	9.2	5.7×10^9, 4.0×10^9 [b]
Oxamide	$H_2NCOCONH_2$	9.0	3.3×10^{10}
Malonamide	$H_2C(CONH_2)_2$	7.0	1.1×10^9
Succinamide	$(-CH_2CONH_2)_2$	7.1	2.0×10^8
Succinimide		6.5	1.1×10^{10}, 7.2×10^9 [b]
		11.4	9.2×10^8
N-Methylsuccinimide	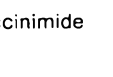	6.9	1.3×10^{10}
N-Ethylmaleamic acid		7.9	8.5×10^9 [d]
N-Ethylmaleimide	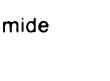	6.0	3.8×10^{10} [d]

[a] Determined in presence of ~0.1–1.0 *M* *t*-BuOH and argon by following decay kinetics of e_{aq}^- at 700 nm. [b] From ref 2. [c] From ref 3. [d] From ref 4.

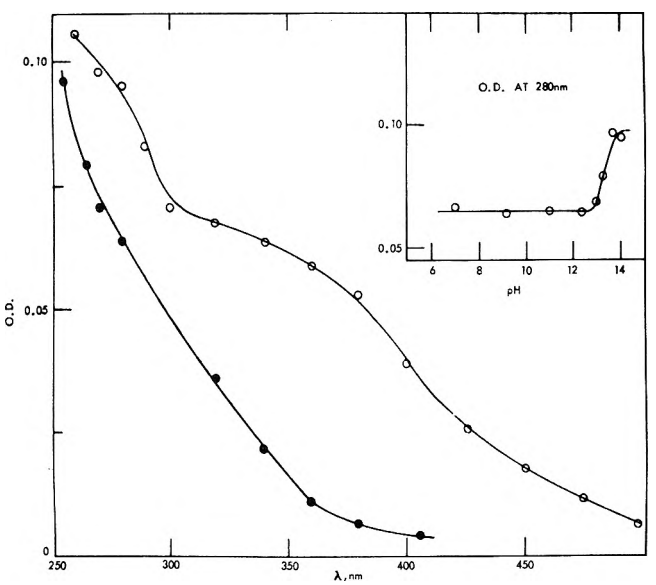

Figure 1. Transient absorption spectra resulting from the addition of e_{aq}^- to aqueous solutions of acetamide (1.0 *M*, in presence of 1.0 *M* *t*-BuOH and argon) at pH 7.0, ●, and 14.0, ○. Total dose ~8 krads/pulse. Insert shows change in absorbance at 280 nm with pH.

the high reactivity of oxamide toward e_{aq}^- (Table I), the red-shift in the absorption maxima of the radicals (Figure 2), the relatively high extinction coefficients (Table II), and the low ionization constant of the semidione radical.

Reactions 4–6 are suggested.

$$e_{aq}^- + H_2NCOCONH_2 \longrightarrow H_2N\dot{C}(O^-)CONH_2 \quad (4)$$

$$H_2N\dot{C}(O^-)CONH_2 + H_2O(\text{or } H^+) \longrightarrow H_2N\dot{C}(OH)CONH_2 + OH^- \quad (5)$$

$$H_2N\dot{C}(OH)CONH_2 \underset{pK_a \sim 3.7}{\rightleftharpoons} H_2N\dot{C}(O^-)CONH_2 + H^+ \quad (6)$$

A rapid interchange between tautomeric forms, as well as cis and trans isomers, are expected[11] for this semidione radical. The transient optical absorption cannot, however, distinguish between these forms. The strong delocalization of the unpaired electron in oxamide leads to a $pK_a \sim 3.7$ for the radical. This is a relatively very low pK_a value for radical anions.

The interaction of electrons with oxamic acid, $H_2NCOCOOH$, is expected to be dependent on the ionization constant of the carboxyl group. When protonated, the molecule should react like an α diketone, as in oxamide. Thus one finds $k(e_{aq}^- + H_2NCOCOO^-) = 5.7 \times 10^9\ M^{-1}$ sec^{-1} and expect $k(e_{aq}^- + H_2NCOCOOH) \sim 3 \times 10^{10}\ M^{-1}$ sec^{-1}. The addition of electrons to oxamic acid can occur at two different sites to produce $H_2N\dot{C}(OH)COOH$ and $H_2NCO\dot{C}(OH)_2$ radicals. Furthermore a number of ionization constants can be expected. Experimentally, only two pK_a values of the radicals were observed due, presumably, to the overlap of some of the ionization constants in the acid pH region. It was not possible to study the reaction of e_{aq}^- with nonionized oxamic acid because of the low pH required. The first observed pK_a (Figure 3) is tentatively suggested to be due to the equilibrium

$$H_2N\dot{C}(OH)COOH \underset{pK_a = 5.2}{\rightleftharpoons} H_2N\dot{C}(OH)COO^- + H^+ \quad (7)$$

Similar ionization constants for α-carboxylic acid radicals have been reported.[12] Interchange between the forms $H_2N\dot{C}(OH)COOH$ and $H_2NCO\dot{C}(OH)_2$ can be expected. In alkaline solutions another equilibrium is established which is assigned to

$$H_2N\dot{C}(OH)COO^- \underset{pK \geq 12.5}{\rightleftharpoons} H_2N\dot{C}(O^-)COO^- + H^+ \quad (8)$$

This radical carries two negative charges and was found to decay slowly with mixed kinetics (Table II).

Malonamide and Succinamide. The effect of isolating

(11) H. Zeldes and R. Livingston, *J. Phys. Chem.*, **74**, 3336 (1970).
(12) P. Neta, M. Simic, and E. Hayon, *J. Phys. Chem.*, **73**, 4207 (1969); M. Simic, P. Neta, and E. Hayon, ibid., **73**, 4214 (1969).

TABLE II: Absorption Maxima, Extinction Coefficients, Decay Kinetics, and Ionization Constants of the Radicals Produced from the Interaction of e_{aq}^- with Amides and Imides in Water

Compound	pH	λ_{max}, nm	ϵ_{max}, M^{-1} cm^{-1} [a]	$2k$, M^{-1} sec^{-1} [a]	$pK_{\epsilon(radical)}$	Suggested radical
Acetamide	7.0	<255	>2,200	1.5×10^9	≥13.5	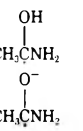
	14.0	<260	>2,400	8.7×10^8		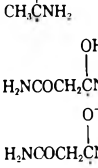
Malonamide	6.8	255	2,400	3.0×10^9	9.8 ± 0.1	
	11.4	260	2,200	1.4×10^9		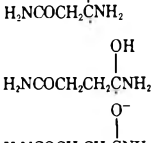
Succinamide	5.0	<245	>1,000	2.0×10^9	11.3 ± 0.1	
	13.0	<255	>1,800	9.0×10^8		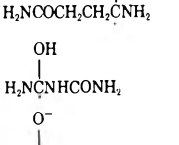
Biuret	5.5	<240	>3,800	1.6×10^9	7.3 ± 0.1	
	9.7	<250	>2,300	6.3×10^8		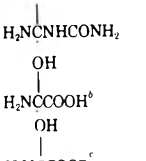
Oxamic acid	3.5	265	6,800	2.0×10^9	5.2 ± 0.1	
	9.2	277	6,000	3.8×10^8	≥12.5	
	13.7	285	7,800	Mixed		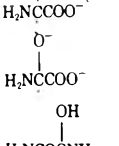
Oxamide	3.2	275	5,100	1.4×10^9	~3.7	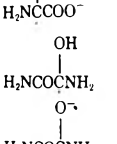
	7.3	285	6,700	4.0×10^8		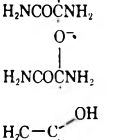
Succinimide	4.0	<245	>1,300	1.8×10^9	8.4 ± 0.1	
	11.0	<255	>1,800	7.0×10^8,		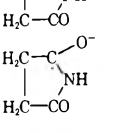
N-Methylsuccinimide	4.0	<245	>1,300		8.4 ± 0.1	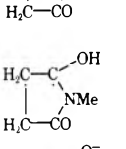
	11.0	<255	>1,800			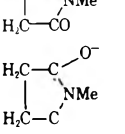
N-Ethylmaleamic[d] acid	6.5	360	15,000	5.0×10^8	10.4	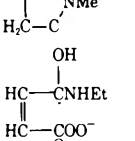
	12.0	360	15,000	Mixed		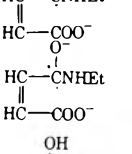
N-Ethylmaleimide	1.0	260	13,000		2.85	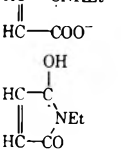
	6.0	270	16,000	4.0×10^9		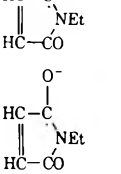

[a] Values to ±10%. [b] Also $H_2NCOC(OH)_2$ in resonance. [c] Also $H_2NC(O^-)COOH$. [d] From ref 4.

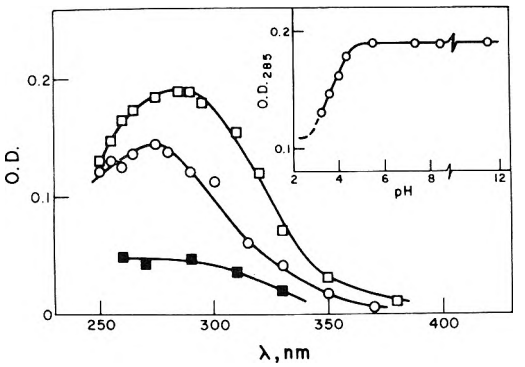

Figure 2. Transient absorption spectra resulting from the addition of e_{aq}^- to 5 m*M* oxamide in presence of 1.0 *M* *t*-BuOH and argon at pH 3.2, O, and 7.3, □. Slow decaying transient at pH 7.3 read at 500 μsec after the pulse, ■. Total dose ~5.1 krads/pulse. Insert shows change in absorbance at 285 nm with pH.

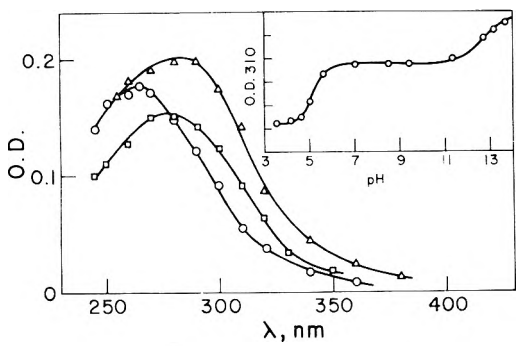

Figure 3. Transient absorption spectra resulting from the addition of e_{aq}^- to oxamic acid in presence of 1.0 *M* *t*-BuOH and argon at pH 3.5 (O, 15 m*M*), 9.2 (□, 2 m*M*), and 13.7 (△, 2 m*M*). Total dose ~4.5 krads/pulse. Insert shows change in absorbance at 310 nm with pH.

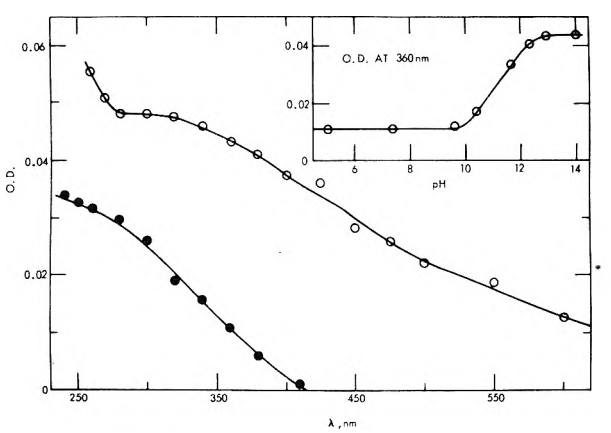

Figure 4. Transient absorption spectra resulting from the addition of e_{aq}^- to 20 m*M* malonamide in presence of 1.0 *M* *t*-BuOH and argon at pH 6.8, ●, and 11.4, O. Total dose ~5.6 krads/pulse. Insert shows change in absorbance at 355 nm with pH.

the two amide groups in oxamide first by one methylene group (malonamide) and then by two methylene groups (succinamide) was investigated. Very sharp decreases in the reactivity with e_{aq}^- were observed, Table I. The rate decreased from 3.3×10^{10} to 1.1×10^9 to 2.0×10^8 M^{-1} sec^{-1} for oxamide, malonamide, and succinamide, respectively. The reduced resonance and reduced electronic overlap probably account for these results.

Similar changes have been found in the absorption maxima, the extinction coefficients, and the ionization

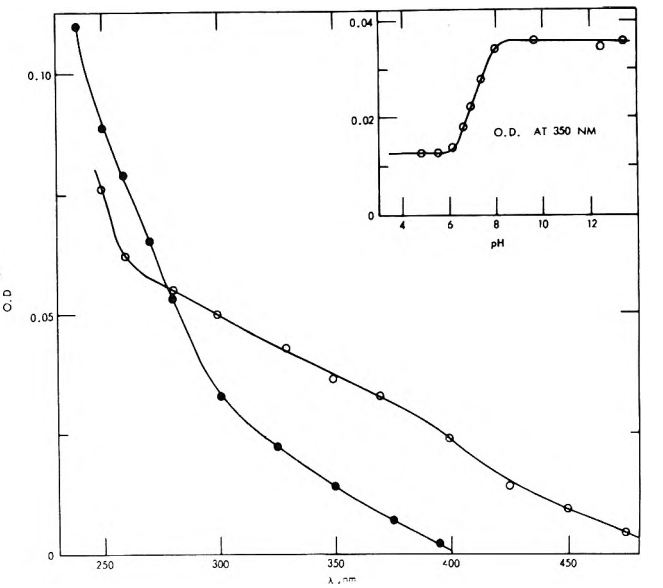

Figure 5. Transient absorption spectra resulting from the addition of e_{aq}^- to 20 m*M* succinamide in presence of 1.0 *M* *t*-BuOH and argon at pH 5.0, ●, and 12.9, O. Total dose ~5.6 krads/pulse. Insert shows change in absorbance at 360 nm with pH.

constants of the radicals, see Figures 4 and 5 and Table II. Thus, λ_{max} of the $R\dot{C}(OH)NH_2$ radicals shifted from 275 to 255 to <245 nm for oxamide, malonamide, and succinamide, respectively. The corresponding ionization constants of $R\dot{C}(OH)NH_2$ were ~3.7, 9.8 ± 0.1, and 11.3 ± 0.1.

$$H_2NCOCH_2\dot{C}(OH)NH_2 \underset{pK_a = 9.8 \pm 0.1}{\rightleftharpoons} H_2NCOCH_2\dot{C}(O^-)NH_2 + H^+ \quad (9)$$

$$\begin{matrix} CH_2\dot{C}(OH)NH_2 \\ | \\ CH_2CONH_2 \end{matrix} \underset{pK_a = 11.3 \pm 0.1}{\rightleftharpoons} \begin{matrix} CH_2\dot{C}(O^-)NH_2 \\ | \\ CH_2CONH_2 \end{matrix} + H^+ \quad (10)$$

It can be concluded that with further increase in $H_2NCO(CH_2)_nCONH_2$, where $n > 3$, the amide groups are completely isolated from each other and the ionization constant of these $R\dot{C}(OH)NH_2$ radicals approaches that of acetamide, $pK \geq 13.5$. These conclusions were important in interpreting the results obtained[5] from the interaction of e_{aq}^- with oligopeptides. These latter molecules have repetitive units -CHRCONH-, *i.e.*, each -CONH- group is isolated from each other by only one carbon atom.

Biuret. Biuret is an interesting molecule in that two amide groups are separated from each other by an -NH- group, instead of a $-CH_2-$ group as in malonamide; it also has the imide structure -CONHCO- and can be compared with other imides (see below). The reactivity of e_{aq}^- with biuret is 2.5×10^8 M^{-1} sec^{-1} and is to be compared with that of malonamide which is 1.1×10^9 M^{-1} sec^{-1}. One can assume the -NH- group to weaken the conjugation between the two carbonyl groups. However, the rate of e_{aq}^- with diacetamide, $CH_3CONHCOCH_3$, was found to be 1.1×10^{10} M^{-1} sec^{-1}.

The transient optical spectra, extinction coefficients, and decays kinetics of the radicals are given in Figure 6 and Table II. The ionization constant of the intermediate produced was found to be 7.3 ± 0.1. This pK_a is significantly lower than that of malonamide (pK_a = 9.8 ± 0.1), and is suggested to be a result of ionization of the ketyl radi-

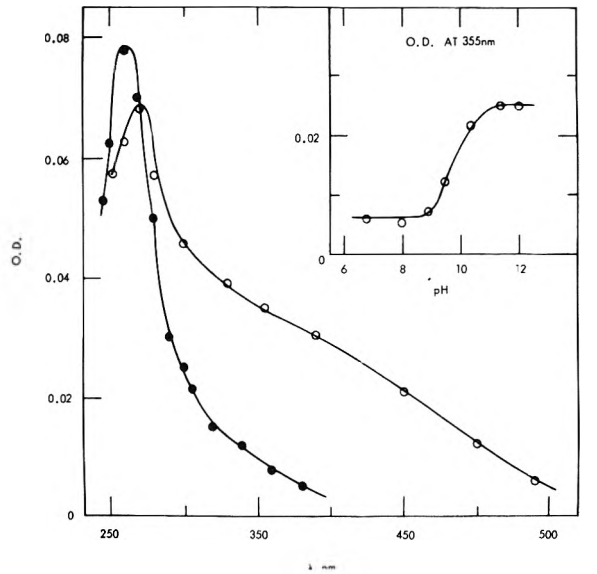

Figure 6. Transient absorption spectra resulting from the addition of e_{aq}^- to 20 m*M* biuret in presence of 1.0 *M* *t*-BuOH and argon at pH 5.5, ●, and 9.7, O. Total dose ~5.6 krads/pulse. Insert shows change in absorbance at 350 nm with pH.

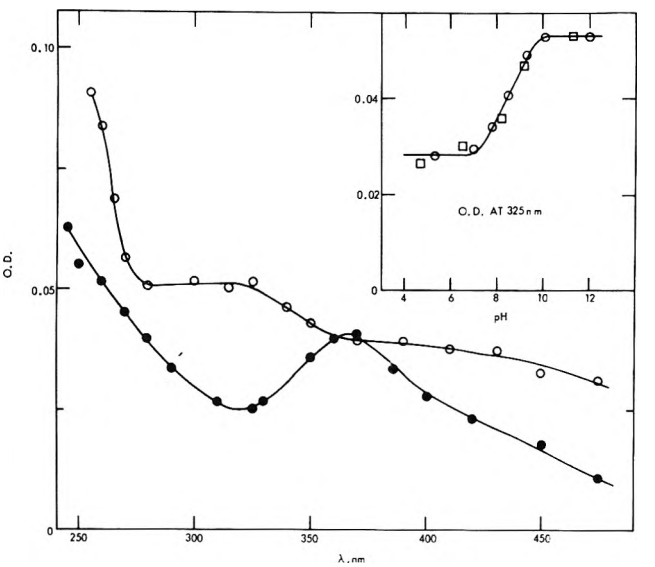

Figure 7. Transient absorption spectra resulting from the addition of e_{aq}^- to 10 m*M* succinimide in presence of 1.0 *M* *t*-BuOH and argon at pH 3.9, ●, and 11.0, O. Total dose ~9 krads/pulse. Insert shows change in absorbance at 325 nm with pH using succinimide, O, or *N*-methylsuccinimide, □.

cal

$$H_2N\dot{C}(OH)NHCONH_2 \underset{pK_a = 7.3 \pm 0.1}{\rightleftharpoons} H_2N\dot{C}(O^-)NHCONH_2 + H^+ \quad (11)$$

The ionization of the -NH- proton is excluded based on the results obtained from succinimide and *N*-methylsuccinimide (see below).

Imides. Succinimide reacts very fast with hydrated electrons, $k = 1.1 \times 10^{10}\ M^{-1}\ sec^{-1}$. This rate is identical with the rate of e_{aq}^- with diacetamide (see Table I) which has an open structure. The reactivity of succinimide was explained[2] on the basis of the formation of the tautomeric form -CON=C(OH)-, with nitrogen becoming a highly electrophilic center. The reactivity of e_{aq}^- toward *N*-methylsuccinimide was found, however, to be equally high with $k = 1.3 \times 10^{10}\ M^{-1}\ sec^{-1}$ (no tautomerism could take place in this case). Succinimide has a high pK_a, and it is interesting to note that on ionization of the -CONHCO- group the rate of reaction with e_{aq}^- decreases substantially to $k = 9.2 \times 10^8\ M^{-1}\ sec^{-1}$. The high reactivity of *N*-ethylmaleimide, compared to succinimide, toward e_{aq}^- must be due to the increased conjugation introduced by the carbon-carbon double bond (Table I).

While the electron adduct to *N*-ethylmaleimide (NEM) produced[4,13] numerous absorption bands with high extinction coefficients, the transient optical spectra of the electron adduct to succinimide (Figure 7) did not. Similarly, the acid-base properties of the radicals are significantly different: pK_a are 8.2 ± 0.1 and 2.85 ± 0.1 (ref 4 and 13) for succinimide and NEM, respectively.

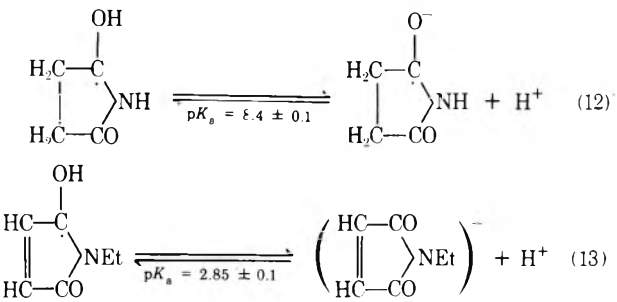

The interaction of e_{aq}^- with *N*-methylsuccinimide produced a similar transient spectrum and an identical ionization constant (see Figure 7 and Table II). This result supports the dissociation mechanism given in reaction 12 and shows that ionization of the proton in the -CONHCO- group does not occur at these relatively low pH values.

Conclusions

It is apparent that the reactivity of e_{aq}^- with amides can be correlated to the structure of the reacting amide. Increased conjugation of electrophilic centers leads to higher electron reactivities. Further addition of electrophilic centers and cyclization to form imides leads to diffusion-controlled rates. Separation of electrophilic centers with insulating groups (*e.g.*, $-CH_2-$ groups) invariably leads to a decrease of $k(e_{aq}^- + S)$.

The pK_a values of the electron adduct radicals can be seen, to a first approximation, to relate to the $k(e_{aq}^- + S)$ values for the amides and imides. Other factors such as spatial distribution of the extra electron may play an important role too. pK_a values as low as ~3 have been observed for electron adducts with highly resonating configurations.

The observed absorption spectra of the electron adducts are also quite different. Those of simple amides have weak absorptions at low wavelengths. In contrast, some highly conjugated systems have high extinction coefficients and, in general, absorption maxima at longer wavelengths.

Information obtained in this work is expected to contribute toward understanding of the interaction and migration of electrons in complex biological systems.

Acknowledgment. One of us (M. S.) acknowledges support under NIH Grant No. GM-13557 and AEC Contract No. AT-(40-1)-3408.

(13) M. Simic and E. Hayon, *Int. J. Radiat. Biol.*, **20**, 589 (1971).

Pulse Radiolysis Studies. XXII. Spectrum and Kinetics of the Sodium Cation–Electron Pair in Tetrahydrofuran Solutions[1]

Bradley Bockrath and Leon M. Dorfman*

Department of Chemistry, The Ohio State University, Columbus, Ohio 43210 *(Received November 20, 1972)*

Publication costs assisted by the U. S. Atomic Energy Commission

The optical absorption band of the sodium cation–electron pair, (Na^+,e_s^-), in tetrahydrofuran solution has been determined in pulse radiolysis studies. The absorption maximum is at 890 nm at 25°, and shows a temperature coefficient of -7 cm^{-1} deg^{-1}. The molar extinction coefficient at the maximum is 2.4×10^4 M^{-1} cm^{-1}, and the oscillator strength is $f = 1.0$. The large shift from the maximum of the solvated electron in THF, which is at 2120 nm, suggests strong coupling with the cation. The absolute rate constant for the reaction of the solvated electron with free sodium cation is 7.9×10^{11} M^{-1} sec^{-1}, with an activation energy of 1.4 kcal/mol. Rate constants were also determined for several reactions of e_{sol}^- with organic molecules. For comparison rate constants for a number of reactions of (Na^+,e_s^-) were also determined. These were found to be roughly an order of magnitude lower than the rate constants for the analogous reactions of e_{sol}^-. The free-ion yield for e_{sol}^-, determined using sodium cation as scavenger, was found to be 0.39 molecule/100 eV.

Introduction

The optical properties of alkali metal–electron pairs in polar liquids have been shown to differ, in some liquids, from those of the solvated electron. Evidence has been presented for the existence in sodium ethylenediamine solutions,[2-4] as well as in other amines,[4a] of the species with stoichiometry Na^-, consisting of two electrons coupled with a sodium cation. In sodium solutions in diglyme an adsorption band attributed to the cation–electron pair, (Na^+,e_s^-), consisting of a single electron coupled with a sodium cation, has been identified.[5,6] Differences in the reactivity of this species, compared with that of the solvated electron itself, have also been reported.[7]

We have recently obtained the complete spectrum of the (Na^+,e_s^-) ion pair in tetrahydrofuran at room temperature, for which only a partial spectrum, with the absorption maximum undefined, had previously been known.[8] From this information, comparison with the spectrum of the solvated electron in pure tetrahydrofuran can now be made since the latter spectrum has recently been reported[9] from our laboratory.

In the course of these observations of the spectrum by the pulse radiolysis method, an accurate absolute rate constant for the formation of (Na^+,e_s^-) by the reaction of e_{sol}^- with Na^+ was determined. Rate constants were also determined for several reactions of e_{sol}^- and of (Na^+,e_s^-) with various organic compounds in THF solution.

Experimental Section

The source of the electron pulse, as in our earlier studies,[10] was a Varian V-7715A electron linear accelerator, delivering 3-4-MeV electrons at a pulse current of about 350 mA for pulse duration of 100 to 1500 nsec and about 600 mA for pulse duration less than 80 nsec. Electron pulses of 20- to 80-nsec duration were used in this work. Dose determinations were based on observation of $(CNS)_2^-$ formation in N_2O-saturated aqueous solutions of 0.1 N potassium thiocyanate, with appropriate corrections for the density of THF and of water. In most runs, the transient optical absorptions were observed using an H.T.V. 196 detector with an S-1 response. In a few cases, where detection in the infrared was required, our fast, indium antimonide ir detector[11] was used. A Baush and Lomb grating monochromator, type 33-86-25, f/3.5 was used. Corning filters were used to eliminate second-order components from the analyzing light beam.

Our standard reaction cells,[10] with high-purity silica windows and a cell length of 20.0 mm, were used in most runs with a double pass of the analyzing light beam. Accordingly the optical path length was 40.0 mm. At wavelengths in excess of 1400 nm, a 3.0-mm cell was used with a single pass because of absorption by the solvent.

The THF was purified first by refluxing under argon, for several hours, a solution containing benzophenone and excess sodium metal. This was then distilled through a glass bead-packed column, the middle fraction being retained. It was then degassed and vacuum distilled into a bulb containing a mirror of freshly triple-distilled potassium. From this bulb it was vacuum distilled into the reaction cells just prior to the runs.

The aromatic compounds used were zone refined, commercially supplied, with a nominal purity of at least 99.9%. *n*-Butyl bromide (Fisher reagent grade) and *n*-

(1) This work was supported by the U. S. Atomic Energy Commission under Contract No. AT(11-1)-1763.
(2) A Gaathon and M. Ottolenghi, *Isr. J. Chem.*, **8**, 165 (1970).
(3) D. Huppert and K. H. Bar-Eli, *J. Phys. Chem.*, **74**, 3285 (1970).
(4) J. L. Dye, M. G. DeBacker, J. A. Eyre, and L. M. Dorfman, *J. Phys. Chem.*, **76**, 839 (1972).
(4a) S. Matalon, S. Golden, and M. Ottolenghi, *J. Phys. Chem.*, **73**, 3098 (1969).
(5) J. G. Kloosterboer, L. J. Giling, R. P. H. Rettschnick, and J. D. W. Van Voorst, *Chem. Phys. Lett.*, **8**, 462 (1971).
(6) L. J. Giling, J. G. Kloosterboer, R. P. H. Rettschnick, and J. D. W. Van Voorst, *Chem. Phys. Lett.*, **8**, 457 (1971).
(7) G. Ramme, M. Fisher, S. Claesson, and M. Szwarc, *Proc. Roy. Soc., Ser. A*, **327**, 467 (1972).
(8) M. Fisher, G. Ramme, S. Claesson, and M. Szwarc, *Proc. Roy. Soc., Ser. A*, **327**, 481 (1972).
(9) L. M. Dorfman, F. Y. Jou, and R. Wagemar, *Ber. Bunsenges. Phys. Chem.*, **75**, 681 (1971).
(10) W. D. Felix, B. L. Gall, and L. M. Dorfman, *J. Phys. Chem.*, **71**, 384 (1967).
(11) F. Y. Jou and L. M. Dorfman, *J. Chem. Phys.*, submitted for publication.

butyl iodide (Matheson Coleman and Bell) were purified by washing with several portions of concentrated H_2SO_4, followed by several portions of 10% sodium carbonate, and finally distilled water. The washed materials were distilled through a glass bead-packed column and the middle fraction retained. *n*-Butyl iodide was stored in the dark over mercury.

Sodium ion was added to the THF by dissolving an appropriate amount of sodium tetraphenylboron, which was Fisher reagent grade, recrystallized as recommended[12] and stored *in vacuo* until used. The spectral mapping was performed on solutions 2.7×10^{-3} *F* in sodium tetraphenylboron.

Results and Discussion

Optical Absorption Spectrum. The optical absorption band of the sodium cation-electron pair, with a maximum at 890 nm, is shown in Figure 1. The identification of this absorbing transient as the pair (Na^+,e_s^-), quite apart from prior evidence[5,6,8] or speculation, is clear from the formation kinetics of the transient, described in a subsequent section, and from our independent information about the formation and the lifetime of the solvated electron in pure THF.[9,11] The immediate precursors of the 890-nm band are the solvated electron (which, in our solutions containing Na^+, has a very short lifetime) and the sodium cation.

Comparison of the band maximum for (Na^+,e_s^-) with that of e_{sol}^- in THF[9,11] shows that coupling of the electron with the sodium in THF at room temperature produces a profound shift in the electron spectrum, the latter species exhibiting its band maximum at 2120 nm. If these band maxima correspond to individual transition energies, then the difference between e_{sol}^- and (Na^+,e_s^-) in THF is fully 0.8 eV, a very large perturbation indeed. Although this large effect, produced by the proximity of the positive charge, would seem to imply strong coupling, it should be noted that it is not known how much of the shift is to be ascribed to the ground-state level and how much to the excited-state level. It is interesting to compare this effect of sodium cation pairing with the observations in ethylenediamine[13] where (M^+,e_s^-) is readily formed,[14,15] yet where this cation-paired species shows no discernible difference in λ_{max} from that of the solvated electron.

The width at half-height of this 890-nm band in THF is 7000 cm^{-1}. The absorption band is thus substantially broadened by sodium cation coupling since the width at half-height of the solvated electron[11] in pure THF is only 3500 cm^{-1}. The solid curve in Figure 1, incidentally, is the result of a fit to the spectral data of a shape function consisting of a Gaussian curve on the low-energy side of the maximum and a Lorentzian curve on the high-energy side.

The molar extinction coefficient of (Na^+,e_s^-) was determined by comparison of the optical density of this species with that of the biphenylide ion in solution, formed in the reaction

$$(Na^+, e_s^-) + C_{12}H_{10} = Na^+,C_{12}H_{10}\cdot^- \qquad (1)$$

The molar extinction coefficient for biphenylide ion in sodium-THF solutions is reasonably accurately known,[16] having the value 12,500 M^{-1} cm^{-1} at 630 nm. If a biphenyl concentration is selected to limit the lifetime of (Na^+,e_s^-) to a value very much lower than its lifetime in solution not containing biphenyl, then all the (Na^+,e_s^-) present at some time after the pulse will be scavenged to form biphenylide ion, and a plateau in the rate curve will be observed since the radical ion lifetime is very long in this system. The biphenyl concentration used gave a half-life for (Na^+,e_s^-) on the order of 100 nsec, whereas its lifetime in the absence of biphenyl but under the same pulse conditions was at least 2000 nsec. Material balance in reaction 1 was thus assured. If the rate curve is observed at a wavelength for which $\epsilon(Na^+,e_s^-) < \epsilon(Na^+,Ph_2^-)$ a formation reaching a plateau will be seen. If the rate curve is observed at a wavelength for which $\epsilon(Na^+,e_s^-) > \epsilon(Na^+,Ph_2^-)$ a decay reaching a plateau will be seen, since the absorptions of the two species overlap extensively. At the wavelength for which $\epsilon(Na^+,e_s^-) = \epsilon(Na^+,Ph_2^-)$ the rate curve will simply be a horizontal line. If such a wavelength can be accurately determined, the value for $\epsilon(Na^+,e_s^-)$ can be determined.

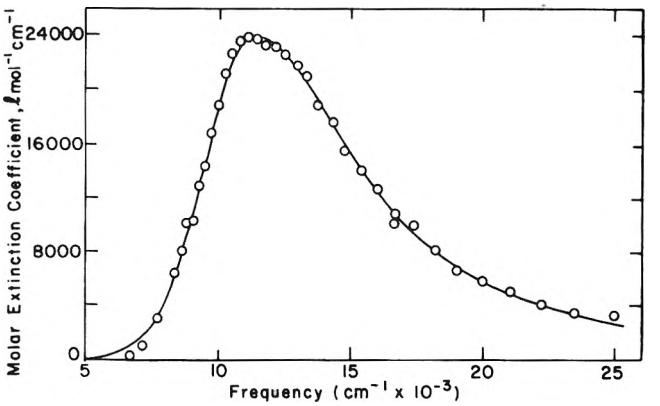

Figure 1. Spectrum of (Na^+,e_s^-) in THF at 25° recorded at the end of a 80-nsec electron pulse in a THF solution of 2.7×10^{-3} *F* sodium tetraphenylboron. The absorption maximum is at 11,300 cm^{-1} with an extinction coefficient of 24,000 and width at half-height of 7000 cm^{-1}. The circles are experimental points and the line is calculated using a Gaussian curve on the low-energy side of the maximum and a Lorentzian curve on the high-energy side. The oscillator strength from the calculated curve is 1.0.

This wavelength was accurately determined by a graphical treatment of the data. Rate curves were recorded at various wavelengths near the equivalency point. The degree of deviation of a given rate curve from the horizontal line which corresponds to equivalency of the extinction coefficients was expressed as the change in optical density from the end of the pulse to the plateau relative to the total optical density change at the plateau. This function, $(A_\infty - A')/A_\infty$, where A_∞ is the optical density change from the beginning of the pulse to the plateau and A' is the change from the beginning of the pulse to the end of the pulse, was plotted against wavelength as shown in Figure 2. The crossover point or the maximum, where $A_\infty - A' = 0$, is thus accurately determined. From the data, the optical density change comes within about 2% of satisfying the condition $\epsilon(Na^+,e_s^-) = \epsilon(Na^+,Ph_2^-)$ at the wavelength 630 nm, very close, incidentally, to an absorption band maximum for biphenylide ion. From the spectra of the two species and the molar extinction coefficient for biphenylide ion,[16] we obtain $\epsilon^{890}(Na^+,e_s^-) = 2.4 \times 10^4$

(12) C. Carvajal, K. J. Tolle, J. Smid, and M. Szwarc, *J. Amer. Chem. Soc.*, **87**, 5548 (1965).
(13) R. R. Dewald and J. L. Dye *J. Phys. Chem.*, **68**, 121 (1964).
(14) R. R. Dewald and J. L. Dye *J. Phys. Chem.*, **68**, 128 (1964).
(15) J. L. Dye, M. G. DeBacker, and L. M. Dorfman, *J. Chem. Phys.*, **52**, 6251 (1970).
(16) J. Jagur-Grodzinski, M. Feld, S. L. Yang, and M. Szwarc, *J. Phys. Chem.*, **69**, 628 (1965).

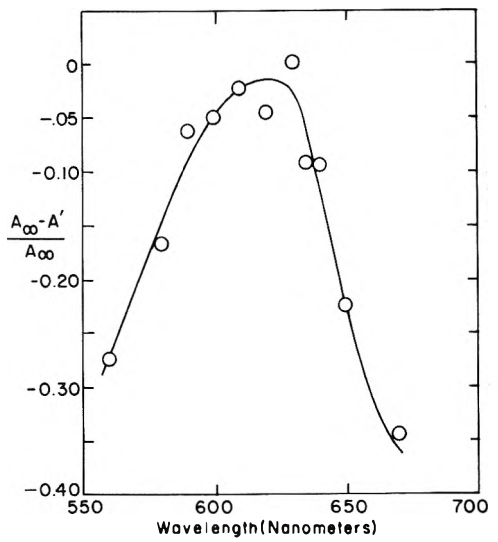

Figure 2. Plot of the function $[(A\infty - A')/A\infty]$ *vs.* wavelength. From the data, the extinction coefficients of (Na^+,e_s^-) and sodium biphenylide are taken to be equal at 630 nm.

M^{-1} cm^{-1}, in agreement with a recent value[7] obtained by other methods. As a confirmation, similar experiments were carried out with naphthalene, for which the absorption band is not quite as suitable because of smaller overlap, and for which the extinction coefficient of the ion may not be as accurately known.[17] A value of $\epsilon^{890}(Na^+,e_s^-) = 2.6 \times 10^4\ M^{-1}$ cm^{-1} was obtained, the value with biphenylide probably being more accurate.

On the basis of $\epsilon^{890}(Na^+,e_s^-) = 2.4 \times 10^4\ M^{-1}$ cm^{-1} we may determine the oscillator strength

$$f = 4.32 \times 10^{-9} \int_{E1}^{E2} \epsilon\, dE \qquad (2)$$

from the data in Figure 1 in two ways: from the width at half-height of the absorption band, and by graphical integration of the area under the entire absorption band.

f was determined from the width at half-height using the equation[18]

$$f = 4.32 \times 10^{-9}(1.065 W_{1/2}^{G} + 1.571 W_{1/2}^{L})\, \epsilon_{max} \qquad (3)$$

where $W_{1/2}{}^G$ and $W_{1/2}{}^L$ are those portions of the width on the Gaussian side and the Lorentzian side, respectively, of the absorption band, and ϵ_{max} is the molar extinction coefficient at the maximum. The value obtained is f = 1.0. Graphical integration of the area under the curve yields f = 0.84, a slightly lower value, as is to be expected, because a small area under the high-energy tail, beyond 25,000 cm^{-1}, the limit of our spectral determination, is neglected. The value f = 1.0 is similar to that typically found for solvated electrons in a variety of liquids, and is consistent with the assignment of the band to a transition involving one electron.

The 890-nm band shifts toward the blue with decreasing temperature. The band maximum was found to be 840 nm at −59°, corresponding to a blue shift of −7 cm^{-1} deg^{-1}. This is somewhat less than the blue shift of −10 cm^{-1} deg^{-1} reported[5] for the solvated electron in diglyme. These authors point out the similarity of blue shifts in diglyme for three different bands assigned to the solvated electron, to (Na^+,e_s^-), and to a higher aggregate of two electrons associated with one or two sodium cations. On the basis of these large spectral shifts, a strong solvent–electron interaction must occur in the ion-paired species.

TABLE I: Rate Constant for the Reaction of e_{sol}^- with Na^+

Concn of $(Na^+Ph_4B^-)$, $M \times 10^5$	Concn of free Na^+, $M \times 10^5$	k_4, M^{-1} sec^{-1} $\times 10^{-11}$
1.83	1.56	7.4[a]
2.41	1.97	9.0
3.15	2.46	7.6
4.31	3.17	7.0
4.38	3.21	7.2
5.18	3.66	8.6
6.16	4.18	8.3
7.03	4.62	8.1

[a] Each rate constant is the average of two to five runs.

Reaction Kinetics of e_{sol}^-. Absolute rate constants for the reaction of the solvated electron with sodium cation

$$e_{sol}^- + Na^+ \longrightarrow (Na^+,e_s^-) \qquad (4)$$

and for the attachment of e_{sol}^- to several compounds in THF solution have been determined by observation of rate curves for the formation of a reaction product, or for disappearance of e_{sol}^-.

k_4 was determined from rate curves for the growth of the 890-nm band observed following a 20-nsec pulse in THF solutions of sodium tetraphenylboron at the concentrations shown in Table I. These concentrations gave a sodium cation concentration which was always high enough to ensure pseudo-first-order kinetics and to give a half-life for reaction 4 in the range 70–20 nsec. The half-life for e_{sol}^-, in the absence of $Na^+Ph_4B^-$ salt, under otherwise identical conditions was greater than 600 nsec so that complete scavenging of e_{sol}^- by Na^+ was assured, as is borne out by the data in Table I. Furthermore the growth curves reach a well-defined plateau since the half-life for decay of (Na^+,e_s^-) is greater than 2000 nsec.

A typical first-order plot for the appearance of (Na^+,e_s^-), showing $-\ln [(D_\infty - D_t)/D_\infty]$ as a function of time, in accord with the integrated form of the differential rate expression for reaction 4, is shown in Figure 3. A linear least-squares fit with a high correlation coefficient was obtained for each run. The first-order rate constants were obtained from the slope of such lines. The sodium cation concentrations, necessary for the determination of k_4, were determined from the concentrations of salt used and the dissociation constant for

$$Na^+Ph_4B^- \longrightarrow Na^+ + Ph_4B^- \qquad (5)$$

which has the value[12] $K_5 = 8.8 \times 10^{-5}\ M$. The values for k_4, obtained in this way, and showing excellent constancy over a 3.5-fold concentration range of $[Na^+]$ are shown in Table I. The average value is $k_4 = (7.9 \pm 0.7) \times 10^{11}\ M^{-1}$ sec^{-1}.

A confirmation that the reaction is first order in free sodium cation was obtained from a plot of log $[Na^+]$ against the log of the pseudo-first-order constant for (4), which gave a straight line with a slope of 1.03. By contrast a plot of log $[Na^+Ph_4B^-]$ against log k_4' gave a straight line with slope 0.835.

The value $k_4 = (7.9 \pm 0.7) \times 10^{11}$ is twice that of an estimate reported earlier.[7] The value reported here is

(17) Y. Karasawa, G. Levin, and M. Szwarc, *Proc. Roy. Soc., Ser. A*, **326**, 53 (1971).
(18) J. G. Calvert and J. N. Pitts, "Photochemistry," Wiley, New York, N. Y., 1966, p 172.

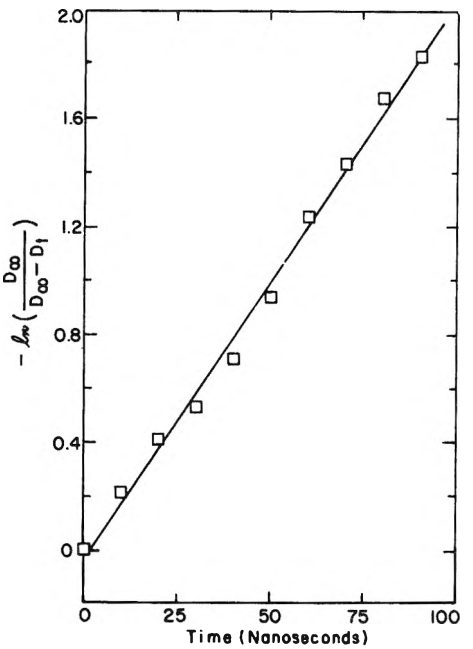

Figure 3. First-order plot of the appearance of (Na^+,e_s^-) in THF observed at 890 nm at 25° after an 80-nsec pulse. The free sodium ion concentration is 2.5×10^{-5} *M*.

more reliably established as may be seen from the individual results in Table I. Direct comparison of k_4 with k_{diff} as calculated from the Debye equation may be instructive even though the uncertainty in the calculated value is large because the interaction radius for e_{sol}^- + Na^+ is not precisely known. If we substitute $a > 4$ Å for the interaction radius on the basis of a Stokes radius of 4 Å for Na^+ in THF, and $D = 7.2$ as the macroscopic dielectric constant, we obtain $k_{diff} < 3 \times 10^{11}\ M^{-1}\ sec^{-1}$. The observed value of $k_4 = 7.9 \times 10^{11}$ is, if anything, somewhat larger than the estimated diffusion-controlled rate constant. If this difference represents a real anomaly it should be noted that reaction 4 is not a unique case, for reactions 7, 8, and 9, which follow, show an even slightly larger ratio for $k_{obsd}/k_{diff}^{calcd}$. This would seem to suggest that transport of the solvated electron need not involve molecular mobility only. Reactions of the sodium cation coupled electron, as in (10–13) and (1), exhibit rate constants fully an order of magnitude lower, and are thus more closely consistent with calculated diffusion-controlled rate constants.

The temperature coefficient of reaction 4 was determined over the range from −60 to 27°. The calculation of the rate constants at each temperature included appropriate corrections to the sodium cation concentration due to the density change of solvent and the temperature coefficient of the dissociation constant for sodium tetraphenylboron. An activation energy of 1.4 kcal/mol was obtained. The corresponding enthalpy and entropy of activation are 0.8 kcal/mol and −1 eu, respectively. The very low activation energy is qualitatively consistent with a simple diffusion-controlled association of two oppositely charged species. The value for the entropy of activation is also consistent with this description.

Taking the dissociation constant[7] for

$$(Na^+,e_s^-) \rightleftharpoons Na^+ + e_s^- \qquad (6)$$

as $K_6 = 3 \times 10^{-8}\ M$, we may calculate $k_6 = 2.4 \times 10^4\ sec^{-1}$.

The fact that the elementary reaction 4 shows kinetics which are first order in both e_{sol}^- and Na^+ establishes that these species are both precursors of the 890-nm band and confirms the 1:1 stoichiometry in the assignment (Na^+,e_s^-).

Several other reactions of e_{sol}^- in THF have been investigated in a similar manner. The decay of e_{sol}^- was monitored at 990 nm following an 80-nsec pulse, in the absence and presence of substrate, for two reactions, and product formation was monitored in a third. For the reactions with *n*-butyl bromide and *n*-butyl iodide, where electron decay was monitored, linear first-order plots of $-\ln D_t$ *vs.* time were obtained over a range of substrate concentrations selected to give pseudo-first-order kinetics. For the reaction

$$e_{sol}^- + n\text{-}C_4H_{11}Br = n\text{-}C_4H_{11}\cdot + Br^- \qquad (7)$$

investigated over a butyl bromide concentration range from 9.4×10^{-5} to $2.9 \times 10^{-4}\ M$, the rate constant is $k_7 = (6.9 \pm 0.5) \times 10^{10}\ M^{-1}\ sec^{-1}$. For the reaction

$$e_{sol}^- + n\text{-}C_4H_{11}I = n\text{-}C_4H_{11}\cdot + I^- \qquad (8)$$

investigated over a butyl iodide concentration range from 4.8×10^{-5} to $1.7 \times 10^{-4}\ M$, the rate constant is $k_8 = (1.1 \pm 0.1) \times 10^{11}\ M^{-1}\ sec^{-1}$. For the attachment to biphenyl

$$e_{sol}^- + C_{12}H_{10} = C_{12}H_{10}\cdot^- \qquad (9)$$

investigated over a biphenyl concentration range from 6.6×10^{-5} to $1.2 \times 10^{-4}\ M$, and monitored by observing the appearance of the biphenylide band at 630 nm, good linear plots of $-\ln [(D_\infty - D_t)/D_\infty]$ *vs.* time were obtained. The rate constant is $k_9 = (1.1 \pm 0.3) \times 10^{11}\ M^{-1}\ sec^{-1}$.

Reaction Kinetics of (Na^+,e_s). For comparison with the reactivity of e_{sol}^-, the corresponding reactions of the ion-paired species, (Na^+,e_s^-), were investigated, along with two other reactions. The reaction

$$(Na^+,e_s^-) + n\text{-}C_4H_{11}Br = n\text{-}C_4H_{11}\cdot + Na^+Br^- \qquad (10)$$

was observed over a butyl bromide concentration range from 9.8×10^{-5} to $9.6 \times 10^{-4}\ M$. The rate constant is $k_{10} = (8.9 \pm 0.8) \times 10^9\ M^{-1}\ sec^{-1}$. For the reaction

$$(Na^+,e_s^-) + n\text{-}C_4H_{11}I = n\text{-}C_4H_{11}\cdot + Na^+I^- \qquad (11)$$

the rate constant, determined over a butyl iodide concentration range from 2.5×10^{-4} to $1.3 \times 10^{-3}\ M$, is $k_{11} = (1.15 \pm 0.10) \times 10^{10}\ M^{-1}\ sec^{-1}$. For the reaction of (Na^+,e_s^-) with biphenyl to form biphenylide ion, reaction 1, good agreement was found between the rate of decay of the 890-nm band and the rate of appearance of the 400-nm band of the biphenylide ion. Over a biphenyl concentration range from 2.6×10^{-4} to $1.36 \times 10^{-3}\ M$ the rate constant is $k_1 = (5.5 \pm 0.2) \times 10^9\ M^{-1}\ sec^{-1}$. For the reaction with pyrene

$$(Na^+,e_s^-) + Py = Na^+,Py\cdot^- \qquad (12)$$

good agreement was found between the rate of decay of the 890-nm band and the rate of formation of the 493-nm band of the pyrenide ion. Over a pyrene concentration range from 4.8×10^{-5} to $1.8 \times 10^{-4}\ M$, we obtain $k_{12} = (2.5 \pm 0.2) \times 10^{10}\ M^{-1}\ sec^{-1}$, which may be compared with an earlier value[8] of 1.7×10^{10}. From the temperature coefficient of reaction 13 over the range from −64 to 25°, the activation energy was found to be 1.8 kcal/mol. The corresponding enthalpy and entropy of activation are 1.3 kcal/mol and −6.6 eu, respectively. The low value for E_{ac} is comparable with that for reaction 4, being consistent with a rate constant very near the diffusion-controlled limit.

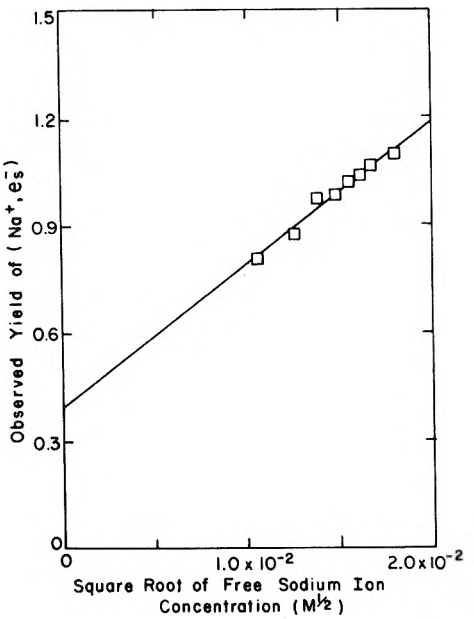

Figure 4. The observed yield of (Na^+,e_s^-) *vs.* the square root of free sodium ion concentration. The intercept, 0.39 ± 0.03, is the free ion yield of the solvated electron in THF. The slope is 39 molecules/100 eV, $M^{1/2}$.

For the reaction with naphthalene

$$(Na^+,e_s^-) + C_{10}H_8 = Na^+,C_{10}H_8\cdot^- \qquad (13)$$

investigated by observing the decay of (Na^+,e_s^-) at 600 nm over a naphthalene concentration range from 3.8×10^{-5} to 6.9×10^{-4} M, the rate constant is $k_{13} = (1.02 \pm 0.10) \times 10^{10}$ M^{-1} sec^{-1}. Comparison of the rate constants of e_{sol}^- with those for (Na^+,e_s^-) for the three common reactants indicates that the latter have values roughly an order of magnitude lower than those for e_{sol}^-. The rate data for such reactions in sodium–THF solutions do not, therefore, constitute a unified set of data with those values obtained in the absence of sodium, nor do they, indeed, represent data for the same species.

Two observations pertaining to the disappearance of the (Na^+,e_s^-) ion pair in solutions containing sodium tetraphenylboron without any other added reactant are worthy of note. (1) The decay was found to obey a first-order rate law, which permits us to conclude that it cannot be attributed solely to the reaction with the solvent counterion. (2) The half-life varied from sample to sample within the range from 2 to 5 μsec in the sodium tetraphenylboron solutions, and was found to be 6 μsec in a single experiment with sodium iodide as the added salt. The rate of this first-order decay, in competition with reactions 10–13 was thus small or negligible and was, in any event, taken into account in calculating k_{10} to k_{13}.

The mechanism of the decay was not investigated, but may very well involve, in addition to the counterion reaction, reactions with radiation produced free radicals the yield of which may be considerably in excess of the electron yield. This would account for the first-order decay and for the substantially shorter lifetime than was observed in photochemical investigations[8] where it was reported to be 175 μsec. The short half-life precludes any observation, under our conditions, of the reported[8] collapse of (Na^+,e_s^-). We have not detected any growth of other absorption bands concurrent with the decay of the (Na^+,e_s^-) band in the spectral range from 400 to 1800 nm.

Radiation Yield. The radiation yield of (Na^+,e_s^-), or of e_{sol}^-, has been determined in this work using sodium cation as scavenger. The sodium cation is a rather different scavenger for the solvated electron than the organic halides or aromatic compounds commonly used, and is particularly effective because of the high extinction coefficient and high formation rate constant of (Na^+,e_s^-).

To determine the free ion yield for e_{sol}^-, the observed G values for (Na^+,e_s^-) were obtained at several different concentrations of sodium cation up to the limit of the range originally used to establish the dissociation constant of sodium tetraphenylboron.[12] This concentration range is sufficiently low so that the following relationship[19] is valid

$$G(Na^+,e_s^-) = G_{fi} + K[Na^+]^{1/2} \qquad (14)$$

where $G(Na^+,e_s^-)$ is the observed yield at a given concentration of sodium cation, G_{fi} is the free ion yield, and K is a constant. A plot of $G(Na^+,e_s^-)$ *vs.* $[Na^+]^{1/2}$, as shown in Figure 4, is linear and has the intercept $G_{fi} = 0.39$ molecules/100 eV. This value for the free ion yield of the solvated electron in THF is in excellent agreement with a similar value obtained in current work[11] using pyrene as scavenger, and with a value cited in a preliminary report[20] using anthracene. It is a source of some confidence that identical yields are obtained with aromatic molecules and with sodium cation.

The effectiveness of sodium cation as a scavenger may be seen by evaluating the α parameter in the yield equation[19]

$$G_{obsd} = G_{fi} + G_{gi}\left[\frac{(\alpha[S])^{1/2}}{1+(\alpha[S])^{1/2}}\right] \qquad (15)$$

in which G_{obsd} is the observed yield, G_{gi} is the yield of geminate ions, and [S] is the concentration of scavenger. This equation is valid at any concentration of scavenger. To a first approximation, in the scavenger concentration range used, the constant of eq 15 is given by

$$K = G_{gi}\alpha^{1/2} \qquad (16)$$

Taking the slope from our plot in Figure 4 and Baxendale's value of $G = 2.6$ for the total yield,[21] we find $\alpha = 20$ M^{-1}. Even if the total yield were as high as 4, we would obtain $\alpha = 120$ M^{-1}. Values for α on the order of 15 to 20 have been cited as typical for scavengers such as alkyl halides in hydrocarbons. The α value for Na^+ in THF is thus roughly an order of magnitude higher. Since α is the ratio of the scavenging rate constant to the frequency factor for geminate ion recombination, it is apparent that the value will depend both on k_4 and on properties of the solvent. Other electron scavengers in THF have been found to have relatively high α values in recent work[22] on the γ-radiolysis of THF.

Acknowledgment. We are indebted to Mr. John Richter and Mr. Amin Bishara for maintaining the effective operation of the linear accelerator and the detection equipment.

(19) S. J. Rzad, P. P. Infelta, J. M. Warman, and R. H. Schuler, *J. Chem. Phys.*, **52**, 3971 (1970).
(20) J. H. Baxendale, D. Beaumond, and M. A. J. Rodgers, *Int. J. Radiat. Phys. Chem.*, **2**, 39 (1970).
(21) J. H. Baxendale, D. Beaumond, and M. A. J. Rodgers, *Trans. Faraday Soc.*, **66**, 1966 (1970).
(22) K. N. Rao, G. C. Goyal, and G. Ramanar, *Radiat. Eff.*, **14**, 101 (1972).

Photochemical Studies on Ozone with Carbon Disulfide and with Carbonyl Sulfide in Low-Temperature Matrices

Patrick R. Jones[1] and Henry Taube*

Department of Chemistry, Stanford University, Stanford, California 94305 *(Received January 5, 1972)*

Publication costs assisted by Stanford University

Reactions of $O(^1D)$ produced by uv photolysis of ozone were studied for dilute mixtures containing O_3 and CS_2 or OCS, in xenon or argon at temperatures between 15 and 60°K, using ir spectrophotometry to identify products. The products observed for O_3–CS_2 mixtures are OCS, SO_2, and SO_3, with CO being produced in minor amounts. For the O_3–OCS system, CO_2, CO, SO_3, and SO_2 are produced. Each of the products, OCS, CO_2, CO, SO_2, and SO_3, appeared at a rate which, except for a short induction period, was constant throughout the time of photolysis. It is suggested that the reaction of $O(^1D)$ with CS_2 produces the sets of primary products OCS + S and CO + S_2, and that with OCS as substrate the primary products are CO_2 + S and CO + SO. No evidence was found for species CS_2O or CO_2S analogous to CO_3 which is formed by the addition of $O(^1D)$ to CO_2.

Introduction

Addition reactions of $O(^1D)$ in the gas phase are dependent on third body collisions. In the matrix isolation technique, it is usually assumed that the host material will provide efficient energy dissipation on the way to the formation of atom–molecule addition products. The reaction of $O(^1D)$ with CO_2 to produce CO_3 does occur readily in a low-temperature matrix,[2-5] but in the gas phase a dissociative process has been shown to compete with the deactivation of the CO_2–$O(^1D)$ collision complex.[6] The evidence presented in this paper indicates that even in a low-temperature matrix, atom–molecule addition reactions similar to that by which CO_3 is formed are not necessarily efficient compared with dissociative processes.

Experimental Section

The studies were conducted using a liquid helium dewar, Model MHD 3L-15N, from the Andonian Associates. The design has been described previously.[3,4] Modifications of the basic dewar were made so that solid nitrogen could be used as a coolant to obtain sample temperatures near 60°K.[4] In addition, sample temperatures down to 15°K were accessible using liquid helium.

The samples were prepared on a standard Pyrex vacuum line using Kel-F Number 90, or halocarbon stopcock grease from the Halocarbon Corp. These greases were necessary for all portions of the vacuum line which were exposed to ozone. The CS_2 and OCS samples were stored in blackened Pyrex bulbs fitted with greaseless, Kel-F bore, high-vacuum stopcocks from the Kontes Co.

Gas samples were prepared by condensing each gas into a calibrated volume. The pressure in the calibrated volume was measured using a quartz spiral null manometer made by Texas Instruments Co. The measured amounts of gas were then transferred to 1-l. Pyrex bulbs containing glass beads so that mixing could be accelerated by shaking the bulbs.

Carbonyl sulfide (Matheson) was purified by scrubbing the gas through three consecutive, fritted wash flasks containing concentrated sodium hydroxide solution at 0°. The gas was then freeze–pumped repeatedly and distilled through a trap packed with glass wool and cooled to 143°K with a *n*-pentane slurry. Carbonyl sulfide enriched in ^{18}O was prepared by heating sulfur in a sealed Pyrex bulb with an excess of $C^{18}O$ at 300° for 36 hr.

Ozone enriched in ^{18}O was prepared by silent electrical discharge through oxygen in a closed system cooled with liquid nitrogen. The ^{18}O content of the enriched oxygen obtained from Miles Laboratories was 95.90 atom %. Ozone of normal isotope abundance was prepared similarly using Matheson research grade O_2.

Carbon disulfide enriched in ^{34}S was prepared by heating sulfur and a rigorously degassed charcoal alumina mixture in a sealed Vycor tube at 600° for 11 days. The labeled CS_2 was then purified by preparative gas chromatography using a Porapak-Q column. Product analysis by mass spectrometry gave the following results: 73% $C^{34}S_2$, 25% $SC^{34}S$, and 2% $C^{32}S_2$.

The matrix isolation experiments were monitored using a Perkin-Elmer Model 21 spectrophotometer with a NaCl prism.

The photolysis sources included (1) a 450-W medium-pressure mercury lamp (Hanovia), used for $\lambda \simeq 260$ nm and for $\lambda \geq 300$ nm; (2) a low-pressure mercury resonance lamp (Osram, Hg/3), for 253.7 nm; and (3) a cadmium resonance lamp (Osram, Cd/1), for 228.8 nm. For all three light sources, filters were always used to preclude problems from the lack of monochromicity. The Hanovia lamp was used for uv photolysis of ozone with a chemical filter[7] which excludes light in the 282–600-nm region, as well as light of $\lambda \leq 218$ nm. The maximum transmittance was at λ 260 nm. Interference filters (Baird-Atomic, Inc.) were used with the resonance lamps. One was appropriate for

(1) National Academy of Sciences Overseas Research Fellow, University of Sao Paulo, Brazil, 1971–1973.
(2) N. G. Moll, D. R. Clutter, and W. E. Thompson, *J. Chem. Phys.*, **45**, 4469 (1966).
(3) E. Weissberger, W. H. Breckenridge, and H. Taube, *J. Chem. Phys.*, **47**, 1764 (1967).
(4) P. R. Jones and H. Taube, *J. Phys. Chem.*, **75**, 2991 (1971).
(5) M. E. Jacox and D. E. Milligan, *J. Chem. Phys.*, **54**, 919 (1971).
(6) W. B. DeMore and C. Dede, *J. Phys. Chem.*, **74**, 2621 (1970).
(7) The quartz filter cell consisted of three compartments of path lengths 5, 5, and 1 cm, which were filled respectively with (1) an aqueous solution of nickel(II) sulfate hexahydrate, 28 g per 100 ml; (2) chlorine gas at 1 atm; and (3) a saturated aqueous solution of cobalt(II) sulfate.

use with the low-pressure mercury lamp since it blocked the regions with λ ≤235 and ≥287 nm, and had a maximum transmittance at λ 250 nm. The other interference filter was suitable for the isolation of the 228.8-nm output of the cadmium lamp. That filter blocked λ 200 and 274 nm, with maximum transmittance at 215 nm. The wavelength limits given above correspond to transmission of approximately 1% of the incident light and are applicable to the range 200–600 nm.

Results

The reaction mixtures were 0.2–1.5 mol % in each of CS_2 (or OCS) and O_3 in solid argon (15 or 30°K) or xenon (usually 60°K) as the matrix material. The deposits were photolyzed using the uv light of either a medium- or a low-pressure mercury arc lamp.

Several precautions were taken to ensure that adequate matrix isolation was attained in our systems. A comparison of the results obtained at dilution higher by a factor of 3 than those reported here showed no discrepancies either in product formation or in infrared matrix shifts. Although in other systems we experienced problems with the rigidity of xenon as a matrix host at 60°K, none were found for OCS or CS_2 with O_3. Results in xenon at 30°K agreed with those at 60°K, and results in argon at 15°K agreed with those at 30°K. Moreover, the relative matrix shifts of the infrared bands for both products and reactants were monitored, and were found to be both consistent throughout for a given matrix host, and typical for that particular material. The alternative matrix materials OCS, SO_2, O_2, and CO_2, when used in place of argon or xenon, gave rise to distinct and characteristic sets of matrix shifts.

Figure 1 shows the spectrum observed for CS_2–O_3 mixtures in xenon before and after photolysis. Before photolysis, the prominent peaks are ascribable to O_3 and CS_2 but some CO_2 as well as OCS is present. The latter species probably arise from the thermal reaction of O_3 with CS_2. It is clear, however, that the samples can be laid down with little interference from thermal reaction products. The absence of SO_2 in the starting sample is especially noteworthy as is the fact that little, if any, SO_3 is formed prior to photolysis. On photolysis using light at λ 254 nm, O_3 decreases rapidly, a small decrease in CS_2, which in this experiment was present in greater proportion, is also evident, and prominent peaks characteristic of SO_2, SO_3, and OCS appear. A weak product peak at 2140 cm^{-1} (2146 cm^{-1} in Ar) can confidently be assigned to CO. The identification of the four products named rests not only on the correspondence of the peaks to known absorptions for these species, but also on shifts observed when ^{18}O-labeled O_3 is used, and in the case of SO_2 and SO_3 making use also of the shifts with $C^{34}S_2$ as substrate. In every case, the expected isotopic shifts were observed. The weak peak at 1112 cm^{-1} (1123 cm^{-1} in Ar) is attributed to a sulfur- and oxygen-containing compound, and it was observed to occur in both the CS_2–O_3 and the OCS–O_3 systems. An experiment was done in which a stream of pure SO_2 gas was passed through an rf discharge and the resulting mixture of sulfur and oxygen compounds were frozen on the sample plate. The ir spectrum indicated SO_2, SO_3, and O_3 to be present, and showed an additional strong band at 1126 cm^{-1}, with a weaker one at 678 cm^{-1}. The latter correlates with the S_2O band which occurs at 679 cm^{-1} in the gas phase.[8] The band at 1126 cm^{-1} is too strong to be an impurity and must be attributed to an oxide of sulfur. On the basis of the band at 1126 cm^{-1} in the SO_2 discharge experiment, the weak peak at 1112 cm^{-1} in Xe (1123 cm^{-1} in Ar) may be considered to be a sulfur oxide that remains unidentified.

Another weak new band at 1045 cm^{-1} in Xe (1058 cm^{-1} in Ar) was evident in some of our experiments. Often, however, the region of interest was obscured by the strong O_3 band (*cf.* Figures 1 and 2). The important observation concerning this band is that it was found unshifted in experiments with OCS–O_3, CS_2–O_3, and ^{18}OCS–O_3. Thus, it also is ascribed to a sulfur oxide. Experiments using $^{18}O_3$ with OCS or CS_2 indicated that the band at 1058 cm^{-1} in argon is shifted to 1016 cm^{-1} when ^{18}O is used. The experiments with $C^{34}S_2$ were unfortunately inconclusive in the matter of isotopic shift.

In Figure 2 are shown the results for an experiment with O_3–OCS again using Xe as a host material. In this system SO_2, SO_3, and CO_2 appear as prominent product peaks and a weak peak attributable to CO is observed. The identification of the products SO_2, SO_3, CO_2, and CO rests on evidence of the kind which has been described for the CS_2 and O_3 system.

Tracer experiments were done using $^{16}O_3$ and ^{18}OCS in argon matrices at 30°K. In a mixture of this composition, $C^{18}O$ was produced, but not $C^{16}O$; and $S^{16}O_2$, but not $^{16}OS^{18}O$. Conversely, in experiments using ^{16}OCS and $^{18}O_3$, $C^{16}O$ but not $C^{18}O$ was observed.

Our previous experience[4] showed that the changes in infrared absorbance on photolysis of a given matrix sample are reasonably reproducible, and are useful, therefore, for monitoring relative concentration changes. Figures 3 and 4 show quantities which are proportional to the concentrations of the particular species dealt with, plotted against the time of photolysis. After an initial induction period in each case, during which O_3 is "wasted" (presumably by net conversion to O_2), O_3 decreases linearly with time, and the several products CO, SO_3, OCS, and SO_2 when CS_2 is substrate, and SO_3, SO_2, CO_2, and CO when OCS is substrate, increase linearly with time of photolysis.

In neither the O_3–CS_2 nor O_3–OCS system were peaks observed attributable to the addition products COS_2 and CO_2S, which can be regarded as the analogs of CO_3 which is formed when $O(^1D)$ reacts with CO_2. Acting on a concern that the putative intermediates COS_2 and CO_2S might be cophotolyzed, the reactions were studied also at λ 2288 nm (Osram Cd/1) and at λ >300 nm using a medium-pressure mercury arc filtered by Pyrex. In addition, in a crude flash photolysis experiment, the light transmitted from a conventional photographic flash bulb was used. In no case were the results different qualitatively, and in particular no ir absorption peaks were observed other than those already described.

Experiments were done under conditions similar to those above using SO_2 as substrate. The chemistry of the system in its qualitative aspects is simple, and possibly the quantitative aspects as well. At least at relatively short ozone photolysis times, SO_3 is the only product observable by ir spectrophotometry. As SO_3 accumulates, complications arise which were separately studied in SO_3–O_3 mixtures. Those with CO_2 as the host material appear to be the most promising, and give evidence of the formation of a new species which we take to be SO_4. Work on this system is being continued.

(8) P. W. Schenk and R. Steudel, *Angew. Chem., Int. Ed. Engl.*, **4**, 4021 (1965).

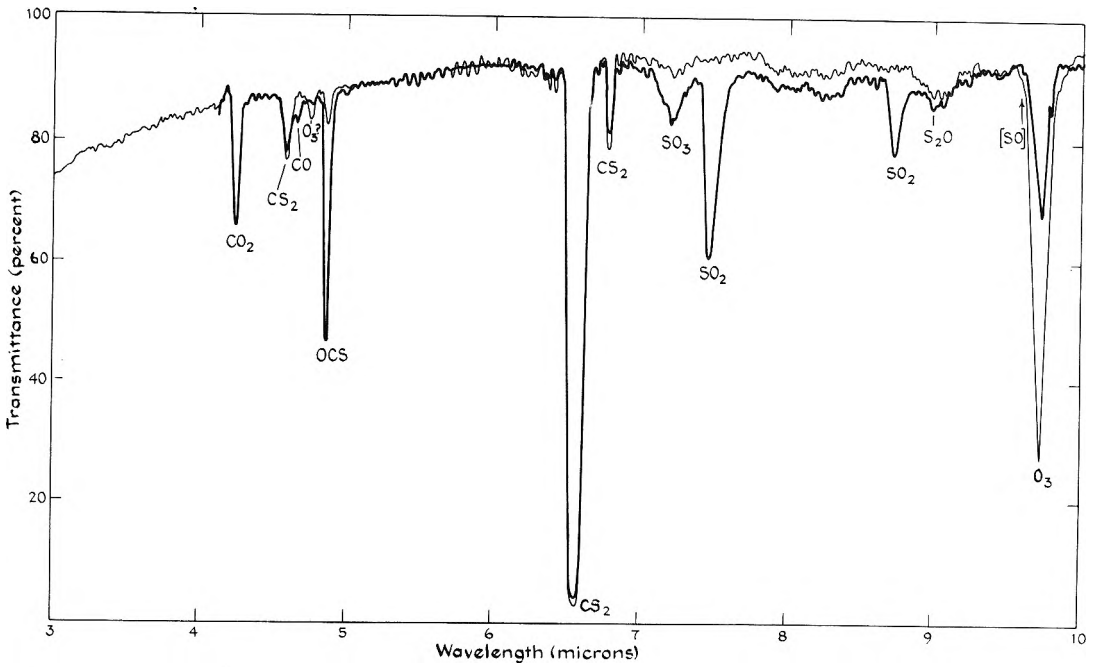

Figure 1. CS_2–O_3 in Xe at 60°K, showing ir trace after laying down sample deposit (light trace) and after photolysis for 5 min, λ 254–260 nm (heavy trace).

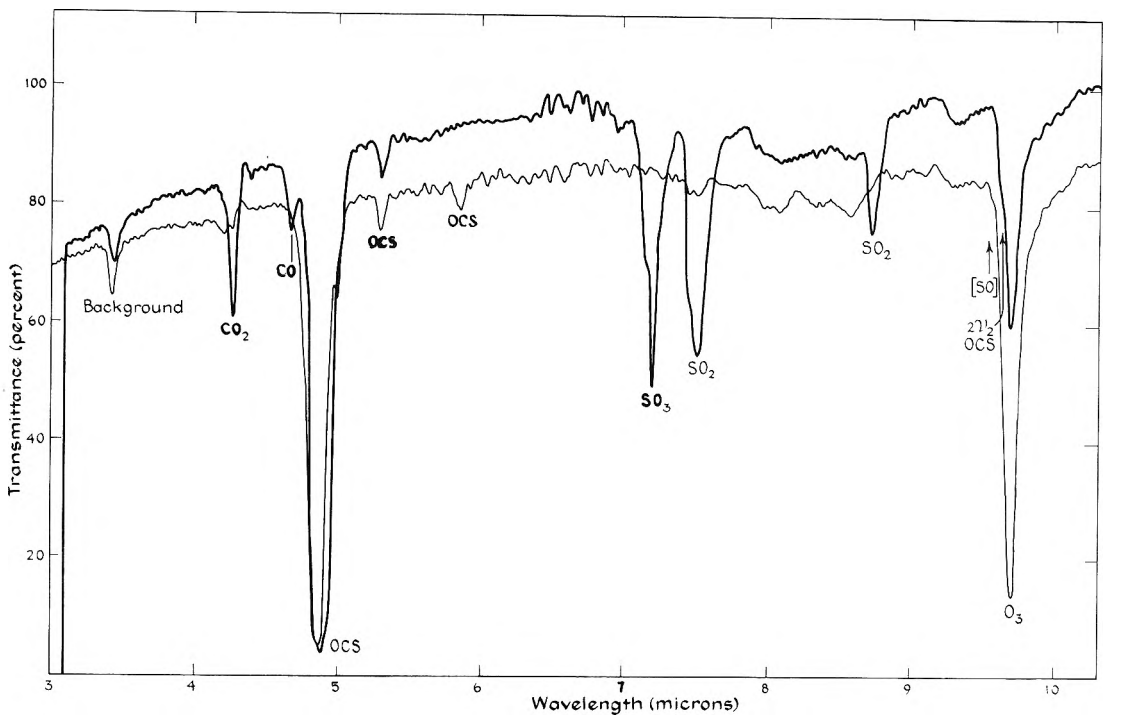

Figure 2. COS–O_3 in Xe at 60°K, showing ir trace after laying down sample deposit (light trace) and after photolysis, λ 254–260 nm (heavy trace).

Discussion

The most striking result in comparing the CS_2–O_3 or OCS–O_3 system with CO_2–O_3 is that no evidence for addition products is encountered with the sulfur-containing reactants. Before the conclusion that such addition products are not formed in the CS_2 and OCS reaction systems can be accepted, the possibilities that the species are formed and are rapidly destroyed or simply escape detection need to be examined.

The possibility that the intermediates, though produced, escape detection as a result of accidental overlapping of the absorption bands by those of species known to be present, is rendered unlikely by (a) the consideration that the spectra of the intermediates should be rich in ir frequencies and (b) by the fact that isotopic substitution failed to resolve structure assignable to addition products.

In investigating the possibility that the intermediates do form but are destroyed efficiently, three mechanisms for destruction must be considered: (1) scavenging by $O(^3P)$ or $O(^1D)$; (2) photochemical decomposition; and (3) thermal decomposition.

Alternative 1 does not explain the failure to observe addition products. $O(^3P)$ reacts efficiently with O_2 even at

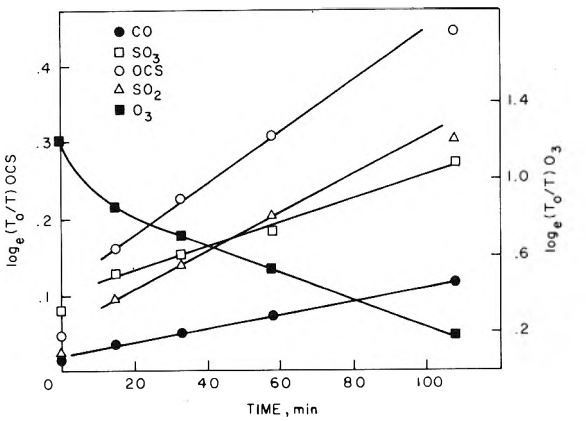

Figure 3. Progress of reactions which occur in mixture of O_3 with CS_2 in xenon at 60°K during photolysis at 260 nm, indicated by plots of ln $(T_0/T)O_3$ *vs.* photolysis time for O_3 and each of the prominent products OCS, SO_2, CO, and SO_3. Quantity ln (T_0/T) related to concentration of particular species where T_0 and T are base and nominal per cent transmittances for infrared band characteristic of that species. Ordinate scale for products on left.

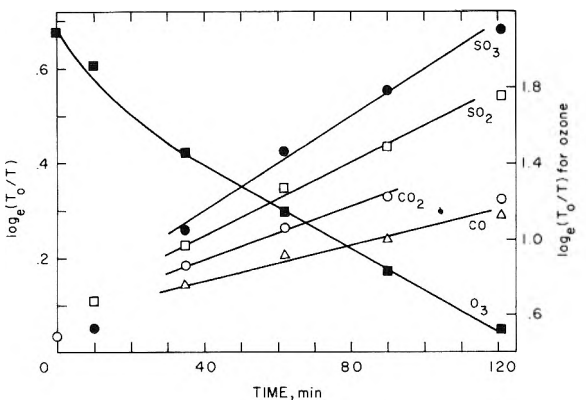

Figure 4. Progress of reactions which occur in mixture of O_3 with OCS in xenon at 60°K during photolysis at 260 nm indicated by plots of ln (T_0/T) *vs.* photolysis time for O_3 and for CO_2, SO_2, CO, and SO_3. Ordinate scale of products on left.

low temperatures, and the specific rate of reaction of $O(^3P)$ with the hypothetical intermediates can hardly be much greater. Thus, the intermediates, if formed and then destroyed by reaction with $O(^3P)$, would be expected to build up to steady-state levels equivalent to O_2 in the matrices. Similar arguments, but now taking account of the efficient reactions of $O(^1D)$ with electron-rich species, can be advanced against selective reaction of $O(^1D)$ with addition products such as COS_2 and CO_2S in the presence of copious amounts of O_3 and CS_2 or OCS.

Alternative 2, presupposing cophotolysis of the intermediates, finds precedent in the CO_3–O_3 system. We have observed[4] that the yield of CO_3 in the CO_2–O_3 system is greatly enhanced when a narrow-band pass filter is used which restricts the photolytic light to the 254–260-nm range, the wavelength region of maximum absorbance for ozone. In the present systems, even using such a filter, and moreover, using various wavelengths for photolysis, no evidence was found for species not already accounted for. It seems highly unlikely that for two different systems, under such a variety of photolysis conditions, addition intermediates would have escaped detection as a result of decomposition by secondary photolysis.

A detailed examination of the requirements which must be met for cophotolysis to account for the failure to observe an intermediate also makes alternative 2 seem very unlikely. The requirements are that the intermediate must have a large extinction coefficient in the 254–260-nm region, that the quantum yield for decomposition be high (*i.e.*, near unity), and that the quantum yield for the photolysis of ozone to produce the intermediates be small. Even making each of these conditions most favorable for cophotolysis, the concentration of the intermediates is expected to be about 5% that of ozone, and that is an amount which is expected to be detectable. (On the basis of observations with CS_2 and OCS, there is no reason to believe that the intensity of ir allowed frequencies would be particularly low for molecules such as COS_2 and CO_2S.) Furthermore, the calculation, favorable to alternative 2, is based on the assumption that O_3 absorbs only a fraction of the light, while, in fact, in most of the experiments, 99% or more of the light was absorbed by ozone.

The alternative that ground-state CO_2S and COS_2 are formed and readily decompose thermally can be set aside on the basis of the following arguments. First, we note that there is no evidence for the intermediates either at 15 or 60°K. Secondly, we note that there is no oxygen scrambling in the OCS–$^{18}O_3$ or ^{18}OCS–O_3 experiments. In analogous experiments in the CO_2–O_3 system is was observed[2,3] that scrambling is complete when CO_2 reacts with $O(^1D)$. Any adduct of $O(^1D)$ to COS_2 or CO_2S is likely to be formed in an excited state and O isotopic scrambling would therefore be expected if the intermediate had an appreciable lifetime.

On the basis of the arguments presented we conclude that decomposition rather than addition (to form ground-state species) is the dominant process when $O(^1D)$ encounters CS_2 or OCS in the matrix.

For CS_2, the spin-allowed reactions

$$CS_2 + O(^1D) = CO(^1\Sigma) + S_2(^1\Delta) \quad (1)$$

and

$$CS_2 + O(^1D) = OCS(^1\Sigma) + S(^1D) \quad (2)$$

are calculated to be exothermic by 115 and 73 kcal, respectively, and the reactions producing S_2 and S in the triplet ground states would be even more exothermic. The above reactions, or the corresponding ones to produce ground state S_2 and S, with reaction 2 dominant, readily account for the major reaction products. A point of interest, and this applies to the OCS system as well, is that SO_2 is not a precursor for the SO_3 produced. Thus, there must be parallel processes for the production of the two oxides of sulfur. If atomic sulfur is mobile in the matrix, the processes for the production of SO_2 and SO_3 can be assumed to be reaction with O_2 and O_3, respectively.

We have already noted that the chemistry of the OCS–$O(^1D)$ system is such that SO_2 is not a precursor to SO_3, and we should note in addition that CO is not a precursor to CO_2 in the OCS–O_3 system. For the decomposition of the $O(^1D)$–OCS encounter complex, the following processes seem the likely possibilities

$$O(^1D) + OCS(^1\Sigma) = CO_2(^1\Sigma) + S \quad (3)$$

$$O(^1D) + OCS(^1\Sigma) = CO(^1\Sigma) + SO \quad (4)$$

When S and SO are in the states (^1D) and $(^1\Delta)$, the reactions are exothermic by 74 and 73 kcal, respectively, and the spin-forbidden processes to form the ground states

would be correspondingly more exothermic. Taking into account the intensity of the product absorption bands, we conclude that reaction 3 is the dominant process in this system. As before, we take S to react with O_2 or with O_3. No evidence was found for the reaction of atomic sulfur with OCS even under the favorable conditions obtaining when OCS is used as matrix host for O_3. In these experiments, some of the light was absorbed by OCS, but this introduced no new reaction products. Other work[9] has shown that there is very little net photodecomposition of OCS, either neat or dispersed, in a rigid inert medium at low temperature using either 228.8- or 253.7-nm light.

The tracer experiments show the isotopic course of reaction 4 to be

$$^*OCS + O(^1D) \longrightarrow C^*O + SO$$

and show that the oxygen in the SO_2 originates in the $O_3(O_2)$ component of the reaction system. This is expected on the basis of the major path assumed for the production of SO_2

$$S + O_2 \longrightarrow SO_2$$

and on the basis of the isotopic course assigned to the minor reaction path (4). The clean isotopic stoichiometry shows that the OCS–$O(^1D)$ encounter complex does not last long enough to bring about scrambling of the oxygen atoms.

Several factors may contribute to the observed differences between the reaction of $O(^1D)$ with CO_2, on the one hand, and with CS_2 and OCS, on the other. First, the reactions of $O(^1D)$ with CS_2 and/or OCS are very exothermic, requiring a large number of collisions to thermalize the adduct. A second consideration rests on the substitution of the heavier sulfur atom for oxygen. Spin–orbit interaction may considerably reduce the forbiddenness of a transition to a dissociative triplet state. DeMore and Raper estimate that in the case of $O(^1D)$ reacting with N_2, only one in about 75 collision complexes are deactivated to produce an N_2O molecule.[10] Also, a study of the formation of CO_2 by the reaction of $O(^1D)$ in liquid CO has led to the conclusion that predissociation of the initially formed collision complex is the dominant process.[11] Since we have observed only products which are attributable to dissociative paths from the reaction of $O(^1D)$ with either CS_2 or OCS, and since sulfur is likely to enhance spin conversion, it is believed that for the collision complex with $O(^1D)$ deactivation of the encounter complex to an oxygen adduct is precluded by dissociation to the triplet sulfur products $S_2(^3\Sigma)$ or $SO(^3\Sigma)$ and $S(^3P)$.

Acknowledgment. Financial support for this research, both for Grant No. GP 5322 and for Jones' Traineeship, 1967–1970, by the National Science Foundation, is gratefully acknowledged.

(9) W. H. Breckenridge, Ph.D. Thesis, Stanford University, 1968.
(10) W. B. DeMore and O. F. Raper, *J. Chem. Phys.*, **37**, 2048 (1962).
(11) O. F. Raper and W. B. DeMore, *J. Chem. Phys.*, **40**, 1053 (1964).

Excited State p*K* Values from Fluorescence Measurements

Nechama Lasser and Jehuda Feitelson*

Department of Physical Chemistry, The Hebrew University, Jerusalem, Israel *(Received August 17, 1972)*

Aromatic acids and bases have often different p*K* values in the excited and in the ground states. Attempts have been made to determine these excited state p*K** values from the fluorescence-pH dependence of the acidic or the basic form of the molecule. Here we show that such data generally do not yield the excited state p*K*, and what often is measured is the rate of the back reaction in $AH^* \rightleftarrows A^{-*} + H^+$. This is shown for riboflavin monophosphate (FMN) by measuring the fluorescence–pH dependence in the presence of various concentrations of Br^- ions. Br^- is a known quencher for the FMN fluorescence and consequently it shortens the FMN* lifetime. Different "p*K**" values, as measured by the FMN fluorescence, are obtained for different Br^- concentrations. This is due to the fact that at shorter lifetimes higher H^+ concentrations are required for the same degree of FMN fluorescence quenching. A similar effect is described for a series of indole derivatives.

It is well recognized now that acids and bases in their excited states are characterized by dissociation constants which could differ by several orders of magnitude from the corresponding ground-state values.[1] The few experimental methods available for the determination of the p*K** values of aromatic molecules in their lower excited singlet state are based mainly on absorption and emission spectra of these molecules.

One method,[1,2] based on thermodynamic considerations and known as the Förster cycle, attributes the difference between the absorption (or emission) peaks of the acidic form and its conjugate base to the difference in p*K* values for the ground and the excited states. This method in-

(1) T. Forster, *Z. Elektrochem.*, **54**, 42 (1950); **54**, 531 (1950).
(2) A. Weller, *Z. Elektrochem.*, **56**, 662 (1952).

volves an approximation; it is assumed that the entropies associated with the ground and excited state dissociations are equal.

An alternative kinetic approach has been developed by Weller,[3] which is based on the pH dependence of the fluorescence of the acid and its conjugate base, respectively. This method is applicable to acids (or bases) in which the prototropic equilibrium is at least partially established within the lifetime of the excited system.

Following Weller's work a number of studies on aromatic systems based on fluorescence measurements have been published. In some of these[4-7] pK^* values were determined by fluorimetric titration of one member of a conjugate acid–base pair, the other member being nonfluorescent. The fluorescence intensity as a function of pH yielded in these cases a sigmoid curve, whose inflection point was considered to correspond to the excited state pK.

The aim of the present study is to show what really is being measured when the fluorescence as a function of pH is recorded for one member of the conjugate acid–base pair, and that these data do not necessarily yield a pK value of the excited state.

Experimental Section

Materials and Solutions. Tryptophan, tryptamine, 3-β-hydroxyethylindole, and tryptophanamide were purissimim grade, and β-aminoindole-3-propanol and FMN (riboflavine-5′-monophosphate sodium salt) were purum grade Fluka (Switzerland) products. N-Acetyltryptophan methyl ester and N-acetyltryptophanamide were obtained from Miles-Yeda (Rehovot) and N-acetyltryptophan from Matheson Coleman and Bell. All other solutes were analytical grade reagents. Triply distilled water was used throughout.

Fresh solutions were prepared before each experiment, so as to minimize photolytic degradation of the substances (which was especially important in the case of FMN).

Absorption spectra were measured on a Cary 14 spectrophotometer.

The fluorescence intensity was measured at right angles to the incident light in an apparatus consisting of a Xe arc, two Bausch and Lomb 500-mm focal length monochromators, an EMI 6256 S photomultiplier, and an EIL electrometer. The apparatus has been described previously.[8] The solutions were of optical density less than 0.1. Spectrosil cells, 1-cm optical path, were used.

FMN containing solutions were excited at λ 375 nm and indole derivatives at λ 280 nm. Since the shape of the fluorescence spectra of both FMN and of the indole derivatives do not change with pH, the peak emission intensity was taken as a measure for the relative quantum yield.

Lifetime measurements were carried out with the aid of an apparatus basically similar to that described by Berlman[9] (Figure 1). The equipment consisted of a nanosecond light pulser (TRW Instrument) with a deuterium lamp of about 4-nsec flash half-width, a Jarrel-Ash Model 82-410 monochromator, a Philips DUVP photomultiplier, a sampling oscilloscope (Tektronix 535 A with 1S1 sampling unit), a Computer of Average Transients (TMC, CAT 400^c), and a X-Y recorder (Electro Instruments Inc.).

The fluorescence intensity as a function of time was measured at right angle to the incident light in 1-cm optical path quartz cells. The optical densities of the solutions in these experiments were between 0.2 and 0.3. Corning

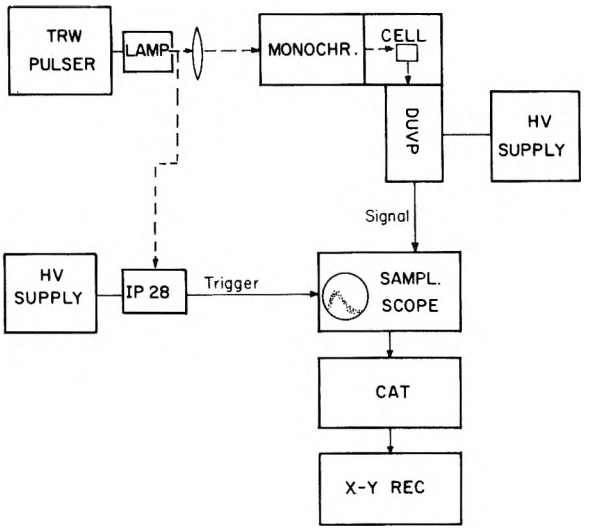

Figure 1. Scheme of lifetime measuring apparatus.

filters (3-73 for FMN and 0-54 for indole derivative solutions) were used to cut off the scattered light from the exciting source. The sampling oscilloscope was triggered by an IP28 photomultiplier which received part of the light flash from the lamp *via* a quartz fiber light guide.

The lifetime was calculated with the aid of the "convolution integral"

$$R(t') = \int_0^{t'} Y(t)P(t' - t)\, dt \qquad (1)$$

in which $R(t')$ is the intensity of fluorescence at a given time t', $Y(t)$ is the intensity of the exciting light at time t, and $P(t' - t)$ is the response function of the experimental system.

Since, in all the systems measured, we could expect an exponential decay (according to a first-order decrease in the number of excited molecules)

$$P(t' - t) = e^{-(t'-t)/\tau} \qquad (2)$$

and therefore

$$R(t') = e^{-t'/\tau} \int_0^{t'} Y(t)e^{t/\tau}\, dt \qquad (3)$$

The values of $R(t')$ and $Y(t)$ as a function of time, which were measured in the apparatus, were fed into a 6400 CDC computer to determine the value of τ which would give the minimum deviation between the experimental and the calculated curves.

Because of the relatively long lifetime of the deuterium lamp, the above procedure results in an increase in the relative error of our measurements as the measured lifetime decreases.

Results

(a) *Quenching Effect of Br^- on FMN Fluorescence.* Halogen ions are known to quench the fluorescence of FMN in the order $I^- > Br^- > Cl^- = F^-$.[10] Since it is

(3) A. Weller, *Progr. React. Kinet.*, **1**, 189 (1961), and references therein.
(4) R. E. Ballard and J. W. Edwards, *Spectrochim. Acta*, **20**, 1275 (1964).
(5) S. Schulman and Q. Fernando, *Tetrahedron*, **24**, 1777 (1968).
(6) S. G. Schulman, *J. Pharm. Sci.*, **60**, 628 (1971).
(7) E. Vander Donckt, *Progr. React. Kinet.*, **5**, 273 (1970).
(8) J. Feitelson, *J. Phys. Chem.*, **68**, 391 (1964).
(9) I. B. Berlman, "Handbook of Fluorescence Spectra of Aromatic Molecules," Academic Press, New York, N. Y., 1965.
(10) H. Theorell and A. P. Nygaard, *Ark. Kemi*, **7**, 205 (1954).

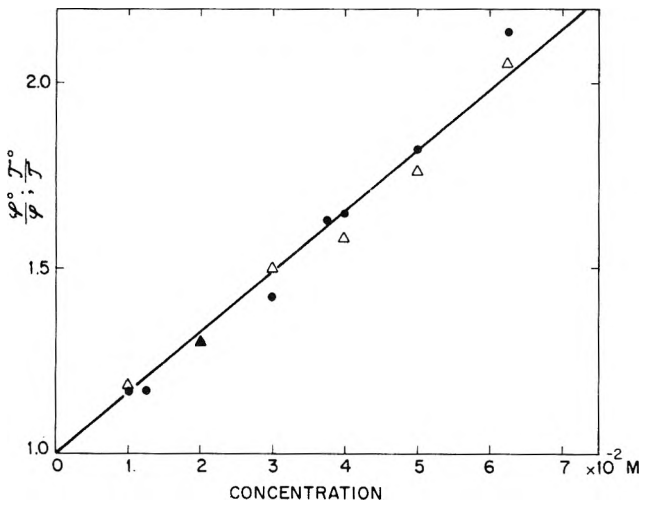

Figure 2. Stern–Volmer plot of the quenching of FMN fluorescence by Br^- ions. Full circles indicate the ratio of quantum yields ϕ^0/ϕ (in absence and in presence of Br^-) from steady-state measurements. Triangles show the same ratio as obtained from the corresponding lifetime measurements (τ_0/τ).

much more convenient to work with Br^- than with I^- solutions, we studied the character of the quenching process by this ion.

It had been assumed that the quenching of FMN fluorescence by Br^- ions is a static process,[10] *i.e.*, that a nonfluorescent complex (in this case 1:1) between the Br^- ion and the FMN molecule in its ground state is formed. It follows that fewer of the absorbing FMN molecules will be able to emit light, *i.e.*, the quantum yield will decrease. However, the lifetime of the excited molecule should be independent of the quencher concentration, and would equal the lifetime in the absence of a quencher.

On the other hand, dynamic quenching of excited molecules is characterized by a parallel decrease in lifetime and quantum yield of the fluorescence as a function of the quencher concentration. This was found to be the case for the quenching of FMN fluorescence by Br^- ions, and contrary to the earlier assumption therefore, FMN is quenched by Br^- in dynamic process. From steady-state kinetics the reciprocal relative fluorescence $-\phi^0/\phi$ plotted against quenching substance (Br^-) concentration (Figure 2), *i.e.*, the Stern–Volmer equation,[11] yields a quenching constant $k_{Br^-} = (17 \pm 1)\ M^{-1}$.

(b) *Quenching Effect of H^+ on FMN Fluorescence.* The quenching of FMN fluorescence by H^+ was studied by Weber in HCl solutions.[12] It was found that this process too is a dynamic one. We confirmed this conclusion by direct measurements of the fluorescence lifetimes of FMN, as a function of H^+ concentration, using $HClO_4$ as the acid. The results, which are an average from several measurements, are shown in Table I.

These data were then used to obtain the Stern–Volmer constant for the quenching of FMN by H^+ ions from lifetime measurements. By plotting τ_0/τ against $[H^+]$ (where τ_0 is the FMN lifetime in absence of H^+ ions), one obtains $k_H = (85 \pm 5)\ M^{-1}$.

(c) *Quenching of FMN Fluorescence by H^+ Ions as a Function of Br^- Ion Concentration.* As shown above, both Br^- and H^+ could be used to shorten the lifetime of the FMN fluorescence. However, in the presence of both ions, we had to make sure that H^+ and Br^- interact independently with excited FMN molecules. In other words, the reaction rate constant between FMN* and Br^- is not influenced by the presence of the acid in the solution and *vice versa*.

TABLE I: Lifetime of FMN as a Function of H^+ Ion Concentration

τ, nsec	$[H^+]$, M	τ, nsec	$[H^+]$, M
4.5 ± 0.1[a]		1.4 ± 0.3	3.3×10^{-2}
4.1 ± 0.2	10^{-3}	<1.0	6.6×10^{-2}
3.1 ± 0.2	5×10^{-3}	<1.0	10^{-1}
2.5 ± 0.3	10^{-2}		

[a] The value of 4.5 ± 0.1 nsec for FMN in neutral solution agrees with 4.6 nsec as measured by A. Bowd, D. Byron, J. B. Hudson, and J. K. Turnbull, *Photochem. Photobiol.*, 11(6), 445 (1970).

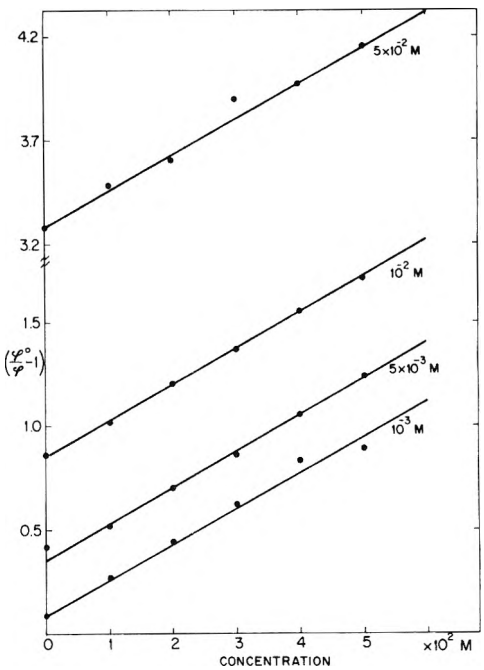

Figure 3. Stern–Volmer plots of the quenching of FMN fluorescence by Br^- ions in presence of various concentrations of H^+ ions ($[H^+] = 10^{-3}, 5 \times 10^{-2}, 10^{-2}, 5 \times 10^{-2}\ M$).

Under these conditions, steady-state kinetics leads immediately to

$$\frac{\tau_0}{\tau} = \frac{\phi^0}{\phi} = 1 + k_H c_{H^+} + k_{Br} c_{Br^-} \qquad (4)$$

where τ_0 and τ are the lifetimes and ϕ^0 and ϕ the quantum yields in absence and in presence of quencher. k_H and k_{Br} are the Stern–Volmer constants for H^+ and Br^- ions, respectively.

Equation 4 predicts that, using, for example, a constant concentration of H^+ ions, a plot of ϕ^0/ϕ as a function of Br^- ion concentration will give a straight line, the slope of which is k_{Br^-}, while its intercept is a measure for k_H. Figure 3 shows such plots for a number of concentrations of H^+. One sees that the lines are parallel to each other, with a slope of $k_{Br} = (17 \pm 1)\ M^{-1}$.

A similar plot for constant concentrations of Br^- and variable H^+ ion concentrations yields also a series of parallel lines, the slope of which is constant and equals $k_H = (85 \pm 5)\ M^{-1}$. The same values for k_H and k_{Br} were obtained by direct lifetime measurements (see eq 4) as a function of Br^- and H^+ ion concentrations as shown in

(11) O. Stern and M. Volmer, *Phys. Z.*, **20**, 183 (1919).
(12) G. Weber, *Biochem. J.*, **47**, 114 (1950).

TABLE II: Comparison of Lifetimes Obtained by Direct Measurements and from Steady-State Fluorescence Quenching by Eq 4[a]

$[Br^-]$, M	5×10^{-2}	3×10^{-2}	10^{-2}
τ_{meas}, nsec	1.9 ± 0.2	2.3 ± 0.2	2.7 ± 0.2
$\tau_{std\ st}$, nsec	2.0	2.3	2.8

[a] H^+ ion concentration was 5×10^{-3} M in all experiments.

Table II. We therefore conclude that Br^- and H^+ ions interact independently with excited FMN molecules.

Figure 4 shows the pH dependence of the FMN fluorescence at various Br^- ion concentrations. The data are normalized to equal quantum yields for high pH values. We denote that pH at which the fluorescence drops to half its value from that at high pH by "pK^* apparent."

(d) *Quenching of Indol Derivative Fluorescence by H^+ Ions.* Relative fluorescence yields as a function of $HClO_4$ concentrations were measured for several indol derivatives in the concentration range between 10^{-3} and 1 M acid.

Again, as with FMN, a plot of ϕ^0/ϕ against H^+ concentration yields the Stern–Volmer constant for the interaction between the excited indole derivative and the proton. It was found that except for very high acid concentrations (>0.5 M) $|(\phi^0/\phi) - 1|/[H^+] = k_H$ is constant over the whole pH range.

These constants for a variety of indole derivatives are presented in Table III. This table also shows the relative quantum yields with respect to β-hydroxyethylindole (which we used as a standard) and the fluorescence lifetimes of these compounds. From the Stern–Volmer constants, we can calculate the H^+ concentration at which the fluorescence intensity decreases to 50% of its value in neutral solutions, $[H^+]_{50\%}$. These $pH_{50\%}$ values or apparent pK^* values are also shown in Table III for the different indole derivatives.

Discussion

In acid–base dissociation equilibria

$$HA + H_2O \underset{k_{-1}}{\overset{k_1}{\rightleftharpoons}} H_3O^+ + A^-$$

the rate of the "back reaction" is usually diffusion controlled, with a bimolecular rate constant k_{-1} in the 10^{10} M^{-1} sec^{-1} range. It follows that the dissociation constant of HA is primarily determined by the rate constant of the forward reaction, k_1. If the dissociation takes place in the excited singlet state the following scheme applies

$$\begin{array}{ccc} H_2O + AH^* & \underset{k_{-1}^*}{\overset{k_1^*}{\rightleftharpoons}} & A^{-*} + H_3O^+ \\ \updownarrow k_f' + k_d' & & \updownarrow k_f'' + k_d'' \\ H_2O + AH & \underset{k_{-1}}{\overset{k_1}{\rightleftharpoons}} & A^- + H_3O^+ \end{array} \qquad (5)\ (6)$$

where k_f and k_d are the rate constants for fluorescence and for the other deactivation steps which compete for the excited molecule, because of the various reactions taking place during the singlet lifetime of 10^{-9}–10^{-8} sec. The above equilibrium is never fully established. Nevertheless, if both moieties AH* and A^-* are fluorescent the dissociation constant can be computed as shown by Weller[3] from the pH dependencies of the two fluorescence quantum yields. We shall now enquire whether it is possible to obtain the K^* value in those cases where only one of the two forms, HA* or A^-*, is fluorescent which means that the other form usually has a lifetime of $\tau < 5 \times 10^{-11}$ sec.

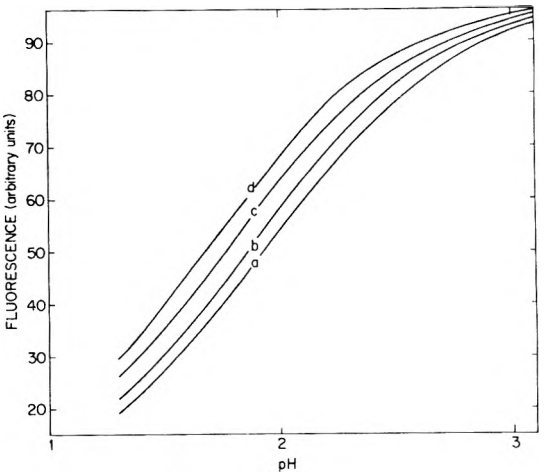

Figure 4. FMN fluorescence intensity as a function of pH for various Br^- ion concentrations: $[Br^-] = 0.0$ M (a), 0.01 M (b), 0.03 M (c), 0.05 M (d).

The Acidic Form HA Only is Fluorescent.* This means that $k_d'' \gg k_f''$ and the lifetime of A^-* is so short that the association reactions A^-* + H_3O^+ cannot take place. The forward dissociation reaction AH* + H_2O → is pH independent and therefore the pH dependence of the AH* fluorescence will be determined by the ground-state AH concentration and will therefore follow the ground-state titration curve. The excited state pK^* will only determine the absolute fluorescence quantum yield of AH* in that the lower the pK^* the faster does the dissociation take place and the shorter the lifetime of AH* will be.

The Basic Form A^- Only is Fluorescent.* The molecular systems described in this study all belong to this class of compounds. Here the concentration of A^- ions which are excited at a given pH is determined by the degree of dissociation of the HA molecules in the ground state. If the ground-state pK is sufficiently low, A^- ions can be excited in the presence of a comparatively high H^+ ion concentration. The fluorescence of A^-* will then be at least partly quenched due to the back reaction A^-* + H_3O^+ (eq 5). In such a case, therefore, the fluorescence yield of A^-* at low pH will be smaller than in the high pH region and the fluorescence *vs.* pH curve will be displaced toward higher pH values when compared to the ground-state titration curve. This shift in the fluorescence–pH curve is in fact a measure of the rate of protonation $k_{-1}[H^+]$ (eq 5) and of the lifetime of A^-*, but it is entirely independent of the dissociation of (the very short lived) HA*. If the ground-state pK is higher, say pK > 2 or 3, the available H^+ ion concentration might become too small for protonation to occur during the lifetime of the excited A^-*. The fluorescence will then follow the ground-state titration curve.

We see that in all the cases discussed the fluorescence of either the acidic or the basic form of a molecule alone is insufficient to determine pK^*.

In the above two cases where excited state pK^* values are apparently obtained we can show that the data do not really represent the dissociation constant. The pH dependence of the fluorescence of FMN shows an inflection point from which Schulman[6] has concluded that pK^* = pK + 1.7. In the Results section we have shown that

TABLE III: Quenching of Indole Derivative Fluorescence by H^+ Ions

Indole derivative	Relative[a] quantum yield	Measured lifetime	Stern-Volmer constant k, M^{-1}	pK_{app}	$\phi_{HEI}{}^b/\phi$	$k_{HEI}{}^c/k$	$\frac{k_{HEI}/k}{\phi_{HEI}/\phi}$
1 3-β-Hydroxyethyl-indole	1	7.7 ± 0.2	110	2			
2 *N*-Acetyltryptophan-amide	0.37	2.7 ± 0.2	28	1.77	2.68	3.95	1.47
3 *N*-Acetyltryptophan methyl ester	0.17	<1.0	11.5	1.26	5.95	9.6	1.6
4 *N*-Acetyltryptophan[d]	0.25		22	1.35	4	5	1.25
5 L-Trytophanamide HCl	0.23	1.7 ± 0.2	6.5	0.86	4.3	17	3.95
6 Tryptamine	0.72	5.2 ± 0.2	29.3	1.47	1.385	3.89	2.83
7 β-Aminoindole-3-propanol	0.58	4.0 ± 0.2	22	1.35	1.73	5	2.89
8 Tryptophan	0.37	2.7 ± 0.2					
9 Indole[e]				2.1			
10 1-methylindole[e]				1.8			
11 2-methylindole[e]				1.2			

[a] The quantum yield of compound **1** was arbitrarily taken to be unity. [b] ϕ_{HEI}, quantum yield of compound **1**. [c] k_{HEI}, Stern-Volmer constant for the quenching of compound **1** fluorescence by H^+. [d] The acidic form of compound **4**. [e] From ref 7.

quenchings of FMN fluorescence by both H^+ ions and Br^- ions are dynamic processes which are characterized by Stern-Volmer constants. If these fluorescence quenching data are displayed on a fluorescence *vs.* pH plot, a sigmoidal curve similar to a titration curve is obtained. That the apparent pK^* as derived from this curve is simply due to quenching by H^+ ions is seen from the fact that in the presence of different Br^- ion concentrations different pK^* values are obtained (see Figure 4). Each of the two ions, H^+ and Br^-, quenches the fluorescence of FMN* separately and thereby decreases its lifetime. It follows that at a given Br^- concentration a higher H^+ concentration is required to attain a certain degree of quenching. This in turn results in a shift of the above sigmoid curve toward lower pH yielding a lower apparent pK^* value. From here we deduce that in fact FMN belongs to the compounds whose A* form only fluoresces and in fact the true pK^* might be lower (as required by the Förster cycle) or higher than the ground-state pK. The value of pK^*, however, cannot be deduced from these measurements.

The indole derivatives in Table III have a similar absorption and fluorescence spectra but they differ widely in their quantum yields and lifetimes. Vander Donckt[7] has concluded that the 3 position of indole can become protonated upon excitation of the molecule. The ordinary indole therefore can be looked upon as the anion of this (protonated) acid and from the pH dependence of its fluorescence he has derived pK^* values for substances **9**, **10**, and **11** of Table III.

All the compounds in Table III have identical chromophores and their excited state pK^* values should therefore be very similar. The differences in their fluorescence quantum yields are due to quenching through interactions with the terminal groups of the aliphatic side chain.[13] These differences in quantum yields are reflected in the lifetimes which show that the quenching by the side chains is a dynamic process.

The indole ring is also quenched by protons. This is seen both in steady-state and in direct lifetime measurements which show that this quenching too is a dynamic process. Since all the compounds in Table III are quite similar we can assume that their rate constant for association with H^+ ions, k_{-1}^* (eq 5), if diffusion controlled, will be of the same magnitude for all of them. The Stern-Volmer quenching constant $k_H = k_{-1}^*\tau_0$ should then be determined solely by τ_0, the excited state lifetime in the absence of protons. In this case, however, a "built in" quencher, the amino acid side chain is present and no external quenching agent like Br^- ions for FMN is required. As in FMN the shorter the lifetime the higher a H^+ ion concentration would be required to attain 50% quenching, the point which determines the apparent excited state pK^* value. This is indeed borne out in Table III. For k_{-1}^* in the 10^{10} M^{-1} sec^{-1} range and τ_0 values of 2–8 nsec the above proton concentration would be 10^{-2}–10^{-1} M. Therefore the curves in Figure 5 will yield pK_{app}^* values of between 1 and 2 in all cases as indeed is seen to occur in Table III.

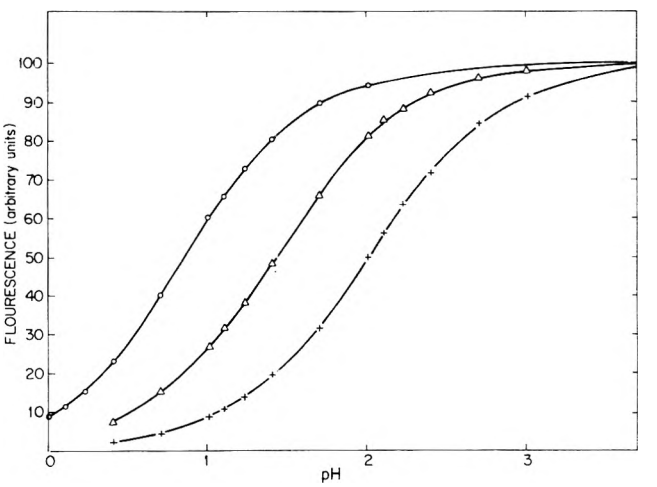

Figure 5. Fluorescence intensity of indole derivatives as a function of pH: +, β-hydroxyethylindole, Δ, *N*-acetyltryptophanamide; O, 1-tryptophanamide hydrochloride.

(13) J. Feitelson, *Isr. J. Chem.*, 8, 241 (1970).

Again, as with FMN, these values do not represent the true excited state pK^* but must be attributed to the quenching reaction only.

With respect to the indole derivatives one discrepancy should be noted. If our assumptions are correct then since $k_q = \tau_0 k_{-1}^*$ the ratio of any directly measured lifetime to that of another substance should equal the ratios of their quenching constants. In Table III the reference compound is β-hydroxyethylindole (HEI) and we see that for substances 2, 3, and 4 the agreement is fairly good. For compounds 5 to 7 however k_{HEI}/k is too large. However it should be noted that the latter compounds all carry an ionized $-NH_3^+$ group. We feel therefore that the above discrepancy might be attributed to a lower rate constant for the reaction between H^+ and the positively charged indole derivative.

Fluorescence Lifetimes of Neodymium-Doped Glasses and Glass–Ceramics

Charles F. Rapp[1]

Owens-Illinois, Corporate Research Laboratories, Technical Center, Toledo, Ohio

and John Chrysochoos*

Department of Chemistry, The University of Toledo, Toledo, Ohio 43606 *(Received December 11, 1972)*

Publication costs assisted by Owens-Illinois

The fluorescence lifetimes of Nd^{3+} in neodymium-doped glass-ceramics are much shorter than the lifetimes in neodymium-doped glasses under comparable Nd^{3+} concentrations, although the absorption and emission spectra are identical. These results indicate that the neodymium ions are excluded from the crystalline phase of the glass-ceramic and they are entirely accumulated in the glassy phase. Under these conditions shorter lifetimes result due to enhanced concentration quenching. The self-quenching rate in the glasses varies linearly with the $[Nd^{3+}]^2$ which is proportional to $1/R^6$. This dependence may imply either a dipole–dipole type of energy transfer or a rapid energy migration to "ion pairs" in which energy may dissipate by exchange interactions.

Introduction

It has been shown recently that lasing action can be obtained from a transparent neodymium-doped glass–ceramic.[2] The glass–ceramic is a two-phase material, whereas almost all previous solid-state laser materials have been either single crystals or glasses.

Since the glass–ceramic is a two-phase material, a significant question arises regarding the distribution of the neodymium ions between the crystalline and the residual glassy phases and the effect of such a distribution upon the emission characteristics of the Nd^{3+} ions. A preferential segregation of the neodymium ions into one of the two phases would be accompanied by an increase in the concentration quenching of the Nd^{3+} fluorescence. To gain some insight into this question, the fluorescence lifetimes of Nd^{3+} were measured in neodymium-doped glasses and in glass–ceramics at various extents of crystallization.

Experimental Procedures

The base composition, in mole percentages, of the glasses and the glass–ceramics used is SiO_2 73.24%, Al_2O_3 13.73%, Li_2O 8.69%, BaO 1.75%, TiO_2 1.51%, and ZrO_2 1.08%. Melts were prepared containing 0.097, 0.189, 0.361, 0.550, and 0.907% Nd_2O_3 which replaces SiO_2. The glasses were melted at 1600° and they were annealed. Small samples, 2 in. × ⅞ in. × 0.25 in., were cut and were given additional one- and two-stage heat treatments to produce glass–ceramics with up to 70% crystallinity. An X-ray diffraction pattern was obtained for each of the heat-treated samples to identify the phases present and to determine their contribution to the composition of the glass-ceramic. The main crystalline phase present, in addition to a small quantity of cubic ZrO_2, was a high-quartz solid-solution phase.[2-4] The percentage of the glass remaining in each sample was estimated by comparing the intensity of the broad maximum in the diffraction pattern of the glass-ceramic to that for the original glass.[5a] The fluorescence lifetimes were measured by exciting the samples with a xenon flashlamp and by photographing the oscilloscope display of the intensity of fluorescence *vs.* time. The duration of the xenon flash was about 20 μsec.

Results and Discussion

As it is commonly observed with neodymium-doped glasses,[5b] the fluorescence decays in the systems studied

(1) This work is based in part on a thesis submitted in partial fulfillment of the Ph.D requirement at the University of Toledo.
(2) C. F. Rapp and J. Chrysochoos, *J. Mater. Sci.*, **7**, 1090 (1972).
(3) S. Ray and G. M. Muchow, *J. Amer. Ceram. Soc.*, **51**, 678 (1968).
(4) R. Roy, *Z. Kristallogr.*, **111**, 185 (1959).
(5) (a) S. M. Ohlberg and D. W. Stricker, *J. Amer. Ceram. Soc.*, **45**, 170 (1962); (b) E. Snitzer and C. G. Young, "Lasers," Vol. 2, A. K. Levins, Ed., Marcel Dekker, New York, N. Y., 1963, p 202.

TABLE I: Fluorescence Lifetimes of Neodymium-Doped Glasses and Glass-Ceramics

Mol % Nd_2O_3	Nd^{3+}, M	% glass	τ at $\frac{1}{2}I_{20}$, μsec
0.097	0.073	100	415
0.097	0.073	40	348
0.189	0.141	100	380
0.189	0.141	98	358
0.189	0.141	40	239
0.189	0.141	45	254
0.189	0.141	40	243
0.189	0.141	55	291
0.189	0.141	40	253
0.189	0.141	40	241
0.189	0.141	35	245
0.189	0.141	30	224
0.361	0.269	100	316
0.361	0.269	95	347
0.361	0.269	80	302
0.361	0.269	40	155
0.550	0.411	100	229
0.907	0.672	100	134

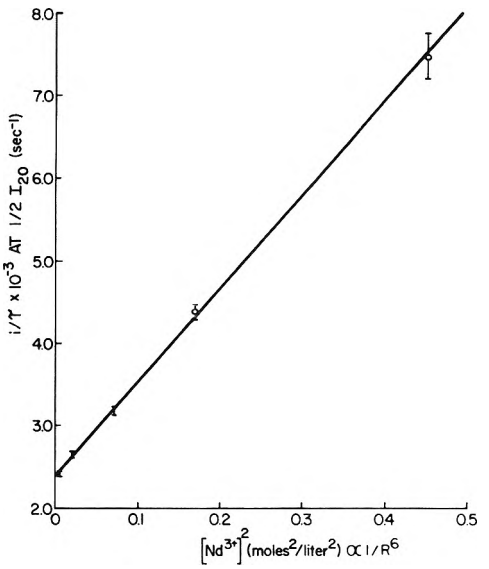

Figure 1. Dependence of the reciprocal fluorescence lifetimes of Nd^{3+}, measured at $\frac{1}{2}I_{20}$, upon the square of the concentration of Nd^{3+} in neodymium-doped glasses.

were not simple exponentials. Therefore, to obtain a decay time characteristic of the "average" ion, the fluorescence lifetimes were measured at the time at which the fluorescence intensity had decayed to one-half of I_{20} where I_{20} represents the fluorescence intensity at 20 μsec after the initiation of the flash. Results obtained in this way for various glasses and glass-ceramics are given in Table I.

The fluorescence lifetimes of Nd^{3+} decrease as the concentration of the rare earth ion increases. This was observed in all glasses and glass-ceramics employed. This is known as concentration quenching and it is attributed[6] to a nonradiative exchange of energy between an excited Nd^{3+} ion in the metastable $^4F_{3/2}$ state and a neighboring Nd^{3+} ion in the $^4I_{9/2}$ ground state. The energy exchange is of the type

$$Nd^{3+}\ (^4F_{3/2}) + Nd^{3+}\ (^4I_{9/2}) \rightarrow 2Nd^{3+}\ (^4I_{15/2}) \rightsquigarrow 2Nd^{3+}\ (^4I_{9/2})$$

It has also been suggested that the transition $^4F_{3/2} \rightarrow {}^4I_{13/2}$ coupled with the transition $^4I_{9/2} \rightarrow {}^4I_{15/2}$ may contribute to the quenching process.[7] Although there has been considerable uncertainty regarding the energy transfer mechanism,[8] *i.e.*, dipole-dipole, dipole-quadrupole, etc., it has been observed that the rate of quenching increase linearly with the square of the neodymium concentration.[7,9] This would imply a dependence of the quenching rate upon $1/R^6$ which in turn may indicate energy transfer *via* a dipole-dipole interaction.[10,11]

A very strict dependence of the quenching rate upon the square of the neodymium concentration was observed in this study for all neodymium-doped glasses. This dependence is shown in Figure 1 where $1/\tau$ (the reciprocal of the fluorescence lifetime) is plotted *vs.* $[Nd^{3+}]^2$. Since the square of the neodymium concentration is proportional to $1/R^6$, where R is the distance between two Nd^{3+} ions, it may appear that the quenching rate varies linearly with $1/R^6$. Therefore, one could speculate that these results imply a correlation between the self-quenching process and a dipole-dipole type of energy transfer. However, it should be pointed out that there is an alternative interpretation for the linear dependence of the quenching rate upon the square of the neodymium concentration. If the resonant energy transfer from one neodymium ion to a neighboring one (which will be excited to the $^4F_{3/2}$ state) is sufficiently rapid, the quenching rate will be proportional to the number of neodymium ions which have another neodymium ion as a nearest neighbor in the glass (not considering the anion positions). Therefore, the excitation energy will migrate from neodymium to neodymium until it reaches a neodymium "pair." The rate of quenching will be proportional to the concentration of such pairs which in turn will be proportional to the square of the neodymium concentration. Since it has been reported that the resonant energy transfer is completed in nanoseconds[12] for Nd^{3+}, such an interpretation is possible. This effect has been observed experimentally[13] in the quenching of Eu^{3+} fluorescence by Nd^{3+}. In the case of different donor and acceptor ions, the number of pairs, and therefore the quenching rate, are proportional to the first power of the quencher concentration. In the case in which both the donor and the acceptor are the same species, the number of pairs will be proportional to the square of the concentration.

The neodymium absorption spectra in the glasses and in glass-ceramics were nearly identical. No differences were found between the line widths of the neodymium absorption bands in the two materials. This would imply that the neodymium ions are excluded from the crystalline phase and are accumulated in the residual glassy phase of the glass-ceramic. Narrowing of the absorption lines should be observed if the neodymium ions were entering the crystalline phase (decreased inhomogeneous line broadening).

(6) G. E. Peterson and P. M. Bridenbaugh, *J. Opt. Soc. Amer.*, **54**, 664 (1964).
(7) L. G. Van Uitert, E. F. Dearborn, and J. J. Rubin, *J. Chem. Phys.*, **47**, 547 (1967).
(8) J. S. Stroud, *Appl. Opt.*, **7**, 751 (1968).
(9) W. W. Holloway, Jr., and M. Kestigian, *J. Chem. Phys.*, **43**, 147 (1965).
(10) T. Foerster, *Z. Naturforsch. A*, **4**, 321 (1949).
(11) D. L. Dexter, *J. Chem. Phys.*, **21**, 836 (1953).
(12) D. K. Duston, Thesis, Rensselaer Polytechnic Institute, 1969.
(13) L. G. Van Uitert, E. F. Dearborn, and J. J. Rubin, *J. Chem. Phys.*, **46**, 420 (1967).

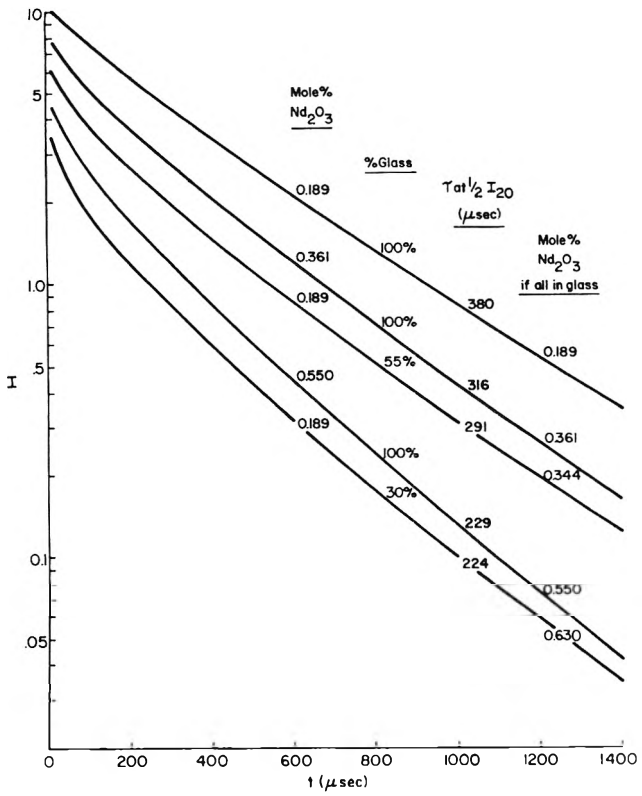

Figure 2. Fluorescence decay in neodymium-doped glasses and glass-ceramics.

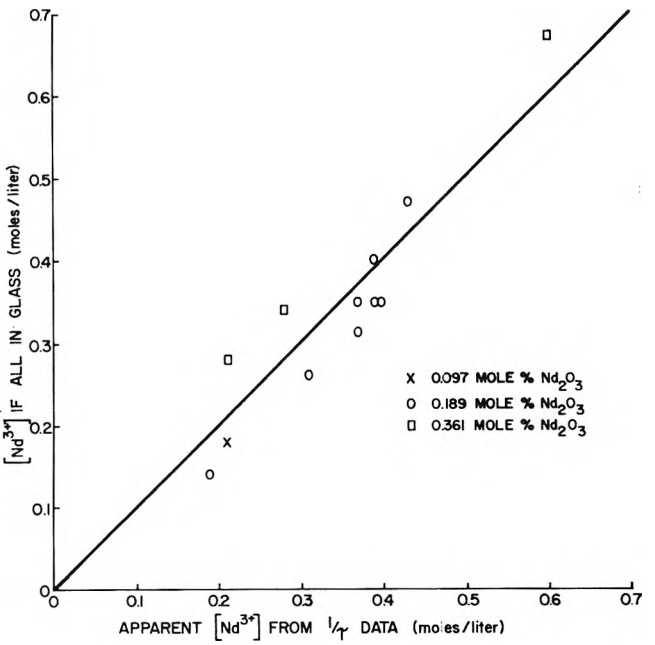

Figure 3. Correlation between the apparent neodymium concentrations obtained *via* the observed fluorescence lifetimes and Figure 1 and the calculated neodymium concentration assuming that the neodymium ions are excluded from the crystalline phase of the glass-ceramic. Solid line represents a theoretical correlation with slope equal to unity.

Any segregation of the neodymium ions in the glass-ceramic should also be accompanied by an increase in the rate of concentration quenching because of the decreased Nd-Nd distance. This would result in a decrease in the fluorescence lifetime. Since the neodymium absorption spectra are identical in both materials, the neodymium transition probabilities and the energy overlap of the transitions involved in the quenching process would be the same in both materials. Therefore, any differences observed in the fluorescence lifetimes of the two materials could only be the result of different neodymium concentrations. If it were assumed that all the neodymium ions were segregated into the glassy phase present in the glass-ceramic, a local neodymium concentration could be calculated from the percentage of the glass present. Figure 2 depicts plots of log I *vs.* t for several glass and glass-ceramic samples with different total $[Nd^{3+}]$ and calculated local $[Nd^{3+}]$. As it can be seen in the figure, the fluorescence lifetimes of the glass-ceramics are in close agreement with the lifetimes expected for their calculated local neodymium concentrations. For example, the lifetimes in a 100% glass containing 0.550 mol of Nd_2O_3 and in a glass-ceramic with 30% glass containing 0.189 mol of Nd_2O_3 are almost the same (229 and 224 μsec).

From the fluorescence decay times of the glass-ceramics and from Figure 1, it is also possible to determine "apparent" neodymium concentrations for the glass-ceramics, that is, neodymium concentrations which should produce the observed decay times. If all of the neodymium ions were being segregated into the glassy phase of the glass-ceramic, these apparent neodymium concentrations should be the same as those calculated from the per cent glass in the glass-ceramics. A correlation between the values obtained *via* both ways is shown in Figure 3. A fairly straight line is obtained with a slope equal to one. It should be pointed out that the percentage of glass can be determined with an accuracy of ±5 to ±10%.

It appears from these data on absorption and decay times that all or nearly all of the neodymium ions in the Li_2O-Al_2O_3-SiO_2 based glass-ceramics are entering the residual glassy phase.

The present data are not sufficient in distinguishing between the dipole-dipole interaction or the participation of neodymium pairs in the concentration quenching of the fluorescence of neodymium. Studies along these lines are under way.

Carbon Monoxide Adsorption on Magnesium Oxide

R. St. C. Smart,[1a] T. L. Slager,[1b] L. H. Little,*[1a] and R. G. Greenler[1b]

School of Chemistry, The University of Western Australia, Nedlands, Western Australia, 6009 and Laboratory for Surface Studies and Department of Physics, University of Wisconsin—Milwaukee, Milwaukee, Wisconsin 53201 *(Received October 12, 1972)*

The adsorption of carbon monoxide onto magnesium oxide was investigated. The formation of surface carbonate groups was observed on samples prepared in high vacuum while added oxygen was necessary for carbonate formation with magnesium oxide subject to more vigorous outgassing in ultrahigh vacuum. Carbon dioxide produced similar carbonate species to that formed by carbon monoxide.

Introduction

Several spectroscopic investigations of the adsorption of carbon monoxide on oxide surfaces have shown that surface carbonate-type species are formed on the surface.[2] In many instances the surface species produced are identical with those obtained in the adsorption of carbon dioxide. In order to investigate the possible origin of the additional oxygen needed to convert carbon monoxide to adsorbed carbonate radicals an infrared spectroscopic study has been made of the adsorption of carbon monoxide onto magnesium oxide samples prepared under different conditions of evacuation. In one set of experiments, adsorption studies were made on samples prepared in a system capable of producing 10^{-5} Torr, while in another an ultrahigh vacuum system producing 10^{-8}–10^{-9} Torr was employed. In the latter experiment it was found that carbon monoxide did not produce the typical spectra of adsorbed carbonate surface species unless additional oxygen was supplied to the system.

The adsorption of carbon dioxide on magnesium oxide was used in the work as a basis for comparison of the species produced by adsorbed carbon monoxide. Evans and Whateley[3] have recorded infrared spectra from 4000 to 700 cm^{-1} of various coordinated carbonate species from carbon dioxide adsorbed on magnesium oxide at temperatures in the range 20–500°. They have also investigated the interaction of adsorbed carbon dioxide with water and deuterium oxide. The spectrum of carbon dioxide adsorbed at room temperature is complex and at present is not fully understood. It is apparent, however, that the method of preparation of the surface, influencing the degree of dehydroxylation of the surface, has a considerable effect on its adsorptive properties. The studies of Evans and Whateley were carried out on a surface prepared at 850°, corresponding to a substantially dehydroxylated surface. The work described here shows the effect on the infrared spectrum of carbon dioxide adsorbed on samples not subjected to extreme dehydroxylation.

Experimental Section

10^{-5} Torr Experiments. Magnesium oxide was obtained by decomposition at 600° in air for 3 hr of precipitated magnesium hydroxide prepared from AR reagents. Pellets of the oxide were prepared and immediately placed in the infrared cell which was evacuated promptly to minimize adsorption of atmospheric carbon dioxide. The infrared cell employed in this study was described by Cant and Little.[4] Before adsorption was commenced the sample was heated in oxygen for 0.5 hr at 400° and evacuated at 450° for 2.5 hr at 10^{-5} Torr. Under this treatment the sample surface was substantially hydroxylated as shown in its spectrum.

Pressures between 20 and 200 Torr of carbon monoxide and carbon dioxide were employed. All spectra were recorded using a Perkin-Elmer 521 spectrophotometer. The cell used in the adsorption studies was connected directly to a vacuum line enabling all evacuation, heating, and adsorption processes to be carried out in the infrared beam. A similar sample, pretreated in the same manner as the adsorbent, was set up in the reference beam of the spectrometer. Both cells were connected to the vacuum line and evacuated similarly. Carbon monoxide or carbon dioxide was admitted to the cell in the sample beam and an equal pressure of helium was admitted to the reference cell to balance any difference in the thermal emission from the compensating sample.

Exchange of the surface hydroxyl groups was effected by admitting deuterium oxide for 0.5 hr at 80° then evacuating at 300° for 1 hr. A second admission of D_2O was made to achieve more complete exchange.

10^{-8}–10^{-9} Torr Experiments. The infrared spectra in this section of the work were recorded with a Beckman IR9 spectrometer under conditions giving a resolution of 1 cm^{-1}. The vacuum system was constructed of stainless steel using a 1.5-in. disk of Irtran II (Eastman Kodak) as infrared windows. These windows were attached to the vacuum system as described by Kottke and Greenler[5] with GeVac sealant obtained from General Electric. The pressure was monitored with a diaphram gauge, a thermocouple gauge, and an ion gauge. The composition of residual gas in the system at a total pressure of 10^{-5} Torr or below was determined with a Veeco MMII mass spectrometer. The sample was heated by radiation from a wire enclosed in an evacuated quartz envelope constructed of two concentric quartz cylinders, 48 and 58 mm in diameter. This arrangement eliminated contamination of the sample from the tungsten wire filament.

The magnesium oxide was obtained from Electronic Space Products, Inc., and was quoted at 4 *N* purity. Carbon monoxide, oxygen, and carbon dioxide were obtained from Matheson as analyzed research grade at a purity of 99.9% or better. The water used was distilled water which had been degassed prior to use.

(1) (a) School of Chemistry, The University of Western Australia. (b) Laboratory for Surface Studies and Department of Physics, University of Wisconsin.
(2) Reviewed by L. H. Little, "Infrared Spectra of Adsorbed Species," Academic Press, London, 1966, p 74.
(3) J. V. Evans and T. L. Whateley, *Trans. Faraday Soc.*, **63**, 2769 (1967).
(4) N. W. Cant and L. H. Little, *Can. J. Chem.*, **46**, 1373 (1968).

A sample of magnesium oxide was pressed at 4000 lb/in.^{2} and fired for 1 hr at 950° in air prior to placing it in the vacuum system. The sample was then heated to 500°. A pressure of 8×10^{-8} Torr was recorded while at 500°. The major residuals were H_2, H_2O, CO, and CO_2. Upon cooling to room temperature the pressure dropped to 5×10^{-9} Torr. Either carbon monoxide or carbon dioxide was then added and spectra were run at various time intervals.

Results

Adsorption of Carbon Monoxide (10^{-5} Torr Evacuation). The adsorption of carbon monoxide (100 Torr) at room temperature on a magnesium oxide surface prepared by 10^{-5} Torr evacuation at 450° is shown in the spectra of Figure 1. The absorption bands are similar to those observed for carbon dioxide adsorption (Figure 5) with an additional band discernable at 1595 cm^{-1}. However the extent of the initial rapid adsorption is not as great nor is the subsequent rate of growth of the bands as rapid as that observed for carbon dioxide adsorption. The intensity of carbon monoxide bands is approximately one-fifth that of the carbon dioxide bands at similar pressures.

Similar changes in the spectrum of the surface hydroxyl groups (or deuterioxyl groups) on the magnesium oxide were observed with increasing adsorption of carbon monoxide to those observed during carbon dioxide adsorption. Deuterium exchange of the hydroxyls to deuterioxyl groups improved the quality of the spectra since the displacement to lower frequencies moved the bands to a spectral region where the scattering losses were less severe. The sharp ν OD band at 2766 cm^{-1} from isolated OD groups decreased in intensity with increasing adsorption while the broad band of perturbed OD groups at 2750–2100 cm^{-1} intensified (Figure 7B) as the surface concentration of adsorbed carbonate radicals increased with more CO_2 adsorption. Similar effects were observed during CO adsorption except that the gaseous CO_2 band at 2330 cm^{-1} was absent.

The addition of gaseous oxygen (100 Torr) to the system produced changes in the relative band intensities (Figure 1F). The 1660- and 1390-cm^{-1} bands increased in intensity more rapidly than the other bands. By comparing the growth of bands during adsorption and the disappearance of bands during desorption studies, it was possible to assign pairs of bands to individual surface species. The band pairs are as follows: 1520 and 1400 cm^{-1}, 1660 and 1390 cm^{-1}, and 1690 and 1310 cm^{-1}. Similar pairs of bands were found for adsorbed CO_2. An additional pair at 1595 and approximately 1350 cm^{-1} were observed during CO adsorption. Similar spectra for adsorbed carbon monoxide on magnesium oxide were reported by Kölbel, *et al.*[6]

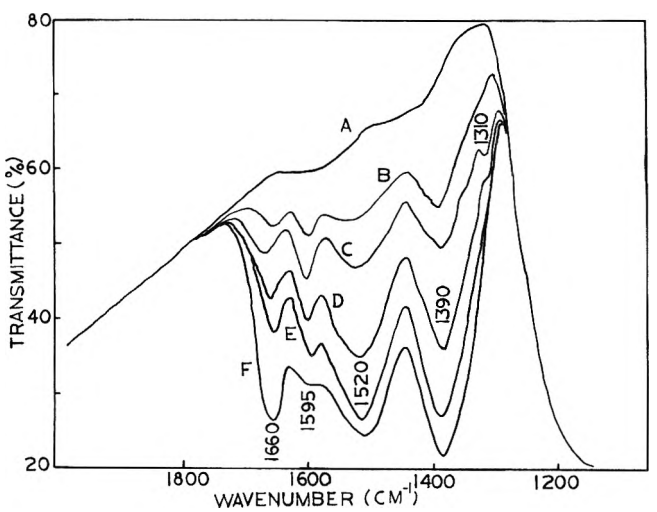

Figure 1. (A) Spectrum of magnesium oxide. (B) 100 Torr of carbon monoxide admitted for 10 min, (C) for 6 hr, (D) for 24 hr, (E) for 72 hr, (F) 100 Torr of oxygen added to carbon monoxide in the cell. Spectrum recorded 24 hr after oxygen admission.

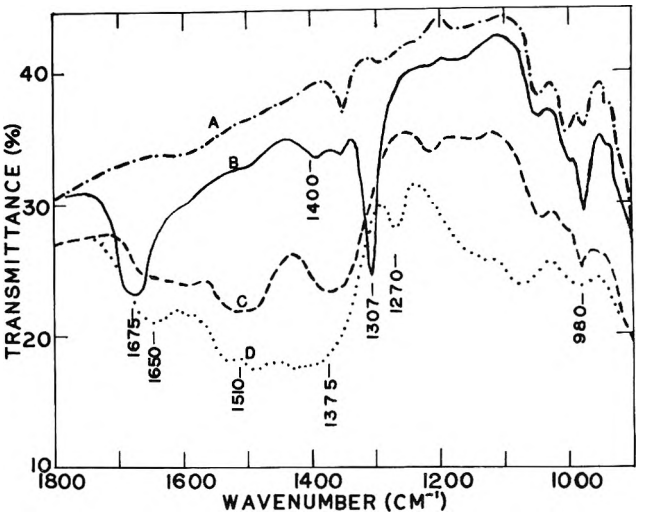

Figure 2. Adsorption of CO on MgO in a leaking system: (A) background and initial CO spectrum; (B) 2.4 hr later; (C) 5.8 hr later; (D) 69.7 hr later.

CO Adsorption in UHV System. One of the early experiments with this system produced the spectra (Figure 2) showing the very rapid growth by bands in the region 1700–1000 cm^{-1}. When evacuation was attempted a large leak was found to have developed during the experiment. No changes were detected immediately after addition of the carbon monoxide shown as trace A. The spectrum at 2.4 hr (B) showed three major bands at 1675, 1307, and 980 cm^{-1} and a minor band at 1400 cm^{-1}. Further standing (C) produced major changes seen as a loss or serious shift of the bands at 1675 and 1307 cm^{-1} to give peaks at 1650, 1510, and 1375 cm^{-1}. The 1400-cm^{-1} absorbance was either lost under the 1375-cm^{-1} peak or shifted to this frequency. Standing for another 64 hr (D) yielded a further loss of detail and a new band at 1270 cm^{-1}.

A fresh sample was placed in the repaired system and surprisingly no change was observed from the background spectrum upon addition of 24 Torr of carbon monoxide to the system. Trace A of Figure 3 represents both the background and magnesium oxide in a carbon monoxide atmosphere after 22 hr. Addition of 26 Torr of oxygen produced an immediate change in the spectrum (Figure 3B) and standing for 6 hr (Figure 3C) amplified these new peaks. They appear at 1670, 1307, 1275, and 980 cm^{-1}. Further standing for 69 hr (Figure 3D) produced a shoulder at 1375 cm^{-1} and a broadening of the 1670-cm^{-1} band to lower frequency. Spectrum A of Figure 4 is a repeat of D in Figure 3 to allow the investigation of the effect of evacuation on the spectrum. Pumping at 10^{-7} Torr for 2 days (B of Figure 4) resulted in a decrease at 1275 and 980 cm^{-1} and the shoulders at 1535, 1375, and 1055 cm^{-1} be-

(5) M. Kottke and R. G. Greenler, *Rev. Sci. Instrum.*, **42**, 1235 (1971).
(6) H. Kölbel, M. Ralek, and P. Jiru, *Z. Naturforsch. A*, **25**, 670 (1970).

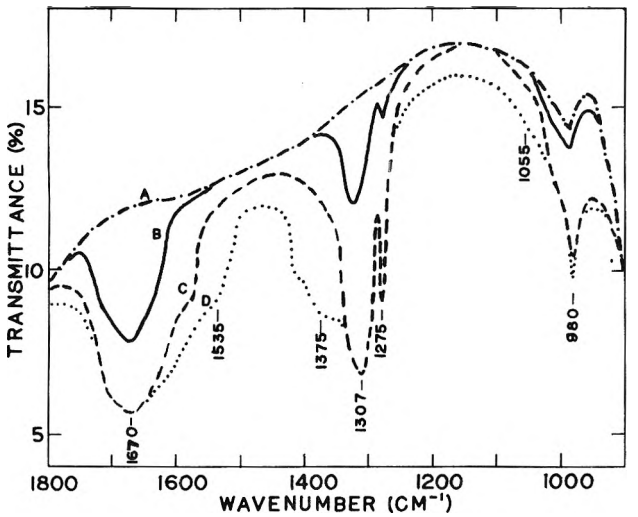

Figure 3. Adsorption of CO on MgO: (A) background and 22 hr after 24 Torr of CO addition; (B) addition of 26 torr O_2; (C) 6 hr after B; (D) 74.7 hr after B.

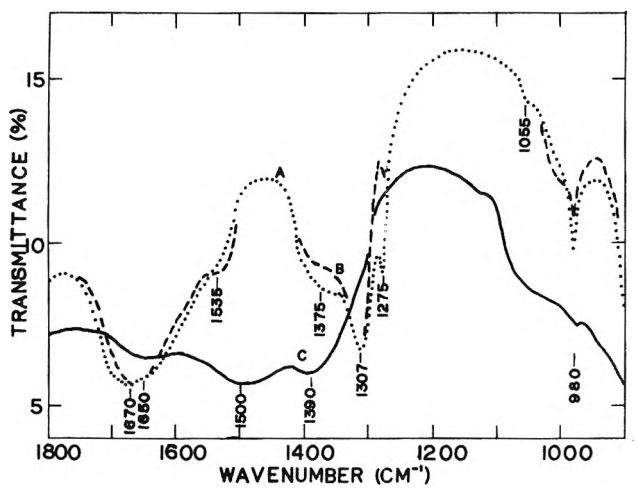

Figure 4. Evacuation and further reaction of the sample of Figure 2: (A) 74.7 hr after addition of O_2; (B) evacuation to 2 × 10^{-7} Torr; (C) addition of 1 Torr of H_2O.

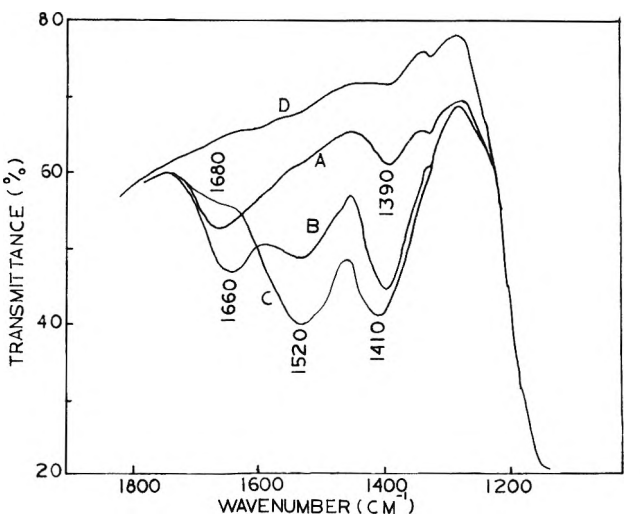

Figure 5. (A) 2 cm of carbon dioxide admitted to magnesium oxide for 0.5 hr; (B) 2 cm of carbon dioxide admitted for 12 hr; (C) the sample in B heated to 150° in the presence of the carbon dioxide; (D) background spectrum of magnesium oxide.

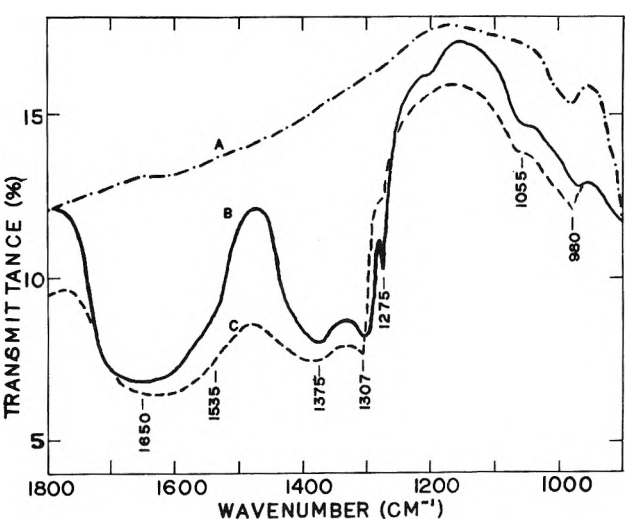

Figure 6. Adsorption of CO_2 on MgO: (A) background; (B) after addition of 27 Torr of CO_2; (C) 26 hr later and evacuation to 2 × 10^{-7} Torr.

came more defined. The subsequent addition of 1 Torr of water to the system (C of Figure 4) produced three major bands at 1650, 1500, and 1390 cm^{-1}.

CO_2 Adsorption (10^{-5} Torr System). The adsorption of CO_2 (20 Torr) at room temperature on a magnesium oxide surface prepared by 10^{-5} Torr evacuation at 450°, is shown in the spectra of Figure 5. Initial adsorption produced bands at 2330, 1680, 1520, and 1390 cm^{-1} (with a shoulder at 1330 cm^{-1}). The growth of the bands with time shows that the 1520- and 1400-cm^{-1} bands increase most rapidly, particularly after heating the sample in the presence of CO_2 at 150°. Transmission through the sample in the region 1100–800 cm^{-1} was poor although bands formed during the adsorption of CO_2 were detected at 1000–900 cm^{-1} and at approximately 850 cm^{-1}.

Desorption studies showed that the 2330-cm^{-1} band was removed immediately on evacuation at room temperature. The remaining bands in the 1800–1200-cm^{-1} region were removed in reverse order of their appearance on adsorption. Thus the species producing bands at 1520 and at 1400 cm^{-1} is only removed by evacuation for several hours at 400° and is clearly the most stable carbonate species on the surface.

CO_2 Adsorption in UHV System. The adsorption of 27 Torr of carbon dioxide on the magnesium oxide sample produced immediate and large changes from the background (A of Figure 6) at 1650, 1375, 1307, 1275, 1055, and 980 cm^{-1} (B of Figure 6). A very broad shoulder was also detected at approximately 1535 cm^{-1}. Standing for 26 hr and pumping to 2 × 10^{-7} Torr (C of Figure 6) gave a broadening in the 1650–1500-cm^{-1} region and at 1375 cm^{-1} and a decrease in intensity at 1275 cm^{-1}.

Heat Treatment and Evacuation. When the carbon monoxide or the carbon dioxide experiment was terminated prior to the addition of water, heating to 500° and evacuation to 8 × 10^{-8} Torr reproduced the background. During this evacuation procedure the maximum pressure was detected between 200 and 300°. A mass spectrum taken during the pressure maximum showed that CO_2 was the major component discharged from the surface whether CO or CO_2 was admitted initially.

Discussion

The results show that uncontrolled leaking of atmosphere into the UHV system could be duplicated by con-

trolled addition of oxygen (Figure 3B) with the addition of water vapor as discussed below. A surprising feature was the complete absence of bands detected in the infrared spectrum (Figure 3A) when only carbon monoxide was placed in the system. With the addition of oxygen, absorption bands are produced in the spectral region characteristic of carbonates. However, adsorption of carbon monoxide proceeds readily to produce surface carbonate species in the system evacuated at 10^{-5} Torr. It has not been determined whether the additional oxygen needed for carbonate formation is supplied by the residual gas atmosphere in this system or by oxygen or some weakly held oxide species in the adsorbed state which is not removed in the less severe evacuation conditions of this system.

Assignment of Bands to Surface Carbonates. Characteristic vibrational band assignments in the infrared spectra of various carbonate complexes have been reviewed by Little.[2] In brief, bands at 1520 and 1370 cm^{-1}, together with bands in the region 1060 and 850 cm^{-1}, can be assigned to a unidentate carbonate ligand. Bands at 1630 and 1270 cm^{-1} with others at 1030 and 830 cm^{-1} may be assigned to bidentate carbonate ligands.

The spectra (Figure 3B) obtained when oxygen and carbon monoxide are admitted to magnesium oxide suggest that two bidentate surface ligands are formed with bands at 1670, 1307, and 980 cm^{-1} and 1670, 1275, and 980 cm^{-1}. The broadness of the 1670-cm^{-1} band (Figure 3B) suggests that two overlapping bands occur here, although no broadening or splitting of the 980-cm^{-1} band is apparent. These bands arise from the carbon–oxygen stretching modes of the adsorbed bidentate species.

An additional form of adsorbed carbonate species is produced on standing oxygen and carbon monoxide over magnesium oxide or on heating the sample. Shoulders appear at 1535, 1375, and at 1055 cm^{-1} (Figure 3D). These bands are also produced when CO_2 is adsorbed on magnesium oxide and can best be assigned to unidentate carbonate groups. The two bands at high frequency arise from the asymmetric and symmetric stretching modes of the two uncoordinated carbon–oxygen bonds of the unidentate carbonate ligand and the 1055-cm^{-1} band from the stretching of the bond through which the carbonate is coordinated to the surface magnesium ion. Desorption studies at increasing temperatures show that the stability of the carbonate species follows the order unidentate (1520- and 1390-cm^{-1} band) > bidentate (1670- and 1307-cm^{-1} band) > bidentate (1670- and 1275-cm^{-1} band). No explanation can be given for this order. This order of stability was also found by Kölbel, *et al.*[6]

A comparison with the spectra of other magnesium compounds[7] shows $MgC_2O_4 \cdot 2H_2O$ to be a bidentate structure having bands at 1675, 1380, 1310, 1020, and 815 cm^{-1}, while $MgCO_3$ is a simple carbonate with bands at 1450, 1010, 890, and 750 cm^{-1}. Thus the surface carbonates formed are not the simple carbonate of the normal magnesium carbonate structure, but have bidentate structure similar to $MgC_2O_4 \cdot 2H_2O$. The pressure increase in the system when the adsorbed carbonates are heated shows that these species decompose between 200 and 300° *in vacuo*. Magnesium carbonate decomposes at 365° in air.[8] Since the major decomposition product is CO_2, as detected during the pressure maximum, the carbon monoxide and oxygen must form a carbonate, which subsequently decomposes to magnesium oxide and CO_2.

The addition of water (Figure 4C) produced a structure with very similar spectra to that of $MgCO_3 \cdot Mg(OH)_2 \cdot 3H_2O$.[7] The separate stepwise addition of oxygen and water duplicated the observations of the leaking system.

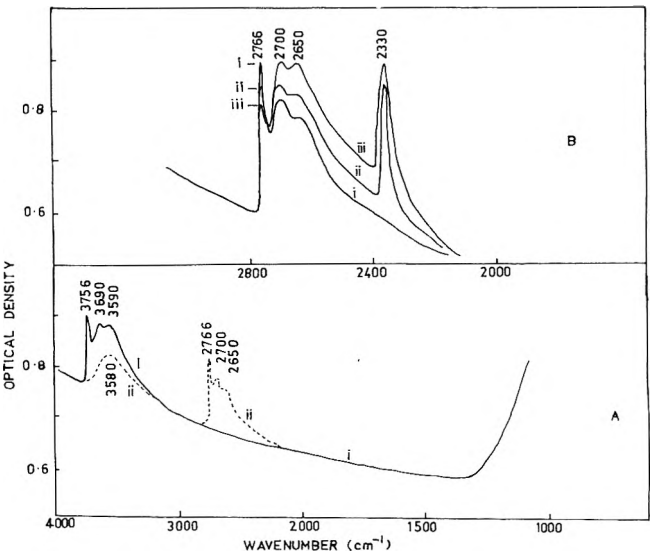

Figure 7 (A) (i) Magnesium oxide spectrum: (ii) after exchange of surface hydroxyl groups with deuterium oxide. (B) (i) Magnesium oxide spectrum after deuterium oxide exchange as in A; (ii) after admission of 2 cm of carbon dioxide for 10 min; (iii) After admission of 2 cm of carbon dioxide for 64 hr.

A very large number of spectra recorded both during adsorption and desorption on the 10^{-5}-Torr vacuum system show that the two carbonate stretching modes at higher frequency (1700–1250 cm^{-1}) are grouped in pairs about the frequency (1450 cm^{-1}) of the isolated carbonate ion. Thus a band of highest frequency, 1670 cm^{-1}, will be associated with one at lowest frequency, 1270 cm^{-1}, while other pairs will be intermediate in spacing.

The band at 2330 cm^{-1} (Figure 7) is due to weakly coordinated or physically adsorbed carbon dioxide and it is readily removed by room temperature evacuation.

Surface Hydroxyls and Interaction with Adsorbed Carbonates. Figure 7 shows the spectrum of a magnesium oxide pellet prepared by 10^{-5}-Torr evacuation at 450°. Malinowski, *et al.*,[9] have investigated magnesium oxide prepared at various temperatures *in vacuo*. Their spectrum in the hydroxyl-stretching region is similar to that in Figure 7 with a sharp and two broad bands. The sharp band at 3756 cm^{-1} is due to free, noninteracting hydroxyl groups, while the broad bands at 3690 and 3590 cm^{-1} indicate hydroxyls involved in weak hydrogen bonding. It is possible that the broad band at 3590 cm^{-1} is due at least in part to internal hydroxyl groups. This is supported by results obtained with deuterium exchange of the hydroxyl groups. After exchange the free hydroxyl band disappears completely and the corresponding free OD band appears at 2766 cm^{-1} (Figure 7). Two types of bonded deuterioxyl groups are also indicated by bands at 2700 and 2650 cm^{-1}. However, a broad band of medium intensity remains at 3580 cm^{-1} after exchange. This may be attributed, as Davydov, Kiselev and Zhuravlev[10] have shown for silica surfaces, to internal hydroxyl groups which are more difficult to exchange. It is possible that some exchange of internal

(7) The Sadtler Standard Spectra, Nos. 1732, 1740, and 1763.
(8) "The Handbook of Chemistry and Physics," 48th ed, Chemical Rubber Publishing Co., Cleveland, Ohio.
(9) St. Malinowski, S. Szczepanska, A. Bielanski, and J. Sloczynski, *J. Catal.*, **4**, 324 (1965).
(10) V. Y. Davydov, A. V. Kiselev, and L. T. Zhuravlev, *Trans. Faraday Soc.*, **60**, 2254 (1964).

hydroxyl groups will take place at 80° when hydrogen- and deuterium-containing species could diffuse into the bulk of the sample. If, in fact, the band at 3580 cm^{-1} in the spectrum before exchange is due to internal hydroxyl groups then the band at 2650 cm^{-1} after exchange is probably due to some internal deuterioxyl groups.

Evans and Whateley[3] have assigned a broad absorption found after water admission in the spectrum below 1200 cm^{-1} to the deformation of surface hydroxyl groups. Hunt, Wisherd, and Bonham[11] found broad absorption in this region with magnesium oxide prepared at room temperature. This absorption, doubtless, contributes to the rising spectrum observed in the present study at frequencies below 1200 cm^{-1}.

The interaction between surface hydroxyl (or deuterioxyl groups) and adsorbed carbonate ligands can be seen in Figure 7B. Gas-phase carbon dioxide has overtone bands in the region 3720–3500 cm^{-1} which overlap the hydroxyl bands of the adsorbent. For this reason, as well as to reduce radiation scattering losses, the interaction of CO_2 with deuterioxyl groups was observed. With increasing adsorption of surface carbonate groups it was found that the sharp free OD band at 2766 cm^{-1} decreased in intensity. A corresponding intensity increase in the bands due to bonded deuterioxyl groups was observed (Figure 7B) in the 2700–2100-cm^{-1} region.

The interaction between adsorbed carbonate species and adsorbed water or surface hydroxyls may occur through hydrogen-bonding interaction as in I or through the production of an adsorbed bicarbonate species as in II.

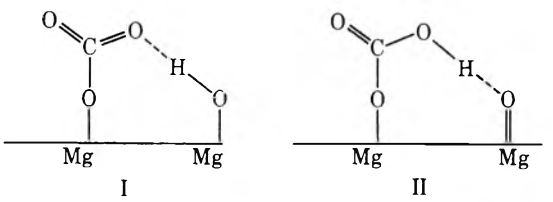

The relatively small deuterioxyl (or hydroxyl) perturbations (Figure 7B) observed are in accord with the formation of a relatively weak hydrogen bond as in I.

Acknowledgment. We gratefully acknowledge grants from the Australian Research Grants Commission to support the work at the University of Western Australia and from the National Science Foundation, to support the work at the University of Wisconsin—Milwaukee.

(11) J. P. Hunt, M. P. Wisherd, and L. C. Bonham, *Anal. Chem.*, **22**, 1478 (1950).

Radicals Bonded to Porous Vycor Glass

E. Melamud, M. G. Reisner, and U. Garbatski*

Department of Chemistry, Technion—Israel Institute of Technology, Haifa, Israel *(Received October 16, 1972)*

Publication costs assisted by the Department of Chemistry, Technion, I.I.T.

In porous Vycor glass surface OH groups were substituted by methoxy, ethoxy, *n*-butoxy, *tert*-butoxy, and acetoxy groups. Various radicals containing a $-\dot{C}H_2$ group were obtained by ultraviolet irradiation and identified by their esr spectra. In most cases the radicals were stable even at room temperature for days and weeks. This stability is probably due to chemical bonding. $\dot{C}H_3$ radicals were also observed when methylated and *tert*-butylated glasses were irradiated at low temperatures. Various possibilities for the mechanism of radical formation are discussed. An important aspect is the fact that the surface concentrations of radicals even at low temperatures and during irradiation are around $10^{14}/m^2$, four orders of magnitude below those of their parent compounds.

Introduction

A number of papers concerning free radicals stabilized on solid surfaces have appeared.[1-7] It seems that this phenomenon of small organic radicals stabilized up to room temperature is restricted to the methyl radical. The exceptional stability of this radical physically adsorbed on the surface is not yet fully understood.

Other stable radicals originally thought to be physically adsorbed were subsequently found to be chemically bonded to the surface. Thus, Vladimirova, *et al.*,[8] assigned the esr spectrum obtained by irradiation of methanol adsorbed in silica and alumina to the $\dot{C}H_2OH$ radical. Ono and Keii[9] found that the signal belonged to the $-O\dot{C}H_2$ group chemically bonded to the surface. Chemical reaction of alcohols with various surfaces has been mentioned by several workers.[10-15]

(1) (a) V. B. Kazanskii and G. B. Pariiskii, *Fiz. Tverd. Tela*, **5**, 473 (1963); (b) *Zh. Strukt. Khim.*, **4**, 336 (1963); (c) *Prepr. Pap. Int. Symp. Free Radicals, 6th, 1963* (1963); (d) *Proc. Int. Congr. Catal., 3rd*, **1**, 367 (1964).
(2) C. L. Gardner and E. J. Casey, *Can. J. Chem.*, **46**, 207 (1968).
(3) J. Turkevich and Y. Fujita, *Science*, **152**, 1619 (1966).
(4) M. Fujimoto, H. D. Gesser, B. Garbutt, and A. Cohen, *Science*, **154**, 381 (1966).
(5) M. Fujimoto, H. D. Gesser, B. Garbutt, and M. Shimizu, *Science*, **156**, 1105 (1967).

In the present work, porous Vycor glass surfaces treated with alcohols, acetic acid, and related compounds were irradiated with ultraviolet light. The resulting radicals were identified and studied by their esr spectra.

Experimental Section

The adsorbent was porous Vycor glass (No. 7930 of Corning) in the form of rods 25 mm long and 3–4 mm in diameter. The glass was treated with boiling concentrated HCl solution, water, and a stream of oxygen at 500° until a colorless sample was obtained. It was introduced into a Spectrosil vacuum cell fitting into the esr cavity. All manipulations were performed in a conventional vacuum system with mercury manometers and a Hg diffusion pump. Degassing was carried out at 400–450° for 4 hr. The surface area of the sample was found by the BET method to be 180 m^2/g.

Methylation was performed by a method similar to that of Folman and Yates[10] and Sidorov.[11] Methanol (0.3 ml) was admitted into the cell and left overnight. Subsequent heating to 270° for 1 hr followed by degassing at this temperature leaves mainly chemically bound methanol in the form of $\equiv Si\text{-}OCH_3$ groups. Only partial methylation of the surface is obtained by this method, but complete methylation was not necessary for our purpose. The same method was used to produce $\equiv Si\text{-}OCH_2CH_3$ groups by ethylation.

Butylation with *n*-butyl alcohol was carried out according to the method of Uytterhoeven and Fripiat,[14] giving $\equiv Si\text{-}O\text{-}CH_2CH_2CH_2CH_3$ groups.

To obtain *tert*-butylated glass, *tert*-butyl alcohol vapor was admitted into the cell. The cell was then gradually heated to 130° for 1 hr and evacuated at the same temperature. In this case desorption was incomplete because of the limitation in raising the temperature due to the tendency of the organic matter to carbonize.

$\equiv Si\text{-}O\text{-}C(=O)CH_3$ groups were obtained by acetylation with acetic acid, acetyl chloride, or acetic anhydride using Young's method.[16]

Surface -OH groups were substituted by ^{17}OH in two steps. Chlorination according to Peri[17] caused a substitution of 95% of the -OH groups by -Cl. Rehydration by two successive amounts of 0.01 ml of H_2O 10 atom % ^{17}O restored almost all the -OH groups.

The materials used were methanol and acetic anhydride, both of analytical grade (supplied by Frutarom), ethanol 99.8% and acetic acid 99% (Merck), *tert*-butyl alcohol and acetyl chloride both puriss (Fluka), *n*-butyl alcohol of spectroscopic grade (Eastman Organic), H_2O and CH_3OH both of 10 atom % ^{17}O (Weizmann Institute of Science), and CD_3OH of 95 atom % D (Merck Sharp and Dohme).

All samples were degassed and used without further purification. The samples were irradiated in the esr cavity with a high-pressure mercury lamp. Esr spectra were recorded on a V-4500 Varian X-band spectrometer equipped with a variable temperature attachment.

Results

The esr spectrum obtained after irradiation of methylated glass at room temperature consisted of three lines (Figure 1). The height ratio of the lines varied from 1.0:13.4:1.0 at −196° to 1.0:6.3:1.2 at +180°. The triplet lines will be named 1,2 and 1a in order of increasing magnetic field. The width of the lines, measured from peak to peak, increases with temperature for line 1 from

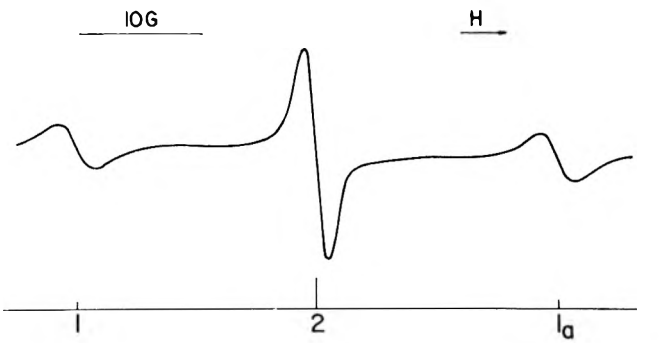

Figure 1. Esr spectrum obtained by irradiation of methylated glass at room temperature.

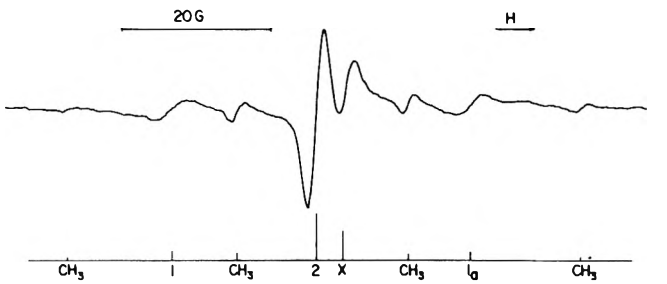

Figure 2. Esr spectrum obtained by irradiation of methylated glass at −100°.

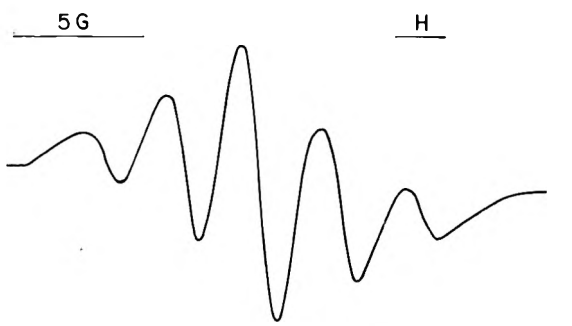

Figure 3. Esr spectrum obtained by irradiat on of glass methylated with CD_3OH at room temperature.

3.2 G at −140° to 4.2 G at +180° and for line 2 from 1.8 to 2.6 G in the same temperature range. The separation between the triplet lines, measured between points of zero derivative, is asymmetric and changes with temperature. The distance between lines 1 and 2 varies from 20.0 G at −140° to 19.1 G at +140°. The distance between lines 2 and 1a varies from 21.0 G at −140° to 19.4 G at +140°. The *g* value of the triplet, taken at the point of zero derivative of line 2, was 2.0031 ± 0.0001. This spectrum could

(6) G. B. Garbutt, H. D. Gesser, and M. Fujimcto, *J. Chem. Phys.*, **48**, 4605 (1968).
(7) E. Melamud, M.Sc. Thesis, Technion, Haifa.
(8) V. I. Vladimirova, G. M. Zhabrova, B. M. Kadenatsi, V. B. Kazanskii, and G. B. Pariiskii, *Dokl. Akad. Nauk SSSR*, **164**, 657 (1965).
(9) Y. Ono and T. Keii, *J. Phys. Chem.*, **72**, 2851 (1968).
(10) M. Folman and D. J. C. Yates, *Proc. Roy. Soc., Ser. A*, **246**, 32 (1958).
(11) A. N. Sidorov, *Zh. Fiz. Khim.*, **30**, 995 (1956).
(12) E. Borello, A. Zecchina, and C. Morterra, *J. Phys. Chem.*, **71**, 2938 (1967).
(13) R. G. Greenler, *J. Chem. Phys.*, **37**, 2094 (1962).
(14) J. Uytterhoeven and J. J. Fripiat, Report of the International Geological Congress XXI, Sess. Norden, 1960, Copenhagen.
(15) L. Abrams and A. O. Allen, *J. Phys. Chem.*, **73**, 2741 (1969).
(16) R. P. Young, *Can. J. Chem.*, **47**, 2237 (1969).
(17) J. B. Peri, *J. Phys. Chem.*, **70**, 2937 (1966).

Figure 4. Esr spectrum obtained by irradiation of ethylated glass at room temperature.

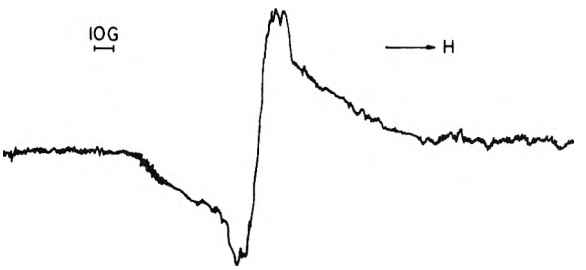

Figure 5. Esr spectrum obtained by irradiation of *n*-butylated glass at room temperature.

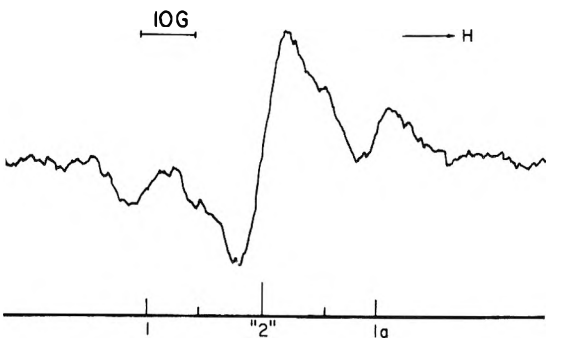

Figure 6. Esr spectrum obtained by irradiation of *t*-butylated glass at −140°.

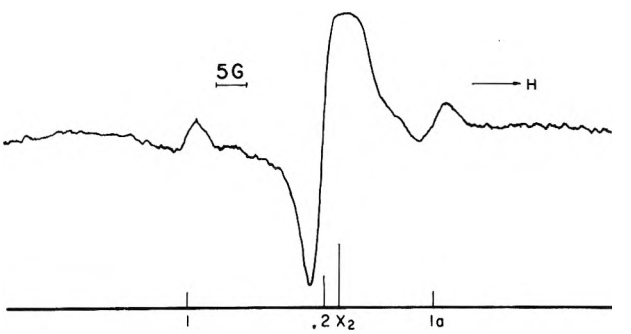

Figure 7. Esr spectrum obtained by irradiation of acetylated glass at room temperature.

be observed immediately following the commencement of irradiation and reached its final intensity after about 20 min.

The number of radicals as estimated by comparison with a known sample of DPPH (diphenylpicrylhydrazyl) was around $10^{14}/m^2$. This number was hardly affected by changing the temperature of irradiation.

The radicals are highly stable; no decay can be detected for days when the glass is held *in vacuo* at room temperature. Even after 5 months the number of radicals decreased only 20%. When H_2 at 0.1 mm pressure was admitted into the cell, the spectrum decayed by 50% in 30 min. The spectrum regained its original intensity when the sample was irradiated again after 10 min of evacuation.

When the methylated glass was irradiated below −100°, five more lines appeared (Figure 2). One of the lines, which will be labeled x, appeared at a slightly higher field than line 2. Because of their partial overlap, the exact *g* value for line x could not be determined. Line x decayed to ⅕ of its intensity after warming to room temperature but did not disappear. The remaining four lines formed a quartet with relative intensities 1:3:3:1 and hyperfine splitting of 22.9 G. At −150° their intensity corresponded to about 3% of the main triplet spectrum. The quartet disappeared at a temperature above −50°.

When glass treated with CD_3OH was irradiated at room temperature, a five-line spectrum was obtained (Figure 3). Exact measurements of the spectral parameters were difficult because of partial overlap of the lines. At room temperature the relative heights of the lines were 1.0:3.0:5.7:3.1:1.1, their width was about 2 G, and the splitting around 3.2 G.

Glass treated with H_2O with 10 atom % ^{17}O was methylated with CH_3OH with 10 atom % ^{17}O. No lines due to ^{17}O hyperfine splitting were observed after irradiation.

Ethylated porous glass gave on irradiation at room temperature a spectrum of at least 15 lines (Figure 4). Difficulty arose in determining the spectral parameters because of partial overlap of the lines. The total width of the spectrum was about 100 G.

When *n*-butylated glass was irradiated at room temperature, a single signal about 125 G wide was observed (Figure 5). The growth and stability of the radicals in the last two cases were similar to those observed for methylated glass.

In the spectrum of *tert*-butylated glass irradiated at −140° five lines could be discerned (Figure 6). The main spectrum consisted of three lines: 1, "2," and 1a. At −140° the distance between lines 1 and "2" was 20.7 G and between lines 1a and "2" 21 G. The *g* value was 2.0030 ± 0.0001. The width of the lines was 9 G. At −140° the spectrum could be observed immediately following the commencement of irradiation and reached "saturation" after about 20 min. The number of radicals at this temperature was $10^{14}/m^2$. The spectrum decayed with increasing temperature and vanished entirely at 20°.

Exact parameter measurements for the other two lines, which looked like a doublet, were difficult because of their low intensity and partial overlap with the triplet lines. The distance between these lines was about 20 G. They could not be seen above −50°.

Porous glass acetylated with acetic acid, acetyl chloride, or acetic anhydride and irradiated at room temperature gave four lines (Figure 7). The same spectrum was obtained at −140°. Three of the lines, 1, "2," and 1a, formed a triplet similar to those described above. The fourth line was labeled x_2. The width of the lines 1, "2," and 1a was about 5 G. The distance between lines 1 and "2" was 21.9

G at +50° and 21.5 G at −140°. The distance between lines 2 and 1a was 18.4 G at +50° and 19.7 G at −140°. The g value at zero derivative was 2.0033 ± 0.0001. The growth and stability of the radicals were similar to those observed on methylated glass. The number of radicals was $10^{13}/m^2$.

Discussion

The triplet observed in most spectra is due to the interaction of an unpaired electron with two identical hydrogen nuclei. The radical responsible for this spectrum is almost certainly the $-\dot{C}H_2$ group. The observed hyperfine splitting (about 20 G) is characteristic of α hydrogens in an organic radical.

Glass methylated with CD_3OH gave a quintet as expected for $-\dot{C}D_2$. The observed hyperfine splitting was 3.2 G, as predicted by the relation between the gyromagnetic ratios of H and D. The measured g factor was characteristic for organic radicals.

The great stability of the radicals, which persist in most cases up to relatively high temperatures, is probably due to their being chemically bound to the surface. These radicals originate in the surface bound molecules whose existence on silica surfaces similarly treated has been proved (ref 10–12, 14–16). No measurable decay with characteristic times of less than hours was observed. This suggests that apart from radicals with high stability there could exist possibly only radicals with very short life time and resulting low steady-state concentration. It is hard to envision a model for this in terms of physical adsorption.

Since the radicals are chemically bonded to the surface, their freedom of rotation is limited and the anisotropic parts of the g and hyperfine tensors should affect the form of the spectra.

The esr spectra of trapped and randomly oriented $-\dot{C}H_2$ radicals, as dependent on the freedom of rotation about the axis bisecting the HCH angle, were calculated by Cochran, *et al.*[18] A good agreement was found between the temperature dependence of our spectrum for methylated glass and the dependence of Cochran's spectrum on the freedom of rotation. The similarity includes height ratios, line widths, and hyperfine splittings. Ono and Keii[9] obtained similar results for the temperature dependence of the spectrum on methylated alumina.

The asymmetry in the separations between line 2 and lines 1 and 1a was probably due to anisotropy of the g value. This anisotropy was neglected in Cochran's calculations.

The triplet obtained for *tert*-butylated glass may be assigned to the $\equiv Si\text{-}O\text{-}C(\dot{C}H_2)(CH_3)_2$ group. The spectrum differs from that of the methylated glass mainly in line width. The greater line width observed here could be the result of a more limited freedom of rotation of the bulky *tert*-butyl group. Small hyperfine splitting from γ hydrogens may also contribute to the line width. The somewhat asymetric shape of line "2" was ascribed to an overlap with another signal.

Although the radical disappears at room temperature the possibility of its being chemically bound as the others cannot be excluded. We tend to ascribe its rapid decay to reaction with adsorbed gases since degassing could not be carried out at temperatures above 130° and was therefore necessarily incomplete.

Irradiation of acetylated glass results in the formation of the $\equiv Si\text{-}O\text{-}C(=O)\dot{C}H_2$ group. The width of the triplet lines in this case lies between those of the methylated and *tert*-butylated glasses. This might be explained by the intermediate volume of this group which influences its ability to rotate. The extraordinary intensity of line "2" and the asymmetry of the spectrum suggest that this line is probably a superposition of line 2 of the triplet and another signal with a smaller g value. The increase of the asymmetry with temperature can then be explained by a more rapid decay of the triplet compared to that of the higher field signal. In ethylated glass, the spectrum could be caused by two radicals: $-\dot{C}H_2CH_2$ and $-\dot{C}HCH_3$. The superposition of the spectra of these two radicals should give 17 lines, as obtained in liquid by Livingston and Zeldes.[19] In our case, the exact number of lines could not be determined because of their partial overlap, but the total width of the spectrum was about 100 G, similar to that found in solution.

The single line seen in the n-butylated glass is presumably due to the superposition of the spectra of the various radicals which could be formed in this case.

The quartet which appeared at low temperatures on methylated glass is to be assigned to the $\dot{C}H_3$ radical. Its parameters are in agreement with those found in the literature. It also seems probable that the additional signals seen at low temperatures on *tert*-butylated glass are the two central lines of this $\dot{C}H_3$ quartet. In this case it was impossible to see the side lines and measure the exact radical parameters because of overlap with the wide triplet lines.

The appearance of the $\dot{C}H_3$ radical suggests the following mechanism of $-\dot{C}H_2$ formation for the methylated glass

$$\text{I} \qquad \equiv Si\text{-}O\text{-}CH_3 \xrightarrow{h\nu} \dot{C}H_3 + \equiv Si\text{-}\dot{O}$$

$$\text{II} \qquad \equiv Si\text{-}O\text{-}CH_3 + \dot{C}H_3 \longrightarrow \equiv Si\text{-}O\text{-}\dot{C}H_2 + CH_4$$

Another mechanism that could be involved in the formation of the $\equiv Si\text{-}O\text{-}\dot{C}H_2$ radical is

$$\text{I} \qquad \equiv Si\text{-}O\text{-}CH_3 \xrightarrow{h\nu} \equiv Si\cdot + \dot{O}CH_3$$

$$\text{II} \qquad \equiv Si\text{-}O\text{-}CH_3 + \dot{O}CH_3 \longrightarrow \equiv Si\text{-}O\text{-}\dot{C}H_2 + CH_3OH$$

Although no signals due to the $\dot{H}$ radical were observed, the existence of the following mechanism cannot be entirely excluded

$$\equiv Si\text{-}O\text{-}CH_3 \xrightarrow{h\nu} \equiv Si\text{-}O\text{-}\dot{C}H_2 + \dot{H}$$

Similar reactions can be envisioned also for the other chemically bound species.

The other radicals involved in these mechanisms, such as $\equiv Si\text{-}\dot{O}$ and in the acetylated glass also $\equiv Si\text{-}O\text{-}\dot{C}(=O)$, may be responsible for lines x, x_2, and the signals which overlapped with the central triplet line.

Since free methanol does not absorb light at wavelengths longer than 2000 Å, it does not seem likely that the first step is a direct photolytic rupture of the C–H bond. It seems probable that photosensitization was involved.

Mercury is known to photosensitize the decomposition of methanol in gas phase.[20] This possibility was checked by excluding all Hg vapors in the preparation of methylated glass, which was sealed afterwards in the cell. The intensity ot the esr signal was similar to that obtained in

(18) E. L. Cochran, F. J. Adrian, and V. A. Bowers, *J. Chem. Phys.*, **34**, 1161 (1961).
(19) R. Livingston and H. Zeldes, *J. Chem. Phys.*, **44**, 1245 (1966).
(20) A. R. Knight and H. E. Gunning, *Can. J. Chem.*, **39**, 1231 (1961).

the presence of Hg vapors. It seems therefore that the photosensitizer must be some other factor in the glass surface. A similar phenomenon was discovered in the photolytic decomposition of hydrogen molecules on a silica gel surface.[21]

It is remarkable that the number of radicals observed in these experiments was always found to be smaller by approximately four orders of magnitude than the substituent groups available.

This cannot be explained kinetically by equilibrium between production and decay, because maximum intensity is reached in minutes whereas half-times of decay are measured in days, sometimes even weeks. Thus one cannot relate the low saturation concentration to a steady state between these two processes and we conclude that the production of these stable radicals must require some additional, rather rare conditions on the surface. One possibility is that the photolytic process needs the presence of some trace impurities which exist only on a few sites. This impurity could be a metal oxide similar to the findings of Fujita, *et al.*,[22,23] who observed photosensitization by trace amounts of V_2O_5 and MoO_3 in the formation of adsorbed methyl radicals.

It would be interesting to try to create different kinds of radicals by irradiation of other chemically bound species. Our attempts to observe radicals by irradiation of aminated glass were unsuccessful.

Acknowledgments. We wish to thank Professor B. L. Silver for his helpful advice. We would also like to thank Professor D. Wolf from the Weizmann Institute of Science, Rehovoth, Israel, for a gift of ^{17}O enriched H_2O and CH_3OH.

(21) G. B. Pariiskii, I. D. Micheykin, and V. B. Kazanskii, *Dokl. Akad. Nauk SSSR*, **1**, 180 (1968).
(22) Y. Fujita, K. Hatano, M. Yanagita, T. Katsu, M. Sato, and T. Kwan, *Bull. Chem. Soc. Jap.*, **44**, 2884 (1971).
(23) T. Katsu, M. Yanagita, and Y. Fujita, *J. Phys. Chem.*, **75**, 4064 (1971).

Equilibrium Studies by Electron Spin Resonance. III. The Nitrobenzene Free Ion as a Hydrogen Bond Acceptor

Gerald R. Stevenson* and Hector Hidalgo

Department of Chemistry, University of Puerto Rico, Rio Piedras, Puerto Rico 00931 *(Received August 28, 1972)*

Publication costs assisted by The University of Puerto Rico

Hydrogen bonding proton donors have been added to the $PhNO_2$ anion radical in hexamethylphosphoramide (HMPA). An equilibrium has been observed between hydrogen bonded HMPA plus the free $PhNO_2$ anion radical and free HMPA plus hydrogen bonded $PhNO_2$. The equilibrium constant for this reaction has been algebraically related to the nitrogen hyperfine coupling constant of the $PhNO_2$ anion radical. A temperature-dependent study of this equilibrium has resulted in the first relative hydrogen bonding energies by electron spin resonance. At lower temperatures (from 0 to $-10°$) line width alternation is observed, due to rapid forming and breaking of the hydrogen bonds to the $PhNO_2$ anion.

The variation of esr coupling constants upon solvent and counterion interactions in organic anion radicals has been a topic of much recent interest.[1] Aromatic anion radicals containing polar groups, such as the nitrobenzene ($PhNO_2$) anion radical, exhibit extreme sensitivity to these effects.[2-4] In the case of the $PhNO_2$ anion radical, the magnitude of the isotopic nitrogen coupling constant, A_n, always increases with external forces such as solvent and counterion interactions.[5]

To date it has been difficult to obtain quantitative solvent effects upon the esr parameters and the thermodynamics of these interactions, since there always existed the possibility of interference with the ion pairing interactions and the interactions of the solvent with itself. Recently, the $PhNO_2$ anion radical has been recorded essentially free from solvent and counterion interactions by lithium reduction in hexamethylphosphoramide (HMPA).[6] This "free" $PhNO_2$ anion radical (α) was observed simultaneously with its ion pair (β), allowing the enthalpy of reaction 1 to be determined from temperature dependent esr studies.[7,8]

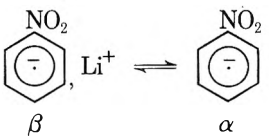

(1)

Utilizing the lowest nitrogen splitting for the $PhNO_2$ anion radical an empirical equation was developed which

(1) M. T. Jones in "Radical Ions," E. T. Kaiser and L. Kevan, Ed., Interscience, New York, N. Y., 1968, Chapter 6.
(2) J. M. Gross, J. D. Barnes, and G. N. Pillans, *J. Chem. Soc.*, 109 (1969).
(3) J. M. Gross and M. C. R. Symons, *Trans. Faraday Soc.*, **63**, 2117 (1967).
(4) W. M. Gulick, Jr., and D. H. Geske, *J. Amer. Chem. Soc.*, **87**, 4049 (1965).
(5) C. Y. Ling and J. Gendall, *J. Chem. Phys.*, **47**, 3475 (1965).

relates the total A_n to the contributions made to it by the counterion and solvent

$$A_n = 8.48 + P_b A_n(\text{solvent}) + P_c A_n(M^+) \quad (2)$$

A_n(solvent) and $A_n(M^+)$ represent the maximum contributions to A_n due to the solvent and cation interactions, respectively. P_b and P_c are the fractions of these interactions found in a particular system.

Several workers have observed line width alternation phenomena, resulting from the modulation of the nitrogen hyperfine splitting, for the $PhNO_2$ anion radical.[8-10] In all cases, however, the line width alternation has been attributed to the rapid equilibrium between two different ion pairs.[6,8,9]

In this report, we wish to communicate the effect of hydrogen bonding upon the nitrogen coupling constant of the $PhNO_2$ free anion radical, the effect of hydrogen bonding upon the equilibrium between the free ion and ion pair (eq 1), and the thermodynamics of this hydrogen bonding.

Results and Discussion

Addition of small amounts of alcohol or water to the system $PhNO_2$–HMPA–Li affords increases in the nitrogen coupling constant for the formally free ion (α) due to hydrogen bonding of the acidic proton of the alcohol with the nitro group of the $PhNO_2$ anion radical. However, no change in the nitrogen splitting of the ion pair (β) is observed (Figure 1). Hydrogen bonding does not occur with the ion pair as evidenced by the lack of change of the nitrogen splitting upon addition of the alcohol or water. This is presumably due to the fact that the nitro group of the ion pair is too strongly complexed with the lithium cation to act as an acceptor in hydrogen bonding. From Figure 1, it is clear that A_n is a linear function of the alcohol or water concentrations for very low concentrations of alcohol or water. Thus $P_b A_n$(alcohol) is equal to a constant times the alcohol concentration. The constant is a function of the alcohol used and the concentration of the anion radical.

Since the observed nitrogen splitting smoothly increases upon addition of proton donor, this value must be a time average between the free ion (α) and the hydrogen bonded ion (α'). As more proton donor is added to the solution the concentration of the time averaged species increases at the expense of the ion pair (Figure 2). From this, it is clear that hydrogen bonding stabilizes the formaly free ion relative to the ion pair. This is an expected result if the enthalpy of hydrogen bonding to α is finite. At high concentrations of proton donor (greater than about 1 M) no esr signal can be observed for the ion paired species.

If our conclusion that the experimental A_n is due to a time averaged between α and α' is correct, we would expect a slower modulation of the nitrogen splitting as the temperature is lowered resulting in line width alternation. The g values of the two radicals should be the same or very close resulting in broadening of the $m = -1$ and $m = +1$ lines in the region of line width alternation. The $m = 0$ lines should remain sharp. In agreement with this prediction, dramatic line width alternation is observed when these systems containing proton donor are studied under low temperature conditions (Figure 3). The line width alternation cannot be due to rapid exchange between α and β, since both can be observed simultaneously at room temperature. The line width alternation is due to the rapid exchange between the free ion and the hydrogen

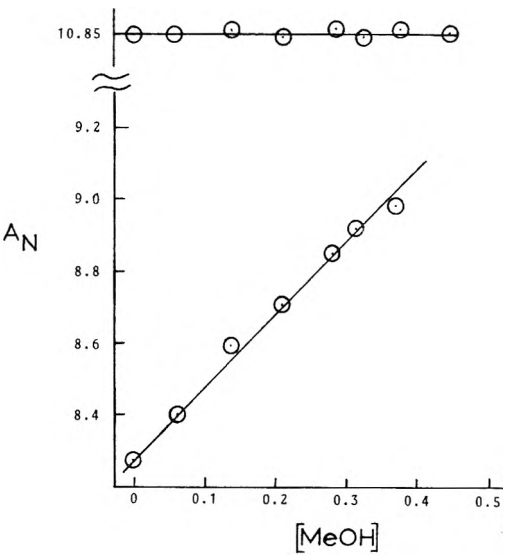

Figure 1. Plot of A_n for the free ion (lower) and the ion pair (upper) *vs.* the methanol concentration (M). The coupling constants are in Gauss.

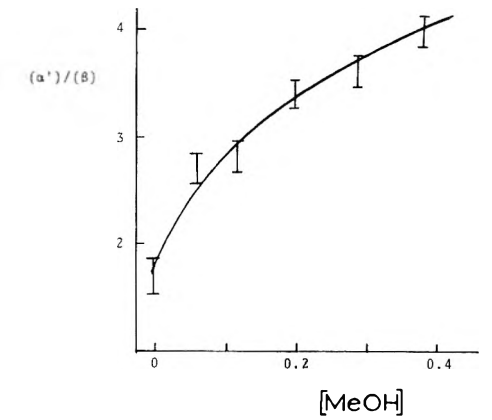

Figure 2. Plot of the concentration of the free ion (α') divided by the ion pair concentration (β) *vs.* the methanol concentration (M).

bonded ion. For dilute solutions of alcohol or water the line width alternation increases rapidly with increasing proton donor concentration. Figure 3 shows that the esr spectrum at $-10°$ for the $PhNO_2$ system containing 0.38 M methanol exhibits strong line width alternation while the same system not containing methanol does not show any line width alternation effect. Essentially only the 18 esr lines resulting from the proton splitting of the $m = 0$ component of the nitrogen coupling can be seen at $-10°$. At still lower temperatures, the simultaneous observation of α and α' would be expected. This cannot be accomplished due to the fact that the solvent freezes at about $-10°$. A simple plot of esr line width *vs.* $1/RT$ allows us to estimate the magnitude of the energy of activation for reaction 3. The energies of activation estimated in this manner are shown in Table I. For the case of water, R

(6) G. R. Stevenson, L. Echegoyen, and L. R. Lizardi, *J. Phys. Chem.*, **76**, 1439 (1972).
(7) G. R. Stevenson, L. Echegoyen, and L. R. Lizardi, *J. Phys. Chem.*, **76**, 2058 (1972).
(8) G. R. Stevenson, L. Echegoyen, and L. R. Lizardi, *J. Phys. Chem.*, submitted for publication.
(9) F. J. Smentowski and G. R. Stevenson, *J. Amer. Chem. Soc.*, **90**, 4661 (1968).
(10) J. M. Gross and J. D. Barnes, *J. Phys. Chem.*, **74**, 2936 (1970).

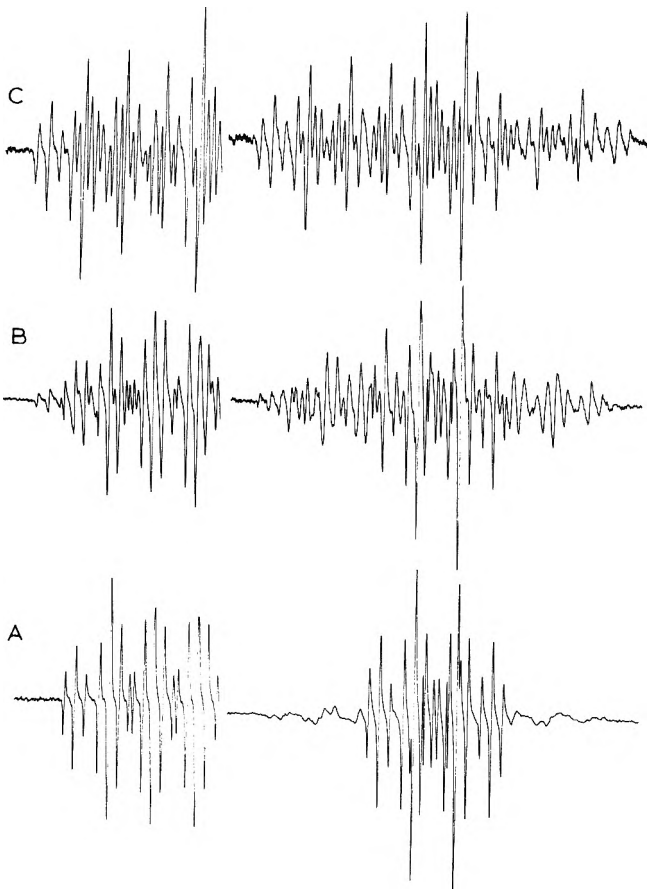

Figure 3. Esr spectra for the $PhNO_2$–HMPA–Li system as a function of temperature. The spectra on the left are the low-field halves for the system without added methanol. The spectra on the right are for the system containing 0.38 *M* methanol: (A) −10°, only the free ion on the left and the time-averaged species on the right can be observed; (B) 25°, the ion pair is observed simultaneously with the free ion and with the time-averaged species; (C) 70°, only the ion pair can be observed.

represents the other proton hydrogen bonded to a molecule of HMPA.

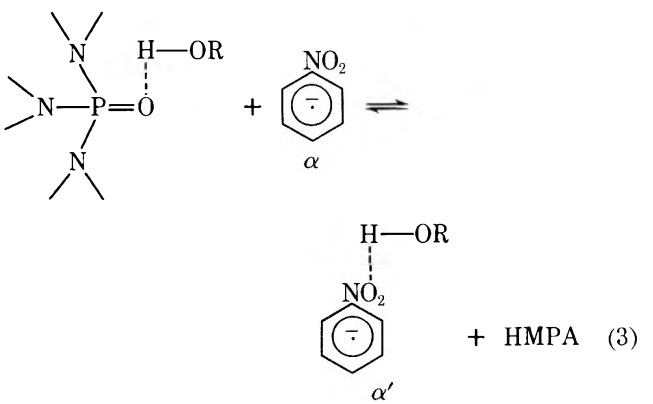

HMPA itself is a good acceptor for hydrogen bonds.[11] For very dilute solutions of alcohol there is very little self-association of the alcohol, and the hydrogen bonding equilibrium can be described by eq 3.

The time averaged esr nitrogen splitting constant, $\bar{A}_n$, is given by

$$\bar{A}_n\{(\alpha) + (\alpha')\} = 8.48(\alpha) + (\alpha')A_n' \quad (4)$$

(α) represents the concentration of the free ion, (α') represents the concentration of the hydrogen bonded ion, A_n' represents the esr splitting for the hydrogen bonded species, and $\bar{A}_n$ is the observed nitrogen splitting.

TABLE I: Thermodynamic Parameters Controlling Equilibrium 3 and A_n' for the Proton Donors

Proton donor	A_n', G	K_{eq} at 25°	$\Delta H°$, kcal/mol	$\Delta S°$, eu	E_a, kcal/mol
Methanol	14	3.5 ± 0.2	1.2 ± 0.2	1.6	1.8
tert-Butyl alcohol	13	1.0 ± 0.4	1		5.0
Water	14.5	0.9 ± 0.1	1.6 ± 0.2	5.5	2.8

The thermodynamic equilibrium constant is given by $K_{eq} = (\alpha')(HMPA)/(\alpha)(HMPA')$, where (HMPA′) represents the concentration of the HMPA hydrogen bonded to the proton donor. Combining this equation for K_{eq} with eq 4, we obtain the expression

$$K_{eq} = (\bar{A}_n - 8.48)(HMPA)/(A_n' - \bar{A}_n)(HMPA') \quad (5)$$

A_n' is estimated from the extrapolation of a plot of $\bar{A}_n$ *vs.* the concentration of the proton donor to infinite concentration. The slope of this plot falls off rapidly at higher concentrations of alcohol (Figure 4). For the case of methanol, this yields a value of 14 G for A_n'. The values used for A_n' are given in Table I for the alcohols and for water. For all cases the observed splitting, $\bar{A}_n$, is much closer to 8.48 than to A_n'. This means that the concentration of the hydrogen bonded HMPA is much greater than that for the hydrogen bonded ion. This is an expected result, since HMPA forms relatively strong hydrogen bonds,[11] and nitrobenzene neutral molecule is a poor proton acceptor.[12] We expect the anion radical of $PhNO_2$ to be a better proton acceptor than the neutral molecule. Since (HMPA′) is much larger than (α'), we can use the concentration of proton donor for the (HMPA′) term in eq 5.

Using the technique described above, the equilibrium constants were determined for the $PhNO_2$–HMPA–Li system with added methanol, *tert*-butyl alcohol, and water. The equilibrium constants determined in this manner gave quantitative agreement for alcohol concentrations between 0.05 and 0.5 *M*. The equilibrium constants are given in Table I together with the standard deviation determined from six measurements.

The enthalpy of the reaction consists of four predominant terms: the enthalpy of hydrogen bonding to the HMPA, the enthalpy of hydrogen bonding to the free $PhNO_2$ anion radical, the heat of solution of the products, and the heat of solution of the reactants. Experimentally the $\Delta H°$ can be determined from a plot of $\ln\{(\bar{A}_n - 8.48)/(A_n' - \bar{A}_n)\}$ *vs.* $1/RT$. This plot should yield a straight line if the concentration of the HMPA′ does not vary appreciably. This condition is met since at all temperatures (HMPA′) is much greater than (α'). All of the systems studied do yield linear plots (Figure 5). The enthalpies for the various systems are given in Table I.

The enthalpy for all three systems studied are positive and between 0 and 2 kcal/mol. This indicates that HMPA is a much better hydrogen bond acceptor than the anion radical of $PhNO_2$. Since $PhNO_2$ is known to be a very weak hydrogen bond acceptor, this small $\Delta H°$ indicates that the anion radical of $PhNO_2$, free from counterion in-

(11) T. Olsen, *Acta Chem. Scand.*, **24**, 3081 (1970).
(12) W. F. Baitinger, P. v. R. Schleyer, T. S. S. R. Murty, and L. Robinson, *Tetrahedron*, 1635 (1964).

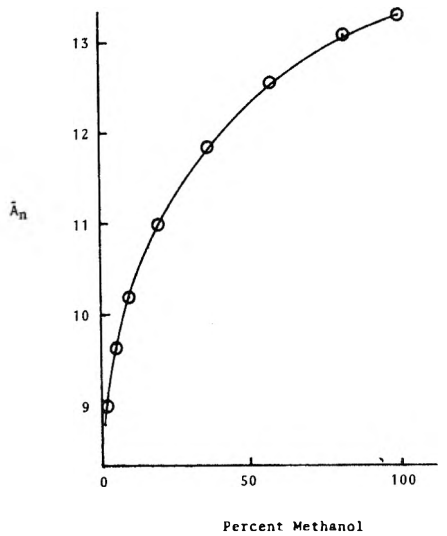

Figure 4. Variation of the nitrogen coupling constant with added methanol for the time-averaged species. The anion radical was generated in HMPA by electrolytic reduction using 0.1 *M* tetra-*n*-butylammonium perchlorate as a counterion.

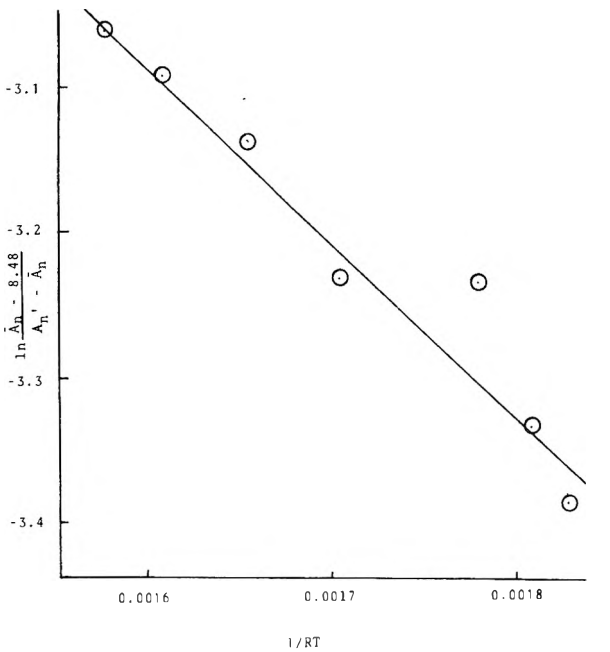

Figure 5. Modified vant' Hoff plot for the system $PhNO_2$–HMPA–Li containing 0.38 *M* methanol.

teractions, is a much stronger hydrogen bond acceptor. The enthalpy for the system containing *tert*-butyl alcohol as a proton donor is too small to yield measurable coupling constant differences at different temperatures. For this system we can only say that ΔH° is greater than zero and less than one.

The entropies have been calculated from the Eyring equation for the three systems and are given in Table I. The signs of ΔS° are positive, indicating that there is a reorganization of the solvent in going from the free ion to the hydrogen bonded ion. The solvent is more ordered around the free ion than it is around the hydrogen bonded ion. This is as expected, since there is more dispersion of charge in the hydrogen bonded ion than there is in the free ion.

Solutions of $PhNO_2$ in HMPA containing 0.1–1 *M* methanol also give line width alternation when reduced electrolytically (tetra-*n*-butylammonium perchlorate), but the effect is not as strong as for the lithium reductions. There is some ion pairing in these systems with the counterion as evidenced by the fact that the A_n is a function of the counterion concentration.[6] This weak ion pairing reduces the ability of the NO_2 group to act as a hydrogen bond acceptor.

Experimental Section

Nitrobenzene (Eastman Organic Chemicals) was vacuum distilled prior to use. Hexamethylphosphoramide was vacuum distilled from calcium hydride and stored over molecular sieves 4A. The HMPA was distilled from the solvated electron under high vacuum (10^{-4} mm pressure) directly into the reaction vessel. Weighed portions of proton donor were added directly to the anion radical solutions through a break seal. The entire system above the reaction vessel was then warmed to ensure that all of the proton donor had entered the reaction vessel.

The esr spectra were recorded on an X-band Varian E-3 esr spectrometer. The temperature was controlled with Varian V-4557 variable-temperature controller.

Acknowledgments. We are grateful to Research Corporation for the support of this work.

Magnetic Circular Dichroism of Molecules in Dense Media. III. Substituted Benzenes

D. J. Shieh, S. H. Lin, and H. Eyring*

Department of Chemistry, University of Utah, Salt Lake City, Utah 84112. *(Received October 28, 1972)*

Publication costs assisted by The National Institute of Health, The National Science Foundation, and the Army Research Office—Durham

The magnetic circular dichroism (MCD) of benzene and 27 derivatives through the absorption region 1850–3000 Å have been measured. Two different electronic transitions in the region 2000–2300 Å (generally assigned to the benzene $^1B_{1u}$ upper state) were observed in some of the compounds. The theory developed by Sklar, Platt, and Petruska for predicting the intensity of the benzene $^1A_{1g} \rightarrow {}^1B_{2u}$ electronic transition is adapted to correlate the sign and intensity of the substituted benzene MCD in this region. The method predicts the correct MCD sign and gives approximate estimates of the magnitude of the $^1A_{1g} \rightarrow {}^1B_{2u}$ MCD transition.

Introduction

The value of magnetic optical activity (the Faraday effect) as a tool in the study of molecular structure has been treated by several investigators. There are three general reviews,[1-3] a general discussion of the theory,[4] and a review of organic chemical applications.[5] We shall consider here the Faraday effect for the electronic transitions of benzene and its derivatives.

The electronic spectra of benzene and its derivatives in dense media were studied extensively in the past. Various investigators including Sklar,[6-8] Forster,[9] Platt,[10,11] Moffitt,[12] Murrell and Longuet-Higgins,[13] and Petruska,[14,15] contributed their efforts toward developing a systematic phenomenological theory capable, to a degree, of explaining and predicting the changes in the absorption wavelengths and intensities of the 2600-Å transition. The 2600-Å band of benzene was ascribed to the forbidden transition $^1A_{1g} \rightarrow {}^1B_{2u}$ in an extensive experimental and theoretical study.[16] The 1850-Å band of benzene is generally assigned to the allowed transition $^1A_{1g} \rightarrow {}^1E_{1u}$.[17] The argument as to whether the forbidden 2100-Å transition of benzene should be assigned to a $^1A_{1g} \rightarrow {}^1B_{1u}$ or a $^1A_{1g} \rightarrow {}^1E_{2g}$ transition is not settled. Some recent calculations[18-22] indicate that the $^1B_{1u}$ state lies at higher energies than the $^1E_{2g}$ level. Dunn and Ingold[23] assigned the second excited singlet π state of benzene to $^1E_{2g}$ symmetry based on their gas-phase experimental data. Nelson and Simpson[24] found a band in the 2350-Å region in the vapor spectrum of hexamethylbenzene. They tentatively assigned the former band to the $^1A_{1g} \rightarrow {}^1E_{2g}$ transition. Petruska's work,[14,15] on the patterns of polysubstitutional shifts in the benzene singlets (which did not include the vibronic effects in the calculation of the changes in electronic energies), indicated $^1B_{1u}$ symmetry for the upper state. In their high-resolution study of electron-impact spectra on benzene Lassettre, *et al.*,[25] found two different electronic transitions, one at 6.2 eV and another having peaks at 6.31, 6.41, and 6.53 eV, but they were not able to assign the symmetry of the excited states. However, the recent experimental studies of the vibrational structures in the 2100-Å spectral region of the benzene molecules in low-temperature rare gas matrices,[26] and of toluene, toluene-d_8, *p*-xylene, and *m*-xylene in a solid krypton matrix,[27] provide strong evidence for the $^1B_{1u}$ assignment. The reflection and absorption spectra of solid benzene and benzene-d_6 at low temperature reported by Brith, Lubart, and Steinberg[28] also favored the assignment of the 2100-Å band to the $^1A_{1g} \rightarrow {}^1B_{1u}$ transition. The present investigation concerns the effects of chemical substitution in aromatic hydrocarbons on the electronic transitions associated with magnetic circular dichroism. The purpose is to find rules which will predict the sign of MCD of substituted aromatic hydrocarbons and describe the behavior of

(1) A. D. Buckingham and P. J. Stephens, *Annu. Rev. Phys. Chem.*, **17**, 399 (1966).
(2) P. N. Schatz and A. J. McCaffery, *Quart. Rev. Chem. Soc.*, **23**, 552 (1969).
(3) D. J. Caldwell, J. M. Thorne, and H. Eyring, *Annu. Rev. Phys. Chem.*, **22**, 259 (1971).
(4) P. J. Stephens, *J. Chem. Phys.*, **52**, 3489 (1970).
(5) C. Djerassi, E. Bunnenberg, and D. L. Elder, *Pure Appl. Chem.*, **25**, 57 (1971).
(6) A. L. Sklar, *J. Chem. Phys.*, **7**, 984 (1939).
(7) A. L. Sklar, *J. Chem. Phys.*, **10**, 135 (1944).
(8) A. L. Sklar, *Rev. Modern Phys.*, **14**, 232 (1942).
(9) T. Forster, *Z. Naturforsch. A*, **2**, 149 (1947).
(10) J. R. Platt, *J. Chem. Phys.*, **17**, 484 (1949).
(11) J. R. Platt, *J. Chem. Phys.*, **19**, 263 (1951).
(12) W. Moffitt, *J. Chem. Phys.*, **22**, 320 (1954).
(13) J. N. Murrell and H. C. Longuet-Higgins, *Proc. Phys. Soc., London, Sect. A*, **68**, 329, 601, 969 (1955).
(14) J. Petruska, *J. Chem. Phys.*, **34**, 1111 (1961).
(15) J. Petruska, *J. Chem. Phys.*, **34**, 1120 (1961).
(16) G. Herzberg, "Electronic Spectra of Polyatomic Molecules," Van Nostrand, Princeton, N. J., 1966, p 555–557.
(17) G. Nordheim, H. Sponer, and E. Teller, *J. Chem. Phys.*, **8**, 455 (1940).
(18) J. E. Bloor, J. Lee, and S. Gartside, *Proc. Chem. Soc., London*, 413 (1960).
(19) J. Koutecky, J. Cizek, J. Dubsky, and K. Hlavaty, *Theor. Chim. Acta*, **2**, 462 (1965).
(20) J. Koutecky, K. Hlavaty, and P. Hochmann, *Theor. Chim. Acta*, **3**, 341 (1965).
(21) J. Koutecky, "Modern Quantum Chemistry-Istanbul Lectures," Vol. 1, O. Sinanoglu, Ed., Academic Press, New York, N. Y., 1965, pp 215–220.
(22) R. J. Buenker, J. L. Whitten, and J. D. Petke, *J. Chem. Phys.*, **49**, 2261 (1968).
(23) T. M. Dunn and C. K. Ingold, *Nature (London)*, **176**, 65 (1955).
(24) R. C. Nelson and W. T. Simpson, *J. Chem. Phys.*, **23**, 1146 (1955).
(25) E. N. Lassettre, A. Skerbele, M. A. Dillon, and K. J. Ross, *J. Chem. Phys.*, **48**, 5066 (1968).
(26) B. Katz, M. Brith, B. Sharf, and J. Jortner, *J. Chem. Phys.*, **52**, 88 (1970).
(27) B. Katz, M. Brith, B. Sharf, and J. Jortner, *J. Chem. Phys.*, **54**, 3924 (1971).
(28) M. Brith, R. Lubart, and I. T. Steinberg, *J. Chem. Phys.*, **54**, 5104 (1971).

the MCD intensity changes with the types and number of substituents and the position of substitution. For this purpose, we have measured MCD of some 27 substituted benzenes. To interpret and correlate the MCD data for these compounds, we shall adopt the theory developed by Sklar,[6-8] Platt,[11] and Petruska[14,15] for the absorption spectra of electronic transitions of aromatic hydrocarbons of MCD. A more detailed theoretical approach has been developed by Caldwell and Eyring[29] which provides additional insight into these problems of symmetry.

Experimental Section

The MCD spectra reported here were measured with a modified Cary Model 60 recording spectropolarimeter with a Varian superconducting solenoid system at a magnetic field of 45 kG. The mechanical slit widths were preprogrammed as recommended by the data manual for the Cary Model 60 spectropolarimeter, with the assumption of a spectral slit width (half-band width) of about 50 Å for the $^1A_{1g} \rightarrow {}^1B_{2u}$ system and 100 Å for the $^1A_{1g} \rightarrow {}^1E_{1u}$ systems. The molar ellipticity

$$[\Theta]_M = (\Theta^\circ/ClH)100^\circ \text{ dl dm}^{-1} \text{ mol}^{-1} \text{ G}^{-1}$$

where Θ° is the ellipticity in degrees, C is the concentration of the solution in mole liter^{-1}, l is the pathlength in centimeters, and H is the magnetic field in Gauss. The spectra were calibrated using a 1 mg/ml aqueous solution of camphor-d_{10}-sulfonic acid in a 1-cm pathlength cell which gives forth a positive natural CD band centered at 2900 Å with an ellipticity (Θ°) of about 0.31° (based on the Cary Model 6001 CD accessory instruction manual). The absorption spectra were obtained using a Cary 14 recording spectrophotometer.

Benzene and n-heptane were Mallinckrodt spectrophotometric grade solvents; toluene and benzonitrile were MC/B spectroquality reagent; fluorobenzene, chlorobenzene, bromobenzene, phenol, nitrobenzene, benzaldehyde, o-dichlorobenzene, and hexafluorobenzene were MC/B reagent grade chemicals; o-xylene, m-xylene, p-xylene, m-dichlorobenzene, 1,2,4-trimethylbenzene, 1,2,4-trichlorobenzene, and pentamethylbenzene were Eastman Organic chemicals with boiling points or melting points ranging over 1 to 2°; iodobenzene was Eastman Organic chemical grade, redistilled once (a colorless liquid at room temperature); aniline was MC/B reagent grade and was redistilled once with some zinc dust (an almost colorless liquid at room temperature); 1,3,5-trimethylbenzene was Baker's reagent (bp 164–166°); 1,2,4,5-tetramethylbenzene was Baker's reagent (mp 79–81°) and was resublimed once; pentachlorobenzene and benzenehexacarboxylic acid were obtained from Aldrich Chemical Co.; 1,2,3,5-tetramethylbenzene was purchased from K & K Laboratories Inc., and hexachlorobenzene was Eastman Organic Chemical's practical grade and was resublimed twice (needle crystal, mp 231–232°). All spectra except benzenehexacarboxylic acid, which was dissolved in methyl alcohol, were obtained using n-heptane as the solvent.

Data Reduction

The method of monents has been used by several investigators in the past to extract the Faraday parameters from the experimental data.[2,30-32] For a nondegenerate electronic transition the magnetic rotational strength is[2,31,32]

$$B = -(33.53)^{-1} \int \frac{[\Theta]_M}{\lambda} \, d\lambda$$

We extract (or reduce) our data by using the following approximate equation

$$B = -(33.53\lambda_m)^{-1} \int [\Theta]_M \, d\lambda$$

where λ_m is the wavelength at the middle of the MCD band. Substituting the experimental magnetic molar ellipticity $[\Theta]_M = (\Theta^\circ/ClH)100$ into the above equation we have

$$B = -100(33.53\lambda_m ClH)^{-1} \int \Theta^\circ \, d\lambda$$

The ordinate of the recording chart paper gives the degree of ellipticity and its abscissas records the wavelength. The area read from the planimeter is in square inches. Their relation is 1 in^2 = 1.5×10^{-8} degree cm so that $\int \Theta^\circ \, d\lambda$ = area (in.^{2}) $\times 1.5 \times 10^{-8}$

$$B = -0.99 \times 10^{-12} \frac{\text{area(in}^2\text{)}}{\lambda_m Cl} \text{D}^2 \, \beta \text{ cm}^{-1}$$

where $H = 4.5 \times 10^4$ G was used. D is the Debye unit and β the Bohr magneton.

The experimental MCD rotational strength for the electronic transition $^1A_{1g} \rightarrow {}^1B_{2u}$ of benzene is $B^0(^1A_{1g} \rightarrow {}^1B_{2u}) = 0.14 \times 10^{-5}$ D^2 β cm^{-1}, and for all of the benzene derivatives with a transition derived from the $^1A_{1g} \rightarrow {}^1B_{2u}$ of benzene B^0 becomes $B = B^0 + \Delta B$. The quantities in Table I are calculated as follows: *e.g.*, 1,2-dimethylbenzene has an MCD rotational strength $B = 2.35 \times 10^{-5}$ D^2 β cm^{-1} (Table II). ΔB is obtained by ignoring $\Delta B(A \rightarrow B)_M$ in eq 4, *i.e.*, $\Delta B(^1A_{1g} \rightarrow {}^1B_{2u}) = B(^1A_{1g} \rightarrow {}^1B_{2u}) - B^0(^1A_{1g} \rightarrow {}^1B_{2u}) = 2.21 \times 10^{-5}$ D^2 β cm^{-1} $\cong \Delta B(^1A_{1g} \rightarrow {}^1B_{2u})_q + \Delta B(^1A_{1g} \rightarrow {}^1B_{2u})_v$. $\Delta B(^1A_{1g} \rightarrow {}^1B_{2u})_v$ is estimated according to the assumptions made in the text, *e.g.*, for singly methylated benzene $\Delta B(^1A_{1g} \rightarrow {}^1B_{2u})_v \simeq \frac{1}{3}B(^1A_{1g} \rightarrow {}^1B_{2u})$ of the 1,3,5-trimethylbenzene and $\simeq \frac{1}{6}B(^1A_{1g} \rightarrow {}^1B_{2u})$ of hexamethylbenzene, *i.e.*, $\simeq -0.27 \times 10^{-5}$ D^2 β cm^{-1}. Finally, the $\Delta B(^1A_{1g} \rightarrow {}^1B_{2u})_q$ of 1,2-dimethylbenzene is calculated from $\Delta B(^1A_{1g} \rightarrow {}^1B_{2u}) - \Delta B(^1A_{1g} \rightarrow {}^1B_{2u})_v = (2.21 + 2(0.27)) \times 10^{-5} = 2.75 \times 10^{-5}$ D^2 β cm^{-1}.

Results and Discussion

Foss and McCarville[33] have reported the correlation between the maximum molar MCD of the $^1A_{1g} \rightarrow {}^1B_{2u}$ band of benzene derivatives and the Hammett σ_{para} constant. Here we present some of our MCD spectra including the 2600-, 2100-, and 1850-Å band (we pushed the instrument to the limit in this region, the baseline was not very stable). There is some evidence of two different electronic transitions in the 2100-Å band, the spectral region from 2300 to 2000 Å, in p-xylene (Figure 1), m-xylene (Figure 2), 1,2,4-trimethylbenzene (Figure 3), and 1,2,4,5-tetramethylbenzene (durene, Figure 4). It is probable that we are observing both the $^1A_{1g} \rightarrow {}^1E_{2g}$ and the $^1A_{1g} \rightarrow {}^1B_{2u}$ transitions in these compounds. The ground states of benzene derivatives are nondegenerate. We should only observe A and B terms. The appearance of an A term in benzene and hexasubstituted benzenes, all having D_{6h} symmetry would prove the existence of the transition to a

(29) D. J. Caldwell and H. Eyring, *J. Chem. Phys.*, to be submitted for publication.
(30) C. H. Henry, S. E. Schnatterly, and C. P. Slichter, *Phys. Rev. A*, **137**, 583 (1965).
(31) P. J. Stephens, *Chem. Phys. Lett.*, **2**, 241 (1968).
(32) J. P. Larkindale and D. J. Simkin, *J. Chem. Phys.*, **55**, 5668 (1971).
(33) J. G. Foss and M. E. McCarville, *J. Amer. Chem. Soc.*, **89**, 30 (1967).

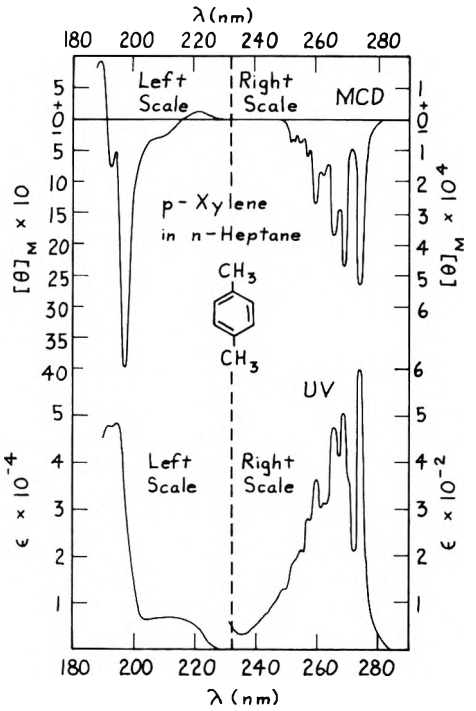

Figure 1. Spectra of 1,4-dimethylbenzene.

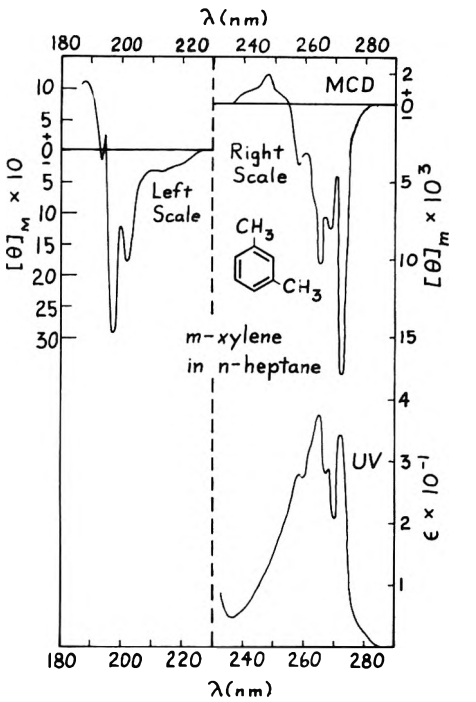

Figure 2. Spectra of 1,3-dimethylbenzene.

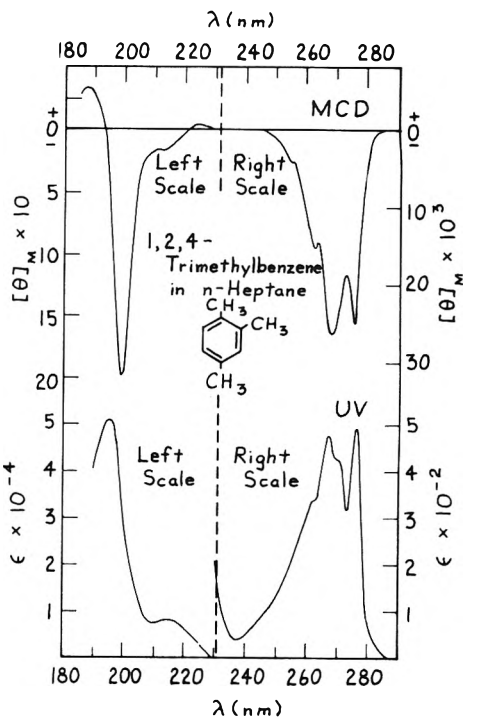

Figure 3. Spectra of 1,2,4-trimethylbenzene.

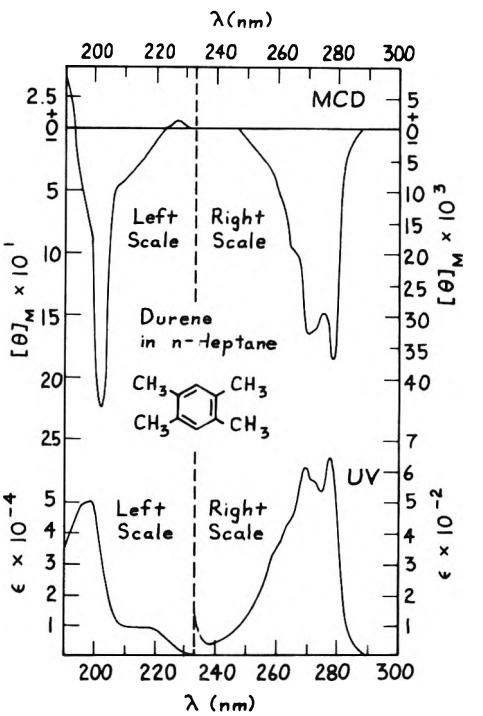

Figure 4. Spectra of durene.

state having $^1E_{2g}$ symmetry. The reason we do not observe A terms in these compounds (see Figures 5–7) could be due to the overlap of the two transitions. p-Xylene, durene, and 1,2,4-trimethylbenzene all show a positive peak around 2200 Å and a negative peak around 2100 Å overlapped with a transition having $^1A_{1g} \rightarrow {}^1E_{1u}$ benzene parentage.

p-Xylene and durene belong to D_{2h}, m-xylene belongs to C_{2v}, and 1,2,4-trimethylbenzene belongs to C_s symmetry. The result of applying the symmetry selection rules indicates that the transition to the excited state $^1E_{2g}$ of benzene for molecules having D_{2h} symmetry is forbidden but the transition to the $^1B_{1u}$ excited state is allowed. The transitions to both of these excited states are allowed for compounds with C_{2v} and C_s symmetry (see Table III where (a) means symmetry allowed and (f) signifies a symmetry forbidden transition). It seems reasonable to speculate, by comparing the MCD line shapes in this region, that the positive peaks in the above-mentioned three compounds belong to the positive troughs of the sinusoidal A term of MCD bands and their negative trough overlaps with the negative B term MCD bands produced by the transition to the upper state derived from the $^1B_{1u}$ of ben-

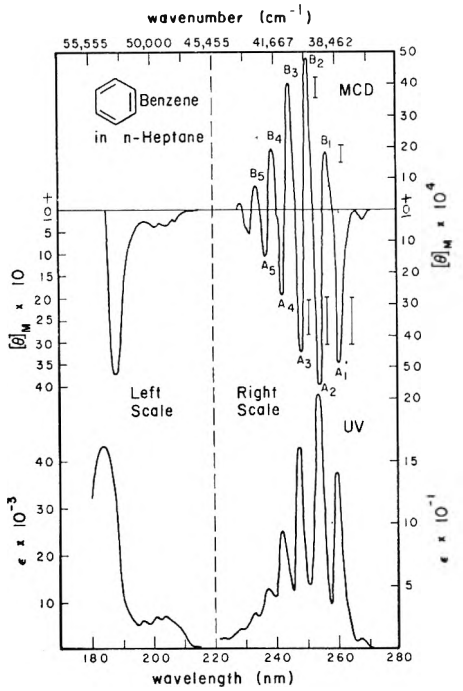

Figure 5. Spectra of benzene.

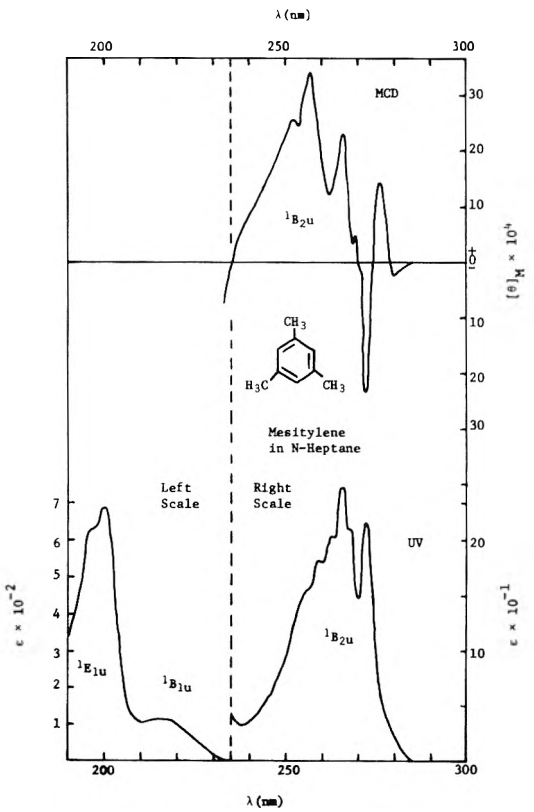

Figure 6. Spectra of 1,3,5-trimethylbenzene.

zene. We observed a large negative A term in the MCD in the spectral region of 1850 Å for most of the benzene derivatives. The positive trough of almost all of the sinusoidal A terms are not recorded adequately (except for hexachlorobenzene which shows a clear A term). The MCD instrument is not very stable in this region, consequently we are not able at this time to make any definite comment on the Jahn-Teller splitting. The possibility of observing this effect has been brought out by Stephens, *et al.*[34] The

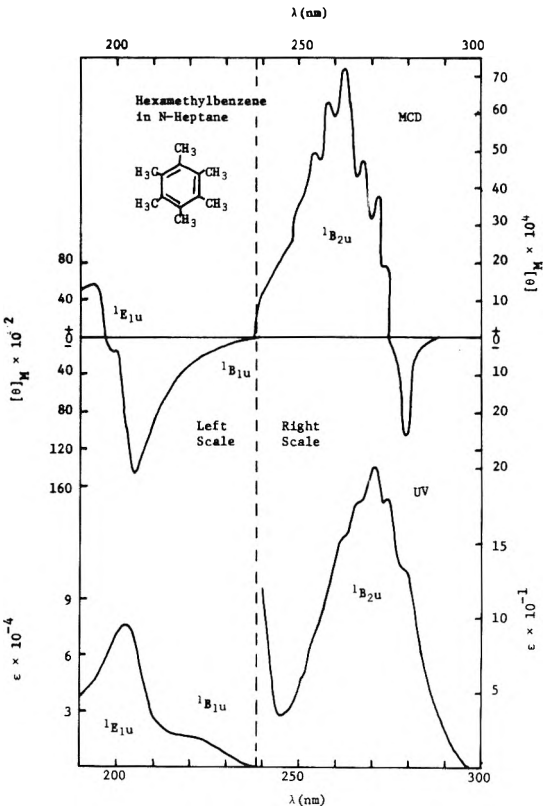

Figure 7. Spectra of hexamethylbenzene.

relative signs of the first and second $\pi \rightarrow \pi^*$ transitions of benzene derivatives are discussed by Caldwell and Eyring.[29]

It has been shown that the rotational strength of the MCD for a nondegenerate electronic transition A → B is determined by $B(\mathrm{A} \rightarrow \mathrm{B})$, which is defined by[4,35]

$$B(\mathrm{A} \longrightarrow \mathrm{B}) = I_{\mathrm{m}}(\vec{r}_{\mathrm{AB}} \cdot \vec{M}_{\mathrm{BA}}) \tag{1}$$

where $\vec{r}_{\mathrm{AB}}$ represents the matrix element of the electric moment and $\vec{M}_{\mathrm{AB}}$ is defined by the relation

$$\vec{M}_{\mathrm{BA}} = \sum_{\mathrm{G}}{}' \frac{\vec{r}_{\mathrm{GA}} \times (\vec{\mu}_{\mathrm{m}})_{\mathrm{BG}}}{h\omega_{\mathrm{GB}}^{\circ}} + \sum_{\mathrm{G}}{}' \frac{\vec{r}_{\mathrm{BG}} \times (\vec{\mu}_{\mathrm{m}})_{\mathrm{GA}}}{h\omega_{\mathrm{GA}}^{\circ}} \tag{2}$$

By $B(\mathrm{A} \rightarrow \mathrm{B})$ we signify the diamagnetic term in the MCD of the A → B transition. In eq 2, $(\mu_{\mathrm{m}})_{\mathrm{BG}}$ and $(\vec{\mu}_{\mathrm{m}})_{\mathrm{GA}}$ denote the matrix elements of the magnetic moment. If we compare the expression for $B(\mathrm{A} \rightarrow \mathrm{B})$ given in eq 1 with the rotational strength of the natural optical activity, we can see that $\vec{M}_{\mathrm{BA}}$ in eq 1 plays the same role as the magnetic transition moment in natural optical rotation.

Now let $B(\mathrm{A} \rightarrow \mathrm{B})$ in eq 1 represent the MCD rotational strength before substitution. After substitution, when the wave functions are changed by small amounts, $\vec{r}_{\mathrm{AB}}$ and $\vec{M}_{\mathrm{BA}}$ are changed by Δr_{AB} and $\Delta\vec{M}_{\mathrm{BA}}$, respectively. The change in $B(\mathrm{A} \rightarrow \mathrm{B})$ that is $\Delta B(\mathrm{A} \rightarrow \mathrm{B})$ caused by $\Delta\vec{r}_{\mathrm{AB}}$ and $\Delta\vec{M}_{\mathrm{BA}}$ to the first order is given by

$$\Delta B(\mathrm{A} \longrightarrow \mathrm{B}) = I_{\mathrm{m}}(\Delta\vec{r}_{\mathrm{AB}} \cdot \vec{M}_{\mathrm{BA}}) + I_{\mathrm{m}}(\vec{r}_{\mathrm{AB}} \cdot \Delta\vec{M}_{\mathrm{BA}}) + I_{\mathrm{m}}(\Delta\vec{r}_{\mathrm{AB}} \cdot \Delta\vec{M}_{\mathrm{BA}}) \tag{3}$$

(34) P. J. Stephens, P. N. Schatz, A. B. Richie, and A. J. McCaffery, *J. Chem. Phys.*, **48**, 132 (1968).
(35) D. J. Shieh, S. H. Lin, and H. Eyring, *J. Phys. Chem.*, **76**, 1844 (1972).

TABLE I: $B(^1A_{1g} \rightarrow {}^1B_{2u})$ and q_m

Substituents	Position	$B(^1A_{1g} \rightarrow {}^1B_{2u})$, $D^2\beta/cm^{-1} \times 10^5$	$q_m \times 10^{10}$
CH_3	1	2.15	5.0
	1,2	2.35	
	1,3	1.34	
	1,4	5.72	
	1,2,4	4.88	
	1,3,5	−0.68	
	1,3,4,5	1.31	
	1,2,4,5	7.23	
	Penta	0.95	
	Hexa	−1.36	
Cl	1	3.38	6.0
	1,2	4.26	
	1,3	3.72	
	1,2,4	11.58	
	Penta	3.27	
	Hexa	−3.45	
F	1	1.16	12.5
	Hexa	−1.34	
Br	1	3.38	6.0
I	1	2.80	8.0
CN	1	−14.61	−11.0
OH	1	16.22	20.0
COOH	1	−28.57	−17.0
	Hexa	−5.29[a]	
NO_2	1	−34.84	
CHO	1	−36.06	−20.0
NH_2	1	46.55	24.0

[a] Methanol solution.

The change in electric transition moment $\Delta\vec{r}_{AB}$ caused by the introduction of substituents consists of two parts, $\Delta\vec{r}_{AB} = (\Delta\vec{r}_{AB})_q + (\Delta\vec{r}_{AB})_v$; $(\Delta\vec{r}_{AB})_q$ represents the substituent induced component (due to the inductive and resonance effects) and $(\Delta\vec{r}_{AB})_v$, the vibronically induced component. The contribution to $\Delta\vec{M}_{BA}$ may originate from the changes in the electric transition moment, the magnetic transition moment, and in the energy levels. For convenience, we shall rewrite eq 3 as

$$\Delta B(A \longrightarrow B) = \Delta B(A \longrightarrow B)_q + \Delta B(A \longrightarrow B)_v + \Delta B(A \longrightarrow B)_M \quad (4)$$

which clearly leads to

$$\Delta B(A \longrightarrow B)_q = I_m[(\Delta\vec{r}_{AB})_q \cdot (\vec{M}_{BA} + \Delta\vec{M}_{BA})]$$

$$\Delta B(A \longrightarrow B)_v = I_m[(\Delta\vec{r}_{AB})_v \cdot (\vec{M}_{BA} + \Delta\vec{M}_{BA})]$$

$$\Delta B(A \longrightarrow B)_M = I_m(\vec{r}_{AB} \cdot \Delta\vec{M}_{BA}) \quad (5)$$

For the $^1A_{1g} \rightarrow {}^1B_{2u}$ transition of benzene, the transition moment $\vec{r}_{AB}$ of benzene itself is small as the transition is symmetry forbidden, and $\vec{M}_{BA}$ for benzene itself also vanishes unless the vibronic effect is considered. From the discussion of the electronic spectra of the $^1A_{1g} \rightarrow {}^1B_{2u}$ transition,[14,15,36] it is found that in most cases $|(\Delta\vec{r}_{AB})_v| < |(\Delta\vec{r}_{AB})_q|$ and thus we expect that $|\Delta B(A \rightarrow B)_q| > |\Delta B(A \rightarrow B)_v|$. In this paper, we shall show how to estimate $\Delta B(A \rightarrow B)_q$ and $\Delta B(A \rightarrow B)_v$, and demonstrate that as far as the prediction of the sign of MCD and the estimation of the order of magnitude of MCD are concerned, we may ignore $\Delta B(A \rightarrow B)_M$.

TABLE II: $\Delta B(^1A_{1g} \rightarrow {}^1B_{2u})^a$

Substituents	Position	$\Delta B(^1A_{1g} \rightarrow B_{2u})$	$\Delta B(^1A_{1g} \rightarrow B_{2u})_v$	$\Delta B(^1A_{1g} \rightarrow B_{2u})_q$
CH_3	1	2.01	−0.27	2.28
	1,2	2.21	−0.54	2.75
	1,3	1.20	−0.54	1.74
	1,4	5.58	−0.54	6.12
	1,2,4	4.74	−0.82	5.56
	1,3,5	−0.82	−0.82	0
	1,2,3,5	1.17	−1.08	2.25
	1,2,4,5	7.09	−1.08	8.17
	Penta	0.81	−1.35	2.16
	Hexa	−1.50	−1.50	0
Cl	1	3.24	−0.60	3.84
	1,2	4.12	−1.20	5.32
	1,3	3.58	−1.20	4.78
	1,2,4	11.44	−1.80	13.24
	Penta	3.13	−3.00	6.13
	Hexa	−3.59	−3.59	0
F	1	1.02	−0.25	1.27
	Hexa	−1.48	−1.48	0
Br	1	3.24		
I	1	2.66		
CN	1	−14.75		
OH	1	16.08		
COOH	1	−28.71	−0.91	−27.80
	Hexa	−5.43	−5.43	0
NO_2	1	−34.98		
CHO	1	−36.20		
NH_2	1	46.41		

[a] $(D^2\beta/cm^{-1}) \times 10^5$.

TABLE III: Correlation Table

C_{0h}	D_{2h}	C_{2v}	C_s
$B_{2u}(f)$	$B_{3u}(a)$	$B_1(a)$	$A'(a)$
$E_{2g}(f)$	$A_g(f) + B_{1g}(f)$	$A_1(a) + B_1(a)$	$2A'(a)$
$B_{1u}(f)$	$B_{2u}(a)$	$A_1(a)$	$A'(a)$
$E_{1u}(a)$	$B_{2u}(a) + B_{3u}(a)$	$A_1(a) + B_1(a)$	$2A'(a)$

According to the Sklar-Platt-Petruska (SPP) theory[6-8,14,15] the change in the electric transition moment $(\Delta\vec{r}_{AB})_q$ induced by substitution can be expressed in terms of the magnitude of the spectroscopic moment q_m. For

$$(\Delta\vec{r}_{AB})_q = \sum_m q_m \hat{t}_{-2m} \quad (6)$$

where q_m represents the magnitude of the spectroscopic moment of the substituent at m, and the unit vector $\hat{t}_{-2m}$ is defined by

$$\hat{t}_{-2m} = \hat{j} \cos(2m\rho) + \hat{i} \sin(2m\rho) \quad (7)$$

where $\rho = \pi/3$ for benzene. The unit vectors $\hat{i}$ and $\hat{j}$ are in the x and y directions, respectively.

For homosubstitutions, the q_m's are equal and eq 6 reduces to

$$(\Delta\vec{r}_{AB})_q = q\sum_m \hat{t}_{-2m} \quad (8)$$

It can easily be shown[6-8,14,15] that $(\Delta\vec{r}_{AB})_q = 0$ for the

(36) P. E. Stevenson, *J. Chem. Educ.*, **41**, 234 (1964).

TABLE IV

Substituents	Position	$\overline{\Delta B_q}$ (exptl)	$\overline{\Delta B_q}$ (theor)	$\overline{\Delta B_q}$ $\alpha = 1/\sqrt{3}$
	a. ΔB_q Experimental and Theoretical			
CH_3	1	1	1	1
	1,2	1.21	$1/2 + \sqrt{3}/2\alpha$	1
	1,3	0.76	$1/2 - \sqrt{3}/2\alpha$	0
	1,4	2.68	2	2
	1,2,4	2.44	$3/2 + \sqrt{3}/2\alpha$	2
	1,2,3	0	0	0
	1,3,5	0	0	0
	1,2,4,5	3.58	$1 + \sqrt{3}\alpha$	2
	1,2,3,4		1	1
	1,3,4,5	0.99	1	1
	Penta	0.95	$1/2 + \sqrt{3}/2\alpha$	1
	Hexa	0	0	0
Cl	1	1	1	1
	1,2	1.38	$1/2 + \sqrt{3}/2\alpha$	1
	1,3	1.24	$1/2 - \sqrt{3}/2\alpha$	0
	1,2,4	3.45	$3/2 + \sqrt{3}/2\alpha$	2
	Penta	1.59	$1/2 + \sqrt{3}/2\alpha$	1
	Hexa	0	0	0

Substituents	Position	$\overline{\Delta B_q}$ (theor)	$\overline{\Delta B_q}$ $\alpha = 0.45/\sqrt{3}$
	b. Calculated ΔB_q		
CH_3	1	1	1
	1,2	$1/2 + \sqrt{3}/2\alpha$	0.725
	1,3	$1/2 - \sqrt{3}/2\alpha$	0.275
	1,4	2	2
	1,2,4	$3/2 + \sqrt{3}/2\alpha$	1.725
	1,2,3	0	0
	1,3,5	0	0
	1,2,4,5	$1 + \sqrt{3}\alpha$	1.45
	1,2,3,4	1	1
	1,3,4,5	1	1
	Penta	$1/2 + \sqrt{3}/2\alpha$	0.725
	Hexa	0	0
Cl	1	1	1
	1,2	$1/2 + \sqrt{3}/2\alpha$	0.725
	1,3	$1/2 - \sqrt{3}/2\alpha$	0.275
	1,2,4	$3/2 + \sqrt{3}/2\alpha$	1.725
	Penta	$1/2 + \sqrt{3}/2\alpha$	0.725
	Hexa	0	0

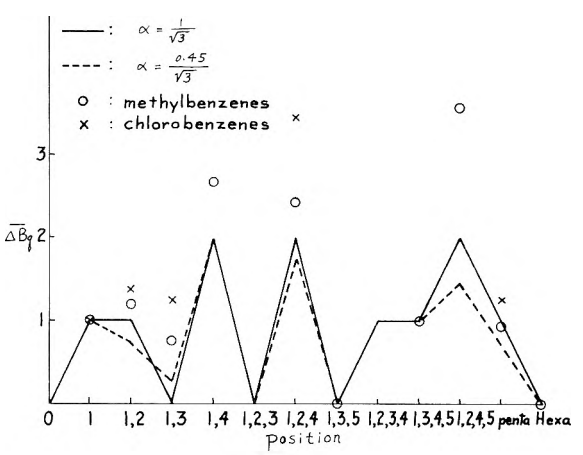

Figure 8. Homosubstitution $\overline{\Delta B_q}$ patterns for the $^1A_{1g} \rightarrow {}^1B_{2u}$ transitions.

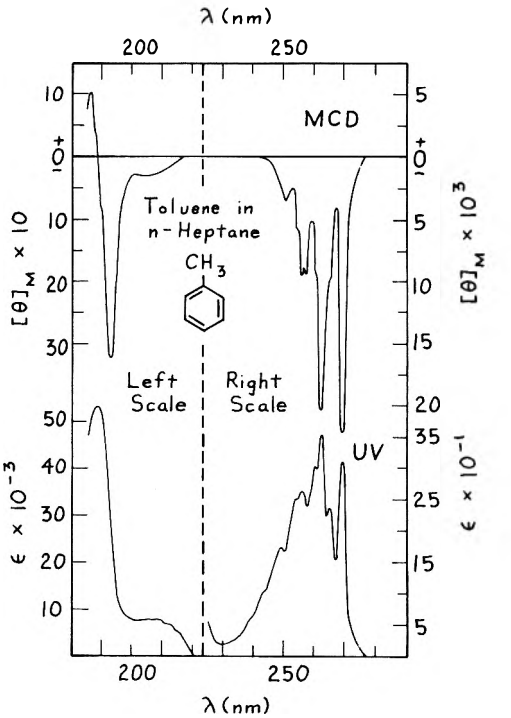

Figure 9. Spectra of toluene.

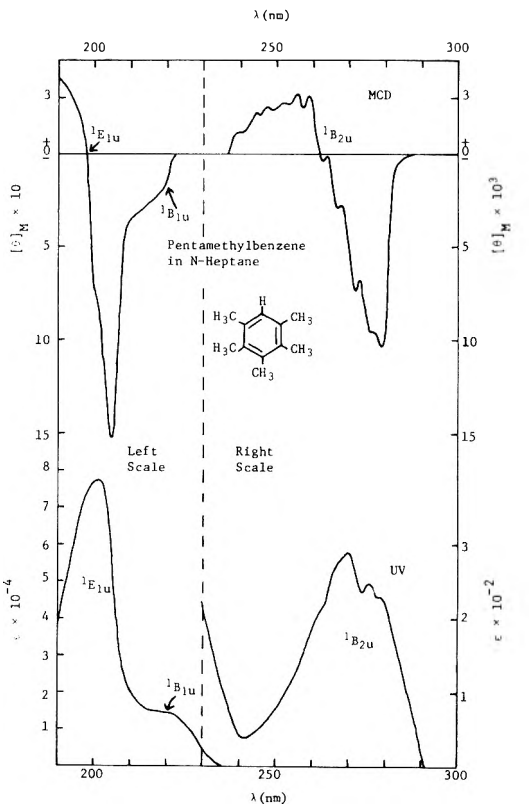

Figure 10. Spectra of pentamethylbenzene.

1,2,3-; 1,3,5-; and hexahomosubstitutions. The q value is positive for ortho–para-directing substituents and negative for meta-direction substituents.[15] *Thus from eq 8 and 4, we expect that for a given type of substituted benzenes other than 1,2,3; 1,3,5; and hexabenzenes, the ortho–para- and meta-directing substituents will give rise to opposite signs in the MCD.* The experimental results of $B(^1A_{1g} \rightarrow$

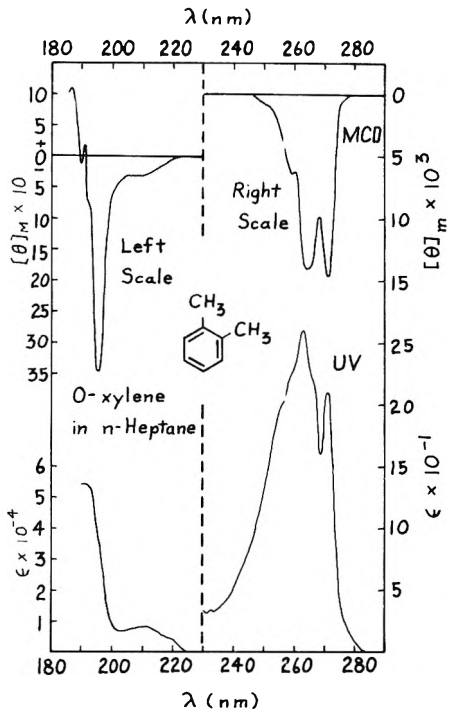

Figure 11. Spectra of 1,2-dimethylbenzene.

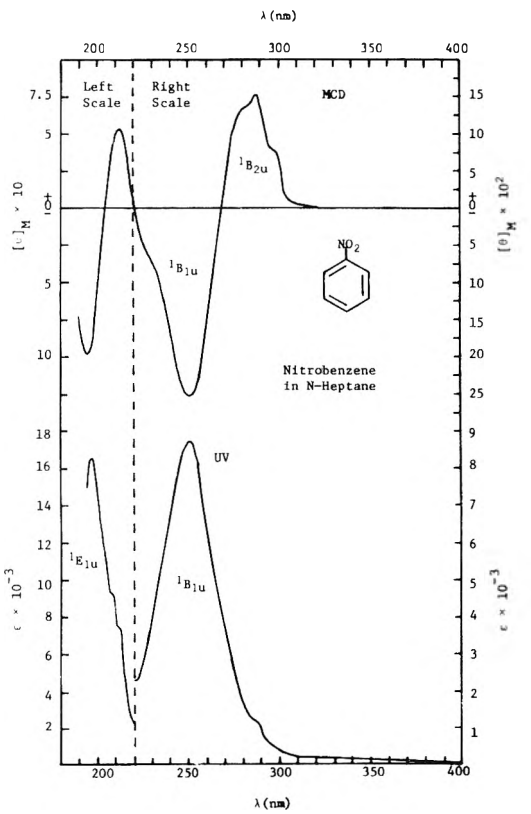

Figure 12. Spectra of nitrobenzene.

$^1B_{2u}$) of substituted benzenes and the transition moment parameter q of some substituents are given in Table II. The experimental observation confirm the italicized rule.

From the three cases of homosubstitution, 1,2,3; 1,3,5; and hexabenzenes, $\Delta B(^1A_{1g} \rightarrow {}^1B_{2u})_q = 0$, as $(\Delta\vec{r}(^1A_{1g} \rightarrow {}^1B_{2u}))_q = 0$. In these cases, the experimental results of $B(^1A_{1g} \rightarrow {}^1B_{2u})$ vary (for example, B(hexa) = $2B(1,3,5)$)

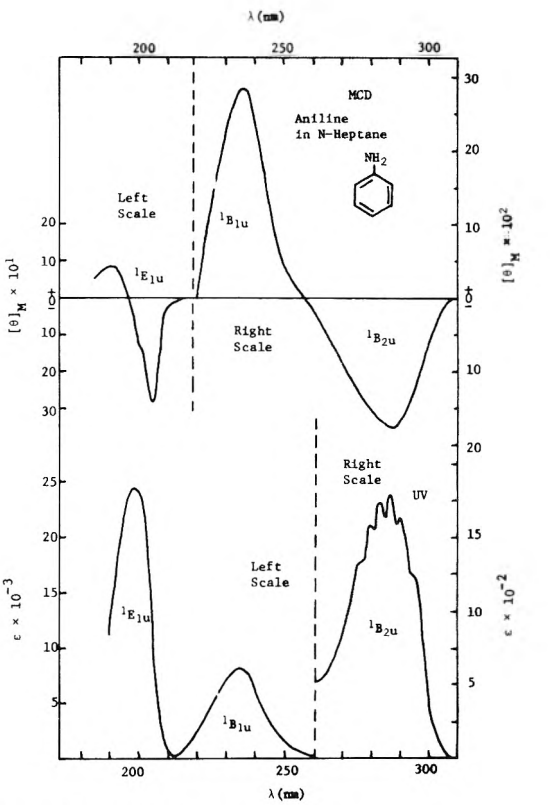

Figure 13. Spectra of aniline.

regularly with the number of substituents, and the sign of the rotational strengths of these homosubstitutions is always negative regardless of the types of substituents.

We now proceed to derive some useful relations for $\Delta B(A \rightarrow B)$. It should be noticed that the rotational strength of pure benzene itself is negligible compared to the rotational strengths of substituted benzenes.[37] Since $(\Delta\vec{r}_{AB})_q$ is in the x-y plane, we may let

$$I_m(\vec{M}_{BA} + \Delta\vec{M}_{BA}) = \hat{i}a + \hat{j}b \qquad (9)$$

where a and b represent two parameters. Substituting eq 9, 7, and 6 into eq 5 yields

$$\Delta B(A \longrightarrow B)_q = \sum_m q_m(a \sin 2m\rho + b \cos 2m\rho) \qquad (10)$$

In particular, for homosubstitution eq 10 reduces to

$$\Delta B(A \longrightarrow B)_q = bq\sum_m(\cos 2m\rho + \alpha \sin 2m\rho) = \Delta B_q(1)\sum_m(\cos 2m\rho + \alpha \sin 2m\rho) \qquad (11)$$

or

$$\overline{\Delta B}_q \equiv \frac{\Delta B(A \longrightarrow B)_q}{\Delta B_q(1)} = \sum_m(\cos 2m\rho + \alpha \sin 2m\rho) = f(\alpha)$$

where $\alpha = a/b$ and $\Delta B_q(1)$ represents the $\Delta B(A \rightarrow B)_q$ value of monosubstituted benzenes. The expression $\overline{\Delta B}_q$ for various substituted benzenes is given in Table IV. The α and b values should vary from one substituted benzene to another, but if $|\vec{M}_{BA}| \gg |\Delta\vec{M}_{BA}|$, then α and b will become the characteristic constants of benzene itself.

$\Delta B(A \rightarrow B)_v$ can be estimated by assuming that ΔB(A

(37) D. J. Shieh, S. H. Lin, and H. Eyring, *Proc. Nat. Acad. Sci. U. S.*, 69(8), 2000 (1972).

$\rightarrow$ B)$_v$ varies regularly with the number of substituents but is independent of their arrangement.[6-8] This amounts to assuming linear superposition of the vibronic effects of the substituents. Thus one may estimate $\Delta B(A \rightarrow B)_v$ for various substitutions from the $\Delta B(A \rightarrow B)_q = 0$ homosubstitution values of $\Delta B(A \rightarrow B)_v$. For convenience, the $\Delta B(A \rightarrow B)_v$ values for the unit substitution of various substituents are tabulated in Table II. From Tables II and IV, we can see that $0 < \alpha < 1/\sqrt{3}$. Using this condition and Table IV, we may assert that for bisubstituted benzenes $|B(1,4)| > |B(1,2)| > |B(1,3)|$, *for trisubstituted benzenes,* $|B(1,2,4)| > |B(1,2,3)| \approx |B(1,3,5)|$, *and for tetrasubstituted benzenes, the magnitude of* $B(1,2,4,5)$ *is the largest among the three substituted benzenes as is verified experimentally.* It should be noticed that for tetrasubstituted benzenes, the sign of $B(1,2,3,5)$ might be opposite to that of $B(1,2,3,4)$, and $B(1,2,4,5)$, if we choose $m = 0,1,2,4$ for $B(1,2,3,5)$, but if we choose $m = 0,2,3,4$ (*i.e.*, rather than designating the compound 1,2,3,5-, it is designated 1,3,4,5- for the MCD) then the signs of $B(1,2,3,4)$, $B(1,2,3,5)$, and $B(1,2,4,5)$ should be the same. Using eq 10, the estimation of $\Delta B(A \rightarrow B)_v$ described above and the spectroscopic moments q_m for various substitutents, one can estimate $B(A \rightarrow B)$ for the mixed substituted benzenes. For monosubstituted benzene $\Delta B_q(1) = bq$ and since q is given by Petruska[14,15] b can be calculated. The average value is found to be $b = 5.48 \times 10^4$. This constant, as we have pointed out, is characteristic of benzene and its derivatives.

To show how well eq 12 correlates the experimental data of $B(A \rightarrow B)$ of homosubstituted benzenes, we define $\overline{\Delta B}_q = \Delta B(A \rightarrow B)_q / \Delta B_q(1)$ and since α is a characteristic constant of benzene itself, we can plot for various substitutents $\overline{\Delta B}_q$ for the different types of substitution. Here $\Delta B(A \rightarrow B)_M$ is assumed to be negligible. In Figure 8 are shown the homosubstitution $\overline{\Delta B}_q$ patterns for the $^1A_{1g} \rightarrow {}^1B_{2u}$ transition of benzene for two different values of the parameters α. From Figure 8, we can see that the agreement between the theoretical predictions and the experimental observations are only fair. In other words, to obtain quantitative agreement, we will have to consider the contribution arising from changes in $B(A \rightarrow B)_M$, as well as improvements in the SPP theory. Since the performance of the SPP theory in the prediction of the spectral intensity itself is only fair, the results are as good as could be expected. The theoretical method for estimating $B(A \rightarrow B)$ of substituted benzenes described in this paper thus suffice to predict the sign of $B(A \rightarrow B)_q$ and to obtain approximate estimations of its magnitude.

Acknowledgment. We wish to thank Mr. Jack Adams for technical assistance, Mr. Alan Weeks for drawing the figures, and Mr. BC. Robertson for typing the manuscript.

The authors wish to thank the National Institutes of Health, Grant No. GP 12862, National Science Foundation, Grant No. GP 28631, and the Army Research-Durham, Contract No. DA-ARO-D-31-124-72-G15, for support of this work.

An Ion Aggregate–Solvent Interaction Studied by Nuclear Magnetic Resonance

H. E. Zaugg* and R. S. Egan

Research Division, Abbott Laboratories, North Chicago, Illinois 60064 *(Received November 8, 1972)*

Publication costs assisted by Abbott Laboratories

The effect of varying proportions of diethyl sodio-*n*-butylmalonate on the chemical shifts of the CH_2 and CH_3 protons of 1,2-dimethoxyethane (DME) in benzene and cyclohexane is examined. Upfield shifts for both groups with decreasing mole ratio of DME to sodium salt are observed in both solvents, the shifts being greater for the CH_2 group. Despite these marked shielding effects the interaction is very weak and nonstoichiometric. It is concluded that the observed shielding is simply a consequence of adsorption of DME molecules on the negatively charged surface of the micellar particles known to exists in solutions of this salt in nonpolar media.

In their nmr examination of the interaction of donor molecules with sodium tetrabutylaluminate ($NaAlBu_4$) in cyclohexane, Day and coworkers[1,2] assumed that the complex produced by the donor (*e.g.*, tetrahydrofuran (THF) or diethyl ether) was in equilibrium with an ion pair aggregate, the nature of which was not defined.

Sedimentation studies have recently revealed[3] that the sodium salt of diethyl *n*-butylmalonate exists in benzene or cyclohexane solution as an inverse micellar system. In benzene the nearly spherical particles are composed of about 50 ion pair units (molecular weight 11,400) with the exterior lipophilic anions serving to insulate the hydrophilic sodium ions from the otherwise incompatible nonpolar environment. This note reports an nmr study of the

(1) E. Schaschel and M. C. Day, *J. Amer. Chem. Soc.*, **90**, 503 (1968).
(2) C. N. Hammonds, T. D. Westmoreland, and M. C. Day, *J. Phys. Chem.*, **73**, 4374 (1969).

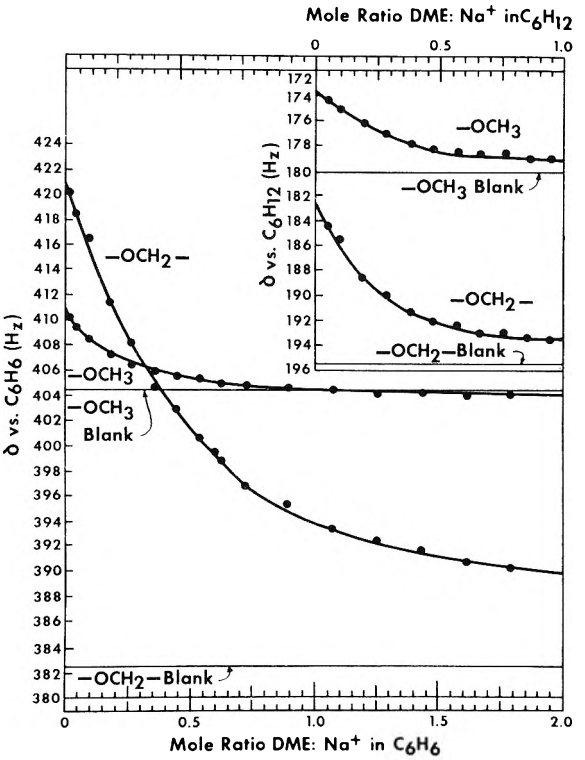

Figure 1. Chemical shifts of DME protons *vs.* DME:Na^+ mole ratio in benzene and cyclohexane.

interaction of this relatively well-defined system with the donor molecule, 1,2-dimethoxyethane (DME). The technique used was a classical mole ratio study in which the concentration of the sodium salt was kept constant and the DME concentration was varied.

Experimental Section

Materials were prepared and purified in the manner previously described.[3] Solutions were prepared in the usual way in Hamilton gas-tight syringes and injected directly into nmr tubes filled with dry nitrogen and then quickly capped for the spectral run. The temperature of all nmr determinations was 31 ± 0.5°. All solutions were 0.09 *M* in diethyl sodio-*n*-butylmalonate.

Nmr spectra were obtained on a Varian Associates HA-100 spectrometer operating in frequency sweep. The solvent resonance was used as an internal lock; therefore, the chemical shifts are reported either upfield from benzene or downfield from cyclohexane. The chemical shifts are reported in hertz and were measured from calibrated chart paper and are accurate to 0.1 Hz.

Results

The chemical shifts (δ) of the CH_2 and CH_3 protons of DME are given graphically in Figure 1 as a function of mole ratio. In benzene, the protons of both groups show increased shielding as the mole ratio of DME to sodium salt is decreased. However, the upfield shift of the CH_2 groups is greater than that of the methyl group so that at a mole ratio of about 0.32 their relative positions are reversed. Significantly, there is no detectable maximum (or even discontinuity) in either curve down to mole ratios as low as 0.01. Also noteworthy is the observed instability of these solutions in air. Replacement of the nitrogen in the nmr tube by dry air resulted in marked and *immediate* shifts of both resonance peaks (CH_2 and CH_3) toward the blank values. Prolonged contact with air (2–6 hr) eventually resulted in essentially complete return to the blank values regardless of the magnitude of the initial shifts. It should be noted that the nmr spectrum of the sodio-*n*-butylmalonate remained unchanged during these experiments, showing that the integrity of the micellar system was unaffected.[4]

Results in cyclohexane were qualitatively similar to those in benzene, but not identical (Figure 1). Although the upfield shift of the methyl peak is essentially the same (~6 Hz) in both solvents, the shift of the methylene peak is much lower in cyclohexane than in benzene (~15 Hz *vs.* ~40 Hz). Consequently, in cyclohexane, the relative positions of the two peaks do not undergo a reversal. Other points of similarity are the absence of any detectable discontinuity in either curve and a marked air sensitivity of all shifts.

Discussion

Previous workers have observed both shielding and deshielding of a donor molecule as a result of its association with alkali salts. The presence of $LiClO_4$,[5] $NaClO_4$,[5] and $NaAlBu_4$[1] leads to a downfield shift of the resonance peaks of a number of ethers, the α protons being affected more than the β protons. Similarly, the methyl groups of dimethyl sulfoxide are deshielded by $LiClO_4$, LiI, and NaI.[6] In contrast, $LiB(C_6H_5)_4$,[5] $NaB(C_6H_5)_4$,[5] and fluorenyllithium[7] produce marked upfield shifts of the resonances of a number of ethers including DME. It was demonstrated[5,7] that in the latter instances, the field caused by the aromatic rings in the anion opposes the magnetic field in the vicinity of the ether protons by an amount more than sufficient to neutralize the deshielding effect of the associated cation.

In view of the relative inaccessibility of the sodium ions encapsulated within the micellar particles of our system, the absence of a net deshielding effect on the donor molecule is not surprising. The lack of any cation–donor interaction is further indicated by the continuity of the experimental curves (Figure 1) The appearance of well-defined maxima in similar plots for other systems[1,5] has clearly indicated the occurrence of stoichiometric donor–acceptor interactions. By contrast, our system exhibits no maxima at mole ratios as low as 0.01, where only one donor molecule (DME) is present for two micellar particles (assuming an association number of 50). Finally, the marked air sensitivity of our system further demonstrates the feebleness of the interactions involved. Apparently, what is being observed is a weak surface interaction in which adsorbed DME molecules enter a shielded environment provided by the negatively charged micellar surface.

(3) G. H. Barlow and H. E. Zaugg, *J. Org. Chem.*, **37**, 2246 (1972).
(4) It can be estimated from the sedimentation studies[3] that at least 92% of the sodium salt is in the micellar form even at the highest mole ratio (*i.e.*, 2.0) given in Figure 1. The concentration of DME at this mole ratio is 0.18 *M* (<2% v/v). At this solvent composition the critical micelle concentration is less than 0.007 *M* (see Figure 4 of ref 3). Hence, the proportion of monomeric ion pairs in this solution must be less than 0.007/0.09 or 8%.
(5) D. Nicholls and M. Szwarc, *J. Phys. Chem.*, **71**, 2727 (1967).
(6) B. W. Maxey and A. I. Popov, *J. Amer. Chem. Soc.*, **90**, 4470 (1968).
(7) J. A. Dixon, P. A. Gwinner, and D. C. Lini, *J. Amer. Chem. Soc.*, **87**, 1379 (1965).

Radiative Processes of the Solvated Electron in Polar Fluids

Neil R. Kestner*[1] and Joshua Jortner

Department of Chemistry, Tel-Aviv University, Tel-Aviv, Israel *(Received December 13, 1972)*

In this paper we present a theoretical study of the physical properties of solvated electrons in ammonia based on the Copeland–Kestner–Jortner model, which incorporates short-range interactions *via* a first solvation layer and long-range interactions *via* polaron modes. We have studied bound–bound and bound–continuum optical transition emphasizing the problem of line shapes in absorption and emission. The total energy of the ground and excited states and its dependence on nuclear configurations was handled by three successive approximate calculations: (a) a temperature dependent potential including short-range radial displacements; (b) a temperature independent potential incorporating both radial and angular short-range displacements; (c) a multidimensional potential surface including both short-range and long-range (polaron) nuclear displacements. The calculated line shapes in absorption for a single solvent configuration include major contributions from short-range radial displacements and from the polaron modes. The energy and line shape for the 2p → 1s emission band is predicted. A general formula is presented for photoionization cross section including the contribution of all medium modes and in this case the role of the polaron modes is crucial.

I. Introduction

In our previous paper,[2] we advanced a model for the solvated electron in polar fluids which took into account the strong short-range interactions of the electron and the first coordination layer solvent molecules as well as the long-range interactions with the bulk medium. This model was capable of yielding quantitative information on the properties of solvated electrons in ammonia as well as providing qualitative data on excess electrons in other polar solvents. In the latter cases we did not attempt a detailed study. Recently, Fueki, Kevan and Christoffersen, in particular, have applied a similar model to study solvated electrons in water and alcohols.[3a,b] Although many questions remain concerning the trends observed in widely differing solvents[4] and solvent mixtures,[4-7] these are predicted well enough by our model to allow us to consider an entirely different set of problems, namely the details of radiative processes in which the state of the electron changes.

In this paper we will use metal–ammonia solutions as a representative system for the study of these processes. We expect the same general behavior in other polar fluids except that the relative rates of the various processes could change in different solvent systems. We will begin with a display of the latest calculations on our model[2] as well as an improved version. These new results provide a better insight into the physical properties of the solvated electron. We shall focus attention on the radiative processes of the solvated electron and, in particular, the observed absorption line shapes for bound–bound and for bound–continuum transitions as well as the yet unobserved emission line shape and the photoionization profile. The study of optical line shapes provides a starting point for the understanding of nonradiative processes of the solvated electron, such as electron capture from the conduction band to form the localized ground state, or the reverse process of thermal ionization of the ground state and of excited states. In general, the nonradiative transition probability can be expressed in terms of a generalized line shape function in the limit of zero frequency. However, in view of the special nature of the problem, where the localized excess electron wave function is strongly dependent on the (short-range and polaron type long-range) nuclear coordinates, the theory of the optical line shapes presented herein requires a gross modification before it can be applied for the elucidation of the nonradiative decay processes of the solvated electron.

II. Calculations

A. Temperature Dependent Potentials—One-Coordinate Model. Let us briefly review the Copeland–Kestner–Jortner model[2] which incorporates the following features.

(a) We assume that in the first coordination layer around the electron there will be a small fixed number, N, of solvent molecules. In this work we will assume values of $N = 4$, 6, 8, and 12, although the first two numbers seem to be most physically relevant.

(b) The solvent molecules in the first layer interact with the electron *via* their permanent and induced moments and with other solvent molecules in the first coordination layer *via* their repulsive forces, *i.e.*, primarily hydrogen–hydrogen repulsions and dipole–dipole repulsions.

(c) The electron interacts with the continuum beyond the first coordination layer in two ways. First of all it reacts with the inertial polarization field in the same way as in polaron theory. The use of adiabatic polaron theory is justified since we have treated the strong short-range interactions separately. The additional interactions with the solvent are contained in the V_0 term. The quantity V_0 represents the energy of a quasifree electron in the same medium.[8]

(1) Address correspondence to this author at the Department of Chemistry, Louisiana State University, Baton Rouge, La. 70803.
(2) D. A. Copeland, N. R. Kestner, and J. Jortner, *J. Chem. Phys.*, **53**, 1189 (1970).
(3) (a) K. Fueki, D. F. Feng, L. Kevan, and R. Christoffersen, *J. Phys. Chem.*, **75**, 2297 (1971); (b) D. F. Feng, K. Fueki, and L. Kevan, *J. Chem. Phys.*, **56**, 5351 (1972); **57**, 1253 (1972).
(4) L. Dorfman, *Proc. Colloq. Weyl III*, in press.
(5) J. Dye, M. G. DeBacker, and L. M. Dorfman, *J. Chem. Phys.*, **52**, 6251 (1970).
(6) L. M. Dorfman, F. Y. Jou, and R. Wageman, *Ber. Bunsenges. Phys. Chem.*, **75**, 681 (1971).
(7) R. Olinger and U. Schindewolf, *Ber. Bunsenges. Phys. Chem.*, **75**, 693 (1971).

(d) The energy to form the cavity will involve surface tension work, E_{ST}, hydrogen repulsions between solvent molecules, E_{HH}, dipole repulsions between solvent molecules in the first coordination layer, E_{dd}, pressure volume work, E_{PV}, and since we will use the adiabatic theory, an energy to polarize the medium.

The electron wave function $\psi_i(r)$ will be determined by the solution of the adiabatic equation (in atomic units)

$$(-\frac{1}{2}\nabla^2 + V(r))\psi_i(r) = W_i\psi_i(r) \qquad (1)$$

where the potential is

$$V(r) = -N\mu e/r_d^2 - \beta e^2/r_c \qquad (0 < r < R)$$

$$V(r) = -N\mu e/r_d^2 - \beta e^2/r_c + V_0 \qquad (R < r < r) \qquad (2)$$

$$V(r) = -\beta e^2/r + V_0 \qquad (r_d < r)$$

The relevant coordinates are defined as in Figure 1. In this model (referred to as Model 3 in our previous paper[2]) r_d is the distance to the dipole from the center of the cavity and r_c is the distance to the start of the continuum which lies beyond the first coordination layer. In this model it is assumed that the parameter, V_0, the energy of the quasifree electron in the medium also represents the interaction of the electron with the molecules in the first layer beyond that due to inertial polarization effects and the small electronic polarization contribution.[9] V_0 is not known experimentally. It has been estimated as -0.5 eV in liquid ammonia,[10] but we shall report calculations for $V_0 = 0.5$, 0.0, and -0.5 eV.

The value of the effective dipole moment, μ, is equal to

$$\mu = \mu_0 \cos\theta \qquad (3)$$

where θ is the angle between the radius vector and the dipole moment vector. In the calculations of this section we will assume that the cosine can be replaced by its average value which can be calculated by the Langevin function, *i.e.*

$$\langle\cos\theta\rangle = \coth\chi - \chi^{-1} \qquad (4)$$

$$\chi = \mu_0 eC/kTr_d^2 \qquad (5)$$

and C is the charge enclosed. When considering the ground state or any state arrived by a vertical (Franck–Condon) excitation C is that for the ground or 1s state, C_{1s}, which is

$$C_{1s} = \int_0^R |\psi_{1s}|^2 d^3\mathbf{r} \qquad (6)$$

This calculation will be referred to a temperature-dependent model since at each temperature a different equation is solved so that the potential (2) and the resulting configurational diagrams are temperature dependent. This approach slightly complicates matters, if one wishes to consider temperature dependent properties.

The total electronic energy for state i will be given by

$$E_{el}^{\ i} = W_i + S_i \qquad (7)$$

where the small polarization term is

$$S_i = -N\alpha C_i^2/r_d^4 - e\gamma_0 C_i^2/2r_c \qquad (8)$$

where C_i is the charge enclosed within radius R for the state i in question.

The medium reorganization energy is the same as calculated in our earlier paper and outlined elsewhere.[2,11] It

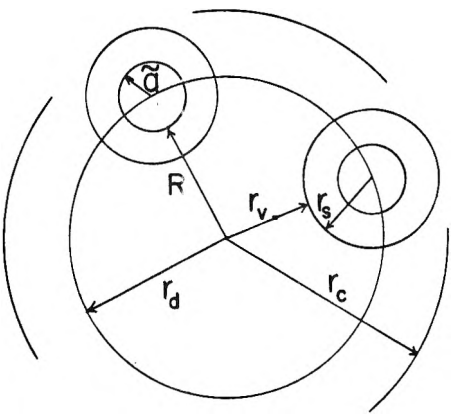

Figure 1. Definitions of the distances involved in the molecular models. r_v is the void radius of the cavity, r_s is the effective solvent radius, and ã is the effective hard core of the molecules located at a distance r_d from the center of the cavity. The continuum begins at r_c (see ref 22).

is the sum of the terms listed above under item (d)

$$E_{mi} = E_{ST} + E_{HH} + E_{ddi} + E_{pv} + \pi \qquad (9)$$

One modification of the earlier work is the term E_{ddi}, the repulsion of the oriented dipoles.

$$E_{ddi} = \frac{D_N \mu_T^2}{r_d^3} \qquad (10)$$

where

$$\mu_T = \mu_0\langle\cos\theta\rangle + e\alpha C_i/r_d^2 \qquad (11)$$

includes the correct induced dipole moment.[12] The constants, D_N, are listed in our earlier paper.[2] The hydrogen–hydrogen repulsion term is modified from earlier work[2] as

$$E_{HH} = C_{HH}^{(N)}\{\exp[-4.6(A_N R - B_N)]\langle\cos\theta\rangle\} \qquad (12)$$

where the constants are listed in ref 2.[13] The modification is in the last factor. This is added so that when $\langle\cos\theta\rangle$ goes to zero this contribution will vanish; *i.e.*, the interactions will be the same as those in the bulk liquid. The remaining terms of eq 9 are evaluated as in ref 2 and 11.

In our calculations we assume that the 1s and 2p functions can be represented by single Slater type atomic orbitals whose exponents can be determined by the variational method. This choice is not ideal as the potential which traps the electron is very deep and near the center of the cavity resembles a particle in a box.[9,14] Nevertheless, at larger distances the potential is coulombic. The error in this approximation is calculated[9] to be about 10% for the ground-state energy. The general features of the results are not affected by this assumption. The electronic energy is minimized for a fixed temperature and then the polarization and medium reorganization energy terms are

(8) This quantity is presented in detail in the work on nonpolar fluids; *e.g.*, B. E. Springett, M. H. Cohen, and J. Jortner, *Phys. Rev.*, **159**, 183 (1967).

(9) An improved model has been used by A. Gaathon and J. Jortner (unpublished research). In that model two V_0 values are used, one in the first layer and another for the continuum. In that case electronic polarization with the first layer is not included separately. For ordinary liquid densities this improved model is similar to our results. In polar gases the results are quite different.

(10) A. Gaathon and J. Jortner, *Proc. Colloq. Weyl III*, in press, have a more accurate estimate of -0.22 eV for ammonia.

(11) J. Jortner, *Ber. Bunsenges. Phys. Chem.*, **75**, 696 (1971).

(12) In ref 2, C_s is incorrectly written for C_i.

(13) In ref 2 there is another misprint in Table II for the constants in the hydrogen–hydrogen repulsion. A_6 should be 1.414 and B_6 should be 0.600.

(14) J. Logan and N. R. Kestner, *J. Phys. Chem.*, **76**, 2738 (1972).

TABLE I: Results of Model 3 Calculations One-Electron Cavity (Ammonia) (203°K)

	$V_0 = 0.5$ eV	$V_0 = 0.0$ eV	$V_0 = -0.5$ eV
		$N = 4$	
E_t ($= \Delta H_1$)	−0.537 eV	−0.909 eV	−1.30 eV
E_{el}	−1.668	−2.010	−2.404
R_0	−1.75 Å	1.75 Å	1.70 Å
R_0^{eff} [a]	3.1 Å	3.1 Å	3.0 Å
$h\nu$	1.16 eV	1.03 eV	0.94 eV
		$N = 6$	
E_t	−0.678 eV	−0.972 eV	−1.294 eV
E_{el}	−2.069	−2.326	−2.603
R_0	2.20 Å	2.15 Å	2.15 Å
R_0^{eff}	3.1 Å	3.0 Å	3.0 Å
$h\nu$	1.30 eV	1.15 eV	0.99 eV

[a] R_0^{eff} is the effective cavity radius measured by volume expansion experiments and $h\nu$ is the lowest allowed optical transition.

subsequently added. The optimum cavity size, R_0, is determined by minimizing the total energy

$$E_t^i(R) = E_{el}^i + E_{mi}(R) \tag{13}$$

so that

$$(\partial E_t/\partial R)_{R_0} = 0 \tag{14}$$

The results of these calculations at 203°K and for $N = 4$ and 6 are listed in Table I and plotted in Figures 2 and 3. These results supercede those published in ref 2. Logan and Kestner have also evaluated the first excited s type state (2s) of this system[14] obtained by vertical excitation from the ground state. It is shown in Figures 2 and 3 for comparison and labeled as the 2s curve.

In the above calculations we have evaluated the energy and properties of excited states as they arise in a Frank–Condon transition from the ground state; *i.e.*, the inertial polarization of the first coordination layer and the continuum is fixed at the values appropriate for the charge density of the ground or 1s state. If the excited state is sufficiently long lived the inertial polarization could relax to a value appropriate for the equilibrium nuclear configuration of the excited state in question. We have evaluated the relaxed 2p states and the relaxed 1s state in which the inertial polarization is determined by the charge density of the relaxed 2p state. This means that in the average of $\cos\theta$ and in μ_T we use the 2p charge density and the relaxed 2p wave functions. The results are summarized in Table IV where the maximum of the 2p → 1s emission is also listed. It is significantly red shifted from the absorption. The potential curves for these states are also shown in Figures 2 and 3 for two typical cases.

Also shown in Figures 1 and 2 are curves for the vertical continuum level, V_c, *i.e.*, the energy of the quasifree electron if the cavity and medium have their inertial polarizations fixed at the values dictated by the charge density of the ground state.

$$V_C = E_{ST} + E_{HH} + E_{PV} + E_{dds} + \pi_s + V_0 \tag{15}$$

The curves represented by Figures 1 and 2 along with others to be presented below can now be used to study the details of electronic excitations as well as radiationless processes.

B. Temperature Independent Potentials—Two-Coordinate Model. In our previous work temperature has entered our calculations in two different ways. First of all, temperature modifies the physical parameters characterizing the medium. Secondly, the electron-medium potential explicitly contains the temperature in that we use a temperature averaged cosine of the dipole orientation. The medium parameters change slowly with temperature whereas the average of the cosine changes rapidly. Thus it is advisable to advance a model in which temperature effects are kept out of the quantum mechanical calculation. One can always reintroduce thermal averages by the appropriate Boltzmann weighted average. In addition, however, one can consider the effects of the fluctuations in the $\cos\theta$ term as they affect various properties.

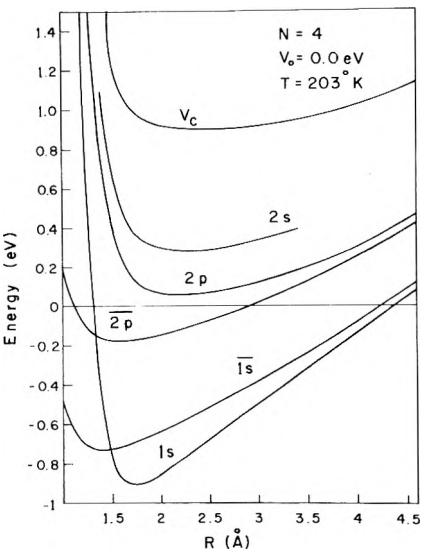

Figure 2. Configurational diagrams for the total energy as a function of the radius R for various electronic states when $N = 4$, $V_0 = 0.0$ eV, and $T = 203$°K. The ground state is denoted by 1s and the two bound excited states and the continuum level which exist when the polarization field is determined by the ground state are denoted by 2s, 2p, and V_c, respectively. The $\overline{2p}$ state is the lowest energy P state when the polarization is determined by the 2p excited state, and the $\overline{1s}$ state is the lowest energy level under the same polarization.

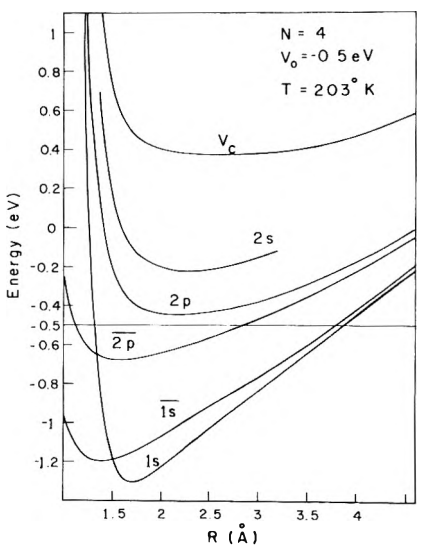

Figure 3. Configurational diagrams for the total energy as a function of the radius R for various electronic states when $N = 4$, $V_0 = -0.5$ eV, and $T = 203$°K. The notation is the same as in Figure 2.

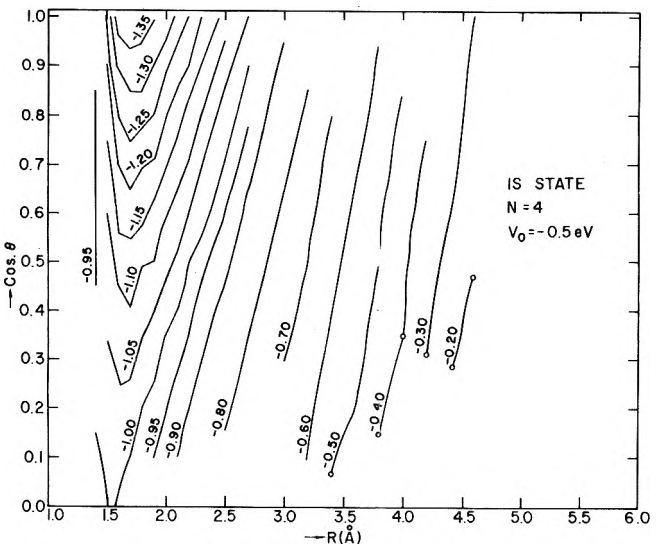

Figure 4. Configurational diagrams for the ground-state total energy as a function of R and θ. $N = 4$, $V_0 = -0.5$ eV. The numbers refer to constant potential surfaces in eV.

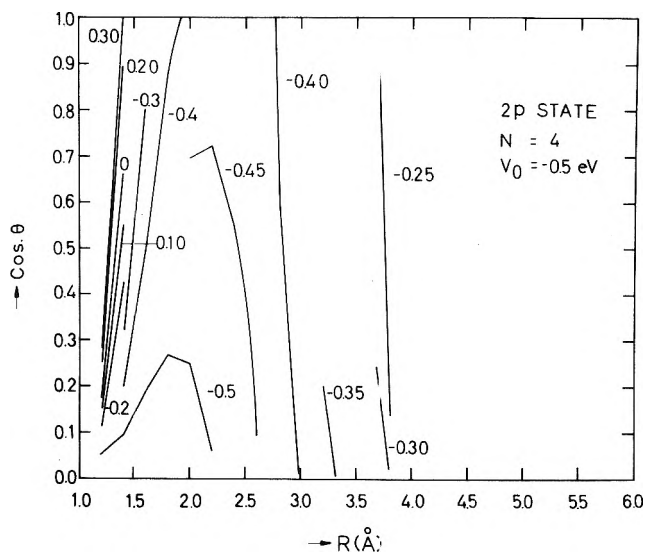

Figure 5. Configurational diagrams for the 2p excited state as a function of R and θ. Notation and parameters identical with those in Figure 4.

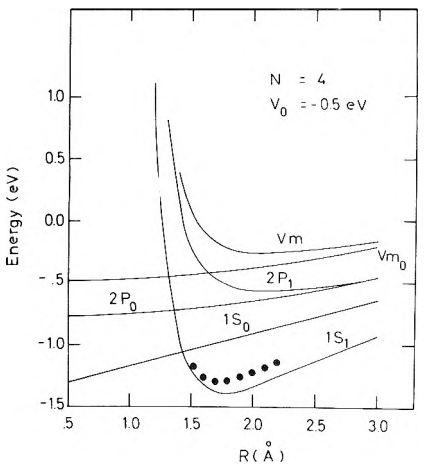

Figure 6. Temperature-independent potential model configuration diagrams for the total energy as a function of the radius R for $N = 4$ and $V_0 = -0.5$ eV. The last subscript now refers to the value of cos θ. Only curves for two values of cos θ are plotted. Each state has the bulk medium polarized according to its electron density (see text). The dots labeled 1s denote the temperature averaged result where $\langle \cos\theta \rangle_{1s} = 0.8$–$0.9$. V_M is the medium or continuum level.

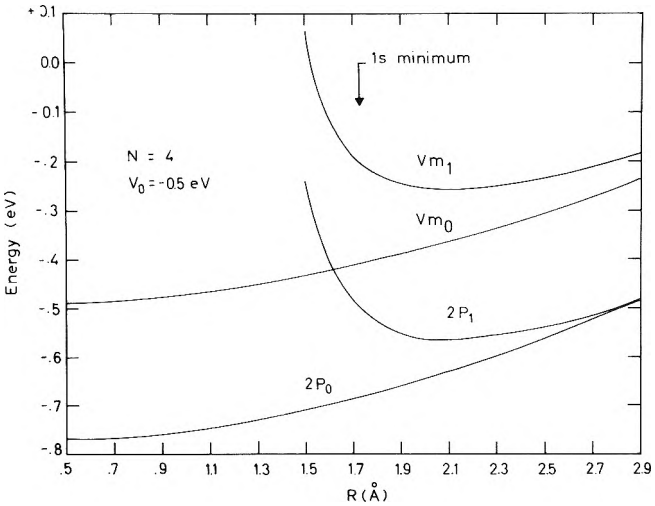

Figure 7. An expanded view of the upper portions of Figure 7 including the completely oriented dipole curve for the continuum or medium level. The arrow indicates the position of the minimum for the 1s state.

It is a simple matter to extend our previous formalism for the calculation of temperature-independent energies. Instead of using the temperature averaged values of cos θ in eq 3, 11, and 12, we evaluate the energy as a function of both R and cos θ where cos θ can range from 0.0 to 1.0. Such potential energy surfaces (*i.e.*, configurational coordinates) for the 1s and 2p states are displayed in Figures 4 and 5.

There is still one problem in defining how that energy is to be calculated since we have averaged the set of coordinates representing the medium quasi-polaron modes. The thermally average effect is included in β and their effective displacement is included in the π term. There is a choice as to what π value should be included with each energy state. We have included in the curves of Figures 6, 7, and 8 the value of π appropriate to the state in question. Thus the difference between curves do not represent vertical excitations in terms of the medium coordinates. To obtain vertical excitations from these curves one needs to correct for the difference in π values. Thus it is important to note that the 2p curves contain π_p calculated with 2p wave functions, the 1s curves contain π_s calculated with 1s functions, and the continuum or V_m curves do not contain any contribution of π. The last subscript on the curves refers to the value of cos θ. We have presented in Figures 6–8 only the cos $\theta = 0.0$ and cos $\theta = 1.0$ results. At small radii the one term wave function is inadequate. In addition, remember the π term is not the same for any two curves and for a vertical process they will be separated by the differences in the values of π appropriate to the various states and this is a few tenths of a volt.

To relate this to our previous work,[2] we must remember that before we used $\langle \cos\theta \rangle_{1s}$ for all Franck-Condon transitions. The value of $\langle \cos\theta \rangle_{1s}$ for the ground state is about 0.85. In Figure 6 we indicate for reference the position of the thermally averaged results for 1s versus $1s_1$.

The use of this temperature-independent potential to calculate the thermally averaged energy of the bound

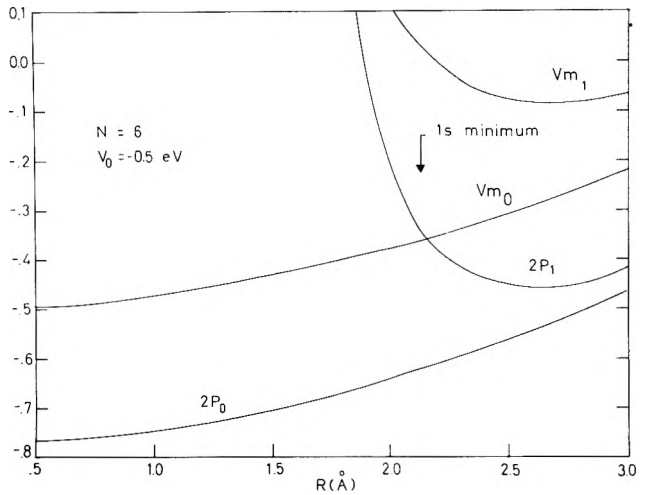

Figure 8. Temperature-independent potential model configuration diagrams for the total energy as a function of the radius R for $N = 6$ and $V_0 = -0.5$ eV. Notation is the same as in Figures 7 and 8.

states leads to almost exactly the same answers as in our previous calculation since for values of cos θ above about 0.6 the energy is a linear function of cos θ and thus averaging yields the same Langevin result as before. However, for weakly bound states and small values of cos θ this approximation is poor and thus the relaxed 2p states would probably change slightly if the proper averaging were done with a temperature-independent potential. It is unlikely that the *relative* behavior of the previous relaxed 2p and 1s states would change greatly.

III. Radiative Processes

A. Absorption Line Shape for the 1s → 2p Transition. In the previous section we have presented configuration diagrams for the ground (1s) and excited (2p) states of the solvated electron in ammonia. With these curves and a few reasonable assumptions we can calculate the line shape expected from this model. These assumptions are as follows. (a) The classical high-temperature limit for the absorption line shape can be safely used. This approximation implies that the relevant frequencies are lower than the thermal energies. The fundamental totally symmetric radial vibration of the electron cavity is about 80 cm^{-1}, while the characteristic frequencies of the medium modes are estimated[15] to be of the order of 1 cm^{-1}. Thus in the relevant temperature region 200-300°K this approximation is valid. (b) The semiclassical Condon approximation is invoked, whereupon the electronic transition moment is independent of the nuclear configuration. This is also reasonably good for the ranges of R considered (see section A4). The intensity distribution function, $F(E)$, for optical excitation at energy E for one configuration of the cavity can be recast in the general form

$$F(E) = \frac{|M|^2}{Z}\sum_{\alpha}\sum_{\beta} \exp(-\epsilon_\alpha/kT) \times |\langle\chi_\alpha(\mathbf{X})|\chi_\beta(\mathbf{X})\rangle|^2\delta(E + \epsilon_\alpha - \epsilon_\beta) \quad (16)$$

where M is the electronic transition moment, Z is the ground state partition function, and α and β represent the vibronic levels of the initial (1s) and the final (2p) states, respectively. These vibronic levels are characterized by the energies ϵ_α and ϵ_β and by the vibrational wave functions $\chi_\alpha(\mathbf{X})$ and $\chi_\beta(\mathbf{X})$, respectively. The generalized coordinate $\mathbf{x}$ represents the set of the radical, R, and angular θ coordinates of the first coordination layer and the solvent polar modes $\{q\}$ outside this first layer whereupon $\mathbf{X} \equiv (R, \theta, \{q_k\})$.

Extensive theoretical studies have been performed[16,17] to derive explicit expression for the line shape function (16). General closed expressions can be derived only within the framework of the harmonic approximation which is inapplicable for the present problem as the potential surfaces for the R and θ coordinates exhibit large deviations from the harmonic model. However, in the high-temperature limit, Kubo and Toyozawa[17] have derived a general expression for the line shape which is valid for any set of potential surfaces

$$F(E)\frac{|M|^2}{Z}\int d\mathbf{X}\, \exp[-U_i(\mathbf{X})/kT] \times \delta(E + U_i(\mathbf{X}) - U_f(\mathbf{X})) \quad (17)$$

where $U_i(\mathbf{X})$ and $U_f(\mathbf{X})$ correspond to the potential surfaces of the initial (1s) and the final (2p) electronic states. Thus, in the present case, we can write

$$F(E) = \frac{|M|^2}{Z}\int d\mathbf{X}\, \exp[-E_t^{1s}(\mathbf{X})/kT] \times \delta(E + E_t^{1s}(\mathbf{X}) - E_t^{2p}(\mathbf{X})) \quad (17a)$$

Equation 17a demonstrates that in the high-temperature limit the radiative transition occurs at energies $E = E_T^{2p}(\mathbf{X}) - E_T^{1s}(\mathbf{X})$ in accordance with the classical Franck-Condon principle.

A1. One-Configurational Coordinate Model. Neglecting the role of the medium modes and utilizing the temperature dependent potential the energies $E_t^{1s}(\mathbf{X})$ and $E_t^{2p}(\mathbf{X})$ are a function of a single radial coordinate $\mathbf{X} \equiv R$, which corresponds to the cavity radius. We thus assume that the dependence of the energy on the nontotally symmetric vibrations is small and that the major contribution to the line width originates from the totally symmetric mode. In addition, the triply degenerate 2p electronic state is not split by this symmetric mode.

The line shape is now obtained from eq 17a in the form

$$A(E) = \frac{|M|^2}{Z}\exp[-E_t^{1s}(R)]\left|\frac{dR}{dE}\right| \quad (18)$$

In Figure 9 we show the results of one calculation of the line shape for a particular choice of parameters. This figure is similar to that of our earlier paper.[2] We include it in this paper in reference to the more detailed calculations to be presented below. The conclusions regarding this curve are the same as we presented earlier.[2] We have observed, however, that when cos θ is fixed at 1.0 rather than its thermal average the line shape is more asymmetric toward lower energies. This observation can be rationalized by noting that the cos θ dependence of the excited 2p state is very weak around cos $\theta \approx 1$. Thus by utilizing equation 17 for the medium one can show that the contribution of this mode to the line shape will result in a broadening only toward lower energies. This one coordinate (cos θ) line shape will be an exponentially decaying function with a width of (ln 2)kT, which is quite small. Detailed numerical calculations presented in the next section confirm this qualitative conclusion.

(15) V. G. Levich, *Advan. Electrochem. Electrochem. Eng.*, **4**, 249 (1966).
(16) M. Lax, *J. Chem. Phys.*, **20**, 1752 (1952).
(17) R. Kubo and Y. Toyozawa, *Progr. Theor. Phys.*, **13**, 160 (1955).

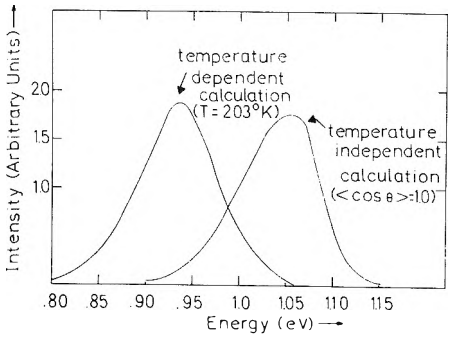

Figure 9. Optical lineshape for 1s → 2p transitions calculated from the potential dependent configurational diagrams with a single (R) mode. $N = 4$, $V_0 = -0.5$, and $T = 300°K$.

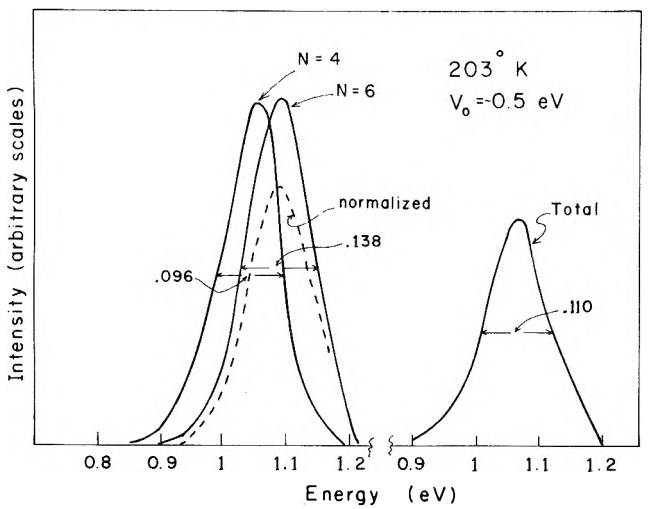

Figure 10. Line shapes calculated at 203°K and $V_0 = -0.5$ eV by the temperature-independent two (R, θ) mode potential model. On the left are the line shapes for the $N = 4$ and $N = 6$ cavities including the $N = 6$ results normalized by its relative Boltzmann factor. On the right is the composite line shape obtained from the $N = 4$ and $N = 6$ cavities following eq 19 in the text.

A2. Two-Configurational Coordinates (R, cos θ). In addition to the configurational coordinate, R, the cavity radius, it is very easy for us to study the dependence of another set of short range coordinates on the energy and line shape, namely cos θ. We will assume that the cavity is still spherical but that the dipole can move together in a way described by their collective coordinate, cos θ. It is now a simple matter to take the various potential curves and properly weight the transition energies, according to eq 17a. This was done for the absorption spectra by fitting the ground state energy and the excitation energy to a power series in cos θ (a linear relation is sufficient for large values of cos θ).

On the left side of Figures 10 and 11 we have plotted line shapes for $N = 4$ and 6 and $V_0 = -0.5$ eV for two temperatures, 203 and 300°K. By comparing Figures 9 and 10 we see that the cos θ mode results in small broadening at low energies and contributes little to the half-width. Within our curve fitting error of about ±0.004 eV we can see no effect on the half-width.

In Table I we see that the calculated ground state energy for the cavity with four and six coordination numbers are very similar. In our earlier work[2] it was also pointed out that the oscillator strengths of the two cavity models were similar.[18] With these conditions and our previous assumptions we can write for the total expected compound line shape involving contributions for different short range configurations

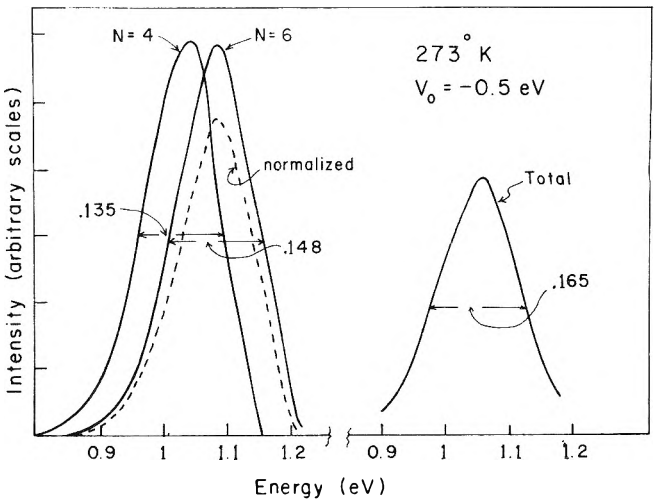

Figure 11. Line shapes calculated at 273°K and $V_0 = -0.5$ eV by the temperature independent two mode potential model. The notation is the same as in Figure 10.

$$F_T(E) = F_4(E) + \exp(-\Delta E°/kT)F_6(E) \quad (19)$$

where $\Delta E°$ is the difference between the ground state energy for the 4 and 6 member cavities. This is calculated at the minimum of potential curves. In our two-coordinate model it is calculated at the radius corresponding to the lowest energy for cos $\theta = 1.0$. On the right side of Figures 10 and 11 we plot the total line shape calculated by eq 19. In principle one should also add contributions for $N = 8$ but since it has a significantly higher total ground state energy in our model it would contribute very little.

A3. Role of Solvent Modes. Thus far we have neglected or rather suppressed another set of coordinates, namely the solvent polaron modes. These are included in our calculation in an average way *via* the β parameter in the potential and the π contribution. The general potential energy surfaces including the polaron modes can be recast by separating the long-range and the short-range nuclear displacements, so that

$$E_t^{1s}(\mathbf{X}) = f_{1s}(R,\theta) + g_{1s}(\mathbf{q}_x) + E_t^{1s}(\mathbf{X}_0^{1s}) \quad (20)$$

$$E_t^{2p}(\mathbf{X}) = f_{2p}(R,\theta) + g_{2p}(\mathbf{q}_x) + E_t^{2p}(\mathbf{X}_0^{2p}) \quad (21)$$

where the f and g functions describe the contribution of the first coordination layer and the medium to the total energy when these coordinates are displaced from their minima.

Following Levich we shall invoke two approximations to specify the contribution of the medium modes:[15] (a) the harmonic approximation whereupon small displacements of the medium modes are considered around the equilibrium configurations $\{q_\kappa°(1s)\}$ and $\{q_\kappa°(2p)\}$ in the two electronic states; (b) the medium modes will be approximated by the single mean frequency ω_0 in both electronic states. Qualitative estimates yield[19] $\hbar\omega_0 \approx 10^{12}$ sec^{-1} ≈ 1 cm^{-1}.

(18) This is confirmed by unpublished calculations of A. Gaathon and J. Jortner. The previous values of the oscillator strengths published in ref 2 are in error due to a numerical error and the use of the dipole length formula. For further discussion see A. Gaathon, J. Jortner, and N. R. Kestner, *Chem. Phys. Lett.*, in press.

(19) R. Dogonadze, *Ber. Bunsenges. Phys. Chem.*, **75**, 628 (1971).

Thus we write

$$E_t^{1s}(\mathbf{X}) = f_{1s}(R,\theta) + \frac{\hbar\omega_0}{2}\sum_\kappa (q_\kappa - q_\kappa^\circ(1s))^2 + E_t^{1s}(\mathbf{X}_0^{1s}) \quad (22)$$

$$E_t^{2p}(\mathbf{X}) = f_{2p}(R,\theta) + \frac{\hbar\omega_0}{2}\sum_\kappa (q_\kappa - q_\kappa^\circ(2p))^2 + E_t^{2p}(\mathbf{X}_0^{2p}) \quad (23)$$

Defining a new set of medium polaron coordinates $Q_\kappa = q_\kappa - q_\kappa^0(1s)$ at reduced shifts of the minimum configuration $\delta_\kappa = q_\kappa^\circ(1s) - q_\kappa^\circ(2p)$ we can write

$$E_t^{1s}(\mathbf{X}) = f_{1s}(R,\theta) + \frac{\hbar\omega_0}{2}\sum_\kappa Q_\kappa^2 \quad (24)$$

$$E_t^{2p}(\mathbf{X}) = f_{2p}(R,\theta) + \frac{\hbar\omega_0}{2}\sum_\kappa Q_\kappa^2 + \hbar\omega_0\sum_\kappa \delta_\kappa Q_\kappa + E_s + \Delta E \quad (25)$$

where the energy gap is

$$\Delta E = E_t^{2p}(\mathbf{X}_0^{2p}) - E_t^{1s}(\mathbf{X}_0^{1s}) \quad (26)$$

represents the difference between the energies of the two states at equilibrium nuclear configurations. We have also defined an energy (Stokes) shift

$$E_s = \frac{\hbar\omega_0}{2}\sum_\kappa \delta_\kappa^2 \quad (27)$$

Levich has shown[15] that E_s can be expressed in the form

$$E_s = \frac{1}{8\pi\beta}\int (D_s - D_p)^2 dV \quad (28)$$

$$= 2\pi\beta\int (P_s - P_p)^2\, dV \quad (29)$$

where D_s and D_p are the electric displacement vectors in the s and p states while P_s and P_p are the corresponding polarizations of the two states.

It is possible to make some very rough statements concerning E_s. It behaves somewhat like the difference in the π term calculated using the 1s wave function and that calculated using the 2p wave function. Since we know these are two magnitudes similar, we expect E_s is small. To obtain a reliable value of E_s we have used the wave functions obtained to calculate D_s and D_p. For $N = 4$ and $V_0 = -0.5$ we obtain a value for E_s of 0.024 eV.

Focusing attention on the line shape (eq 17) we note that the factorization of the potential surfaces into short- and long-range contributions enables us to recast $F(E)$ in the form of a convolution. Neglecting the contribution of the θ mode (see section A3) we can write

$$F(E) = \int dR \prod_\kappa dq_\kappa \int d\epsilon \exp[-f_{1s}(R)/kT] \times \delta(E + f_{1s}(R) - f_{2p}(R) - \Delta E - \epsilon) \times \exp[-\hbar\omega_0\sum_\kappa Q_\kappa^2/2kT]\ \delta(\epsilon - \hbar\omega_0\sum_\kappa Q_\kappa\delta_\kappa - E_s - \Delta E) \quad (30)$$

Defining the line shape functions for the two modes

$$\alpha(E-\epsilon) = \int dR \exp(-f_{1s}(R)/kT)\delta(E + f_{1s}(R) - f_{2p}(R) - \epsilon) \quad (31)$$

$$\gamma(\epsilon) = \int \prod_\kappa dq_\kappa \exp[-\hbar\omega_0\sum_\kappa Q_\kappa^2/2kT]\delta \times (\epsilon - \hbar\omega_0\sum_\kappa \delta_\kappa Q_\kappa - E_s - \Delta E) \quad (32)$$

The line shape takes the form of a convolution

$$F(E) = \int d\epsilon\, \alpha(E-\epsilon)\gamma(\epsilon) \quad (33)$$

The line shape α originating from the radial cavity displacement was calculated previously and is given by

$$\alpha(E-\epsilon) = A(E-\epsilon) \quad (34)$$

where A is given by eq 18. The line shape (E) for the harmonic medium displacements can be easily evaluated utilizing the techniques of Kubo, Toyozawa,[17] and Lax[16] and is given by the Gaussian distribution

$$\gamma(\epsilon) = \exp\left[\frac{-(\epsilon - E_s - \Delta E)^2}{4kTE_s}\right] \quad (35)$$

The half-width of this distribution is given by

$$\Gamma_\gamma = 4(kTE_s \ln 2)^{1/2} \quad (36)$$

Numerical calculations yield for $V_0 = -0.5$ and $N = 4\Gamma_\gamma = 0.07$ eV. On the other hand, the width of the distribution $A(E-\epsilon)$ is $\Delta \approx 0.12$ eV at 300°K. As the A distribution can be reasonably well approximated by a Gaussian the total width, Γ, of the line shape (33) is given by the sum of the two widths

$$\Gamma \approx \Delta + \Gamma_\gamma = 0.19 \text{ eV} \quad (37)$$

We thus conclude that the contribution of the medium polaron modes to the line broadening of the bound–bound 1s → 2p transition is relatively important; however, it still cannot explain the discrepancy between theory and experiment.

A4. Conclusions and Other Possible Source of Line Broadening. Based on our calculations several general comments can be made. (1) Even though the calculated 1s → 2p absorption lines we have are quite broad they are narrower than the experimental widths by almost a numerical factor of 2. (2) The particular vibrational motion of the first coordination layer dipoles, namely cos θ, does not contribute significantly to line broadening. Almost all of the line shape arises from the spherically symmetric vibrations and from the long-range polaron modes. (3) The contribution of several types of cavities does contribute to line broadening but is not capable of leading to extremely wide lines. Furthermore, if this were the primary reason for broad line shapes then the half-width should be greatly dependent on the density of the fluid, and the best available data[10,20] for electrons in supercritical vapors suggest it is not the case. In the case of dense water vapor the line width does not vary greatly even when the gas density is reduced to 2% of the normal liquid water density.[10] (4) The theoretical line shapes are slightly asymmetric on the low-energy side while the experimental results are very skewed towards high energy. This asymmetry originates from the contribution of the θ mode. This slight low-energy asymmetry is removed if one properly includes the variation of the oscillator strength across the band. This variation of the oscillator strength across the band is about 30% and it will produce a more symmetrical line of almost the same width. (5) The theoretical line widths behave as $(T)^{1/2}$ contrary to experimental data[21] which show

(20) R. Olinger, U. Schindewolf, A. Gaathon, and J. Jortner, *Ber. Bunsenges. Phys. Chem.*, **75**, 690 (1971).

(21) D. F. Burrow and J. J. Lagowski, *Advan. Chem. Ser.*, **No. 50**, 125 (1965). I. Hurley, T. R. Tuttle, Jr., and S. Golden, "Metal Ammonia Solutions," J. J. Lagowski and M. J. Sienko, Ed., Butterworths, London, 1970.

a much weaker temperature dependence in dilute metal ammonia solutions.

The final comparison between the latest theoretical and experimental results are summarized in Figure 12. The fact that the maxima of the two curves do not agree is not important, but their great difference of shapes is crucial. There are many possible explanations for this qualitative discrepancy.

First of all, it is possible that our model is not accurate enough especially with regard to the small differences between the $N = 4$ and $N = 6$ cavities. This is possible but rather unlikely since no matter what relative energies are assigned to the two species the observed spectra cannot be duplicated. For example, if they are moved far apart the composite spectrum will have a dip between the two peaks.

Another explanation commonly proposed is that the high energy tail of the absorption involves higher excited states (3p, 4p, even continuum levels). Within our model this can also be ruled out. The higher excited states should have electronic energies given by a Rydberg-like formula

$$E_n = -\frac{\beta^2}{2n^2} + V_0 \qquad (38)$$

This works well even for the 2p state and should be even better for the 3p and 4p levels. Using eq 38 we can locate the 1s → 3p and 1s → 4p transitions relative to the 1s → 2p transition. However, as shown in Figure 12 these lie at very high energies and in order to explain the experimental data even approximately they would have to be extremely broad and carry an extremely large oscillator strength. From the calculation of all previously considered line broadening factors it is unlikely that they would have half-widths over 0.4 eV. Other calculations indicate that the oscillator strength available to all excited states beyond 2p is small.[18] These excited levels should also be greatly affected by the density of the fluid since they depend directly on β and yet lines in very low density water vapor[10] are as broad as those in the liquid. Also, Lugo and Delahay[22] were not successful in a phenomenological fitting the solvated electron spectrum with up to four gaussian distributions. These remarks apply to water and ammonia.

Thus the question of the extremely broad lines remains. Two other explanations have been proposed which have not been fully evaluated as yet.

Thus far we have assumed spherical cavities with spherically symmetrical vibrations. Asymmetric fluctuations might lead to an appreciable increase in the half-width. However, the 2p excited state energy is almost independent of any nonspherical vibrations of the first coordination layer and since the estimates indicate that asymmetric modes have a very small force constant one calculates that *at most* they could contribute kT ln 2 or 0.012 eV to the half-width. Less well understood is the Jahn-Teller effect on the line shape but in any case it will lead to asymmetric lines and increase the width as $\sqrt{T}$,[23] both ideas contrary to experimental data.

Another possible explanation of the line shape is a permanent distortion of the cavity from its spherical shape. It is hard to justify such a model but it could arise from the rapid exchange of solvent molecules between the first coordination layer and the bulk medium. At any one instant one would have a variety of cavity shapes. The average would be represented by our model but large deviations from it would be possible. This was considered for

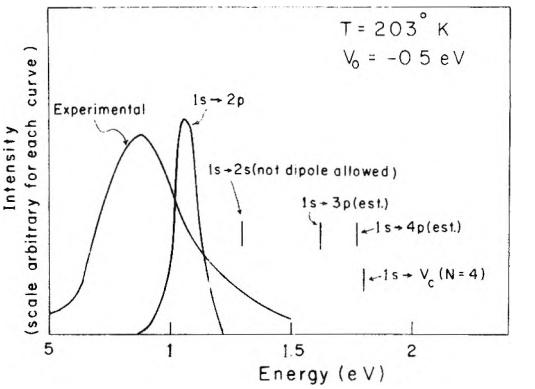

Figure 12. Typical transition energies and line shapes obtained from these models in comparison with typical experimental data. The 1s → 2p line shape is the total curve in Figure 10. The other lines indicate where the various bound-bound and bound-continuum (1s → V_0) levels are located for this model. These curves incorporate the contribution of the short-range R and θ displacements, disregarding the role of the long range polaron displacements.

TABLE II: Metal-Ammonia Solutions Relaxed States at 203°K

	V_0 = 0.5 eV	V_0 = 0.0 eV	V_0 = −0.5 eV
	$N = 4$		
E_t (2p)	0.3160 eV	−0.1826	−0.6811 eV
$h\nu$ (emission)	0.594 eV	0.548 eV	0.506 eV
E_t (1s)	−0.2780 eV	−0.7301 eV	−1.1873 eV
P	1.55 Å	1.55 Å	1.55 Å
C_s	0.197	0.09	0.08
C_p	0.007	0.007	0.007
	$N = 6$		
E_t (2p)	0.3839 eV	−0.1126 eV	−0.6093 eV
$h\nu$ (emission)	0.627 eV	0.535 eV	0.467 eV
E_t (1s)	−0.2429 eV	−0.6477 eV	−1.0765 eV
R	2.05 Å	2.05 Å	2.00 Å
C_s	0.181	0.153	0.126
C_p	0.020	0.019	0.017

the case of electrons in helium.[24] Although we cannot treat this problem easily without major variations in our model, one can argue that this could lead to asymmetric lines if nonspherical cavities had larger transition energies, becoming slightly more asymmetric at higher temperatures (for the case where density is constant), and total half line widths increasing more slowly than $\sqrt{T}$ due to the many contributions to the total line shape. It would suggest that lines in dense polar fluids could be as broad as those in polar liquids. However, although there is evidence for all these predictions, in the absence of quantitative evidence all of this is speculation. At the moment we cannot see how to calculate any of these features from first principles.

B. Emission Line Shapes (2p → 1s). If the 2p state exists long enough for the medium to relax to the new charge density, then it may be possible to see an emission from the relaxed 2p level to the relaxed 1s level. The energies of such states were given in Table II. Using the curves

(22) R. Lugo and P. Delahay, *J. Chem. Phys.*, **57**, 2122 (1972). Note, however, that this present paper emphasizes the need to use different line widths for the bound-bound and bound-continuum transitions.
(23) Y. Toyozawa in "Dynamical Processes in Solid State Optics," R. Kubo, Ed., Benjamin, New York, N. Y., 1969.
(24) B. Fowler and D. L. Dexter, *Phys. Rev.*, **176**, 337 (1968).

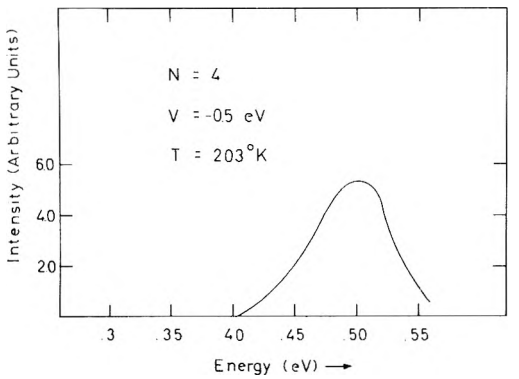

Figure 13. 2p → 1s emission line shape calculated from the temperature-dependent one-mode model.

of Figure 3 it is possible to calculate using formulas 16-18 the emission line shape inverting the sign of E in the δ function. The only change is that $A(x)$ refers to points on the relaxed 2p configuration curves. The resulting line shape is plotted in Figure 13. It is again quite broad, especially considering the very low energy of the emission. The emission is Stokes shifted about 0.4 eV to the red from the absorption. This emission would be extremely interesting if it could be observed since it could have a rather different line shape from the absorption as the emitting state has a very different electronic structure.

C. Photoionization. Using the calculated curves for the energy of various states we can calculate the photoionization profile[25,26] as a function of the photon energy. This calculation differs from that in the previous section in two ways: first of all, there are additional line broadening effects and secondly we cannot invoke the Condon approximation and remove the energy dependence of the transition matrix element or cross section from the integral over all possible configurational states. Thus we need to evaluate the following integral

$$L(\nu) = \int \sigma(\nu, \nu_1) F(\nu_1) \mathrm{d}\nu_1 \tag{39}$$

where $F(\nu_1)$ is related to the quantity we have calculated in the previous section and it is proportional to the line shape if one can neglect the energy dependence of the cross section or transition matrix element σ. The reason for the integral is that a photon of energy ν can ionize all configurations with energy less than ν. To reduce this result to the previous case we not only factor out σ but replace it with a δ function since $F(\nu_1)$ contains all contributions of energy E which is equal in that case to ν.

In our considerations $F(\nu_1)$ represents the probability for finding states with an ionization energy ν_1 at a temperature T. The ionization energy is evaluated as

$$\nu_1 = E_c(R) - E_t^{1s}(R) \tag{40}$$

i.e., the difference between the total energy of the continuum and the total energy of the ground state. In Table III we present values for this quantity at the most probable radius as determined by our temperature dependent calculations.

Using the same procedure as in the previous section we evaluate the $F(\nu_1)$ including the contributions from the symmetric vibration, *i.e.*, changes in R. The results are very similar to those for the 1s → 2p transition and we shall use those values here. In addition, however, we must consider the effect of broadening by polaron modes. This

TABLE III: The 1s Continuum Thresholds for the Most Stable Cavity Radius (Using Temperature-Dependent Model and T = 203°K)

	V_0 = 0.5 eV	V_0 = 0.0 eV	V_0 = −0.5 eV
N = 4	2.071 eV	1.976 eV	1.846 eV
N = 6	2.364 eV	2.138 eV	2.004 eV
N = 8	2.461 eV	2.164 eV	1.890 eV

is a very small contribution for bound-bound states (especially for the 1s → 2p transition) but it is large for bound-continuum transitions since the electric displacement in the continuum states is zero and thus in eq 28 the value of E_s is simply the value of π_s for the ground state. This value is 0.78 eV for N = 4 and V_0 = −0.5 eV. Substituting this value into eq 36 we find an additional line broadening of 0.388 eV. If the two contributions are independent we predict at T = 203°K a line half-width for the transition of 0.096 + 0.388 = 0.484 eV. For the N = 6 cavity and V_0 = −0.5 eV we obtain 0.138 + 0.369 = 0.507 eV since the value of π is 0.75 eV.

If we assume a Gaussian distribution we can write an explicit expression for $F(\nu_1)$ in terms of the half-width, w, using the notation of Delahay.[26]

$$F(\nu_1) = \exp(-y^2) \tag{41}$$

where

$$y = \frac{1.665}{w}(\nu_1 - \nu_1(R_0)) \tag{42}$$

where $\nu_1(R_0)$ is tabulated in Table III. The temperature dependence is contained in the half-width which was found theoretically to vary as $\sqrt{T}$ thus further justifying eq 26.

More complicated is the calculation of the energy-dependent cross section. This is dependent on the square of a matrix element of the form

$$\langle \psi_i | \vec{r} | \psi_f \rangle \tag{43}$$

in the dipole length formulation. ψ_i and ψ_f are the initial and final state wave functions. We have a good idea of the initial wave function but we have only approximate ideas of the form of ψ_f. We notice, however, that this matrix element involves radial integrals of the form

$$\int \psi_i^* r^l \psi_f \, \mathrm{d}r \tag{44}$$

and thus they are very dependent on the behavior of the wave functions at larger r. Furthermore, ψ_f by symmetry must have orbital angular momentum l = 1. We have already seen that even the 2p state is well approximated by a purely Coulombic potential with its long-range behavior. Therefore in order to get the proper energy dependence of the cross section we can use the exact formulas appropriate to a hydrogen atom (or a screened hydrogen-like atom) as derived in Bethe and Saltpeter.[27] Except for some constants the results are proportional to

$$\sigma(\nu_1 \nu) = \nu_1^3 \nu^{-4} f(\nu/\nu_1) \tag{45}$$

where

$$F(\nu/\nu_1) = 1 + \frac{4}{3}\left(\frac{(\nu - \nu_1)}{\nu_1}\right) = \frac{4}{3}\left(\frac{\nu}{\nu_1}\right) - \frac{1}{3} \tag{46}$$

if

(25) J. Hasing, *Ann. Phys.* **37**, 509 (1940).
(26) P. Delahay, *J. Chem. Phys.*, **55**, 4188 (1971).
(27) H. A. Bethe and E. E. Saltpeter, "Quantum Mechanics of One- and Two-Electron Atoms," Academic Press, New York, N. Y., 1957, pp 303-308.

$$(\nu - \nu_1) < \sqrt{3}\,\nu_1$$

or so.

For very small $(\nu/\nu_1 - 1) < 0.2$ or so, this result has often been expanded as

$$F(\nu/\nu_1) = (\nu/\nu_1)^{4/3} \tag{47}$$

leading to a cross section varying as

$$\sigma(\nu_1, \nu) = \frac{1}{\nu_1}(\nu_1/\nu)^{8/3} \tag{48}$$

except for the $(1/\nu_1)$ factor this is in the form used by Delahay.[28] Delahay was able to very nicely express $L(\nu)$ in terms of the line width and the maximum of the line, $\nu_1(R_0)$.[26] Because he used the ⅔ power expression he had to evaluate the integrals numerically. We will show now that if we use the full low-energy expressions (45) and (46) one can evaluate the answer analytically and in the case of reasonable line widths obtain a very simple expression.

Because the photoionization profiles are of interest to many people we will present our derivation in some detail. Following Appendix A in Delahay's paper,[26] we can express eq 39 using eq 41, 42, 45, and 46 as

$$L(z_p) = \frac{4}{3}y_c(|1 + z_p|)^{-3}\int_{-1}^{z_p}(|1 + z|)^2 \exp(-z^2y_c^2)\,dz - \frac{1}{3}y_c(|1 + z_p|)^{-4}\int_{-1}^{z_p}(|1 + z_p)^2 \exp(-z^2y_c^2)\,dz \tag{49}$$

using Delahay's notation in terms of our parameters

$$y_c = \left(\frac{1.665}{w}\right)\nu_1(R_0) \tag{50a}$$

and

$$z_p = \frac{\nu_1 - \nu_1(R_0)}{\nu_1(R_0)} \tag{50b}$$

The integrals in eq 49 can be evaluated in terms of error functions and their derivatives as well as ordinary exponential integrals (for odd powers of z). To carry out the analysis one must perform a separate calculation for $z_p > 0$ and for $z_p < 0$, as the functional dependence is quite different in the two regions. To simplify the result we shall define

$$\Phi(x) \equiv \operatorname{erf}(x) = \frac{\sqrt{\pi}}{2}\int_0^x e^{-t^2}\,dt$$

$$\Phi'(t) = d\Phi/dx|_{x=t} \tag{51}$$

furthermore

$$(\sqrt{\pi}/2)\,\Phi'(t) = e^{-t^2}$$

For $z_p < 0$ we find

$$P(z_p) = \frac{2}{\sqrt{\pi}}L(z_p) = \frac{4}{3}(1 + z_p)^{-3}\{(1 + (2y_c^2)^{-1}[\Phi(y_c) + \Phi(y_cz_p)] - (2y_c)^{-1}[\Phi'(y_c) + z_p\Phi'(y_cz_p)] + \Phi'(y_c)(y_c^{-1} + y_c^{-3}) - \Phi'(y_cz_p)(z_p^2y_c^{-1} + y_c^{-3})\} - \frac{1}{3}(1 + z_p)^{-4}\{(1 + (\tfrac{3}{2})\,y_c^{-2})\,[\Phi(y_c) + \Phi(y_cz_p)] - (\tfrac{3}{2})y_c^{-1}[\Phi'(y_c) + z_p\Phi'(y_cz_p)] + (\tfrac{3}{2})\Phi'(y_c)(y_c^{-1} + y^{-3}) - (\tfrac{3}{2})\Phi'(y_cz_p)[z_p^2y_c^{-1} + y_c^{-3}] + \Phi'(y_c)y_c^{-5}[1 + (y_c^2y_c^4)/2] - \Phi'(y_cz_p)y_c^{-5}[1 + y_c^2z_p^2 + (z_p^4y_c^4)/2] \tag{52}$$

For $z_p = 0$ we obtain

$$P(0) = \Phi(y_c)[1 + (\tfrac{1}{6})y_c^{-2}] - (\tfrac{5}{6})y_c^{-3} + (\tfrac{1}{3})y_c^{-5} + \Phi'(y_c)[(\tfrac{1}{2})y_c^{-1} + (\tfrac{1}{2})y_c^{-3} - (\tfrac{1}{3})y_c^{-5}] \tag{53}$$

The expression for $z_p < 0$ is given in Appendix I.

Before proceeding with our calculations it is important to estimate the size of our parameters. We have $\nu_1(R_0) \approx 2$ eV, $W \sim 0.5$ eV, so $y_c \sim (1.7)(2)/0.5 \sim 6.6$. Also from the calculations of Delahay[26] we know that the integration changes very rapidly for values of z_p around zero; for $z_p > 0.5$ or so the integral is almost constant. In addition, for $z_p < 0.5$ the answer is almost zero. These values suggest that some very important approximations can be made since $y \geq 5$. In this limit we can neglect to within a few per cent $\operatorname{erf}(y^{-2})$ *vs.* 1 and e^{-y^2} *vs.* 1, or $\Phi'(y)$ *vs.* 1.

These results greatly simplify the expressions. Consider P(0) in these limits

$$P(0) \approx \Phi(y_c)[1 + (\tfrac{1}{6})y_c^{-2}] - (\tfrac{5}{6})y_c^{-3} \simeq 1.00 \tag{54}$$

to about three significant figures for $y \geq 5$.

Likewise for the other limits we obtain

$$P(z_p > 0) = \frac{4}{3}(1 + z_p)^{-3}[1 - \Phi(y_cz_p) - \Phi'(y_cz_p)((\tfrac{1}{2})z_py_c^{-1} + z_p^2y_c^{-1} + y_c^{-3})] - (\tfrac{1}{3})(1 + z_p)^{-4}[1 + \Phi(y_cz_p) - \Phi'(y_cz_p)(\tfrac{3}{2})z_py_c^{-1} + (\tfrac{3}{2})z_py_c^{-1} + 3y_c^{-3} + y_c^{-5} + z_p^2y_c^{-3} + (z_p^4y_c^{-1})/2) \tag{55}$$

$$P(z_p < 0) = \frac{4}{3}(1 - \eta_p)^{-3}\{1 - \Phi'(y_c\eta_p)[\eta_p^2y_c^{-1} + y_c^{-3} - (\tfrac{1}{2})\eta_py_c^{-1}] - \Phi(y_c\eta_p)\} - \frac{1}{3}(1 - \eta_p)^{-4}\{1 - \Phi(y_c\eta_p) - \Phi'(y_c\eta_p)[(\tfrac{3}{2})\eta_p^2y_c^{-1} + y_c^{-3} - (\tfrac{3}{2})\eta_py_c^{-1} + y_c^{-5} + \eta_p^2y_c^{-3} + (\tfrac{1}{2})\eta_p^4y_c^{-1}]\} \tag{56}$$

where $n_p = -z_p > 0$, but less than 1.0.

For the regions of interest it was found that terms involving $\Phi'(y_c\eta_p)$ are very small (3 parts in 1000 or less) and thus very reliable, very simple expressions can be used over all regions of z_p.

$$P(z_p > 0) = (1 + z_p)^{-3}[(\tfrac{4}{3}) - (\tfrac{1}{3})(1 + z_p)^{-1}] \times [1 + \Phi(y_cz_p)] \tag{57}$$

$$P(z_p < 0) = (1 + z_p)^{-3}[(\tfrac{4}{3}) - (\tfrac{1}{3})(1 + z_p)^{-1}] \times [1 - \Phi(y_cz_p)] \tag{58}$$

$$P(z_p > 0) = [1 - (\tfrac{8}{3})z_p + (\tfrac{14}{3})z_p^2][1 + \Phi(y_cz_p)] \tag{59}$$

(when $z_p < 0.5$).

The region in which the asymptotic result holds is therefore when $\Phi(y_cz_p) \sim 1$. The exact limit depends on the precision required. This simple result occurs because of the large value of y in the present examples. In that case

$$\int_{-1}^{z_p}(1 + z)^n e^{-y_c^2z^2}\,dz \approx \int_{-1}^{z_p} e^{-y_c^2z^2}\,dz \tag{60}$$

since only small values of z contribute to the integral. Thus the integral depends very weakly on the power of n. Therefore, the results of Delahay at large y_c are equivalent to the above calculations. For small values of y_c both our approximate formulas (eq 57-59) and those of Delahay need further corrections. In that case the complete expressions of eq 52, 53, and Appendix A are required.

(28) P. Delahay (ref 26) neglected to include the ionization potential contained in the factor in front of eq 71.11 of ref 27. His results in his Appendix A are thus slightly narrower than our calculations. However, for large values of y, *i.e.*, narrow lines, the integral is almost independent of the specific power law and thus his results are good. See eq 60.

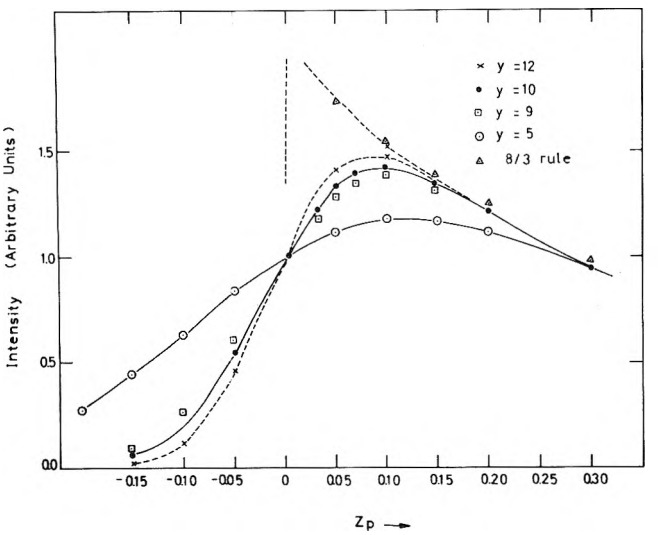

Figure 14. Photoemission profiles calculated for various values of y_c.

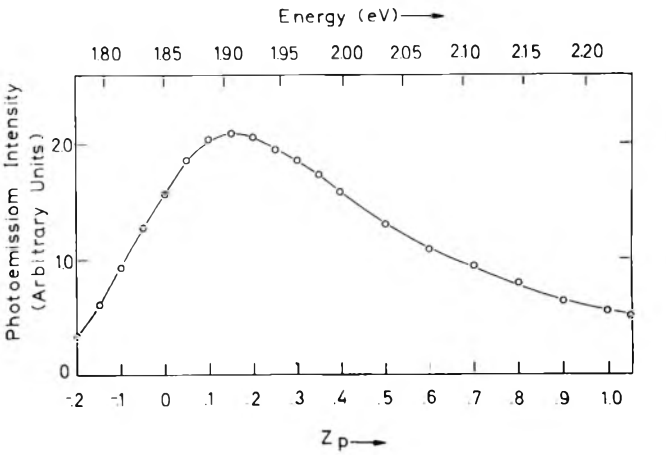

Figure 15. Predicted photoionization line shape for the solvated election in liquid ammonia.

In Figure 14 we present the reduced plots of the photoionization energy profile for various values of y in the region of interest. The points were calculated using the expressions 39 and 40 but in most cases, eq 57 and 58 yield results within a per cent or so of these answers. We have also plotted the asymptotic behavior which departs significantly from the integrated result for $z_p < 0.1$ when $y_c \sim 10$ and for $z_p < 0.2$ when $y_c \sim 5$. The points marked A are for the $\frac{8}{3}$ low asymptotic behavior. It differs very little from the complete result for $z_p < 0.3$.

Since our calculations indicate that both $N = 4$ and $N = 6$ cavities are energetically stable we have calculated the total contribution (unnormalized) from both cavities at a temperature corresponding to about 240°K. This is plotted in Figure 15 for suitable parameters. For the $N = 4$ state we used $\nu_1(R_0)$ from Table III for $T = 203$°K and $V_0 = -0.5$ eV and $y = 5$ for a reasonable line width at 240°K. For $N = 6$ we also used $y = 5$, the corresponding energy from Table III and a weighting factor of 0.8 relative to the $N = 4$ case. It is apparent that with several cavity types the profile is very broad and very complicated. For values of $z_p > 0.2$ the total result behaves as if the ionization potential were 1.9 eV and not either 1.85 or 2.00 eV. In general no simple power law behavior is expected to work.

The only data with which we can compare our results is the photoelectron emission spectrum of metal–ammonia solutions of Häsing.[25] To apply our calculations to that case involves some drastic assumptions but if we assume that this spectrum behaves as $E^{-8/3}$ down to 2 eV and if extrapolated to zero current in that way one obtains 1.85 eV. Our curve in Figure 15 deviates from any simple law in the region near the maximum or at about 2.2 eV, but again we emphasize that these interpretations are risky and one needs direct measurements of the photoionization. More experimental data is desperately needed.

It has been suggested that the high energy tail of the optical absorption is in fact the bound–continuum transition.[26] Delahay has even analyzed the spectra of hydrated electron and electrons in 3-MP, THF, and HMPA in terms of such an assumption. They obey an $E^{-8/3}$ plot. However, the calculations presented in section A suggest that the high energy tail in these cases may not necessarily be part of the bound–continuum transition. (For further evidence in the last two cases, see ref 22.) It is also important to note that if several types of cavities with different $E_1(R_0)$ contribute the true photoemission line profile, it will very likely not have a simple $E^{-8/3}$ or any other power law dependence except at extremely high energies where only the highest value of $\nu_1(R_0)$ remains important. Unfortunately, the experimental data are not yet available to check on this feature.

Appendix

Total Expression for $P(z_p < 0)$. Using the notation of eq 56 and setting $\eta_p = -z_p$ for $z_p < 0$, we find

$$P(z_p < 0) = \frac{4}{3}(1 - \eta_p)^{-3}\{(1 + (\tfrac{1}{2})y_c^{-2})(\Phi(y_c) - \Phi(y_c\eta_p)) + \Phi'(y_c)(y_c^{-3} + (\tfrac{1}{2})y_c^{-1}) - \Phi'(y_c\eta_p)[\eta_p^2 y_c^{-1} + y_c^{-3} - (\eta_p/2)y_c^{-1}]\} - \frac{1}{3}(1 - \eta_p)^{-4}\{(1 + (\tfrac{3}{2})y_c^{-2})[\Phi(y_c) - \Phi(y_c\eta_p)] + \Phi'(y_c)[(\tfrac{3}{2})y_c^{-3} + y_c^{-5}(1 + y_c^2 + y_c^4/2)] - \Phi'(y_c\eta_p)[(\tfrac{3}{2})\eta_p^2 y_c^{-1} + (\tfrac{3}{2})y_c^{-3} + y_c^{-5}(1 + \eta_p^2 y_c^2 + (\tfrac{1}{2})y_c^2\eta_p^4) - (\tfrac{3}{2})\eta_p y_c^{-1}]\}$$

Digital Simulation of Edge Effects at Planar Disk Electrodes

James B. Flanagan and Lynn Marcoux*

Department of Chemistry, Texas Tech University, Lubbock, Texas 79409 *(Received October 30, 1972)*

Publication costs assisted by The Robert A. Welch Foundation

Digital simulation has proven to be a useful approach to electrochemical problems involving complex geometries. This method was used to take into account the contributions of cylindrical diffusion to diffusion processes at finite planar disk electrodes. The current-time relationship for diffusion-controlled electrolysis at a planar disk electrode with radius R was found to be $it^{1/2} = (nFACD^{1/2}/\pi^{1/2})\{1 + 1.92(Dt/R^2)^{1/2}\}$. For chronopotentiometry the transition time, τ, was found to be given by $i\tau^{1/2} = (nFACD^{1/2}\pi^{1/2}/2)\{1 + 0.72(D\tau/R^2)^{1/2}\}$. The chronoamperometric working curves for the first-order ECE reaction were calculated as a function of kR^2/D and were found to depart significantly from simple theory for values of this parameter which were less than 500. The results are discussed and compared with previous work.

The simplicity of Fick's second law for semiinfinite linear diffusion is often complicated by the fact that semiinfinite linear diffusion does not obtain for real systems of electrochemical interest. The most obvious departures are those geometric ones in which the electrode is nonplanar. The classical example of this is, of course, the spherical mercury drop electrode which was first presented in this context by Lingane.[1] This problem has continued to be a topic for discussion.[2] Noble metal wires were among the first solid electrodes to be used;[3] consequently, cylindrical diffusion became a process to be reckoned with. The effect of cylindrical diffusion upon the potential-time curves of chronopotentiometry has been extensively treated[4-7] and tables of correction factors have been prepared for use with cylindrical electrodes.[8] Cylindrical diffusion is also encountered in the case of tubular electrodes, and the current-time response for this geometry has been predicted and observed.[9]

A less obvious departure from linear diffusion occurs at circular planar electrodes and is due to the finite size of the disk. For disks of large radius, the contribution from the disk edge is small at times of electrochemical interest; however, as the electrode radius decreases, the relative importance of this source of flux increases. The first approach to this problem was an experimental one in which chronoamperometric data were used to obtain an empirically corrected version of the Cottrell equation. At the same time chronopotentiometric data were used to similarly treat the Sand equation.[10] Later the chronoamperometric problem was considered analytically and the experimental result was more-or-less confirmed.[11] The cylindrical component of diffusion to a planar disk has been experimentally eliminated by the use of shielded electrodes,[12-14] and although this approach is quite effective; the difficulties involved in the construction of these electrodes have limited the usefulness of this technique.

Chronoamperometric and chronocoulometric methods are finding increasing use in the study of the mechanisms of reactions coupled to charge transfer.[15-18] As the distinctions between these mechanisms grow more and more subtle it becomes necessary to completely understand the limitations of the method. With this thought in mind, we employed digital simulation[19] in order to consider the two-dimensional diffusion problem encountered at disk electrodes of finite size.

Method

The computational technique was a two-dimensional variation of the explicit difference method described by Feldberg.[19] Certainly many other methods exist[20] including those specifically developed for the solution of discontinuous boundary value problems;[21] however, the present method was chosen because of our own familiarity with the technique as well as the fact that once the basic diffusion problem is solved by this method it is a relatively easy matter to extend these calculations to include any number of kinetic complications. Digital simulation has recently proven to be quite effective in the solution of interesting geometric problems such as those presented by the rotating ring disk electrode,[22-25] thin layer electrodes,[26] and electrochemical esr cells.[27,28]

(1) J. J. Lingane and B. A. Loveridge, *J. Amer. Chem. Soc.*, **72**, 438 (1950).
(2) J. Heyrovsky and J. Kuta, "Principles of Polarography," Academic Press, New York, N. Y., 1966, pp 91-95.
(3) H. A. Laitinen and I. M. Kolthoff, *J. Phys. Chem.*, **45**, 1061 (1941).
(4) J. J. Lingane, *J. Electroanal. Chem.*, **1**, 379 (1960).
(5) D. G. Peters and J. J. Lingane, *J. Electroanal. Chem.*, **2**, 1 (1961).
(6) J. J. Lingane, *J. Electroanal. Chem.*, **2**, 46 (1961).
(7) D. G. Peters and J. J. Lingane, *J. Electroanal. Chem.*, **2**, 249 (1961).
(8) D. H. Evans and J. E. Price, *J. Electroanal. Chem.*, **5**, 77 (1963).
(9) T. O. Oesterling and C. L. Olson, *Anal. Chem.*, **39**, 1546 (1967).
(10) P. J. Lingane, *Anal. Chem.*, **36**, 1723 (1964).
(11) Z. G. Soos and P. J. Lingane, *J. Phys. Chem.*, **68**, 3821 (1964).
(12) M. von Stackelberg, M. Pilgram, and V. Toome, *Z. Elektrochem.*, **57**, 342 (1953).
(13) A. J. Bard, *Anal. Chem.*, **33**, 11 (1961).
(14) J. Zimmerman, Ph.D. Thesis, University of Kansas, 1964.
(15) M. D. Hawley and S. W. Feldberg, *J. Phys. Chem.*, **70**, 3459 (1966).
(16) W. V. Childs, J. T. Maloy, C. P. Keszthelyi, and A. J. Bard, *J. Electrochem. Soc.*, **118**, 874 (1971).
(17) L. Marcoux, *J. Amer. Chem. Soc.*, **93**, 537 (1971).
(18) L. Marcoux, *J. Phys. Chem.*, **76**, 3254 (1972).
(19) S. W. Feldberg, "Electroanalytical Chemistry, A Series of Advances," Vol. 3, A. J. Bard, Ed., Marcel Dekker, New York, N. Y., 1969, p 199.
(20) B. Caranahan, H. A. Luther, and J. O. Wilkes, "Applied Numerical Methods," Wiley, New York, N. Y., 1969.
(21) H. E. Wilhelm, *Z. Angew. Phys.*, **30**, 376 (1971).
(22) K. B. Prater and A. J. Bard, *J. Electrochem. Soc.*, **117**, 207 (1970).
(23) K. B. Prater and A. J. Bard, *J. Electrochem. Soc.*, **117**, 335 (1970).
(24) K. B. Prater and A. J. Bard, *J. Electrochem. Soc.*, **117**, 1517 (1970).
(25) G. Neubert, E. Gorman, R. Van Reet, and K. B. Prater, *J. Electrochem. Soc.*, **119**, 677 (1972).
(26) I. B. Goldberg and A. J. Bard, *J. Electroanal. Chem.*, **38**, 313 (1972).

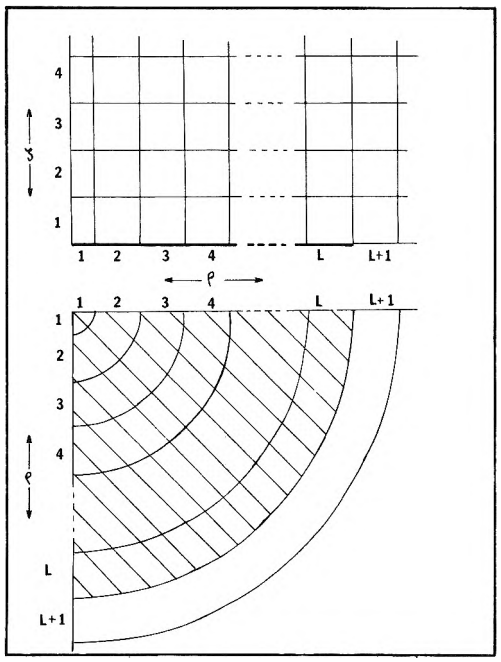

Figure 1. Simulation model of electrode. Cross-hatched area represents electrode surface.

Because of the symmetry of the planar-disk electrode, the system was modeled in circular cyclindrical coordinates. As shown in Figure 1, the electrode model was divided into L annular elements. To simulate radial diffusion, there were annuli beyond the electrode radius. The direction normal to the surface is divided into segments parallel to the electrode surface. Each of these volume elements is designated by its radial component ρ, and its normal component ζ. The dimensionless concentration parameter F is equal to the concentration in that volume element divided by the bulk concentration. These dimensionless concentrations are then stored in an array of the form $F_{\rho,\zeta,K}$. For other notation see Table I.

The explicit difference equations for diffusion in cylindrical coordinates have been given both by Feldberg[19] and in slightly different form by Hartree.[29] For any element except the central element, *i.e.*, $\rho \neq 1$, this expression is

$$F_{\rho,\zeta,K+1} = F_{\rho,\zeta,K} + \delta\{-4F_{\rho,\zeta,K} + F_{\rho+1,\zeta,K} + F_{\rho-1,\zeta,K} + F_{\rho,\zeta+1,K} + F_{\rho,\zeta-1,K} + \frac{1}{2(\rho-1)}(F_{\rho+1,\zeta,K} - F_{\rho-1,\zeta,K})\} \quad (1a)$$

Diffusion into the central element has been treated by Hartree[29] and is of the form

$$F_{1,\zeta,K+1} = F_{1,\zeta,K} + 4\delta(F_{2,\zeta,K} - F_{1,\zeta,K}) + \delta(-2F_{1,\zeta,K} + F_{1,\zeta+1,K} + F_{1,\zeta-1,K}) \quad (1b)$$

The standard boundary condition for chronopotentiometry is that the current, hence the flux at the electrode surface, is constant. Because of the cylindrical contributions present in this particular case this boundary condition becomes more complex, since although the current at each annulus on the electrode surface varies, the total current is held constant. It is thus necessary to solve for the surface concentration (hence the potential) which will cause the total current summed over all the annuli to equal the preset current. It is assumed that, since the electrode and solution are good conductors, the potential difference across the interface will not vary with position.

TABLE I: Explanation of Notation

Variable	Explanation
δ	Dimensionless diffusion coefficient $\delta = D\Delta t/(\Delta R^2)$
$F_{\rho,\zeta,K}$	Dimensionless concentration variable $F = C/C_{bulk}$
K	Dimensionless iteration counter (see eq 14)
L	Number of radial divisions of electrode model (see Figure 1)
ρ	Radial coordinate of model
ζ	Normal coordinate
θ	Dimensionless time parameter (see eq 14)
Z	Dimensionless current parameter (see eq 13)
Φ_ρ	Dimensionless flux to electrode surface in element ρ
$\bar{\Phi}$	Dimensionless average net flux to electrode surface
$F_{\rho,K}{}^s \equiv \bar{F}^s$	Concentration at electrode surface
A_ρ	Area of volume element ρ
A_{tot}	Total electrode area
G	An intermediate concentration variable (see eq 7)
R	Real electrode radius
D	Real diffusion coefficient

This is to be contrasted to with those previously cited examples in which a resistive component is responsible for a nonequipotential surface.[26-28]

Consider the system A ± e $\rightleftarrows$ B where we assume that charge transfer is rapid, A and B have equal diffusion coefficients, and that the potential of the electrode surface remains constant for each iteration. We assume, as did Feldberg, that the surface of the electrode is at the outside of the first volume elements of the electrode. In each time step we have

$$F_{\rho,1,K+1} = F_{\rho,1,K} + \Delta F_{\rho,1,K} - \Phi_{\rho,K} \quad (2)$$

where $\Delta F_{\rho,1,K}$ is the change in concentration due to diffusion and $\Phi_{\rho,K}$ is the change in concentration in each surface element due to electrolysis. Note that if $\bar{\Phi}$ is the preset flux which defines the chronopotentiometric experiment

$$\bar{\Phi} \cdot A_{tot} = \sum_{\rho=1}^{L} (\Phi_{\rho,K} A_\rho) \quad (3)$$

Extrapolating the concentration to the surface

$$F_{\rho,K+1}{}^s = F_{\rho,1,K+1} - \frac{\Phi_{\rho,K}}{2\delta} \quad (4)$$

Combining (2) and (4)

$$F_{\rho,K}{}^s = F_{\rho,1,K} + \Delta F_{\rho,1,K} - \left(1 + \frac{1}{(2\delta)}\right)\Phi_{\rho,K} \quad (5)$$

This leads to

$$\Phi_{\rho,K} = \frac{F_{\rho,1,K} + \Delta F_{\rho,1,K} - F_{\rho,K+1}{}^s}{1 + 1/(2\delta)} \quad (6)$$

In the finite difference approximation, the quantity $(F_{\rho,1,K} + \Delta F_{\rho,1,K})$ may be calculated independently of the flux. For convenience, let

(27) I. B. Goldberg and A. J. Bard, *J. Phys. Chem.*, **45**, 3281 (1971).
(28) I. B. Goldberg, A. J. Bard, and S. W. Feldberg, *J. Phys. Chem.*, **76**, 2550 (1972).
(29) D. R. Hartree, "Numerical Analysis," Oxford University Press, London, 1952, p 219.

$$G_\rho = F_{\rho,1,K} + \Delta F_{\rho,1,K} \tag{7}$$

Invoking (3) and the equipotential surface condition (*i.e.*, $F_{\rho,K}{}^{s} = \bar{F}^{s}$, a constant, for $\rho \leq L$)

$$\bar{\Phi} \cdot A_{tot} = \sum_{\rho=1}^{L} \frac{(G_\rho - \bar{F}^{s})A_\rho}{1 + 1/(2\delta)} \tag{8}$$

Finally

$$\bar{F} = \sum_{1}^{L} G_\rho \frac{A_\rho}{A_{tot}} - \bar{\Phi}(1 + 1/2\delta) \tag{9}$$

From (6) it is possible to calculate the various $\Phi_{\rho,K}$. The electrode potential is simply given by the Nernst equation

$$E = E^\circ \pm \frac{0.059}{n} \log \left\{ \frac{(1 - \bar{F}^{s})}{\bar{F}^{s}} \right\} \tag{10}$$

The transition time is taken to be the time step at which $\bar{F}^{s}$ becomes equal to or less than zero. The boundary condition for chronoamperometry is similar to that for chronopotentiometry, except that the surface concentration is fixed at zero. From eq 6

$$\Phi_{\rho,K} = \frac{F_{\rho,1,K} + \Delta F_{\rho,1,K}}{1 + 1/(2\delta)} \tag{11}$$

Combining (2) and (11) and solving for the new concentration

$$F_{\rho,1,K+1} = (F_{\rho,1,K} + \Delta F_{\rho,1,K})\left(\frac{1}{1 + 2\delta}\right) \tag{12}$$

The correspondence between real and simulation variables is as follows: for current

$$Z = \frac{i}{nFC^{b}\pi D} = \frac{\sum_{1}^{L}(\Phi_{\rho,K} \cdot (2\rho - 1))}{\delta(L - 0.5)} \tag{13}$$

and for time

$$\theta = \frac{tD}{R^2} = \frac{K\delta}{(L - 0.5)^2} \tag{14}$$

The introduction of kinetic complications was done in a fashion similar to that of Feldberg.[19] After establishing the boundary conditions and carrying through the diffusion step the effect of chemical reaction upon the various concentrations was calculated for each volume element. Although myriad kinetic possibilities exist we chose the simple first-order ECE reaction because an analytical solution exists for this problem at the infinite planar disk,[30] and furthermore, this reaction sequence occurs quite often in practice.[31] The sequence is

$$A + n_1 e \rightleftharpoons B \tag{15}$$

$$B \xrightarrow{k} C \tag{16}$$

$$C + n_2 e \rightleftharpoons D \tag{17}$$

The usual simulation approach to a kinetic complication is to calculate the concentration change due to reaction by means of a finite difference equation. For the reaction cited above this is

$$\Delta(B) = (B)_0 k \Delta t \tag{18}$$

One of the deficiencies of the finite difference method has been that this expression is invalid for large values of $k\Delta t$. A more accurate and versatile approach arises from integration of the appropriate differential equation and subsequent utilization of this integrated form. For the sequence 15–17 this is

$$\Delta(B) = (B)_0(1 - e^{-k\Delta t}) \tag{19}$$

This idea may easily be extended to other reaction sequences. For example for the frequently studied second-order coupling ECE reaction[32,33] which is identical with the above case except reaction 16 is given by

$$2B \xrightarrow{k} C \tag{20}$$

The integrated difference form is

$$\Delta(B) = \left\{ -k\Delta t + \frac{1}{(B)_0} \right\}^{-1} - (B)_0 \tag{21}$$

For kinetic cases in which integration of the rate law is more complicated a numerical technique such as the Runge–Kutta method[20] may be used to determine the concentration change of interest. Superficially this approach may seem to destroy the aesthetic simplicity of the simulation method, but the increase in range and accuracy is well worth the sacrifice. Furthermore, because this method converges more rapidly, it permits a savings in both computation time and array size. These latter considerations are often limiting in the case of multidimensional problems.

One of the difficulties of the digital simulation technique arises from the fact that one cannot accurately evaluate the magnitude of the errors inherent in the calculation. This problem is not unique to digital simulation since the authors of the analytical treatment of this problem encountered the same difficulty.[11] For our purposes the criterion for accepting a calculated value was convergence to reproducible values as the number of time iterations became large, or as the $\Delta\rho$ and $\Delta\zeta$ became small. Where analytical solutions were known, comparisons were made. Thus the first-order ECE sequence was simulated for an infinite disk, and the results compared within 0.5% of the analytical solution of Alberts and Shain.[30] The problem of diffusion to the walls of a tube of infinite length is quite similar to the present problem and when our method was applied to this the results came within 0.04% of the solution calculated by Oesterling and Olson.[9] The simulations were also tested by varying internal parameters such as dimensionless diffusion coefficients and the number of annuli in the disk. For a convergent calculation these parameters should not affect the final result, and this was found to be the case. We believe our results to be easily within 1.0% of actual values.

Results and Discussion

The Cottrell equation[34] for an infinite disk is

$$i = \frac{nFAD^{1/2}C^{b}}{\pi^{1/2}t^{1/2}} \tag{22}$$

where all symbols have their usual electrochemical significance. Intuitive[10] and later mathematical[11] arguments have shown that for finite electrodes this equation should be written as the Cottrell term times a power series in

(30) G. S. Alberts and I. Shain, *Anal. Chem.*, **35**, 1859 (1963).
(31) R. N. Adams, *Accounts Chem. Res.*, **2**, 175 (1969).
(32) R. F. Nelson and S. W. Feldberg, *J. Phys. Chem.*, **73**, 2624 (1969).
(33) L. S. Marcoux, R. N. Adams, and S. W. Feldberg, *J. Phys. Chem.*, **73**, 2611 (1969).
(34) P. Delahay, "New Instrumental Methods in Electrochemistry," Interscience, New York, N. Y., 1954, p 51.

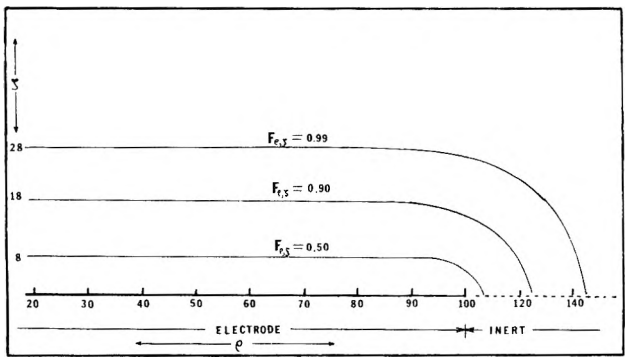

Figure 2. Constant concentration contours after 250 iterations: $L = 100$, $\delta = 0.22$.

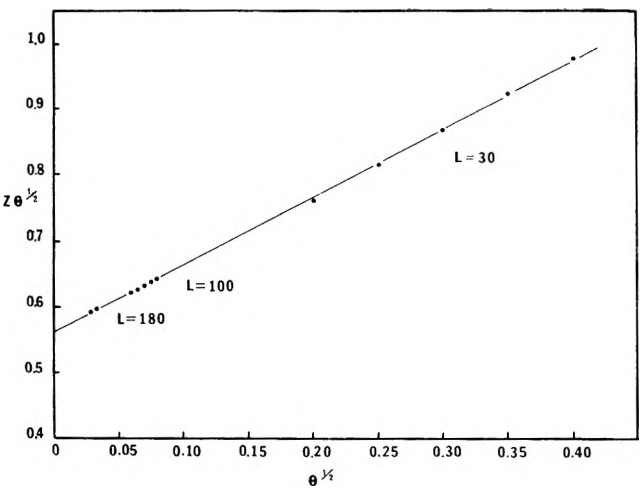

Figure 3. Simulation of chronoamperometry for various values of L. $Z\theta^{1/2} = (\pi)^{-1/2}(1 + a\theta^{1/2})$

$(Dt/R^2)^{1/2}$. It has also been shown that only the first term in the power series is significant[11] so the current-time behavior at a finite disk for applied potentials in the region of diffusion control is given by

$$i = \frac{nFAD^{1/2}C^b}{\pi^{1/2}t^{1/2}}\left\{1 + a\left(\frac{Dt}{R^2}\right)^{1/2}\right\} \qquad (23)$$

where R is the electrode radius. Digital simulation confirmed this result and provided a value of 1.92 for the constant a. The experimental value[10] for this constant was found to be 2.12 ± 0.11 and the analytical treatment yielded a value of 2.26. The discrepancy between the analytical and simulation value is not disturbing since approximations made in the development of the analytical treatment were such that the analytical value was acknowledged to be too large by a small but undetermined amount.[11] The importance of the cylindrical contributions is shown more graphically in Figure 2 which provides concentration profiles for the simple electron transfer case.

The consistency of this simulation is demonstrated by the plot of $Z\theta^{1/2}$ *vs.* $\theta^{1/2}$ given in Figure 3. Several different values of L were used in order to span the range shown. Note the agreement between the slopes and intercepts for each simulation. It should be noted further that the intercept is nearly identical with the theoretical value of 0.564. This provides indirect confirmation of the validity of the calculation.

An accurate evaluation of the constant a of eq 23 is of some practical value since data obtained at a small disk electrode over a sufficient time interval may be used in order to determine n and D independently. The slope of a plot of $it^{1/2}$ *vs.* $t^{1/2}$ divided by the intercept of this plot yields D where the only experimental variable required is the electrode radius, R. The value of D so determined may be used in conjunction with the experimental value of the intercept in order to calculate n. A similar approach has recently been carried out at cylindrical wire electrodes.[35] For constant current experiments the Sand equation[36] is given by

$$i\tau^{1/2} = \frac{nFACD^{1/2}\pi^{1/2}}{2} \qquad (24)$$

where all symbols are standard. For a finite disk it has been argued[10] that the appropriate equation is

$$i\tau^{1/2} = \frac{nFACD^{1/2}\pi^{1/2}}{2}\left\{1 + b\left(\frac{D\tau}{R^2}\right)^{1/2}\right\} \qquad (25)$$

where the constant b was evaluated experimentally and found to be 0.98. Digital simulation provided a similar result; however, the value of b was found to be 0.72. This

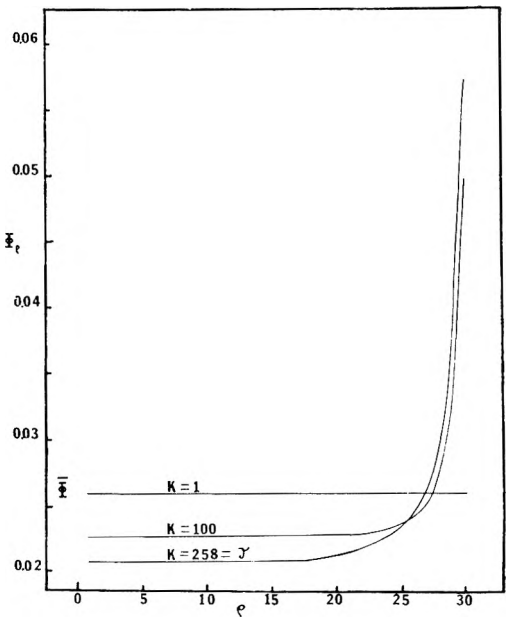

Figure 4. Radial current distribution in chronopotentiometry: $\bar{\Phi} = 0.26$, $\delta = 0.16$, $L = 30$, transition in iteration 258.

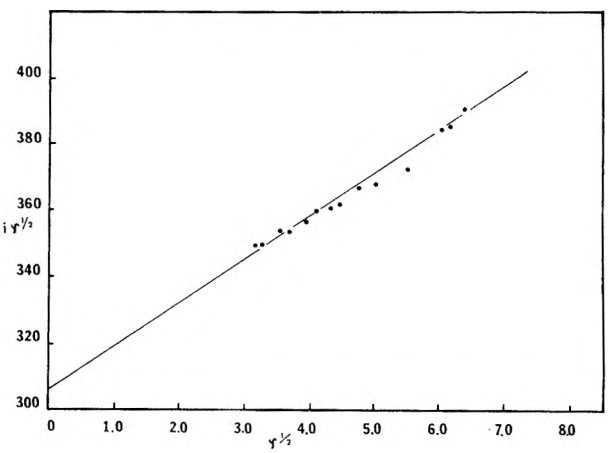

Figure 5. Plot of chronopotentiometric data given in ref 38.

(35) O. R. Brown, *J. Electroanal. Chem.*, **34**, 419 (1972).
(36) Reference 34, p 184.

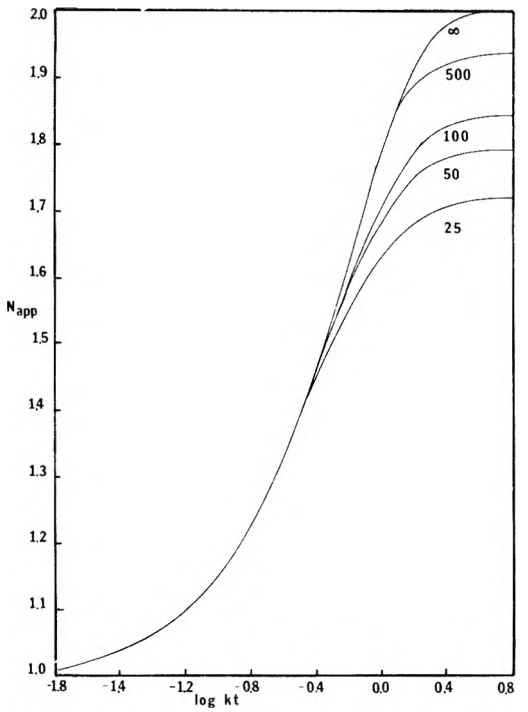

Figure 6. Simulated working curves for the first-order ECE mechanism shown as a function of (kR^2/D).

discrepancy probably arises from the fact that the experimental determination was based upon only 16 data pairs. Furthermore, the experimental difficulty in accurately measuring τ is legendary.[37] Here again the qualitative aspects of the departure are seen in Figure 4 which shows current density as a function of distance across the disk face.

In the past the departures from naive theory have often been ascribed to convective effects when in fact the anomaly was due to edge effects. In order to demonstrate the superiority of propylene carbonate over acetonitrile for chronopotentiometric measurements at long times, Nelson and Adams[38] compared the value of $i\tau^{1/2}$ obtained for 4.0×10^{-3} M 5,10-dihydro-5,10-dimethylphenazine in both acetonitrile and propylene carbonate. The value of $i\tau^{1/2}$ in acetonitrile diverged quite rapidly while for the same time domain it remained fairly constant for propylene carbonate. The departure from constancy for acetonitrile was ascribed to convective effects which were minimized in the case of the more viscous propylene carbonate. Acetonitrile data are shown plotted as $i\tau^{1/2}$ *vs.* $\tau^{1/2}$ in Figure 5. Using the slope to intercept ratio one calculates a value for $D^{1/2}$ of 4.16×10^{-3} cm/sec$^{1/2}$. Using the Sand equation and the extrapolated value of $i\tau^{1/2}$ at the $\tau = 0$ intercept of this plot one finds $D^{1/2} = 4.06 \times 10^{-3}$ cm/sec$^{1/2}$. It seems clear that the departure from constancy that was observed was due to edge effects which are less pronounced in propylene carbonate because of the decrease in diffusion coefficient in the more viscous solvent.

The results of the calculations for the chronoamperometric treatment of the first-order ECE reaction are shown in Figure 6. The format is of the usual working curve type where $N_{app} = it^{1/2}/(it^{1/2})_{k=0}$. This calculation was obviously carried out for the $n_1 = n_2$ case although the extension to nonsymmetrical cases is easily accomplished. The extent of departure from the Alberts and Shain[30] treatment is a function of the parameter kR^2/D where the case $kR^2/D = \infty$ represents the analytical solution for an infinite disk. From this it is clear that in order to attach any degree of confidence to a measured rate constant, the experimental conditions should be such that $kR^2/D > 500$. Due to the size of the commercially available Beckman platinum disk, and because of convenience in constructing carbon paste electrodes many rate constant determinations have been made at electrodes with areas of the order of 0.20 cm^2. Assuming $D = 1.0 \times 10^{-5}$ cm^2/sec, it may be readily seen that there exists little danger of error for cases in which $k > 0.1$ sec^{-1}. The only occasion in which errors incurred in this fashion might lead to seriously incorrect conclusions is when experimental results are used in an attempt to distinguish between mechanisms. For example, the experimental differences between electron transfer in solution (ECC) and electron transfer at the electrode (ECE) are slight[15] and it is reassuring to note that the experimental confirmation of this distinction[39] relied for the most part upon reactions whose rate constants were well within the above stated limits of confidence. Superficially the possibility of error may seem slight because the departure of $(it^{1/2})_{k=0}$ from constancy would seem to be an obvious indication that simple theory did not hold. This is normally not the case, however, because measurements over only one or two decades of time appear correct although in fact cylindrical diffusion is making a meaningful contribution to the process.

For the most part we assume that these results will be used only to assign probable errors to rate constant measurements. Nonetheless the possibility exists of actually using the given curves for measurement purposes. This would seem to be useful since it probably allows measurements to be extended another full decade in time. This is important since it is imperative when attempting to assign a mechanism by chronoamperometry to cover as much of the time range as possible. Measurements have been extended to very short times using carefully designed potentiostats,[40,41] but short time measurements are facilitated by small electrodes which are by geometric necessity more prone to long time departures from simple theory. By actually using these calculations it would seem that small electrodes could be used, thereby extending the time domain in both directions.

Acknowledgment. The support of the Robert A. Welch Foundation (Grant No. D-511) is gratefully acknowledged.

(37) D. G. Davis, "Electroanalytical Chemistry, A Series of Advances," Vol. 1, A. J. Bard, Ed., Marcel Dekker, New York, N. Y., 1966.
(38) R. F. Nelson and R. N. Adams, *J. Electroanal. Chem.*, **13**, 184 (1967).
(39) R. N. Adams, M. D. Hawley, and S. W. Feldberg, *J. Phys. Chem.*, **71**, 851 (1967).
(40) R. R. Schroeder and I. Shain, *J. Phys. Chem.*, **73**, 197 (1969).
(41) R. R. Schroeder and I. Shain, *Chem. Instrum.*, **1**, 233 (1969).

Nuclear Magnetic Resonance Chemical Shift of the Water Proton in Aqueous Alcoholic Solutions at Various Temperatures. Some Thermodynamic Properties of These Solutions

Marie-Madeleine Marciacq-Rousselot

Laboratoire de Physique Expèrimentale Molèculaire, Universitè Paris VI, Paris, France

and Michel Lucas*

Dèpartement de Gènie Radioactif, Centre d'Etudes Nuclèaires, 92260 Fontenay Aux Roses, France *(Received October 6, 1972)*

Publication costs assisted by Commissariat à l'Energie Atomique

In the present article, we report the results of nmr measurements of the chemical shift of the water proton in solutions of methyl, ethyl, *n*-propyl, *n*-butyl, and *tert*-butyl alcohol at various temperatures and concentrations. At low temperature the downfield shift of the water proton is consistent with an increase in water structure promotion by the solutes. At high temperatures, the upfield shift is consistent with a weakening of the water structure by the solutes. These results are also qualitatively consistent with what may be expected of the influence of hard-sphere molecular solutes on the water structure. The enthalpy of transfer of some alcohols from light to heavy water at 51° is given, but the classical interpretation of this type of measurements is questioned. Finally the enthalpy of transfer of *t*-BuOH from H_2O to *t*-BuOH aqueous solutions is also given and discussed according to current interpretations based on the overlap of hydration spheres around a hydrophobic solute. These interpretations are also questioned.

Introduction

A consideration of the influence of hard-sphere molecular solutes on water structure has yield the following interpretation.[1] At temperatures lower than 4°, the temperature at which the pure water expansion coefficient is equal to zero, a hard-sphere solute enhances the bonds between water molecules, and the bigger the solute the more important is the enhancement. When the temperature is raised this enhancement gradually diminishes and at temperatures higher than 4° the solute weakens the bonds between water molecules. This effect increases with the solute size and the temperature.

In order to test this hypothetical behavior, we report here the results of nmr measurements of the chemical shift of the water proton in solutions of methyl, ethyl, *n*-propyl, *n*-butyl, and *tert*-butyl alcohol at various temperatures and solute concentrations.

Alcohols are different from hard-sphere nonpolar molecules, but less dissimilar solutes as hydrocarbons or rare gases are not soluble enough to allow measurements to be performed and it is hoped that the influence of the alcohols on water structure will be somewhat similar to that of hard-sphere solutes. In addition, some results of the molar heat of transfer from H_2O to D_2O for the alcohols at 51°, and from H_2O to *t*-BuOH aqueous solutions at 2 and 60° are also reported and the interpretation of these measurement discussed in relation with what is expected for a hard-sphere solute.

Experimental Section

Chemicals. Reagent grade alcohols were refluxed over CaO and then fractionally distilled. The middle fraction was collected.

Nmr Measurements. Nmr spectra were obtained with a Varian A 60 spectrometer operating at 60 MHz and equipped with the V 6040 temperature controller. The chemical shift between the peak due to the water protons and a peak due to protons in the CH_3 group of the alcohols was measured. The CH_3 protons were used as an internal standard. It has been shown for *t*-BuOH aqueous solutions that similar results are obtained with an external standard as chloroform or an internal standard.[2]

Heat of Transfer. The calorimeter and procedure have already been described in detail.[3] The heat of solution of small quantities of liquid alcohol in H_2O, D_2O, or aqueous *t*-BuOH is measured at given temperatures and the heat of transfer deduced by difference.

Results

In Figure 1 the chemical shift (as ordinate) is plotted against alcohol molality (as abscissa) for different alcohols and temperatures. The temperature in general was controlled within ±2°. The reproducibility of measurements was within 0.5 Hz. Bars of error are shown in the plots. Figure 2 shows the plots of the enthalpy of transfer from light to heavy water for the different alcohols at 25 and 51°. Results at 25° are taken from the literature.[4] Figure 3 shows the plots of the heat of solution of *t*-BuOH solutions at 2 and 60° against the alcohol molality. Bars of error are shown in the figure.

Discussion

1. Nmr Measurements. Using an internal standard, we have found that at 0 and 40° the molal chemical shift caused by *t*-BuOH is respectively 2.5 and 0.8 Hz downfield. Corresponding numbers found in ref 2 are respectively 3.0 and 1.0 Hz using an external standard.

(1) M. Lucas, *J. Phys. Chem.*, **76**, 4030 (1972).
(2) R. G. Anderson and M. C. R. Symons, *Trans. Faraday Soc.*, **65**, 2550 (1969).
(3) M. Lucas, *Bull. Soc. Chim.*, 2902 (1970).
(4) G. C. Kresheck, H. Schneider, and H. A. Scheraga, *J. Phys. Chem.*, **69**, 3132 (1965).

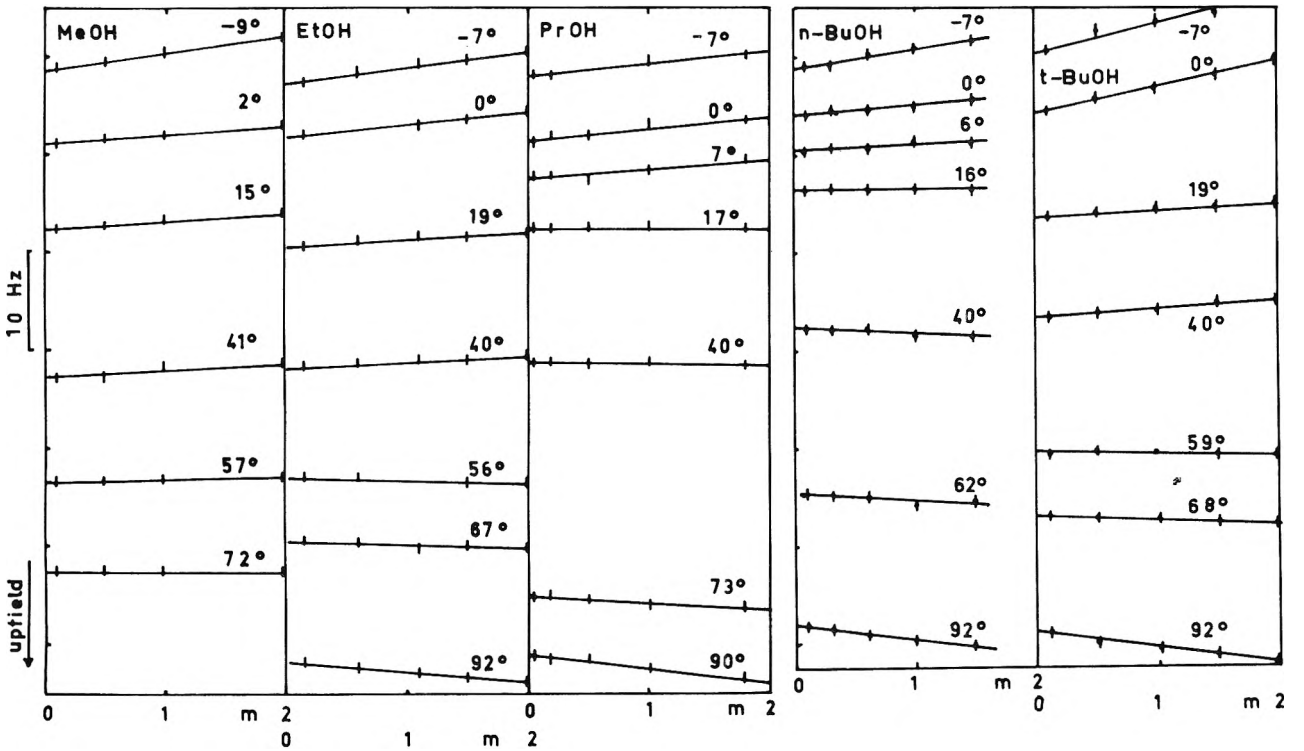

Figure 1. Plots of the chemical shift between the peak due to the water proton and a peak due to protons in the CH_3 groups against the alcohol molality.

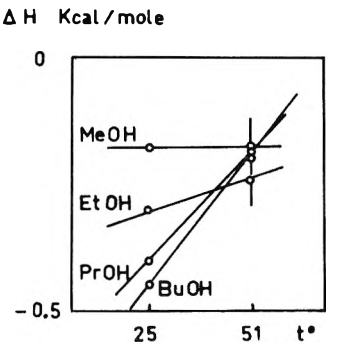

Figure 2. Plots of the enthalpy of transfer from H_2O to D_2O for the alcohols at 25 and 51°.

Another difficulty arises from the contribution of the alcohol hydroxyl proton to the peak due to water protons. The position is given by the mean of the individual water and alcohol resonances weighted with respect to the relative number of each type of protons. At −6° two separate proton resonances were observed in solutions for which the *t*-BuOH mole fraction is higher than 0.2, with a separation increasing slightly from 23 Hz at the mole fraction 0.6 to 26 Hz at the mole fraction 0.2, the water proton resonance lying to higher field. At 25° the separation is about 24 Hz for mole fraction between 0.6 and 0.3.[2] If a downfield shift from 30 to 60 Hz is assumed for the *t*-BuOH hydroxyl resonance at the lowest alcohol concentrations, then the *t*-BuOH contribution to the observed chemical shift should vary from 30 $m/110$ to 60 $m/110$ where m is the *t*-BuOH molality in the solution.

From a nmr study at 60 MHz of some ROH-D_2O mixtures, Cernicki has concluded that the resonances from *n*-PrOH and EtOH hydroxyl protons and HDO-H_2O protons do not coacervate until the alcohol mole fraction is lower than 0.1.[5] At 25° the separation decreases from 55 Hz at a 0.9 *n*-PrOH mole fraction to 30 Hz at a 0.1 *n*-

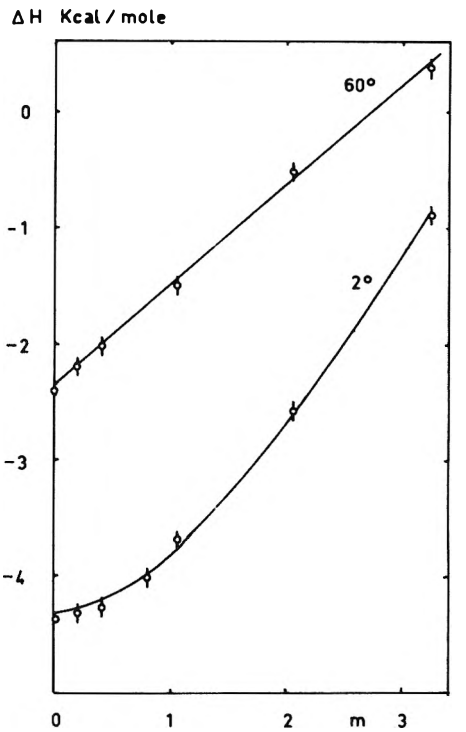

Figure 3. Plots of the enthalpy of solution for liquid *t*-BuOH at 60° and solid *t*-BuOH at 2° in aqueous *t*-BuOH solutions against the alcohol molality.

PrOH mole fraction in the PrOH-D_2O mixture, from 50 to 20 Hz for the corresponding EtOH-D_2O mixtures, and from 55 to 40 Hz when the *n*-BuOH mole fraction in the BuOH-D_2O solution decreases from 0.9 to 0.5. In addition, for the *t*-BuOH-D_2O mixture, the separation de-

(5) B. Cernicki, *Ber. Bunsenges. Phys. Chem.*, **69**, 57 (1965); **70**, 154 (1966).

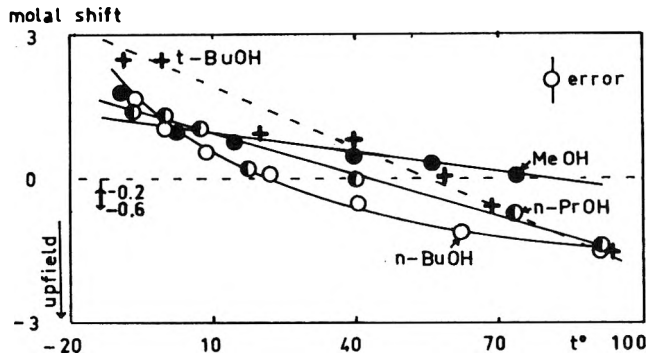

Figure 4. Plots of the alcohols molal chemical shift against the water temperature.

creases from 25 Hz at a 0.4 alcohol mole fraction to 22 Hz at a 0.2 mole fraction, thus being very similar to that found with *t*-BuOH–H_2O mixtures. In all cases the water proton resonance lies to higher fields. Therefore 60 $m/110$ is probably an upper limit for the alcohol hydroxyl proton contribution to the chemical shift measured in our study.

The results given in Figure 1 are summarized in Figure 4 which shows plots of the molal shift caused by alcohols at various temperatures. It is apparent that as the temperature is raised, the shifts downfield at low temperature become upfield at high temperatures. The shift for the water proton only should be more upfield than the shifts plotted in Figure 4, the difference being between 0.2 and 0.6 unit.

A difficulty of another sort arises from the interpretation of nmr measurements. An upfield shift is caused for water protons by addition of a structure breaker as CsI or by higher temperatures. Therefore if the addition of a solute to water at a given temperature causes the water shift to move upfield, this solute may be ascribed as a structure breaker. However, if one assumes that the H bond has some covalent character, then the direction of the shift (upfield with increasing solute concentration) can be explained by an increase in the covalent character in the presence of the solute with an accompanying increase in the proportion of organized water in the solution.[6] On the other hand, if an electrostatic model is assumed for the H bond, an upfield shift on solute addition must be interpreted as a decrease in the H bonding in the water, that is the solute is a structure breaker.

According to this model the plots in Figure 4 may be interpreted as showing the solutes acting as structure formers at low temperature and structure breakers at high temperature. It is difficult to interpret the results if the partially covalent model is assumed since it would then result that the alcohols are structure breakers at low temperature and structure formers at high temperatures, a conclusion difficult to accept.

It is possible to compare the influence of an alcohol on the water structure to that of corresponding hydrocarbons, as deduced from a water two-state model devised by Frank and Franks.[7] In this model water is represented as a two-species mixture of dense and bulky (fully hydrogen bonded) constituents. The dissolved hydrocarbon is represented as dissolving separately in these constituents as if they were two "phases." The mole fraction of the bulky and dense water species is f_0 and $1 - f_0$, respectively, and the fraction of the hydrocarbon in the bulky "phase" is g_0 and that in the dense "phase" is $1 - g_0$. Equation 7 in ref 7 provides a simple measure of the structure promoting or breaking produced by the hydrocarbon solute, as the difference between the two numbers g_0 and f_0. An interpretation of this equation is as follows: if the hydrocarbon is more soluble in the bulky "phase" than in the other, then the addition of the hydrocarbon to water shifts the equilibrium between the two water species toward the more hydrogen bonded. The variation of the two numbers with temperature and hydrocarbon size is given by eq 13 and 14 of ref 7. From Frank and Franks' data, we have computed the values of g_0 and f_0 in a small temperature range around 25°, assuming constant heat of transfer (since the heat capacity of transfer is not known). Plots of $g_0 - f_0$ are shown in Figure 5 for CH_4, C_2H_6, C_3H_8, and C_4H_{10}. The solute is considered a structure former when $g_0 - f_0$ is positive and a structure-breaker when $g_0 - f_0$ is negative. The plots show that the bigger the solute, the more it acts as a structure breaker above 27°. However, at low temperatures, all hydrocarbons are probably structure promoters.

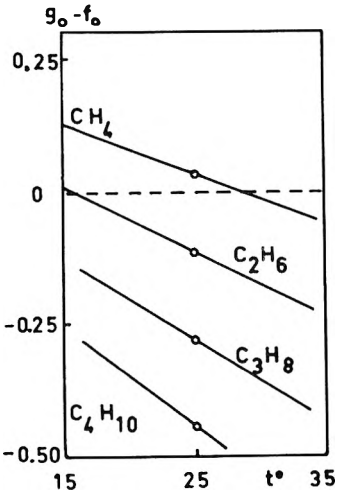

Figure 5. Plots of $g_0 - f_0$ for hydrocarbons in water against the water temperature.

The explicit conclusion of Frank and Franks is that a negative entropy of solution into water is not evidence of water structure promotion by the solute, but rather that water behaves differently from a nonpolar solvent. An implicit conclusion is that a high partial molar heat capacity for a solute is not evidence for water structure promotion by this solute since butane with a partial molar heat capacity of about 130 cal/mole °K is considered a structure breaker.[8] This needs to be outlined since a high heat capacity for Bu_4NBr in water is still considered by many workers as evidence of water structure promotion by this salt.

The comparison between Figures 4 and 5 shows that the influences of alcohols and hydrocarbons on the water structure is qualitatively similar in that an increase in temperature changes the alcohol behavior, being a structure former at low temperature and a structure breaker at high temperature. The temperatures at which the alcohols' structural influences change cannot be determined in view of the uncertainties in the molar chemical shifts and the contributions of alcohol hydroxyl protons to the shifts.

2. Heat of Transfer of the Alcohols from H_2O to D_2O. This type of measurements is often used as a probe for the structural influence of a solute on water.[9] According to

(6) J. Clifford and B. A. Pethica, *Trans. Faraday Soc.*, **60**, 1483 (1964).
(7) H. S. Frank and F. Franks, *J. Chem. Phys.*, **48**, 4746 (1968).
(8) T. J. Morrison, *J. Chem. Soc.*, 3814 (1952).
(9) C. V. Krishnan and H. L. Friedman, *J. Phys. Chem.*, **74**, 2356 (1970).

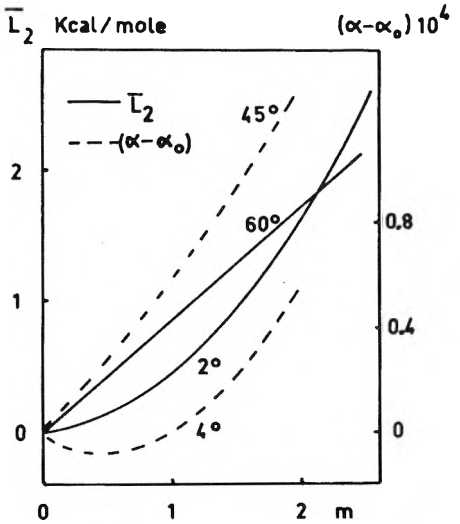

Figure 6. Plots of $\bar{L}$ for *t*-BuOH aqueous solutions against *t*-BuOH molality, and plots of the difference between the expansion coefficient of the solution and that of pure water.

Friedman's interpretation, negative values are taken as evidence for water structure promotion. Then the plots in Figure 2 may be interpreted as showing that at 25° the bigger the alcohol the more it behaves as a structure former. At 51°, all alcohols have the same influence on the water structure and possible at higher temperatures the alcohols with the larger alkyl chain could act as structure breakers.

However, a different interpretation is possible. Eley has derived the relation $\bar{\Delta U} = (\alpha T/\beta)\bar{V}_2$ between the molal internal energy of solution for a solute from the gas state, the solute molar volume $\bar{V}_2$ in solution, the expansion coefficient α, and the isothermal compressibility coefficient β of the pure solvent.[10]

Then the enthalpy of transfer for a hard-sphere solute from H_2O to D_2O should be

$$\Delta H_{(D_2O-H_2O)} = T\left\{\frac{\alpha D_2O}{\beta D_2O}V_2(D_2O) - \frac{\alpha H_2O}{\beta H_2O}V_2(H_2O)\right\}$$

Since βD_2O, βH_2O, and $V_2(H_2O)$, $V_2(D_2O)$ are probably not much different but αD_2O is much smaller than αH_2O at room temperature,[11] ΔH should be negative for a hard-sphere solute.

When the temperature is further raised the expansion coefficients for H_2O and D_2O are less different, so the enthalpy of transfer may become less negative. Then the sign of the experimental enthalpy of transfer should be only the consequence of the fact that alcohols behave somewhat as hard-sphere solutes, and it would not give any information on the structural properties of the solute.

3. Heat of Transfer of t-BuOH to Aqueous t-BuOH Solutions. The difference $\Delta H - \Delta H°$, where ΔH is the molar heat of solution of small amounts of liquid (or solid) *t*-BuOH in the aqueous *t*-BuOH solution of molality m and $\Delta H°$ the heat of solution in pure water, is plotted at two temperatures against m in Figure 6. $\Delta H - \Delta H°$ is also equal to the relative partial heat content $\bar{L}_2$. In the same figure is also plotted the difference $\alpha - \alpha°$ between the expansion coefficient α of the aqueous alcohol solution and $\alpha°$ the water expansion coefficient. Plots at 4° are deduced from the influence of the solute on the TMD (temperature of maximum density) of its solution.[12] Plots at 45° are deduced from a few measurements of the densities of aqueous *t*-BuOH solutions at 40 and 50° made in this

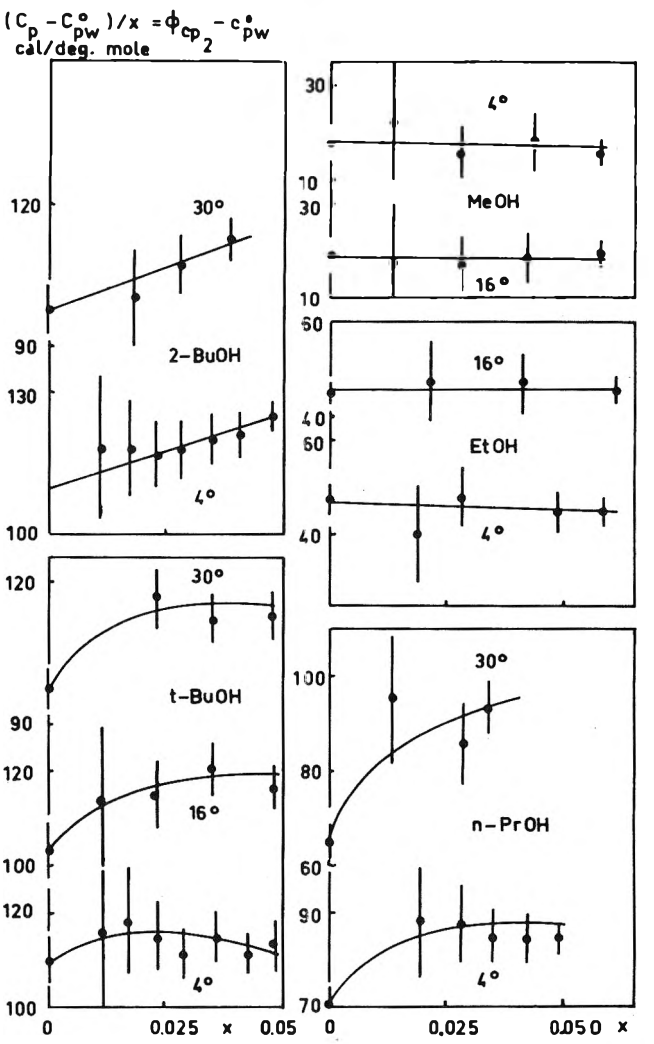

Figure 7. Plots of $\phi c_{p2} - C_{pw}°$ for various alcohols at various temperatures against the alcohol mole fraction in the solution.

laboratory. The initial negative variation of at 4° clearly shows the enhancement of the water structure by the addition of small quantities of *t*-BuOH. The further increase in $\alpha - \alpha°$ may possibly be ascribed to the increasing disruption of water structure as more alcohol is added to water. At 45° the steep increase of $\alpha - \alpha°$ as *t*-BuOH is added may possibly be ascribed to the fact that the alcohol enhances the water structure to a much smaller extent.

The interpretation of $\Delta H - \Delta H°$ for a hard-sphere solute is straightforward since we have shown that a close proportionality exists between $\Delta H - \Delta H°$ and $\alpha - \alpha°$.[13] (At 4° the relation between the two quantities is $\Delta H - \Delta H° = (\alpha - \alpha_0)T/\beta V_2$ where β and $\bar{V}_2$ are respectively the compressibility of the solution and the alcohol partial molal volume.) Then $\Delta H - \Delta H°$ should be positive at high temperature and negative at 4° for a hard-sphere solute in aqueous *t*-BuOH solutions. In addition, since at 4° a hard-sphere solute decreases the expansion coefficient of its solution with water,[1] it results that $\bar{L}_2$ for such a solute should be negative at high dilution. When the solute is not a hard-sphere solute but *t*-BuOH, the relation be-

(10) D. D. Eley, *Trans. Faraday Soc.*, **35**, 1281 (1939).
(11) D. Eisenberg and W. Kauzmann, "The Structure and Properties of Water," Oxford, Clarendon Press, 1969, p 187
(12) G. Wada and S. Umeda, *Bull. Chem. Soc. Jap.*, **35**, 646 (1962).
(13) (a) M. Lucas and A. Feillolay, *J. Phys. Chem.*, **75**, 2330 (1971); (b) A. Feillolay and M. Lucas, *ibid.*, **76**, 3068 (1972).

tween $\bar{L}_2$ and $\alpha - \alpha^\circ$ is not followed since $\bar{L}_2$ is slightly positive at 2° for low *t*-BuOH molalites, but $\bar{L}_2$ is smaller at 2° than at 60°.

The usual interpretation of a positive value for $\bar{L}_2$ is entirely different. The overlap of the more hydrogen-bonded water sphere around a structure-forming solute as its concentration is increased is interpreted as producing a positive contribution to $\bar{L}_2$.[14] Since all other effects on $\bar{L}_2$ are neglected, a positive $\bar{L}_2$ is taken as evidence for water structure promotion, by Bu_4NBr by instance. In our opinion too much importance is given to this particular contribution caused by the overlap of the hydration spheres. For instance, $\alpha - \alpha^\circ$ at 4° for aqueous *t*-BuOH solutions may be equated to $-\alpha_1 m + \alpha_2 m^2$ where $-\alpha_1 m$ may be interpreted as showing the solute influence on the expansion coefficient if no other interaction as solute–solute interaction, overlap of hydration sphere . . . is present. The term $\alpha_2 m^2$ incorporates all these effects. Then the contribution of the overlap to $\bar{L}_2$ should be at most proportional to $\alpha_2 m^2$, provided that other effects are absent. Although this contribution to $\bar{L}_2$ for a water structure former is certainly positive, it cannot be assumed in our opinion that a positive $\bar{L}_2$ is evidence for water structure promotion in view of all the other effects which may exist. In any case such an interpretation would lead to the conclusion that at low molalities *t*-BuOH is a strong structure former at 60°, a weak one at 2° and possibly a structure breaker at lower temperatures if a negative $\bar{L}_2$ is found as the extrapolation of data at 2 and 60° suggests. This conclusion is difficult to accept.

An interesting consequence of the variation of $\Delta H - \Delta H^\circ$ with the temperature is that the partial molal heat capacity of *t*-BuOH around 30° should at first increase with its molality and then should decrease when the molality is further increased.

Figure 7 shows the plots of $\phi c_{p2} - c_{pw}^0$ against the alcohol mole fraction in the aqueous solution at various temperatures for some alcohols, where ϕc_{p2} is the alcohol apparent molar heat capacity and c_{pw}^0 the pure water heat capacity. These plots are drawn from c_p data in the literature.[15] The values of $c_{p2}^0 - c_{pw}^0$ have been computed from Hill's data[16] and the liquid alcohols heat capacities.[17] For all alcohols except MeOH and EtOH these plots show a similar behavior for the variation of ϕc_{p2} with the concentration and support our findings for the variation of the *t*-BuOH partial molar heat capacity.

We do not interpret high solute heat capacity as evidence for water structure promotion by this solute, but rather as showing that the solute structural influence changes much with the temperature.[18] Then an increasing c_{p2} is in our opinion related to a change of the solution structure with the temperature more important than the pure water structural changes, since the solute is assumed to be a structure former at low temperature and a structure breaker at high temperature, at moderate concentration. A possibly similar idea is expressed by Frank: " . . . An appropriate heat capacity contribution must also be expected, arising from the transformation, with rising temperature, of bonded to non bonded species."[19]

(14) R. H. Wood, H. L. Anderson, J. D. Beck, J. R. France, W. E. de Vry, and L. J. Soltzberg, *J. Phys. Chem.*, **71**, 2149 (1967).
(15) W. S. Knight, doctoral dissertation, Princeton, 1962.
(16) D. M. Alexander and D. J. T. Hill, *Aust. J. Chem.*, **22**, 347 (1969).
(17) (a) Landolt-Bornstein, "Physikalische-chemische Tabellen," Vol. 2, Part 4, Julius Springer, Berlin, 1960. (b) F. L. Oetting, *J. Phys. Chem.*, **67**, 2757 (1963).
(18) M. Lucas and A. de Trobriand, *C. R. Acad. Sci., Ser. C*, **274**, 1361 (1972).
(19) H. S. Frank in "Water a Comprehensive Treatise," Vol. 1, F. Franks, Ed., Plenum Press, New York, N. Y., 1972, p 543.

Reactions of Hydrogen Atoms and Hydroxyl Radicals with Hydrogen Bromide

G. A. Takacs and G. P. Glass*

Department of Chemistry, Rice University, Houston, Texas 77001 *(Received October 10, 1972)*

Publication costs assisted by The Petroleum Research Fund

A fast discharge-flow system was used to study reactions of hydrogen atoms and hydroxyl radicals with hydrogen bromide at 295 K. The reactions were followed by monitoring the epr spectra of $H(^2S_{1/2})$, $Br(^2P_{3/2})$, and $OH(^2\pi_{3/2})$ at a number of different reaction times. A fluorinated halocarbon coating, applied to the flow tube, was found to be extremely effective in eliminating wall recombination of $Br(^2P_{3/2})$. Rate constants of $(3.4 \pm 0.8) \times 10^{-12}$ and $(5.1 \pm 1.0) \times 10^{-12}$ cm^3 molecule^{-1} sec^{-1} were obtained for the reactions $H + HBr \rightarrow H_2 + Br$ and $OH + HBr \rightarrow H_2O + Br$, respectively. An unsuccessful search was made for $Br(^2P_{1/2})$.

Introduction

Hydrogen bromide is known to inhibit combustion of hydrogen and hydrocarbon fuels. Numerous studies have demonstrated its effect on flame propagation, flamability, and explosion limits.[1-7] It is generally accepted that the inhibition results from reactions of HBr with chain centers which are important for flame propagation; for example, with H and OH. However, absolute rate constants for

(1) D. R. Clark, R. F. Simmons, and D. A. Smith, *Trans. Faraday Soc.*, **66**, 1423 (1970).

TABLE I: Reaction of Atomic Hydrogen with Hydrogen Bromide

$(HBr)_0$, $\times 10^{14}$ molecule cm^{-3}	$(H)_0$, $\times 10^{14}$ molecule cm^{-3}	Method of data reduction[b]	$(HBr)/(H)$[a]	k_1, cm^3 molecule^{-1} sec^{-1} $\times 10^{12}$
3.88	0.82	First-order H decay	62	2.94
2.75	0.79	First-order H decay	20	3.03
2.21	0.71	First-order H decay	11	3.39
1.78	0.68	First-order H decay	6	3.98
2.21	0.70	First-order H decay	10	3.20
2.21	0.71	Second-order from H decay		3.43
1.78	0.68	Second-order from H decay		4.08
2.21	0.70	Second-order from H decay		3.08
1.25	1.06	Second-order from Br growth		3.57
7.84	10.1	From $1/(H) - 1/(H)_0$		3.33
				Av = $3.4 \pm 0.4 \times 10^{-12}$ cm^3 molecule^{-1} sec^{-1}

[a] Ratio measured 3.3 cm downstream of HBr inlet at the first measuring point. [b] Explained fully in text.

these reactions are not well established. In this study we have measured them directly in a fast discharge-flow apparatus using epr detection.

Experimental Section

The construction and operation of the discharge-flow apparatus used in these experiments has been described in detail previously.[8,9] The 20-mm i.d. flow tube was operated at pressures from 0.5 to 1.5 Torr, and linear flow speeds were maintained in the range 1300–1900 cm/sec.

Atomic hydrogen was produced by microwave discharge of a dilute mixture of H_2 in Ar, and OH was generated from it by reaction with NO_2.[8] A moveable inlet system consisting of two concentric tubes, with the inner tube of 3 mm o.d. extending 2.25 cm beyond the end of the 6 mm o.d. outer tube, allowed the HBr to be added 2.25 cm downstream from the point of production of OH. HBr (Matheson 99.8%) was used without further purification. A liquid nitrogen trap was placed immediately upstream of the pump in order to collect Br_2 and unreacted HBr.

The epr signals were recorded with a Varian V4502 spectrometer. Absolute concentrations were determined from the integrated epr spectra.[8] Transition probabilities for all the observed free radicals have been reported.[10,11]

Results

The effect of the wall treatment of the flow tube on the rate of $Br(^2P_{3/2})$ atom recombination was studied first. Oxy acids, such as sulfuric and phosphoric acid, have been reported to be effective wall poisons.[12] However, other workers claim that measurable bromine atom recombination takes place on both Teflon and phosphoric acid wall coatings.[13] In our studies bromine atoms were produced by the reaction of atomic hydrogen with excess HBr. High reactant concentrations were used to ensure complete production of Br within 1 msec (typically $(H)_0 = 6 \times 10^{14}$ and $(HBr)_0 = 2 \times 10^{15}$ molecules cm^{-3}, thus reaction is 99% complete in less than 1 msec). Bromine atom recombination was studied over a reaction time of 20–25 msec.

Using a clean quartz flow tube, first-order decay of $Br(^2P_{3/2})$ was observed, and a rate constant of 465 sec^{-1} was measured. This corresponds to a surface recombination coefficient for $Br(^2P_{3/2})$ of $\gamma = 1.12 \times 10^{-2}$. When the flow tube was coated internally with ortho boric acid, γ was measured in two different experiments as 5.76×10^{-3} and 5.28×10^{-3}. Three experiments using phosphoric acid as the wall coating gave values of $\gamma = 2.0 \times 10^{-3}$, 2.3×10^{-3}, and 1.0×10^{-3}. Measurable surface recombination was completely eliminated, however, when the flow tube was coated with a fluorinated halocarbon wax,[14] and all further experiments reported in this paper were performed using a flow tube treated in this manner.

Reaction of H with HBr. Ten experiments were performed to determine the ratio of the concentration of $Br(^2P_{3/2})$ formed to the concentration of atomic hydrogen removed by reaction 1. These experiments were performed

$$H + HBr \rightarrow H_2 + Br \qquad (1)$$

at reaction times varying from 1.9 to 15.4 msec, and on a variety of different reaction mixtures. The ratio was measured as 0.91 ± 0.11.

The dynamics of the reaction were studied using the seven reaction mixtures listed in Table I. In order to obtain adequate spacial resolution for the fast reaction of H + HBr, the mixtures were chosen to have relatively low reactant concentrations. Unfortunately, this fact limited the range of mixture stoichiometries that could be investigated at adequate epr signal to noise ratios.

Experimental data were treated in three different ways. (a) When HBr was present in a large excess, the reaction was assumed to be first order, and the integrated rate expression

$$2.303 \log \left(\frac{H}{H_0}\right) = -k_1(HBr)t$$

was used. (HBr) was taken as the average HBr concentra-

(2) C. Powall and R. F. Simmons, *Symp. Combust. 13th*, 585 (1971).
(3) M. J. Day, D. V. Stamp, K. Thompson, and G. Dixon-Lewis, *Symp. Combust. 13th*, 705 (1971).
(4) R. N. Butlin and R. F. Simmons, *Combust. Flame*, **12**, 447 (1968).
(5) W. E. Wilson, Jr., J. T. O'Donovan, and R. M. Fristrom, *Symp. Combust. 12th*, 929 (1969).
(6) D. R. Blackmore, G. O'Donnell, and R. F. Simmons, *Symp. Combust. 10th*, 303 (1965).
(7) W. A. Rosser, H. Wise, and J. Miller, *Symp. Combust. 7th*, 175 (1959).
(8) J. E. Breen and G. P. Glass, *J. Chem. Phys.*, **52**, 1082 (1970).
(9) J. E. Breen and G. P. Glass, *Int. J. Chem. Kin.*, **3**, 145 (1970).
(10) A. A. Westenberg and N. deHaas, *J. Chem. Phys.*, **40**, 3087 (1964).
(11) A. A. Westenberg, *J. Chem. Phys.*, **43**, 1544 (1965).
(12) N. Vanderkool, Jr., and J. S. MacKenzie, *Advan. Chem. Ser.*, **No. 36**, 98 (1962).
(13) P. B. Davies, B. A. Thrush, and F. Tuck, *Trans. Faraday Soc.*, **66**, 886 (1970).
(14) MarChem Inc., Houston, Texas 77005.

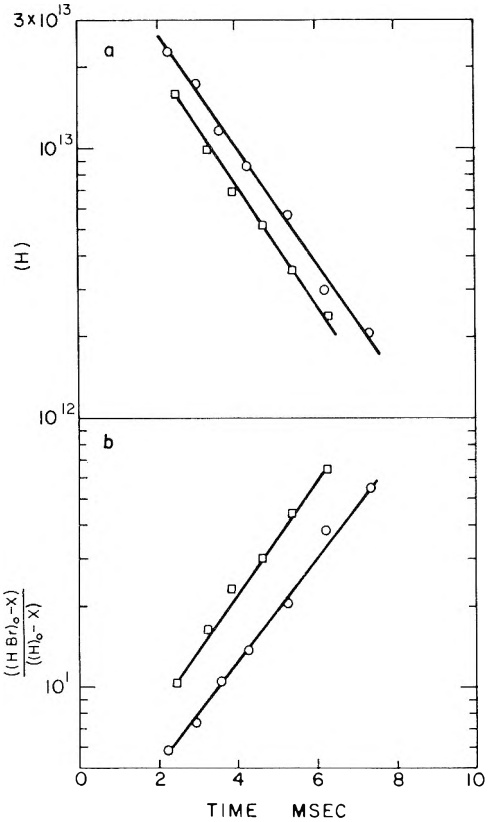

Figure 1. (a) Plot of log (H) *vs.* time for reaction of H + HBr. (b) Plot of log $[(HBr)_0 - (H)/(H)_0 - (H)]$ *vs.* time: O represents $(HBr)_0 = 1.78 \times 10^{14}$, $(H)_0 = 6.7 \times 10^{13}$ molecule/cm^3, flow speed = 1322 cm/sec; □ represents $(HBr)_0 = 2.21 \times 10^{14}$, $(H)_0 = 7.0 \times 10^{13}$ molecule/cm^3, flow speed 1270 cm/sec.

tion over the region in which the reaction was followed, and the reaction time, t, was calculated from the linear flow speed, and the distance from the HBr inlet to the center of the modulating coils of the epr cavity. Log (H) was plotted against t as shown in Figure 1a, and k_1 was calculated from the slope of the plot. (b) The second-order integrated rate equation

$$2.303 \log [(HBr)_0 - x/(H)_0 - x] = k_1[(HBr)_0 - (H)_0]t$$

was used to reduce data from several experiments. Here, x represents the concentration reacted at time t. x was computed from either H decay or the Br($^2P_{3/2}$) growth measurements, and plots of log $[(HBr)_0 - x/(H)_0 - x]$ *vs.* t were made as shown in Figure 1b. (c) When $(H)_0$ and $(HBr)_0$ are nearly equal, method a cannot be used and method b is inappropriate since any small errors in the measurement of $(H)_0$ and $(HBr)_0$ are greatly magnified in their difference term. Under these conditions the expression

$$[(H)^{-1} - (H)_0^{-1}] = kt$$

was used. The expression was derived by integrating the rate equation after setting (HBr) equal to (H). This procedure is strictly justified if $(H)_0 = (HBr)_0$, because the reaction stoichiometry is such that equal amounts of H and HBr react together.

Values of k_1 are listed in Table I. The reactant concentrations and the methods of data treatment for each mixture are also given.

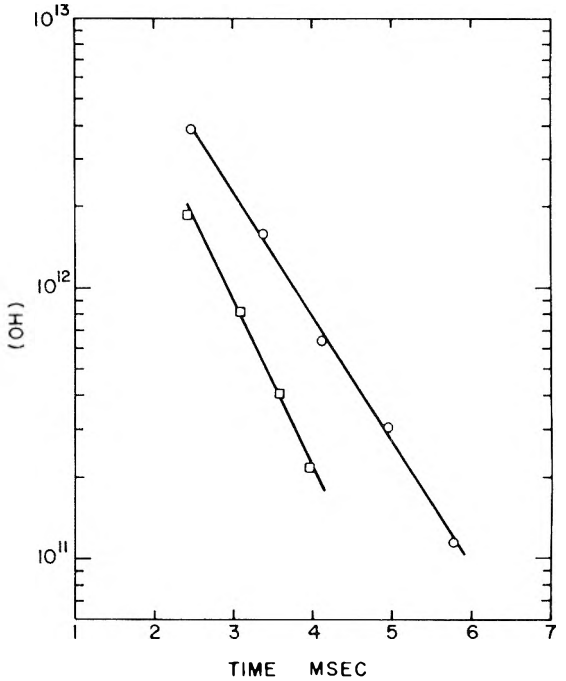

Figure 2. Plot of log (OH) *vs.* time in reaction of OH with HBr: O represents (HBr) = 1.35×10^{14} molecule/sec (in reaction zone; □ represents (HBr) = 2.51×10^{14} molecule/sec, flow speed = 1362 cm/sec.

Reaction of OH with HBr. This reaction was studied by adding HBr to the flow tube 2.25 cm downstream of the point at which OH was generated by reaction of atomic hydrogen with NO_2. The reaction was followed by monitoring the OH and Br($^2P_{3/2}$) concentrations as a function of distance downstream from the HBr inlet. Initial measurements were made at a point 2.5 cm (corresponding to a reaction time of 3.3 msec) downstream of the HBr inlet. At this point, the ratio of the concentration of unreacted HBr (given as $(HBr)_0 - (Br)$) to the measured OH concentration, varied from 34 to 183 in the seven mixtures studied. Thus, all measurements were made in the presence of a large excess of HBr.

The experimental results were analyzed in terms of the following mechanism

$$OH + HBr \rightarrow H_2O + Br \quad (2)$$

$$OH + OH \rightarrow H_2O + O \quad (3)$$

$$OH + O \rightarrow H + O_2 \quad (4)$$

$$OH \rightarrow \text{wall} \quad (5)$$

If reaction 2 is fast and HBr is present in large excess, OH is largely consumed by reaction 2, and, to a first approximation, the removal of OH is described by the equation

$$-d(OH)/dt = k_2(HBr)(OH)$$

which integrates to

$$\ln (OH)_1/(OH) = k_2(HBr)t$$

where $(OH)_1$ is the OH concentration at some arbitrary point chosen to represent $t = 0$.

In our experiments, HBr was present in large excess and this expression was used to determine approximate values for k_2. Log (OH) was plotted against t, and k_2 was calculated from the gradient. Figure 2 clearly shows that such plots remain linear for a variation in OH concentration of a factor of 20–30.

TABLE II: Rate Constants for the Reaction H + HBr → H_2 + Br

k, cm^3 molecule^{-1} sec^{-1}	k at 295 K, cm^3 molecule^{-1} sec^{-1}	Temperature of study, K	Method of study
$2.3 \times 10^{-10} \exp(-3100/RT)$[a]	1.06×10^{-13}	300–523	H_2–HBr photolysis[d]
$1.8 \times 10^{-10} \exp(-3700/RT)$[b]	3.24×10^{-13}	973–1673	Flame propagation[d,e]
$2.1 \times 10^{-11} \exp(-900/RT)$	4.50×10^{-12}	821–984	HBr–H_2 thermal reaction[f]
$1.0 \times 10^{-10} \exp(-2200/RT)$	2.40×10^{-12}	1150–1284	H_2–O_2 ignition[g]
$2.5 \times 10^{-11} \exp(-900/RT)$[c]	5.58×10^{-12}		H_2–Br_2 photolysis[h]
$1.0 \times 10^{-10} \exp(-2900/RT)$[c]	7.43×10^{-13}	500–1700	Critical review[i]
$8.7 \times 10^{-11} \exp(-2900/RT)$[c]	6.20×10^{-13}		Critical review[j]
	3.40×10^{-12}	295	This study

[a] Calculated from a ratio of rate constants, using the value of ref 20 for the reaction H + Br_2 → HBr + H. [b] Estimated by ref 20 from the kinetic data of ref 17. [c] Calculated from values for the reverse reaction together with the equilibrium constant. [d] Reference 16. [e] Reference 17. [f] Reference 18. [g] Reference 19. [h] An interpretation by B. A. Thrush, *Progr. React. Kinet.*, **3**, 88 (1965), of data reported by M. Bocenstein and W. Muller, *Z. Electrochem.*, **30**, 416 (1924); W. Jost, *Z. Phys. Chem.*, **B3**, 95 (1929). [i] Reference 20. [j] Reference 21.

A more sophisticated analysis was made using the computer program described in detail in an earlier paper.[9] This program fits the experimental data to data generated from a reaction scheme involving reactions 2–5. Known values of the rate constants k_3 and k_5 were introduced into the program, and the value of k_2 that gave the best fit between the experimental data and the predictions of the reaction scheme was computed.

In order to determine k_5, which has not been measured in a fluorinated halocarbon coated tube, several measurements were made of the rate of OH decay in the absence of HBr. These were analyzed in a manner identical with that described previously,[8] giving k_3 as $(1.50 \pm 0.40) \times 10^{-12}$ cm^3 $molecule^{-1}$ sec^{-1}, and k_5 as (62 ± 17) sec^{-1}. Using these rate constants k_2 was computed as $(5.1 \pm 1.0) \times 10^{-12}$ cm^3 $molecule^{-1}$ sec^{-1}.

In all of the above calculations, the HBr concentration was computed as $(HBr)_0 - (Br)$. This assumes the stoichiometry of reaction 2 to be as written. The following experiment was made to confirm this fact.

Excess HBr was added to atomic hydrogen, and the $Br(^2P_{3/2})$ signal was recorded 15 cm downstream. Then, NO_2 was added to the system at the HBr inlet. $Br(^2P_{3/2})$ was again recorded, and its concentration compared to that produced in the absence of NO_2. Five experiments were performed and the ratio of $Br(^2P_{3/2})$ formed from reactions of OH, to that formed in reaction 1, was measured as 0.90 ± 0.14. In these experiments, sufficient NO_2 was added to ensure that between 76 and 90% of the atomic hydrogen was converted to OH before reaction with HBr.[15] Corrections were made for that atomic hydrogen that reacted with HBr even in the presence of NO_2, and to account for the small amount of OH (less than 10%) that reacted *via* reactions 3–5.

An unsuccessful search was made for $Br(^2P_{1/2})$ in both reactions 1 and 2. The sensitivity of the apparatus was such that its presence would have been detected if its concentration had been greater than 4–5% of that of $Br(^2P_{3/2})$.

Discussion

In this study, the rate constant for the reaction of atomic hydrogen with hydrogen bromide has been estimated from measurements of hydrogen atom decay, and from measurements of bromide atom growth. Three methods of data reduction have been used. Since the values of k_1 obtained from first-order H decay do not depend on concentrations determined using integrated epr signals, and since values obtained from plots of $1/(H) - 1(H)_0$ against reaction time depend solely on absolute epr measurements, the constancy of the various estimates allows some confidence to be placed in the measured value of $3.4 \pm 0.4 \times 10^{-12}$ cm^3 $molecule^{-1}$ sec^{-1}. The value of the standard deviation is, however, smaller than the estimated calibration uncertainties. These arise mainly from an oversimplified view of the gas flow, and from uncertainties in flow-rate measurements, and amount to ±25%.

There have been a number of previous attempts to determine the rate constant for the reaction of hydrogen atoms with HBr.[16-21] All of these determinations have either inferred the rate of reaction 1 from measurements on the reverse reaction, or have estimated k_1 relative to some other reaction rate (usually H + Br_2 → HBr + Br). No direct measurements have been made. Values of k_1 that have been reported are listed in Table II, and, at 295 K, range from 1.06×10^{-13} to 4.50×10^{-12} cm^3 $molecule^{-1}$ sec^{-1}. At this temperature our measurements are in best agreement with those of Steiner[18] or Steiner and Ringrose,[19] but if our data are combined with previous high-temperature measurements,[16-20] an activation energy of 1.2–2.0 kcal/mol is obtained.

The production of $Br(^2P_{1/2})$ in the reaction of atomic hydrogen with HBr was first observed by Polanyi and coworkers[22,23] in 1966, and a very recent measurement indicates that its formation rate is 8% of that of $Br(^2P_{3/2})$.[24] In this study, nearly quantitative conversion (91 ± 11%) of H to $Br(^2P_{3/2})$ was observed, and no $Br(^2P_{1/2})$ was detected. However, these observations do not preclude its formation, since physical quenching of $Br(^2P_{1/2})$ could have preceded our measurements. Rate constants for quenching of $Br(^2P_{1/2})$ by Ar, HBr, and H_2 are known,[25] and are too small to produce effective quenching of $Br(^2P_{1/2})$ in our system. However, quenching by atomic

(15) The rate constant for H + NO_2 → OH + NO was taken as 4.8×10^{-11} cm^3 $molecule^{-1}$ sec^{-1} as measured by L. F. Phillips and H. I. Schiff, *J. Chem. Phys.*, **37**, 1233 (1962).
(16) R. A. Fass, *J. Phys. Chem.*, **74**, 984 (1970).
(17) S. D. Cooley and R. C. Anderson, *Ind. Eng. Chem.*, **44**, 1402 (1952).
(18) H. Steiner, *Proc. Roy. Soc., Ser. A*, **173**, 531 (1939).
(19) G. B. Steiner and G. H. Ringrose, *J. Chem. Phys.*, **43**, 4129 (1965).
(20) A. F. Trotman-Dickenson and G. S. Milne, "Tables of Bimolecular Gas Reactions," NSRDS-NBS 9, U. S. Government Printing Office, Washington, D. C., 1967.
(21) A. A. Westenberg and R. M. Fristrom, "Flame Structure," McGraw-Hill, New York, N. Y., 1965, p 358.
(22) J. R. Airey, P. D. Pacey, and J. C. Polanyi, *Symp. Combust. 11th*, 85 (1967).
(23) J. C. Polanyi, *Chem. Brit.*, 15 (1966).
(24) P. B. Davies, B. A. Thrush, A. J. Stone, and F. D. Wayne, *Chem. Phys. Lett.*, submitted for publication.

TABLE III: Reaction of OH with Hydrogen Bromide

$(Ar)_0$, 10^{14} molecules cm^{-3}	$(H_2)_0$, 10^{14} molecules cm^{-3}	$(NO_2)_0$, 10^{14} molecules cm^{-3}	$(HBr)_0$, 10^{14} molecules cm^{-3}	$(H)_0$, 10^{14} molecules cm^{-3}	% H removed by NO_2	$(OH)_1$,[a] 10^{13} molecules cm^{-3}	$(Br)_1$,[a] 10^{13} molecules cm^{-3}	k_2[b] First-order plot	k_2[b] From computer
236	2.36	4.81	3.22	4.28	74	2.82	18.7	7.2	6.9
223	2.23	8.90	2.96	4.65	Excess NO_2	3.71	11.3	6.9	6.0
231	2.62	5.80	3.98	4.98	92	3.68	18.4	6.0	5.2
271	0.42	2.90	3.42	1.05	Excess NO_2	1.48	3.54	4.4	3.8
271	0.42	4.14	3.01	0.99	Excess NO_2	1.43	4.24	4.6	4.1
254	0.74	1.98	2.47	1.31	96	2.68	6.35	5.6	5.1
247	0.72	1.92	3.14	1.31	95	2.52	6.16	5.6	4.8
							Av value of k_2	(5.7 ± 0.9)	(5.1 ± 1.0)

[a] Measured 3.3 cm downstream from HBr inlet at the first measuring point. [b] Units of 10^{-12} cm^3 $molecule^{-1}$ sec^{-1}.

hydrogen or wall quenching could have taken place. Atomic hydrogen is known to quench $Cl(^2P_{1/2})$ with unit collisional efficiency,[25] and $I(^2P_{1/2})$ is effectively removed at the walls.[26]

A rate constant of $(5.1 \pm 1.0) \times 10^{-12}$ cm^3 $molecule^{-1}$ sec^{-1} was obtained for reaction 2 from computer analysis of the reaction of hydroxyl radicals with HBr. This number is similar to the average value (5.7×10^{-12}) obtained from plots of log (OH) *vs.* reaction time. Since this latter procedure neglected any contribution from reactions 2-5, the closeness of the two values indicates that these reactions are not very important in determining the rate of removal of OH. This conclusion can be confirmed using known values for k_3 and k_5[27,28] and data from Table III, since it can be estimated that, under the conditions of this study, reaction 2 is always 20 times faster than reaction 5, and 100 times faster than reaction 3. Thus, the present disagreement concerning k_3[8,27,28] does not influence the value measured for k_2.

Only one previous measurement has been made of the rate of reaction 2. From a study of flame inhibition by halogen compounds, Wilson, *et al.*,[29] have estimated k_2 as 2.65×10^{-11} cm^3 $molecule^{-1}$ sec^{-1} at 1875–1975 K. Combining this rate constant with our value at 295 K, k_2 can be estimated as $(3.7 \pm 0.7) \times 10^{-11} \exp\{-(1.15 \pm 0.14)/RT\}$ cm^3 $molecule^{-1}$ sec^{-1}, where the activation energy is expressed in kcal/mole.

Good agreement was obtained between the measured stoichiometry and that predicted for reaction 2. In this system all atomic bromine is expected to be present as $Br(^2P_{3/2})$, since any $Br(^2P_{1/2})$ formed would be rapidly quenched to $Br(^2P_{3/2})$ by collision with NO,[25] which is produced in the initial reaction generating OH, namely, $H + NO_2 \rightarrow OH + NO$.

The value measured for k_3 is higher than that previously reported from this laboratory,[8] although the error bounds placed on the two measurements almost overlap. The reason for this discrepancy is not clear. The present measurement was made using an entirely new apparatus, and a different wall coating, but the experimental procedure used was identical with that described previously. The only significant difference between the measurements was that in the present study OH was followed over a reaction time of 18 msec, while in the previous study, it was followed for only 6–7 msec. At this point, it is worth noting that only a small change in the experimental data is needed to produce a sizeable simultaneous change in k_3 and k_5, since the effects of an increase in k_3 can be largely offset by a decrease in k_5. The new value agrees closely with that measured by Kaufman.[27]

The work presented in this paper was greatly facilitated by the use of the fluorinated halocarbon wall coating. The inertness of this coating to halogen atom recombination allowed reaction stoichiometries to be measured, rate constants to be estimated from measurements of bromine atom concentrations, and the HBr concentration to be calculated at any reaction time using the expression $(HBr) = (HBr)_0 - (Br)$.

Acknowledgments. Acknowledgment is made to the Donors of The Petroleum Research Fund, administered by the American Chemical Society, for the support of this research. The authors would like to thank the Robert A. Welch Foundation of Houston, Texas, for the use of the epr spectrometer, and thank Dr. L. T. Cupitt for assisting in the early work with wall coatings.

(25) R. J. Donovan and D. Husain, *Chem. Rev.*, **70**, 509 (1970).
(26) D. Husain and J. R. Wiensenfeld, *Trans. Faraday Soc.*, **63**, 1349 (1967).
(27) F. Kaufman, *Ann. Geophys.*, **20**, 106 (1964).
(28) (a) A. A. Westenberg and N. deHaas, *J. Chem. Phys.*, **43**, 1550 (1965); (b) G. Dixon-Lewis, W. E. Wilson, and A. A. Westenberg, *ibid.*, **44**, 2877 (1966).
(29) W. E. Wilson, Jr., J. T. O'Donovan, and R. M. Fristrom, *Symp. Combust. 12th*, 929 (1969).

Matrix Reactions of Cesium Atoms with Oxygen Molecules. Infrared Spectrum and Vibrational Analysis of $Cs^+O_2^-$. Infrared Observation of $Cs^+O_2^{2-}Cs^+$ and $Cs^+O_4^-$. Theoretical Structure Elucidation of $M^+O_4^-$

Lester Andrews,* Jenn-Tai Hwang, and Carl Trindle

Department of Chemistry, University of Virginia, Charlottesville, Virginia 22901 *(Received December 29, 1972)*

The simultaneous matrix deposition of cesium atoms and oxygen molecules at high dilution in argon produced infrared absorptions at 1115, 268, and 236 cm^{-1} which are respectively assigned to ν_1, ν_3, and ν_2 of the $Cs^+O_2^-$ species. The use of isotopic mixtures confirmed these assignments and the isosceles triangular structure for $Cs^+O_2^-$. The most intense mode of $Cs^+O_2^{2-}Cs^+$ was observed at 357 cm^{-1}. A strong band at 1002 cm^{-1} showed isotopic splittings for a species containing two O_2 molecules which is assigned to the cesium disuperoxide species $Cs^+O_4^-$. CNINDO calculations were done to investigate possible O_4^- geometries and M^+ position in the $M^+O_4^-$ molecular system.

Introduction

The products of reactions of alkali metal atoms with oxygen molecules have been studied in our laboratory over the past 5 years beginning with the infrared observation of LiO_2 and LiO_2Li.[1,2] Spectra of the mixed oxygen isotopic species indicated equivalent oxygen atoms and the symmetrical structures C_{2v} and D_{2h}, respectively, for LiO_2 and LiO_2Li. The O–O mode for LiO_2 occurred in the O_2^- frequency region suggesting an electronic distribution $Li^+O_2^-$ for the lithium superoxide molecule. Following this example, the lithium peroxide molecule was suggested to exist predominantly as $Li^+O_2^{2-}Li^+$.

Analogous superoxide and peroxide species have been produced and studied for Na, K, and Rb.[3,4] In addition, a new molecule, the disuperoxide species of formula MO_4, was observed for the latter three alkali metals.[4] Spectra for the MO_4 species suggested two equivalent O_2 units with equivalent oxygen atoms in each unit and a single alkali atom;[4,5] accordingly, a D_{2d} structure for the alkali disuperoxide was proposed. In a very recent letter reporting absorptions for CsO_4, Jacox and Milligan[6] suggested a *trans*-O_4^- structure in a molecule $Cs^+O_4^-$ without considering the cation position with respect to O_4^-. Also pertinent, a recent Raman investigation[7] of Cs–O_2 matrix reactions attributed intense bands at 287 and 269 cm^{-1} to the alkali disuperoxide species.

Here follows a detailed infrared study of cesium atom–oxygen molecule matrix reactions. Absorptions of CsO_2Cs and CsO_4 were observed along with the complete vibrational spectrum of CsO_2 which allows a vibrational analysis to be done for the CsO_2 molecule. CNINDO calculations were performed on the $M^+O_4^-$ system searching for the structure which best fits the isotopic frequency and reaction mechanism data.

Experimental Section

The cryogenic refrigeration system, vacuum vessel, and alkali metal atom source have been described earlier.[4] Oxygen gas (Air Products, therapy), isotopic oxygen samples 55% and 99% ^{18}O-enriched (Miles Laboratories), and argon 99.999% (Air Products) were used without purification. A cesium atom beam was provided by the reaction of lithium metal (O.R.N.L.) and cesium chloride (Fisher) in the Knudsen cell maintained at 320°. Analogous rubidium experiments utilized rubidium chloride (Fairmont) heated with lithium to 290°.

Samples of oxygen in argon (Ar/O_2 = M/R = 100) were simultaneously deposited at 15°K with an atomic beam of cesium for 12–24 hr. Infrared spectra were recorded during and after sample deposition on a Beckman IR-12 filter-grating infrared spectrophotometer in the 200–2000-cm^{-1} spectral region. High-resolution spectra were recorded using 8 or 3.2 cm^{-1}/min scanning speeds and 20 cm^{-1}/in. scale expansions. Additional high-resolution spectra were recorded following temperature cycling of the sample to 36°K. Frequencies were measured to the nearest 0.1 cm^{-1}; however, wave number accuracy was ±0.5 cm^{-1}. Spectral slit widths were 2.7 cm^{-1} at 250 cm^{-1}, 2.3 cm^{-1} at 350 cm^{-1}, and 0.9 cm^{-1} at 1100 cm^{-1}.

Results

Cesium Atoms with Oxygen. Several experiments were run depositing cesium atoms from the lithium metal–CsCl source with argon–oxygen samples in order to determine the best conditions to maximize the yield of product absorptions. Operation of the Knudsen cell containing the lithium metal–CsCl charge at 315–320° gave product yields comparable to those in elemental K and Rb experiments using a metal vapor pressure of 1 μ.[4] No feature was observed at 699 cm^{-1} where the most intense LiO_2 band was observed; the lithium vapor pressure in these experiments is a factor of 2000 lower than that used for lithium atom reactions.[2] The spectrum from one of these runs using Ar/O_2 = 100 is depicted at the top of Figure 1; the frequencies are listed in Table I. Of foremost importance are five groups of bands near 1100, 1000, 350, 260, and 230 cm^{-1}. In the first group, sharp, weak bands were observed at 1115.6 and 1103.8 cm^{-1}. The second group contained a band at 1002.5 cm^{-1} (5 cm^{-1} half-width), a weak intermediate feature at 976.5 cm^{-1} (0.05 OD), and a

(1) L. Andrews, *J. Amer. Chem. Soc.*, **90**, 7368 (1968).
(2) L. Andrews, *J. Chem. Phys.*, **50**, 4288 (1969).
(3) L. Andrews, *J. Phys. Chem.*, **73**, 3922 (1969).
(4) L. Andrews, *J. Chem. Phys.*, **54**, 4935 (1971).
(5) R. R. Smardzewski and L. Andrews, *J. Chem. Phys.*, **57**, 1327 (1972).
(6) M. E. Jacox and D. E. Milligan, *Chem. Phys. Lett.*, **14**, 518 (1972).

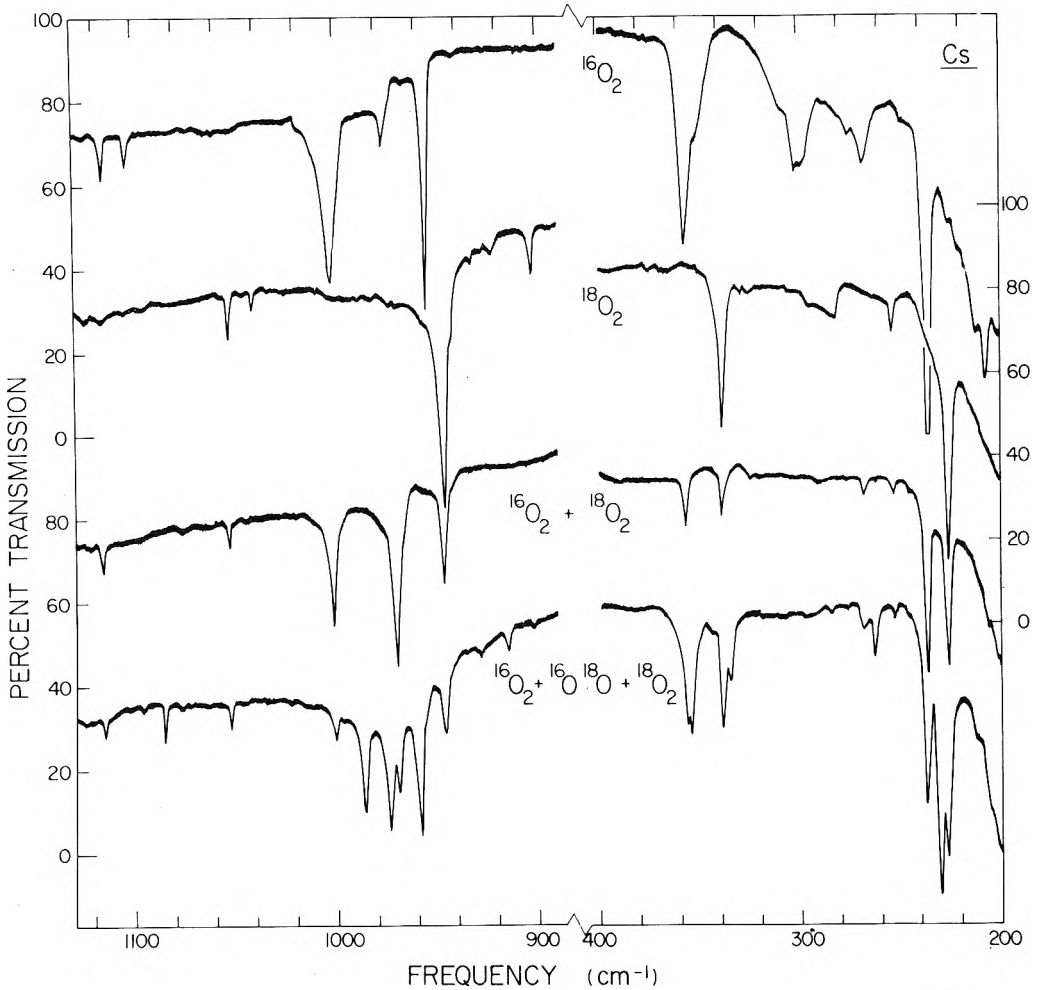

Figure 1. Infrared spectra of the products of cesium atom–oxygen molecule argon matrix reactions, $Ar/O_2 = 100$, deposition of cesium atoms from CsCl(s)/Li(l) reaction, window temperature 15°K.

very sharp band at 954.5 cm^{-1} (1.5 cm^{-1} half-width). The third spectral feature of interest appeared at 357.0 cm^{-1} with a shoulder near 348 cm^{-1}. A weak, sharp band appeared at 268.6 cm^{-1} which had a rubidium counterpart[4] at 282 cm^{-1}. The major feature in the spectrum was observed as a very intense absorption at 236.5 cm^{-1}; this feature was totally absorbing at the end of the sample deposition period.

A similar experiment using a sample with $Ar/O_2 = 200$ produced identical bands, including the sharp, weak features at 1115.8 and 1103.8 cm^{-1}; however, two small differences are worth noting. The very sharp 954.5-cm^{-1} band (0.48 OD) was relatively more intense than the 1102.3-cm^{-1} band (0.14 OD). Instead of a shoulder on the low-frequency side, the 356.8-cm^{-1} band (0.30 OD) had a well-resolved partner at 347.0 cm^{-1} (0.22 OD). This behavior is due to environmental effects owing to different trapping sites in the matrix or perturbations due to nearby molecules. Similar effects were observed for the rubidium counterparts of these absorptions.[4]

The second trace in Figure 1 and the second column in Table I illustrate the effect of $^{18}O_2$ substitution on these new cesium–oxygen species. The first two weak, sharp bands exhibit oxygen isotopic shifts of approximately 63 cm^{-1} to 1052.5 and 1041.5 cm^{-1}. The next two intense features shifted 56 and 52 cm^{-1}, respectively, to 946.5 and 902.5 cm^{-1}. The third band of interest exhibited an 18 cm^{-1} $^{18}O_2$ shift to 339.0 cm^{-1}, while the weak sharp band at 268.6 cm^{-1} shifted 14.6 cm^{-1} and the very intense 236.5-cm^{-1} band was displaced 10.5 cm^{-1} to 226.0 cm^{-1}.

Isotopic mixtures are helpful for revealing the composition of the absorbing species. The third position in the figure and table depict the spectra for an equimolar mixture of $^{16}O_2$ and $^{18}O_2$. All bands were observed, in excellent agreement with measurements made in the $^{16}O_2$ and $^{18}O_2$ isotopic experiments separately. The only new feature appeared as an intense band at 970.2 cm^{-1} having double the intensity of the isotopic counterparts at 1002.0 and 946.5 cm^{-1}. In this experiment, the cesium atom concentration was reduced. Note that the bands near 1000 and 250 cm^{-1} were of comparable intensities whereas the 357–339-cm^{-1} doublet was markedly reduced in intensity, relative to previous experiments.

Finally, a scrambled isotopic sample containing 20% $^{16}O_2$, 50% $^{16}O^{18}O$, and 30% $^{18}O_2$ was reacted with cesium atoms. The product absorptions are contrasted in Figure 1 and Table I with the other isotopic samples. The first group of absorptions was observed as a sharp triplet with bands at 1115.8, 1084.8, and 1052.6 cm^{-1}. It should be noted that this spectral region was scanned at 3.2 cm^{-1}/min; this slow speed was necessary to produce the best spectrum. Counterparts to the 1103.8-cm^{-1} feature were not detected. The feature near 1000 cm^{-1} was split into a sextet of bands; no counterpart of the sharp 954.5-cm^{-1} band was observed. A partially resolved triplet was observed at 356.5, 354.5, and 338.8 cm^{-1}. Presumably the

TABLE I: Absorptions (cm^{-1}) Observed Following Cesium Atom Matrix Reactions with Four Isotopic Oxygen Samples. Optical Densities Given in Parentheses

$^{16}O_2$	$^{18}O_2$	$^{16}O_2 + {}^{18}O_2$	$^{16}O_2 + {}^{16}O^{18}O + {}^{18}O_2$	Sample warming[a]	Identification
1115.6(0.07)		1115.7(0.03)	1115.8(0.02)	dec	$Cs^{16}O_2$
			1084.8(0.05)	dec	$Cs^{16}O^{18}O$
	1052.5(0.06)	1052.3(0.03)	1052.6(0.03)	dec	$Cs^{18}O_2$
1103.8(0.04)				con	$(Cs^{16}O_2)_2$
	1041.5(0.02)			con	$(Cs^{18}O_2)_2$
1002.5(0.31)		1002.0(0.17)	1002.3(0.04)	inc	$Cs(^{16}O_2)_2$
			987.7(0.15)	inc	$Cs^{16}O^{18}O^{16}O_2$
			975.2(0.19)	inc	$Cs(^{16}O^{18}O)_2$
		970.2(0.30)	970.6(0.10)	inc	$Cs^{16}O_2{}^{18}O_2$
			960.0(0.22)	inc	$Cs^{16}O^{18}O^{18}O_2$
	946.5(0.72)	946.5(0.14)	946.8(0.07)	inc	$Cs(^{18}O_2)_2$
954.5(0.53)				dec	i-$Cs(^{16}O_2)_2$
	902.5(0.05)			dec	i-$Cs(^{18}O_2)_2$
357.0(0.32)		356.8(0.05)	356.5(0.12)	dec	$Cs^{16}O_2Cs$
			354.5(0.14)	dec	$Cs^{16}O^{18}OCs$
	339.0(0.28)	338.8(0.05)	338.8(0.13)	dec	$Cs^{18}O_2Cs$
299(0.10)					
	283(0.04)		289	con	
268.6(0.05)		268.6(0.02)	268.4(0.02)	dec	$Cs^{16}O_2$
			262.8(0.05)	dec	$Cs^{16}O^{18}O$
	254.0(0.05)	253.7(0.02)	253.3(0.02)	dec	$Cs^{18}O_2$
236.5(1.0)		236.5(0.24)	236.4(0.24)	dec	$Cs^{16}O_2$
			229.6(0.47)	dec	$Cs^{16}O^{18}O$
	226.0(0.67)	226.0(0.21)	225.9(0.32)	dec	$Cs^{18}O_2$
207.5(0.30)				inc	$(Cs^{16}O_2)_2$

[a] Sample warming behavior: decreases, dec; constant, con; increases, inc.

335-cm^{-1} shoulder was due to a site effect analogous to that reported for the 357-cm^{-1} band. The lower two bands of interest produced well resolved triplets with intense central components which were not observed in the other isotopic experiments. These frequencies are recorded in Table I.

Sample warming operations were conducted on these isotopic samples. Spectra following temperature cycling to 36–37°K and recooling to 15°K were compared to spectra of the final sample before the warm-up. The changes in intensity due to this operation are noted in Table I for each group of bands. The behavior of the first group of sharp, weak bands was the most difficult to discern since the warming operation increases light scattering causing poorer spectral conditions, particularly in the higher frequency spectral region. Nevertheless, the spectra showed a decrease in intensity for the 1115.6-cm^{-1} feature and its isotopic counterparts, whereas the 1103.8-cm^{-1} feature remained approximately constant. The sample annealing had markedly contrasting effects on the 1002- and 955-cm^{-1} bands; the former grew strongly whereas the latter almost disappeared. Sample warming decreased the intensities of the remaining bands of interest; sample warming effects are noted in Table I.

Rubidium Atoms with Oxygen. In order to compare reactions of alkali metal atoms produced by chemical reaction with alkali metal atoms evaporated from the pure element, one experiment was performed using a lithium metal–RbCl charge in the Knudsen cell. The principal features of the spectrum agree with those reported earlier.[4] Very intense sharp bands were observed at 991.6 and 954.3 cm^{-1}. The intense 389.0-cm^{-1} band exhibited weak splittings at 385 and 381 cm^{-1}. The 254.8- and 219.8-cm^{-1} bands were prominent as in the earlier experiments. The 282.3-cm^{-1} feature appeared here as a sharp weak band.

Two new features appeared as weak, sharp bands at 1111.3 cm^{-1} (0.04 OD) and 1101.5 cm^{-1} (0.03 OD). Similar weak features were observed in the previous experiments, but these bands were not reported.[4] A reexamination of the previous Rb + $^{18}O_2$ experiment revealed weak bands at 1040 and 267.5 cm^{-1}. Likewise, the latter band appeared as a weak triplet at 283, 277, and 268 cm^{-1} in the previous Rb + $^{16,18}O_2$ experiment.[4]

Sample warming to 38°K had an analogous effect on the absorptions produced by rubidium atom reactions as those discussed above for cesium. The sharp 1111.3-cm^{-1} feature decreased while the 1101.5-cm^{-1} band remained constant.

Discussion

The first task at hand is to identify the new molecular species and characterize the vibrational modes which produce the observed spectrum. Vibrational analysis of the CsO_2 species is presented followed by CNINDO calculations for a geometry search for the $M^+O_4^-$ species.

$Cs^+O_2^-$. The infrared spectrum of lithium superoxide[2] showed three absorptions, a weak sharp feature near 1100 cm^{-1} which was assigned to the superoxide stretch and very strong bands near 700 and 500 cm^{-1}, respectively, which were assigned to symmetric and antisymmetric interionic Li^+-O_2^- modes. Although the infrared spectra of $Na^+O_2^-$ and $K^+O_2^-$ failed to produce bands near 1100 cm^{-1} in the infrared, Raman bands were observed at 1094 and 1108 cm^{-1}, respectively. Accordingly, the weak, sharp infrared bands at 1115.6 and 1103.8 cm^{-1} must be considered for assignment to the superoxide fundamental in $Cs^-O_2^-$.

The large oxygen isotopic shifts clearly show that the 1115.6- and 1103.8-cm^{-1} features are essentially pure O–O stretching vibrations. The 1115.6-cm^{-1} feature and its isotopic counterparts are observed in two mixed oxygen isotopic experiments which indicate the presence of two equivalent oxygen atoms. Counterparts of the 1103.8-cm^{-1} feature were not observed in the mixed isotopic runs suggesting that this absorption might arise from a dimeric species whose isotopic intensities would be correspondingly weaker. Although it is difficult to determine whether the fate of a weak sharp band upon sample warming is due to chemical reaction or to poorer spectral conditions, the sharp 1115.6-cm^{-1} band does decrease upon sample warming while the 1103.8-cm^{-1} feature remains, further suggesting that 1115.6 cm^{-1} is due to monomeric $Cs^+O_2^-$ while 1103.6 cm^{-1} arises from the corresponding dimer. The Raman spectrum of Cs plus O_2 argon matrix reactions provides the conclusive data.[7] This spectral region showed one sharp Raman band of moderate intensity at 1114 ± 1 cm^{-1} which is in agreement with the 1115.6 ± 0.5-cm^{-1} infrared band reported here. Hence, the sharp, weak 1115.6-cm^{-1} band and its oxygen isotopic counterparts are assigned to the superoxide fundamental ν_1, in monomeric $Cs^+O_2^-$; it is suggested that the 1103.6-cm^{-1} band is due to dimeric $Cs^+O_2^-$.

The rubidium atom–oxygen molecule reactions produce an analogous set of bands at 1111.3 and 1101.5 cm^{-1}. Although the isotopic data are less complete, the sample warming operations suggest assignments analogous to those above for $Cs^+O_2^-$. The Raman spectrum[7] of Rb and O_2 reaction products trapped in solid argon produced a single feature at 1110 ± 1 cm^{-1}. The agreement between the infrared and Raman spectra indicate the assignment of the 1111.3-cm^{-1} infrared band to ν_1, the superoxide fundamental in $Rb^+O_2^-$; similarly, it is suggested that the 1101.5-cm^{-1} band is due to dimeric $Rb^+O_2^-$.

Previous work with the alkali metals K and Rb produced very intense bands at 307.5 and 255.0 cm^{-1} which were assigned to ν_2, the symmetric interionic mode, in $K^+O_2^-$ and $Rb^+O_2^-$, respectively. The very intense band at 236.5 cm^{-1} showed a 10.5-cm^{-1} $^{18}O_2$ shift and a band pattern in mixed oxygen isotopic experiments consistent with two equivalent oxygen atoms. The intense well-resolved triplet at 236.4, 229.6, and 225.9 cm^{-1} clearly indicates that this vibrational mode arises from a structure containing two equivalent oxygen atoms. Accordingly, the 236.5-cm^{-1} feature is assigned to the symmetric interionic mode ν_2 in $Cs^+O_2^-$.

Antisymmetric interionic modes have been reported for $Li^+O_2^-$ and $Na^+O_2^-$; however, these modes were not assigned for $K^+O_2^-$ and $Rb^+O_2^-$. The sharp, weak feature in the clear spectral region at 268.6 cm^{-1} presents itself as a candidate for this antisymmetric mode. The large $^{18}O_2$ shift of 14.6 cm^{-1} is consistent with the antisymmetric interionic motion. As was discussed in detail for $Li^+O_2^-$, the antisymmetric interionic mode exhibits more $^{18}O_2$ shift than the symmetric interionic mode.[2] The mixed oxygen isotopic experiments clearly show that the 268.6 cm^{-1} feature arises from a single O_2 molecule absorption and that the oxygen atoms are equivalent, as evidenced by the triplet at 268.4, 262.8, and 253.2 cm^{-1}. Furthermore, diffusion behavior associates these bands with the other $Cs^+O_2^-$ absorptions. The assignment of the 268.6-cm^{-1} band to ν_3, the antisymmetric interionic mode of $Cs^+O_2^-$, clearly follows.

The present data on $Cs^+O_2^-$ prompted a closer look at the previous $Rb^+O_2^-$ spectra. The weak band reported at 282 cm^{-1} also showed a large $^{18}O_2$ shift of 15 cm^{-1}, which, along with its appearance 14 cm^{-1} higher than the analogous band for $Cs^+O_2^-$, indicated the assignment of the 282-cm^{-1} band to ν_3 of $Rb^+O_2^-$. Unfortunately, the analogous mode for $K^+O_2^-$ was probably obscured by the intense 307-cm^{-1} band.

Table II lists the fundamental frequencies of all of the alkali metal superoxide molecules. The decrease in frequency of the interionic vibrations ν_2 and ν_3 involving the metal cation follows the increase in atomic weight of the alkali cation; notice that the symmetric mode metal dependence is greater than the antisymmetric mode metal dependence, which follows from the G-matrix elements for these modes.[2] The interesting trend in increasing superoxide frequency is explained in terms of the increasing polarizability of the metal cation in a $M^+O_2^-$ ionic model.[8]

$Cs^+O_2^2-Cs^+$. The infrared spectrum of lithium plus oxygen reaction products showed two intense features at 796 and 445 cm^{-1} which were assigned to the ν_5 and ν_6, antisymmetric interionic motions of cations perpendicular and parallel to the O–O bond, respectively, in $Li^+O_2^2-Li^+$. Isotopic mixtures indicated that two equivalent lithium atoms and two equivalent oxygen atoms were present in this lithium peroxide species. Symmetry coordinate arguments were advanced to suggest the D_{2h} structure.[2] Similar features were assigned to the peroxide molecules of Na, K, and Rb at 524.5, 433.0, and 388.8 cm^{-1}. Mixed alkali metal experiments Na and K or K and Rb simultaneously verified that these absorbers contained two equivalent alkali metal atoms. In the Na and Rb cases, well resolved triplets in the scrambled oxygen isotopic experiments indicated two equivalent oxygen atoms in this species.[3,4]

The 357.0-cm^{-1} feature in the present experiments is assigned to ν_5, the antisymmetric interionic mode perpendicular to the O–O axis, of $Cs^+O_2^2-Cs^+$. The $^{16}O_2$, $^{18}O_2$ experiment indicates the incorporation of a single O_2 molecule into this species. Unfortunately, the scrambled oxygen isotopic experiment produced an incompletely resolved triplet at 356.5, 354.5, and 338.8 cm^{-1}. Apparently, the unsymmetrical $Cs^{16}O^{18}OCs$ species absorbs at a frequency almost accidentally degenerate with the $Cs^{16}O_2Cs$ species. A similar observation was reported[4] for $K^{16}O^{18}OK$. The lower frequency mode ν_6 was not observed for the K, Rb, and Cs peroxide molecules; it likely absorbs below 200 cm^{-1}, the low-frequency limit of these experiments.

$Cs^+O_4^-$. In the study of K and Rb matrix reactions with O_2, very intense bands were observed near 993 cm^{-1} which were assigned to an antisymmetric oxygen stretching mode in a species of formula MO_4. Oxygen isotopic experiments suggested two equivalent O_2 molecules, each with equivalent atoms, in the new MO_4 molecule. Detailed concentration studies[4] and mixed Na–K reactions with oxygen[5] showed that the species contained a single alkali atom. An additional band at 955 cm^{-1} in the K and Rb work was attributed to a matrix site effect or isomer of the MO_4 species absorbing at 993 cm^{-1}.

The intense band at 1002.5 cm^{-1} in the present cesium–oxygen study showed a large oxygen-18 shift of 56.0 cm^{-1}. The sharp triplet structure in the $^{16}O_2$, $^{18}O_2$ experiment

(7) R. R. Smardzewski and L. Andrews, *J. Phys. Chem.*, in press.
(8) L. Andrews and R. R. Smardzewski, *J. Chem. Phys.*, in press, (1973).

indicates the presence of two equivalent O_2 units. Furthermore, the sextet in the scrambled isotopic experiment suggests that the atomic oxygen positions in each O_2 unit are equivalent. The sharper, more intense band at 946.5 cm^{-1} showed a 52.0-cm^{-1} oxygen-18 shift; there was a marked change in the relative intensities of these two features between the first two traces in Figure 1. The intense 1002.5- and 945.5-cm^{-1} bands are assigned to different structural isomers of the most intense mode of the MO_4 disuperoxide species. This is an antisymmetric mode involving out-of-phase stretching of the two O_2 parts of the MO_4 species. The MO_4 molecule is relatively large and its incorporation in two different matrix sites or geometric orientations is reasonable. The change of frequency from 1001 cm^{-1} for NaO_4, 933 for KO_4, 992 for RbO_4 to 1002 cm^{-1} for CsO_4 may also be attributed to matrix site or molecular orientation effects as the size of the alkali cation increases.

Jacox and Milligan[6] have suggested a *trans*-O_4^- structure in the MO_4 species since molecular orbital calculations of Conway[9] show the *trans*-O_4^- isomer to be the most stable of several possible structures for the gaseous anion. This structure has the disadvantage of not fitting the observed spectral equivalence of oxygen atoms in each O_2 unit and the advantage of simply accounting for the reduced vibrational frequency of the disuperoxide species (near 1000 cm^{-1}) as compared to the superoxide species itself (near 1100 cm^{-1}). Jacox and Milligan[6] have pointed out that inequivalence between the two oxygen atoms in each O_2 unit could be too small to resolve spectroscopically; hence, the observed spectrum may mislead one to conclude that the oxygen atoms in the O_2 parts of the MO_4 species must be equivalent. We expect the equivalence between the two O_2 molecules to remain approximately; the observed vibrational mode involves both O_2 units in MO_4 and this mode should be sensitive to the isotopic stoichiometry. However, the arrangement of O_2 molecules is expected to have a smaller effect upon the normal mode frequency, and inequivalence between O atoms in each O_2 unit may be too small to resolve spectroscopically.

The Raman spectrum of the $Cs^+O_4^-$ species contained intense bands[7] at 287 and 270 cm^{-1} which were assigned to an intermolecular oxygen stretching mode $(O\text{-}O \leftrightarrow O\text{-}O)^-$. The observation of the Raman mode is much more readily rationalized with a $M^+O_4^-$ species containing a weak bond between the two O_2 parts of the O_4^- species. Again, two bands were observed in the Raman as in the infrared, consistent with two matrix trapping sites or geometric orientations for $Cs^+O_4^-$.

The vibrational data do not allow a detailed picture of the structure of the MO_4 species to be made. Since MO_4 is a secondary reaction product of the MO_2 species [$M + O_2 \rightarrow M^+O_2^-$; $O_2 + M^+O_2^- \rightarrow M^+O_4^-$], the new structure $M^+O_4^-$ should be formed from the $M^+O_2^-$ isosceles triangular arrangement. This secondary reaction even takes place upon sample warming to 37°K as evidence by growth of $M^+O_4^-$ feature and loss of $M^+O_2^-$ bands. Apparently, another O_2 adds to $M^+O_2^-$, bonding simultaneously to O_2^- and M^+ resulting in a weak bond between the two O_2 parts of the O_4^- anion. Clearly, the presence of the alkali cation affects the structure of the O_4^- anion; the cation is intimately surrounded by the anion, bound by strong electrostatic forces. In a following section, we explore possible cation–anion arrangements and anion structures for the $M^+O_4^-$ species.

It is difficult to discriminate between interionic modes which may be due to a $M^+O_4^-$ or $(M^+O_2^-)_2$ species. Clearly, both molecules are expected to be produced upon sample warming and intense infrared bands should increase under these conditions. Considering the observations in Na, K, Rb, and Cs experiments, the 207-cm^{-1} band in cesium–oxygen reactions most probably is due to the $(MO_2)_2$ species giving rise to 296, 255, and 220 cm^{-1} absorptions, respectively, in Na, K, and Rb experiments. However, the 220.8-cm^{-1} band in $K\text{-}O_2$ experiments which grows sharply upon sample warming is relatively more prominent at lower alkali concentrations.[4] This suggests that the 220.8-cm^{-1} feature and its 213.8-cm^{-1} oxygen-18 counterpart might be due to an interionic mode $(K^+ \leftrightarrow O_4^-)$ in the KO_4 species.

TABLE II: Fundamental Frequencies (cm^{-1}) Assigned to C_{2v} Alkali Metal Superoxide Molecules in Solid Argon at 15°K. Raman Measurements Noted with R; All Others Are Infrared Data

Molecule	ν_1	ν_2	ν_3
$^6LiO_2$	1097.4	743.8	507.3
	1097.0 R	740 R	
$^7LiO_2$	1096.9	698.8	492.4
	1096.6 R	694 R	
NaO_2	1094 R	390.7	332.8
KO_2	1108 R	307.5	*a*
RbO_2	1111.3	255.0	282.5
	1110 R		
CsO_2	1115.6	236.5	268.6
	1114 R		

[a] Unobserved, probably absorbs near 300 cm^{-1} which was obscured by the intense 307.5-cm^{-1} feature.

Vibrational Analysis. Since three fundamental frequencies were observed for three isotopic CsO_2 molecules, a straightforward vibrational analysis can be done for this molecule. Calculations were performed using internal coordinates in the usual Wilson FG matrix format and the Schachtschneider program FADJ. Internal coordinates are preferred over symmetry coordinates for inclusion of $Cs^{16}O^{18}O$ isotopic data and to provide a chemical test of the physical model used here. The isosceles triangular structure proposed for CsO_2 should have two equivalent Cs–O bonds, and accordingly, the calculated CsO force constants should agree. Geometric parameters for CsO_2 were estimated as follows: the O–O distance, 1.28 Å, taken from crystalline[10] KO_2, the Cs–O distance of 2.67 Å taken from preliminary estimates of the Cs–O force constant, and the Herschbach-Laurie[11] force constant–bond length relationship.

Table III illustrates the normal coordinate calculations for isosceles triangular CsO_2. The observed frequencies for three isotopic molecules are compared to the calculated frequencies; the agreement is excellent, with an average discrepancy of 0.3 cm^{-1}. The potential function is also listed in Table III. Notice that the two CsO force constants agree quite closely, as they should for a molecular structure with equivalent Cs–O bonds.

Analogous calculations performed for isosceles triangular RbO_2 are described in Table IV. The Raman[7] assignments to ν_1, previous[4] assignments to ν_2 and the present assignments to ν_3 provide the input data for the calculation. Again, notice that the two RbO force constants agree within the error limits of the calculation.

(9) D. C. Conway, *J. Chem. Phys.*, **50**, 3864 (1969).

TABLE III: Normal Coordinate Calculations for Isosceles Triangular CsO_2 in 3 × 3 Matrix Format Using Nine Isotopic Frequencies. Geometry: O–O Distance 1.28 Å; Cs–O Distance 2.67 Å; O–Cs–O Angle 27°

Isotope	Obsd[a]	Calcd[a]	
16-133-16			
ν_1	1115.6	1116.1	
ν_3	268.5	269.0	$F_{O-O} = 5.854 \pm 0.004$[b]
ν_2	236.5	236.6	$F_{Cs-O} = 0.5614 \pm 0.0050$
16-133-18			
ν_1	1084.9	1084.6	$F_{Cs-O,Cs-O} = -0.111 \pm 0.001$
ν_3	262.5	262.6	$F_{Cs-O} = 0.5618 \pm 0.0053$
ν_2	229.8	229.9	$\Delta\nu = 0.3\ cm^{-1}$
18-133-18			
ν_1	1052.4	1052.1	
ν_3	254.5	253.8	
ν_2	226.0	225.7	

[a] Frequencies, cm^{-1}. [b] Units, mdyn/Å, error limits provided by program FADJ.

TABLE IV: Normal Coordinate Calculations for Isosceles Triangular RbO_2 in 3 × 3 Matrix Format Using Nine Isotopic Frequencies. Geometry: O–O Distance 1.28 Å; Rb–O Distance 2.49 Å; O–Rb–O Angle 29°

Isotope	Obsd[a]	Calcd[a]	Potential function
16-85-16			
ν_1	1110.0	1109.6	
ν_3	282.5	283.0	$F_{O-O} = 5.783 \pm 0.003$[b]
ν_2	255.0	255.4	$F_{Rb-O} = 0.610 \pm 0.003$
16-85-18			
ν_1	1078.0	1078.3	$F_{Rb-O,Rb-O} = -0.130 \pm 0.001$
ν_3	277.0	276.8	$F_{Rb-O} = 0.604 \pm 0.004$
ν_2	248.5	248.3	$\Delta\nu = 0.3\ cm^{-1}$
18-85-18			
ν_1	1046.0	1046.0	
ν_3	267.5	267.2	
ν_2	245.0	244.8	

[a] Frequencies, cm^{-1}. [b] Units, mdyn/Å, error limits provided by program FADJ.

Theoretical Elucidation of the NaO_4 Structure. In the foregoing discussion, we have seen that the vibrational spectrum of alkali metal–oxygen systems, concentration dependences, and alterations in the spectrum as the matrix is warmed permitting diffusion and further reaction afford valuable hints on another species present in the matrix, aside from the well established MO_2. The proposed stoichiometry is MO_4. The interaction between O_2 fragments is small, and the low value of the O–O stretching frequency suggests an ionic model for the bonding. Isotopic substitution effects may be interpreted as indicating that the O_2 fragments are equivalent, and that the O atoms within an O_2 are also equivalent. However the 2-cm^{-1} breadth of the multiplet bands observed in the isotopic experiments suggests that small departures from these symmetry-equivalences are possible, especially in view of the weak interaction between O_2 fragments.

With the established stoichiometry and the symmetry constraints deduced from the vibrational spectrum, there is a wide range of conceivable shapes for MO_4, some of which are shown in Figure 2. Further, within each of these general shapes there exist a number of bond lengths, bond angles, and dihedral angles to be specified.

It is experimentally established that MO_4 is formed by reaction of O_2 molecule with an MO_2 species. The MO_2 species is known to be isosceles-triangular and may be presumed to share the electronic structure of isosceles-triangular LiO_2 which has been established by *ab initio* computation.[12] In the language of molecular orbital theory, the MO's of MO_2 and O_2 provide a basis in which we may express the MO's of the composite MO_4. More importantly, the highest occupied and lowest unoccupied MO's of the fragments can provide a guide to the arrangement of atoms in MO_4 if the rules of perturbation theory stated by Hoffmann,[13] Pearson,[14] Fukui,[15] Dewar,[16] and Salem[17] are followed. Figure 3 shows the MO's of the O_2 and MO_2 fragments and the MO's of a possible C_{2v} arrangement of MO_4. This "rectangular pyramid" will have a pair of equivalent O_2 fragments with O–O bonds more nearly typical of O_2^- than of O_2 owing to the substantial population of the π antibonding MO's of O_2, and the weakening of O–O bonding in lower orbitals (not shown) due to delocalization. The odd electron in MO_4 is placed entirely on the O_4 moiety rather than the metal, which tallies with the ionic character of the molecule deduced from the intensities of the Raman transitions. The bonding between O_2 fragments arising from phase matching of the diffuse O_2 π antibonding orbitals will be weak, which is consistent with the observation of an intense low-frequency intra-ionic mode in the Raman spectrum. The arrangement suggested here by the simplest MO arguments also satisfies the most rigorous symmetry constraints deducible from the vibrational spectrum.

We may consider departures from C_{2v} symmetry, if only because interactions in this molecule are so weak that minor nonequivalences may not be distinguished spectroscopically. Inspection of the uppermost occupied orbital in the qualitative MO diagram suggests that metal AO's can stabilize the system if the metal is moved off the symmetry axis. The metal can move toward an O_2 fragment, a dissociative motion producing O_2 and MO_2, or toward one of the weak connections between O_2 fragments. Each of the occupied orbitals sketched in Figure 3 should be stabilized by this motion, due to the exponential character of interaction between orbitals so long as the nuclear repulsion or short range forces do not change substantially.[18] This distortion removes the strict equivalence of oxygen atoms within an O_2 fragment but preserves the equivalence between O_2 molecules.

A further small distortion suggested by the form of the uppermost (half-filled) MO relieves the direct O···O antibonding by twisting the O_2 fragments relative to one an-

(10) S. C. Abrahams and J. Kalnajs, *Acta Cryst.*, **8**, 503 (1955).
(11) D. R. Herschbach and W. V. Laurie, *J. Chem. Phys.*, **35**, 458 (1961).
(12) F. P. Billingsley, II, and C. Trindle, *J. Phys. Chem.*, **76**, 2995 (1972).
(13) R. Hoffmann, *Accounts Chem. Res.*, **4**, 1 (1971).
(14) R. G. Pearson, *J. Amer. Chem. Soc.*, **91**, 1252 (1969).
(15) K. Fukui in "Advances in Quantum Chemistry," Vol. 6, P.-O. Lowdin, Ed., Academic Press, New York, N. Y., 1972.
(16) M. J. S. Dewar "MO Theory of Organic Chemistry," McGraw-Hill, New York, N. Y., 1969.
(17) L. Salem and J. S. Wright, *J. Amer. Chem. Soc.*, **91**, 5947 (1969); L. Salem, *ibid.*, **90**, 543 (1968).
(18) C. T. thanks B. A. Gimarc for a clear explanation, as follows. Consider three (s) orbitals 1, 2, and 3 centered at −a, o, and a on the *x* axis. As the central orbital is displaced a distance *b* to one side its overlap with 3 is increased to $e^{-z(a-b)}$ from e^{-2a}, and with 1 is decreased to $e^{-z(a+b)}$ from e^{-2a}. The net overlap charge is positive $(e^{-z(a-b)} - e^{-2a}) - (e^{-z(a+b)} - e^{2a}) = e^{-z(a-b)} - e^{-z(a+b)} > 0$. (Here *z* is an unspecified positive number typical of the orbital.) The implication is that the system is always electronically stabilized by yielding to long-range attractive forces. This argument neglects core repulsions and short-range repulsions.

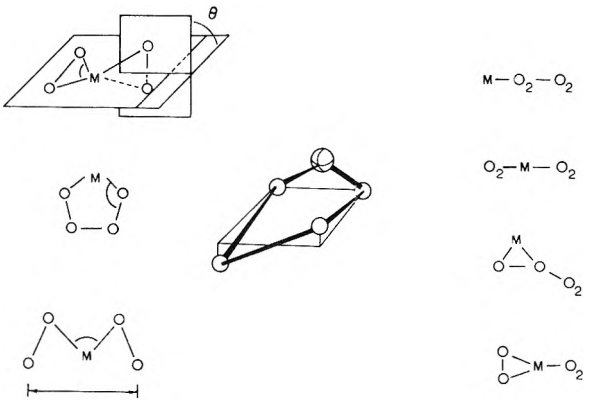

Figure 2. Schematic representations of initial connectivities assumed in NaO_4 geometry searches. The leading candidate for the NaO_4 structure is shown at center the open circles are oxygen atoms. Assumed O–O distances are 2.0 Å for the O_2–O_2 connection in the foreground, 1.3 Å for the strong O–O bond, and 2.0 Å for the Na–O distance. Computed angles are 20° for the twisting of the foreground O–O vector out of a reference plane formed by the oxygen atoms linked to Na and the midpoint of the weak O_2–O_2 connector; 40° between the O–Na–O plane and that reference plane; nearly 90° for the angles between the strong and weak O–O bonds; 110° for the Na–O–O angle.

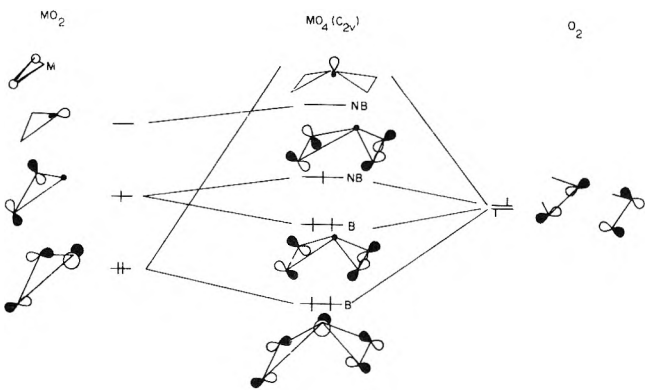

Figure 3. Qualitative interaction diagram for addition of O_2 and MO_2. If the O atoms form a square, the nonbonding M hybrid becomes more stable than the antibonding combination of π antibonding MO's and the system tends to dissociate. This result can be avoided if M is moved off the C_{2v} axis; symmetry breaking allows stabilization of the orbital indicated to be singly occupied (see text).

other. The final shape we propose from qualitative considerations is featured in Figure 2. It remains to estimate approximate bond lengths and angles, which is a matter for more detailed computation.

The large number of geometric parameters necessary to determine the shape of any MO_4 species, even with the guidance of the arguments presented, makes careful planning of the geometry search essential if we wish to avoid (a) forcing a "reasonable" solution by restricting options and (b) bankruptcy. An efficient algorithm which reconciles these aims has appeared,[19] but we completed these computations before McIver's method was available to us. One of us (J.-T. H.) has constructed a program which generates geometries given bond lengths, bond angles, and torsional angles. Special features of this program include the feasibility of incorporating constraints corresponding to maintaining a molecule in a plane, altering angles but not bond distances, and subjecting a ring system to arbitrary puckering without breaking the ring. The latter capabilities are particularly useful in the semiempirical calculation of molecular shapes, which is essentially an optimization of angles.

We have chosen to deal with NaO_4 because it is the only observed MO_4 species within the competence of our MO programs. Estimates of the Na–O and O_2 O–O distances, 2.0 and 1.3 Å, respectively, are available from the known NaO_2 system. To reduce computation, and since semiempirical MO methods are not always reliable for bond length estimation, we adopt these bond lengths without change. If the O_2 fragments are connected in a shape we study, the weak connection is assigned the length 2.0 Å, following Conway's semiempirical computation on O_4^-, which gave special attention to the bond length problem.[9]

Electronic energies were computed using the CNINDO routine by Dobosh based on work by Pople, *et al.*, and distributed by QCPE.[20] For economic reasons, we did not pursue SCF iteration during the geometry search but operated in the extended Hückel mode. Such procedure is suspect if bonds are broken or formed in the course of geometry changes but reliable if the bonding topology is undisturbed, as in our computations. Since the influence of d orbitals may be overestimated by CNINDO in this system, we omit them.

The geometry generator GEO was coupled with the electronic energy program CNINDO by the QCPE program STEPIT[21] which automatically varies the several geometric parameters, monitoring the electronic energy and core repulsion energy, so to seek out the minimum total energy.

The energy hypersurface is sufficiently complex that the minimum energy configuration found by our computation depends on the assumed starting geometries. This multiple minimum problem recurs in any complex optimization problem, and to our knowledge, no general guarantee that the absolute minimum has been found is known. We considered a number of plausible starting geometries (Figure 2); two candidates for the ground state geometry emerged. One was a virtually square pyramidal species, which was in fact the lowest in total energy. Formation of this species from NaO_2 and O_2 is not allowed under thermal conditions, according to Woodward and Hoffmann arguments.[22] The NaO_2 system, which dissociates smoothly to $Na(^2P)$ and $O_2(^3\Sigma_g^-)$ cannot pass directly into the square pyramidal form in which Na would take on ^2S character. As a referee has pointed out, an O_4 species is allowed to form in a rectangular shape by coplanar combination of ground state O_2 molecules. The square pyramid can form from $Na(^2S)$ + O_4 or two O_2. We discount the latter possibility, since the likelihood of a third-order reaction in a matrix seems remote. There is also no experimental evidence for neutral O_4. Moreover, due to the crossing of the Na 3s orbital into the occupied manifold in this form, the odd electron in the square pyramidal species is entirely localized on Na, which then bears a slightly negative charge. Since the highest occupied orbital then has no bonding interaction with the O_4 "ring," the system dissociates

(19) J. W. McIver, Jr., and A. Komornicki, *Chem. Phys. Lett.*, **10**, 303 (1971).
(20) CNINDO by J. A. Pople and P. Dobosh, Quantum Chemistry Program Exchange, No. 91; Quantum Chemistry Program Exchange Chemistry Department, Indiana University, Bloomington, Ind. 47001
(21) STEPIT by J. P. Chandler, Quantum Chemistry Program Exchange, No. 66.
(22) R. B. Woodward and R. Hoffmann, "The Conservation of Orbital Symmetry," Verlag Chemie - Academic Press, Weinheim, 1970.

TABLE V: Force Constants Calculated for the Isosceles Triangular MO_2 Molecules[a]

Molecule	F_{O-O}	F_{M-O}	$F_{M-O,M-O}$
LiO_2	5.547	1.188	−0.203
NaO_2	5.608	0.797	−0.128
KO_2	5.772	(0.66)[b]	(−0.13)[c]
RbO_2	5.780	0.607	−0.130
CsO_2	5.854	0.561	−0.111

[a] All force constants in mdyn/Å units. [b] Calculated from F_{22} and estimate of $F_{M-O,M-O}$. [c] Estimated for KO_2 by comparison with NaO_2 and RbO_2.

easily. The stability of the NaO_4 system to warming, the intensity of the low-frequency Raman mode, and the infrared frequency cannot be rationalized by the square pyramidal geometry.

The second candidate, which is in fact symmetry-allowed to form from NaO_2 and O_2, (a 2s + 2a addition), is the distorted species suggested by the qualitative arguments outlined above. Details of the computed geometry are given in Figure 2. The bond indices[23] of the short O–O bonds are 1.3, while the long O–O bond has an index of 0.4; there is some reason to think that this very weak bond may be longer than 2.0 Å, but the unrealistic description of dissociation provided by CNINDO makes computation of such a bond length chancy.

It is remarkable that none of the symmetry equivalences deduced from isotopic studies of the vibrational spectrum are strictly satisfied by our proposed structure. We are led to ask: what degree of nonequivalence is spectroscopically observable? Inspection of the structure in Figure 2 indicates that the departure from symmetry equivalence of the O_2 fragments is entirely due to the different separation of the foreground oxygen atoms from the sodium atom. The separations are 2.8 and 3.0 Å. We consider it likely that the quartet of bands expected in a $^{16}O^{16}O$–$^{18}O^{18}O$ isotopic mixture would be virtually indistinguishable from the triplet we observe if the *difference* in interaction over 2.8 and 3.0 Å is on the order of a single wave number. Again, in a scrambled isotopic experiment if the inequivalence in O atoms in each O_2 unit were less than one wave number, O atom inequivalence would not be resolved in the observed sharp sextet. [A similar argument has been advanced to support the proposal that the MO_4 system has the equilibrium gas phase *trans* structure of O_4^- with inequivalent O atoms in each O_2 unit, without reference to the metal ion.[6]] However, we find that an isolated Na^+----O_4^- is not competitive in energy with our proposed structure; starting a geometry search with such a model leads to our "puckered five-membered ring" $M^+O_4^-$ structure.

A referee has pointed out the possibility that O_4^- exists with three parallel spins. The computational evidence[9] is not complete, but we do not rule out that possibility in general. Our calculations on the square pyramidal species and the twisted ring indicate that the high multiplicity states are far above the doublet states. However, we have not been able to reproduce singlet-triplet splittings in systems where triplets are very probably the ground states (nitrenes[24]), so we do not offer this statement as proof positive that the quartet is inaccessible.

Conclusions

The metal–oxygen and oxygen–oxygen force constants and bonding in the species reported here merit closer comparison.

Metal–Oxygen Force Constants. Metal–oxygen force constants for the alkali superoxide molecules are tabulated in Table V. The progressive decrease in M–O force constant with increasing alkali atomic weight is noted along with a decrease in the stretch–stretch interaction force constant. The negative sign implies that stretching one M–O bond weakens the other, consistent with the electrostatic $M^+O_2^-$ picture of these molecules; the decrease in M–O force constants with increasing alkali atom size also follows the ionic model.

Oxygen–Oxygen Force Constants. The trend in F_{O-O} shown in Table V for the MO_2 molecules is rationalized on the basis of increasing polarizability of the alkali cation.[8] This gives rise to progressively greater induced dipole moments on the M^+ of opposite sign to the ion dipole which reduces the antibonding electron density and correspondingly increases the O–O frequencies and force constants.

Of particular interest are the oxygen–oxygen force constants in the $M^+O_4^-$ species. Since the two strong O–O bonds have no atom in common, the force constant can be simply calculated using the diatomic approximation. O–O force constants of 4.73 and 4.75 mdyn/Å were determined for $Cs^{16}O_4$ and $Cs^{18}O_4$, respectively; similar values were reported[4] for KO_4 and RbO_4. Now, the observed infrared mode at 1002 cm^{-1} is an antisymmetric or out-of-phase stretching of the two O_2 groups; the symmetric mode counterpart was not observed. For the H_2O_2 molecule, which also has two equivalent, adjacent bonds, the antisymmetric and symmetric OH modes are only a few wave numbers apart.[25] Hence, we believe that interaction between the antisymmetric and symmetric O–O modes in O_4^- is minimal and that the observed frequency of 1002 cm^{-1} adequately reflects the strong O–O bond in O_4^-.

Low-frequency Raman bands of 305, 298, and 287 cm^{-1} were attributed[5,7] to intermolecular $(O_2–O_2)^-$ modes, respectively, in KO_4, RbO_4, and CsO_4. Again, using the diatomic approximation and the KO_4 data,[5] force constants of 0.438 and 0.446 mdyn/Å were determined for $K^{16}O_4$ and $K^{18}O_4$. However, this mode probably involves the intermolecular motion of two O_2 molecules rather than two O atoms; accordingly, these values probably should be doubled, giving an average value of 0.88 mdyn/Å for the intermolecular oxygen–oxygen force constant in O_4^-.

Bonding. The superoxide force constant for the $Cs^+O_2^-$ species (5.85 mdyn/Å) exceeds the strong bond disuperoxide force constant (4.74 mdyn/Å) in the $Cs^+O_4^-$ species. Here the *two* O_2 parts of O_4^- have lower force constants than O_2^- itself, an impossible reduction feat for a single alkali metal atom, without intermolecular oxygen bonding in O_4^-. Hence the low strong bond force constant in O_4^- requires intermolecular oxygen–oxygen bonding for its explanation.

Calculated oxygen–oxygen bond indices in the O_4^- species are consistent with the force constant trend. The strong O–O bond in O_4^- has a bond index of 1.3, just less than the 1.5 bond index for O_2^- itself.[26] Hence the strong O–O bond in O_4^- must be slightly weaker than the O–O bond in O_2^-. The bond index of 0.4 for the weak O_2–O_2

(23) C. Trindle, *J. Amer. Chem. Soc.*, **91**, 219 (1969).
(24) L. Hayes, F. P. Billingsley, and C. Trindle, *J. Org. Chem.*, **37**, 3924 (1972).
(25) R. L. Redington, W. B. Olson, and P. C. Cross, *J. Chem. Phys.*, **36**, 1311 (1962).
(26) C. Trindle, CNDO calculation on O_2^- using 1.28 Å bond length.

bond in O_4^- is consistent with the very low force constant for this Raman mode and the weak intermolecular $(O_2-O_2)^-$ binding which could also be rationalized by the qualitative $\pi^*-\pi^*$ bonding picture of Spratley and Pimentel.[27]

Acknowledgments. The authors gratefully acknowledge financial support for the experimental part of this work by Grant GP-28582 of the National Science Foundation and for the theoretical part by the UVa Computer Science Center, the A. P. Sloan Foundation, and the National Science Foundation under Grant GP-30817. J.-T. H. thanks the Research Corporation for contributions to his research assistantship.

(27) R. C. Spratley and G. C. Pimentel, *J. Amer. Chem. Soc.*, **88**, 2394 (1966).

Dielectric Relaxation of Tetrahedral, Octahedral, and Cubic Complexes of Acetylacetone[1]

E. N. DiCarlo,* Edgar Watson, Jr., C. E. Varga,[2] and W. J. Chamberlain[2]

Department of Chemistry, Saint Joseph's College, Philadelphia, Pennsylvania 19131 *(Received November 22, 1972)*

Publication costs assisted by the National Science Foundation

Recent studies have shown that several octahedral complexes of acetylacetone, which possess very high atom polarizations, exhibit considerable microwave losses in benzene solution which are consistent with unusually short dielectric relaxation times. These earlier observations have been extended to other acetylacetonates in which the linkages have a tetrahedral and cubic disposition to the central metal atom and a fairly clear general picture of the position has evolved. The relaxation times reported previously for Cr(III), Fe(III), Co(III), and Al(III) acetylacetonates are virtually identical with those found in the present investigation for the acetylacetonates of Be(II), Th(IV), and Zr(IV). The latter consistency and the magnitude of the individual relaxation times (in all cases 4–5 psec, 60°) indicate a common relaxation process of surprisingly high frequency for these octahedral, tetrahedral, and cubic complexes. The observed losses are shown not to be relaxation losses of permanent dipoles in agreement with other evidence which favors completely symmetrical structures for these molecules. Consideration of various alternatives suggests that the microwave losses are most probably connected with an intramolecular relaxation process involving highly damped oscillations of the chelate rings relative to the remainder of the molecule. It therefore appears that a considerable fraction of the total atom polarization of each of these substances is associated with absorption in the centimeter and millimeter wavelength region while the remainder arises from the usual infrared absorption.

Introduction

Recent studies[3-5] have shown that several octahedral complexes of acetylacetone, *e.g.*, cobalt(III), iron(III), chromium(III), and aluminum, exhibit considerable dielectric losses in benzene solution in the centimeter wavelength region. The general feature of the relaxation, *i.e.*, it appears at a frequency which is much too high for a dipole rotation, indicates that the observed losses are associated with an intramolecular relaxation mechanism. Of all of the acetylacetonates examined by X-ray diffraction, the most extensive investigations have been made on the iron(III) chelate, $Fe(acac)_3$. A refinement of its crystal structure (by the least-squares method with full three-dimensional data) shows this molecule to be perfectly symmetrical, *i.e.*, the six-membered rings are completely planar within experimental error.[6,7] While the X-ray results obtained for several other acetylacetonates do not exclude the possibility that the metal atom may deviate from the plane of the chelate ring,[8,9] the data, as pointed out by Haigh and Sutton,[10] do not require bent chelate rings. Also, numerous static polarization studies[11-14] which collectively cover a wide temperature range, *ca.* 200°, indicate zero moments and unusually large atom polarizations for $Fe(acac)_3$, $Cr(acac)_3$, and $Al(acac)_3$. In view of the preponderance of evidence which favors completely symmetrical structures for these molecules, it is quite signifi-

(1) This research was supported by the National Science Foundation under Grant No. GP-24935.
(2) This paper represents part of the work submitted by C. E. Varga and W. J. Chamberlain to the Chemistry Department of Saint Joseph's College in partial fulfillment of the requirements for the degree of Master of Science.
(3) S. Dasgupta and C. P. Smyth, *J. Amer. Chem. Soc.*, **89**, 5532 (1967).
(4) E. N. DiCarlo and R. E. Stronski, *Nature (London)*, **216**, 679 (1967).
(5) E. N. DiCarlo, R. E. Stronski, and C. E. Varga, *J. Phys. Chem.*, **73**, 3433 (1969).
(6) R. B. Roof, Jr., *Acta Crystallogr.*, **9**, 781 (1956).
(7) J. Iball and C. H. Morgan, *Acta Crystallogr.*, **23**, 239 (1967).
(8) E. C. Lingafelter, *Coord. Chem. Rev.*, **1**, 151 (1966).
(9) B. Morosin, *Acta Crystallogr.*, **19**, 131 (1965).
(10) J. Haigh and L. E. Sutton, *Chem. Commun.*, 296 (1970).
(11) I. E. Coop and L. E. Sutton, *J. Chem. Soc.*, 1269 (1938).
(12) A. E. Finn, G. C. Hampson, and L. E. Sutton, *J. Chem. Soc.*, 1254 (1938).
(13) J. McQueen and J. W. Smith, *J. Chem. Soc.*, 1821 (1956).
(14) E. N. DiCarlo, T. P. Logan, and R. E. Stronski, *J. Phys. Chem.*, **72**, 1517 (1968).

cant that they show considerable dielectric absorption in benzene solution. From the initial dielectric loss studies, DiCarlo, *et al.*,[5] concluded that the microwave absorption exhibited by these substances is connected with some form of intramolecular polarization not due to the ordering of permanent dipole moment components. It was also suggested that damped oscillation of the chelate rings about the metal atom as a center could possibly account for the observed high-frequency relaxation of these octahedral complexes.[5,10] The present investigation was undertaken to obtain further evidence as to the possible relaxation mechanism. For this purpose, the earlier observations on metal acetylacetonates with octahedral dispositions of the linkages to the central metal atom have been extended to acetylacetonates in which these linkages have a tetrahedral and cubic disposition. In addition, for comparison purposes, the dispersion behavior of an acetylacetonate which is known to be polar has been examined.

Experimental Section

Apparatus. Static dielectric constants were measured with a General Radio GR 716-CS1 capacitance bridge at 1 MHz. The technique and error analysis have been previously reported.[14] A Lipkin bicapillary pycnometer was employed to measure solution densities. Reproducibility of the density measurements was better than 0.0002 g/ml. Dielectric constants, ϵ', and losses, ϵ'', were measured at frequencies of 9133 and 25,680 MHz employing the standing wave method as developed by Heston, Franklin, Hennelly, and Smyth.[15] An error analysis[5] has led to the following estimated accuracies: ϵ', ±0.3 and ±0.2% at 25,680 and 9133 MHz, respectively; ϵ'', ±0.0001 or ±2% (whichever is larger) at 25,680 MHz and ±0.00005 or ±2% (whichever is larger) at 9133 MHz. The experimental details of the microwave techniques have been reported.[5] For all measurements, temperature was maintained to within 0.01° of the desired temperature.

Materials. The source, method of purification, and melting point or refractive index of each substance investigated are listed in Table I. Carbon-hydrogen analysis was performed on $Th(C_5H_7O_2)_4$ and $Zr(C_5H_7O_2)_4$. *Anal.* Calcd for $Th(C_5H_7O_2)_4$: C, 38.22; H, 4.49. Found: C, 38.17; H, 4.55. Calcd for $Zr(C_5H_7O_2)_4$: C, 49.26; H, 5.74. Found: C, 49.56; H, 5.94.

TABLE I: Sources, Method of Purification, and Melting Points or Refractive Index

Compound	Source[e]	Mp, °C
Bis(acetylacetonato)beryllium(II)[b]	A	101.2–101.8
Tetrakis(acetylacetonato)-thorium (IV)[a]	A	172.0–172.5
Tetrakis(acetylacetonato)-zirconium(IV)[a]	A,C	193.8–194.8
Bis(acetylacetonato)mono-(3-chloroacetylacetonato)-chromium(III)[d]	D	
Benzene[c]	B	$n_D^{25} = 1.49786$

[a] Repeated crystallization from benzene-petroleum ether and drying under vacuum over Drierite or P_2O_5. [b] Repeated boiling of a saturated toluene solution with molecular sieve, filtration, low-temperature crystallization from petroleum ether, and drying under vacuum over P_2O_5. [c] Reagent grade, thiophene-free benzene was fractionally distilled over Na and stored over Drierite. [d] Prepared and purified by Professor J. P. Collman, Stanford University. Dried under vacuum over P_2O_5. [e] (A) J. T. Baker Chemical Company, (B) Fisher Scientific Company, (C) Matheson Coleman and Bell, (D) Professor M. Bursey, University of North Carolina.

TABLE II: Total Molar Polarization (Benzene Solution)

Temp, °C	ϵ_1	$10^4\alpha$	$-10^4\beta$	v_1	$P_{2\infty}$, cm³	$P_{2\infty}$, lit, cm³
Tetrakis(acetylacetonato)thorium(IV) (0–0.0612)						
25	2.2748	7565	5523	1.1448	200.4	200.8[a]
55	2.2155	7338	5984	1.1874	199.2	200[b] (vapor at 238°)
Tetrakis(acetylacetonato)zirconium(IV) (0–0.0906)						
25	2.2744	8508	3977	1.1444	186.5	185.4[a]
55	2.2145	8571	4557	1.1880	186.8	

[a] Finn, *et al.*,[12] benzene solution at 25°. The value cited for $Th(acac)_4$, 195.6 cm³, was determined by extrapolating the polarization data to infinite dilution. Treatment of the data by the Halverstadt–Kumler method yielded a value of 200.8 cm³. [b] Reference 11.

Results

Table II contains polarization data obtained at 1 MHz for benzene solutions of zirconium(IV) and thorium(IV) acetylacetonates. Together with the total molar polarizations, $P_{2\infty}$, the derivatives and intercepts of dielectric constant and specific volume with respect to weight fraction (α, β, ϵ_1, and v_1, respectively) are listed. Tabulated in parentheses immediately following the name of the chelate is the concentration range in weight fraction for each set of solutions examined. The total polarizations were calculated by the method of Halverstadt and Kumler.[16] A minimum of seven solutions was employed for the polarization determinations and α, β, ϵ_1, and v_1 were calculated by the method of least squares. The values of $P_{2\infty}$ deduced from the parameters listed in Table II were checked by comparison with the values of the polarization calculated from the dielectric constant and density data for each concentration. No systematic variation of polarization with concentration was observed. An error analysis, which has been previously described[14] and applied to the present results, has led to an absolute error of *ca.* ±3 cm³ in the Halverstadt–Kumler $P_{2\infty}$ values of Table II. The relative error in the $P_{2\infty}$ values determined at the different temperatures was estimated to be ±1.5 cm³.

Table III contains the absorption results obtained at 25,680 and 9133 MHz for benzene solutions of beryllium(II), zirconium(IV), and thorium(IV) acetylacetonates. The concentration range in mole fraction for each set of solutions examined is given in parentheses immediately following the name of the chelate. The derivatives of dielectric loss, ϵ'', with respect to mole fraction, c_2, *i.e.*, a'', were calculated by the least-squares method employing data obtained on five solutions. Arc plots could not be formulated with any degree of certainty because the frequency dependence of the dielectric constant of the solutions investigated was extremely small and only two microwave frequencies were employed in this study. Therefore, the absorption was examined solely in terms of the dielectric losses by assuming the Debye theory to be applicable.[17,18] As a result, the τ values, deduced from the loss data as

(15) W. M. Heston, Jr., A. D. Franklin, E. J. Hennelly, and C. P. Smyth, *J. Amer. Chem. Soc.*, **72**, 3443 (1950).
(16) I. F. Halverstadt and W. D. Kumler, *J. Amer. Chem. Soc.*, **64**, 2988 (1942).
(17) P. Debye, "Polar Molecules," Chemical Catalog Co., New York, N. Y., 1929, Chapter V.
(18) For a critical discussion of this method of analysis, see D. H. Whiffen and H. W. Thompson, *Trans. Faraday Soc.*, **42**, 114 (1946).

TABLE III: Slopes, a'', for the Dependence of the Dielectric Loss of Solutions on Mole Fraction of Solute and Relaxation Times, τ

Temp, °C	a'' 25,680 MHz	a'' 9133 MHz	τ, 10^{-12} sec
Bis(acetylacetonato)beryllium(II) (0–0.0404)			
10	0.110	0.063	5.4
25	0.086	0.051	5.7
40	0.077	0.038	4.2
60	0.062	0.028	3.5
Tetrakis(acetylacetonato)zirconium(IV) (0–0.0131)			
20	0.344	0.282	8.4
40	0.366	0.199	5.0
60	0.374	0.214	5.4
Tetrakis(acetylacetonato)thorium(IV) (0–0.0213)			
20	0.497	0.305	6.0
60	0.486	0.222	3.6

previously described,[5] reflect the Debye form of the absorption curve. The most reliable values of τ (calculated from loss data at only two frequencies assuming a Debye-type absorption) are obtained when the two experimental frequencies are very close to and on opposite sides of the frequency of maximum absorption, ω_{max}. If this condition is not satisfied, the τ values so determined are either low or high estimates depending on whether the two measured losses are on the high- or low-frequency side, respectively, of ω_{max}. (This effect is greatly enhanced if the actual dispersion has a distribution associated with it.) For the unsubstituted acetylacetonates considered in both the present study and in an earlier investigation[5] (Co(III), Cr(III), Fe(III), and Al), the reported τ values are high estimates. For these substances, the 9133- and 25,680-MHz points are on the low-frequency side of ω_{max}. This is reflected in preliminary measurements made from 9133 to 135,000 MHz (2 mm) on $Al(acac)_3$ in benzene solution at 25° which definitely show the maximum loss to be at about 3 mm (τ of about 2 psec). It is to be noted that the latter observation, which by implication suggests the actual τ values of all these complexes to be closer to 1 or 2 psec rather than 4 or 5 psec (see Table III), serves to reinforce the conclusions arrived at in the following Discussion.

Table IV summarizes the results obtained for bis(acetylacetonato)mono(3-chloroacetylacetonato)chromium(III), $Cr(acac)_2$(3-Cl acac), in benzene solution. Due to lack of sufficient material, only one solution was examined. The two measuring frequencies were so far removed from ω_{max} that the τ value of this molecule could not be reliably estimated from the loss data alone. Therefore, both the ϵ' and ϵ'' results were utilized and the values of the relaxation time and permanent moment tabulated are those that gave a best fit of the data to a Debye line shape. Because the losses of the dilute solution studied were very low and the extreme high-frequency side of ω_{max}, the uncertainty in τ is probably quite large and 74 psec should be taken as a rough approximation only in the sense of a lower limit estimate for this molecule.

Discussion

Static Polarization. In a study by Wright, *et al.*,[19] the solution (benzene) total polarizations of Th(IV) and Zr(IV) acetylacetonates were reported to increase greatly with slight increase in temperature (by *ca.* 50 and 30 cm^3 from 20 to 40° for $Th(acac)_4$ and $Zr(acac)_4$, respectively).

TABLE IV: Dielectric Constants and Losses, Relaxation Time, and Dipole Moment of Bis(acetylacetonato)mono-(3-chloroacetylacetonato)chromium(III) in Benzene[a]

Temp, °C	Frequency, MHz	ϵ'	ϵ''	τ, 10^{-12} sec	μ, D
30	25,680	2.269	0.00078	74	1.80
	9,133	2.271	0.00121		(1.73[b])
	1	2.277			

[a] c_2 = 0.001839. [b] R. H. Brook and H. Freiser, *Inorg. Chem.*, 5, 2078 (1966).

These results which are suggestive of temperature-dependent permanent moments which vary from 1.18 (20°) to 2.00 D (40°) and from 1.85 (20°) to 2.26 D (40°) for $Th(acac)_4$ and $Zr(acac)_4$, respectively, are surprising when compared to data obtained previously by other workers for these complexes with cubically disposed donor atoms and several others of different symmetry.[11-14] For example, Be(II) acetylacetonate has been conclusively shown to have a temperature-independent static polarization (from earlier determinations in decalin solution[12] over a temperature range of 298–415° and by vapor-phase measurements[11] from 185 to 255°) confirming the absence of a permanent moment as expected for this tetrahedrally symmetric molecule. Vapor-phase and solution (benzene) polarization investigations[11,12,14] have demonstrated that several octahedral acetylacetonates, Co(III), Fe(III), Cr(III), and Al(III), do not possess a component of orientation polarization. In earlier studies, it was also found that the polarization of $Th(acac)_4$ determined at one temperature in benzene solution[12] (25°) was virtually identical with the vapor-phase value[11] obtained at 238° (see Table II). This agreement between solution and vapor-phase values led to the conclusion that $Th(acac)_4$ is nonpolar, although, for this substance, polarization measurements as a function of temperature were not made either in solution or on the vapor. Finally, the polarization values observed for $Zr(acac)_4$ in benzene solution at 20 and 30° by Wright, *et al.*,[19] do not fall in line with the polarization in this solvent found previously[12] at 25°. (Vapor-phase data are not available for $Zr(acac)_4$.) In summary, the large temperature coefficients reported for $Th(acac)_4$ and $Zr(acac)_4$ in benzene are unexpected in view of earlier published data and raise the question as to the possible polarity of these substances. Therefore, it was decided to redetermine their solution static polarizations as a function of temperature to further investigate this apparent anomaly before examining their dispersion at microwave frequencies.

As seen from Table II, the findings of this study do not agree with those of Wright, *et al.* In particular, no change, within experimental error, of the solution total polarizations of the cubic complexes, $Th(acac)_4$ and $Zr(acac)_4$, was found at the two temperatures employed. It is to be noted that because the present investigation was conducted over a relatively small temperature range (25–55°), the results obtained, considered solely by themselves, certainly can not be used in arriving at a definite conclusion regarding the nonpolarity of these substances. However, considering the relative error (±1.5 cm^3) in the $P_{2\infty}$ values at the different temperatures, the extremely large variations observed previously[19] over an even smaller temperature interval (20–40°) would have been easily detecta-

(19) P. Podleschka, L. Westland, and G. F. Wright, *Can. J. Chem.*, **36**, 574 (1958).

ble. Furthermore, the $P_{2\infty}$ values found for $Th(acac)_4$ in benzene solution at both 25 and 55° are, within the estimated absolute experimental error (±3 cm³), in excellent agreement with the value of 200.8 cm³ reported by Finn, *et al.*,[12] from measurements in the same solvent at 25° and with 200 cm³ obtained by Coop and Sutton[11] from a vapor-phase determination (238°). Therefore, the results of this investigation when considered in conjunction with the findings of the earlier vapor-phase study agree with the original conclusion that $Th(acac)_4$ is nonpolar and possesses an unusually high atomic polarization. Finally, the static polarizations measured for $Zr(acac)_4$, while disagreeing with those reported by Wright, *et al.*, confirm the value, 185.4 cm³, found by Finn, *et al.*,[12] from determinations in benzene solution (25°). Because polarization data at temperatures far removed from those employed in the present work are not available for $Zr(acac)_4$, the question of whether or not this molecule possesses a permanent moment can not be resolved from temperature coefficient considerations.

Although the differences between the present solution results and those of Wright and his coworkers are much greater than can be accounted for by the absolute errors quoted in this investigation, discussion of the reasons for the disagreement would be purely conjecture. However, as will be shown, the dielectric absorption studies offer an independent confirmation of the orginal conclusion that these molecules are nonpolar.

Microwave Absorption. In a previous study,[5] it was shown that several octahedral complexes of acetylacetone exhibit significant dielectric losses in benzene solution in the centimeter wavelength region. These earlier observations have now been extended to other acetylacetonates in which the linkages have a tetrahedral and cubic disposition to the central metal atom. The unusually short relaxation times reported recently for $Al(acac)_3$, $Cr(acac)_3$, $Fe(acac)_3$, and $Co(acac)_3$ in benzene solution[5] are virtually identical with those found for $Be(acac)_2$, $Th(acac)_4$, and $Zr(acac)_4$ in the same solvent. Although the actual line shape of the absorption curve can not be specified from the limited data available, the magnitude of the estimated τ values[20] defintely establish the relaxation process to be insensitive to the overall size of these chelates. In addition, the closeness of the individual τ values (in all cases, 4–5 psec, 60°) indicates that the behavior of the high-frequency relaxation does not significantly depend (within the uncertainty in the representation of the loss data in terms of a Debye line shape) on the particular disposition of the rings to the central metal atom. Any interpretation of these losses must be consistent with the above observation, *i.e.*, in general, these complexes, although of different overall symmetry, appear to relax in the same fashion, the decrease of loss with temperature, and with the fact that their high total polarizations are not peculiar to the condensed phase.[11]

Most evidence favors completely symmetrical structures (zero permanent moments) for these molecules. X-Ray analysis has shown that the acetylacetone portion of the chelate ring (*i.e.*, the set of atoms O-C-C-C-O), in $Be(acac)_2$, $Cr(acac)_3$, and $Zr(acac)_4$ is completely planar within the limits of accuracy of the data.[8] As mentioned earlier, static dielectric constant studies over a wide temperature range have definitely established that $Be(acac)_2$ does not possess a component of orientation polarization.[11,12] While it can be argued that the polarization results obtained for $Th(acac)_4$ and $Zr(acac)_4$ are not quite as conclusive, the relaxation behavior of the latter molecules appears to be identical with that shown by $Be(acac)_2$ (Table III) and is dramatically different than what would be expected for a polar acetylacetonate[5] (Table IV).

While the present results do not, of themselves, definitely exclude the possibility of permanent dipole moments, they do favor their absence. In this connection, the following points are pertinent.

(1) The observed relaxation times are obviously too short to be associated with overall molecular rotation. The magnitude of the τ value found for the substituted complex, $Cr(acac)_2$(3-Cl acac), which indicates that its predominant relaxation mechanism is dipole orientation by molecular rotation (based on comparisons made with polar molecules of similar size and shape),[5] is almost 15 times greater than those of the unsubstituted chelates investigated.

(2) Internal rotation can be eliminated as a possible relaxation mechanism because these molecules, even if they were permanently polar, do not possess the type of polar group capable of orienting in the field by an internal rotation *in the usual sense.*

(3) The inversion mechanism which has recently been suggested to account for the high-frequency relaxation displayed by these chelates is not plausible on several counts. Nelson and White[21] measured the far-infrared molar refraction, R_{FIR} (at 29.7 cm^{-1}), of $Al(acac)_3$ in benzene solution and found it to be smaller than the radio-frequency polarization, P_T. The difference, $P_T - R_{FIR}$, was assigned as orientation polarization, the latter amounting to a permanent moment of 1.1 D. They suggested that the minimum potential energy structure of $Al(acac)_3$ is one in which the Al atom is displaced from the plane of the three carbon and two oxygen atoms, *i.e.*, each ring has two minima of potential energy *vs.* conformation. They interpreted the short relaxation times previously observed for $Al(acac)_3$ in terms of torsional jumps from one polar conformation to another. By implication, Fe(III), Cr(III), and Th(IV) acetylacetonates were presumed to display the same relaxation mechanism. The pertinent motion is pictured as a metal-ligand bending mode which is so strongly perturbed by asymmetric solvent cages that it becomes in effect a hindered inversion motion. (In this model, the time required for the reversal of dipole moment direction is apparently governed by a slowly changing solvent cage.) As pointed out by Haigh and Sutton,[10] the temperature-independent total polarizations of these systems is not consistent with such an interpretation. Inversion between two asymmetric conformations would result in a static polarization inversely proportional to temperature. For example, one would expect to observe a drop of *ca.* 8 cm³ in the P_T of $Al(acac)_3$ from 25 to 225°, considering the difference between P_T and R_{FIR} at 25°, *ca.* 22 cm³ mol^{-1}.[10] (The values actually found are 130.8 cm³ (240°)[11] and 131.7 cm³ (25°).[14]) Correspondingly large drops (8–10 cm³) would also be predicted at 225° for the Cr(III), Fe(III), Co(III), and Th(IV) complexes from the differences between the radio and submillimeter frequency values at 25°.[10] Again, these are much larger than the observed differences (1–3 cm³).[11] Finally, if such a mechanism were operative, one would expect the high solution polarizations at radio frequency to

(20) Recall that the actual τ values of these complexes are probably close to 1 or 2 psec.

(21) R. D. Nelson, Jr., and C. E. White, *J. Phys. Chem.*, **73**, 3439 (1969).

be caused by solvent effect which is definitely not the case, as shown by Sutton, *et al.*,[11,12] so long as the solvent is nonpolar.

(4) The losses are much too high to be accounted for by the presence of polar impurities in the starting materials, complex formation between the solvent and the chelates, or dissociation of the acetylacetonates in solution.[5] Substantial dissociation in solution or significant complex formation would have resulted in differences between solution and vapor polarizations much greater than those actually observed. Also, the infrared spectra of a number of metal acetylacetonates in solution give no indication of absorptions due to dissociation products.[22]

As a result of the foregoing process of elimination, it appears clear that the observed losses are not relaxation losses involving permanent dipoles. Concerning other alternatives, the following is to be noted.

(5) The molecular distortion mechanism (in which the dipole moment and relaxation time arise from environmental conditions unique to the liquid state) suggested by Whiffen[23] to account for the dielectric losses exhibited by benzene and several other nonpolar liquids can not be invoked in the present case. The fact that the unusually large P_T values of the acetylacetonates are not peculiar to the condensed phase[11] does not agree with such a mechanism. Based on this model, large differences between the vapor and solution P_T values of each of these chelates would be expected. For example, assuming a Debye exponential damping process for the relaxation, a contribution of about 14 cm^3 to the solution P_T of $Th(acac)_4$, dispersing with a τ of 6.0 psec, is calculated from the observed loss data at 20°. A solution P_T 14 cm^3 greater than that of the vapor would have been easily detected. (Actually the radio frequency polarizations in the gas phase and in solution agree to within 1 cm^3 for $Be(acac)_2$ and $Th(acac)_4$.[11,12]) This same argument also applies to the octahedral chelates investigated previously.

(6) These absorptions are evidently not related to the (Poley) absorption,[24] characteristic of the structural features of the liquid state and exhibited by both polar and nonpolar molecules in the far-infrared between 30 and 80 cm^{-1}.[25-30]

(7) The measured losses can not be reconciled with the fact that the long-wavelength tails of vibrational, infrared absorption bands are being observed. Preliminary measurements made from 9 to 135 GHz on $Al(acac)_3$ in benzene solution at 25° show ω_{max} to be located between 1 and 10 cm^{-1}. Also, the losses were found to decrease with increase in temperature, whereas an increase of the loss in the low-frequency tail would be expected.[23]

In view of the foregoing arguments, it appears that the absorption exhibited at high microwave frequencies by all of the unsubstituted acetylacetonates investigated to date is connected with some form of intramolecular polarization which is not due to the ordering of permanent dipole moment components. This is equivalent to saying that a considerable fraction of their total atom polarization is associated with absorption in the centimeter and millimeter wavelength region while the remainder arises from the usual infrared absorption. Dasgupta and Smyth[3] and Di-Carlo and Stronski[4] initially arrived at this conclusion in microwave-loss studies on $Al(acac)_3$. The suggestion that oscillations of the rings about the metal atom are involved in the relaxation[4,5,10] appears to be the most plausible explanation of the observations (1–7 above). The oscillations of interest would have to be highly damped because the absorptions seem compatible with an aperiodic process which reflects a liquid viscosity effect (τ decreases with temperature). Such motion may well be relevant to the observed relaxation for the following reasons. (a) The fact that the losses show about the same frequency dependence for the tetrahedral, octahedral, and cubic complexes suggests a common internal process. (b) A large amount of evidence shows these molecules to possess considerable flexibility at the metal[31-35] and therefore it can be reasonably assumed that the lowest lying vibrations are those of the rings, as units, about the metal atom as a center.[36] (c) As pointed out by Haigh and Sutton,[10] such vibrations might be highly damped by collisions because the chelate rings are large and peripheral. They further note that collision damping, while not affecting the polarizations at visible and radio frequencies, would greatly modify the form of the dispersion and absorption curves.

Obviously, further evidence is required before the microwave losses can be definitely correlated with a highly damped oscillation process. More information about the details of the absorption in the millimeter wavelength region is necessary before a conclusion can be reached regarding the validity of the Debye line shape assumption. In this regard, dielectric constant and loss measurements as a function of temperature are being made at 2-mm wavelength. These data together with those which have already been obtained at the submillimeter wavelength[10] (0.337 mm) should further elucidate the mechanism of the relaxation.

Acknowledgment. We gratefully acknowledge financial assistance from the National Science Foundation (GP-24935).

(22) J. P. Dismukes, L. H. Jones, and J. C. Bailar, *J. Phys. Chem.*, **65**, 792 (1961).
(23) D. H. Whiffen, *Trans. Faraday Soc.*, **46**, 124 (1950).
(24) J. Ph. Poley, *J. Appl. Sci., B*, **4**, 337 (1955).
(25) H. A. Gebbie, N. W. B. Stone, F. D. Findlay, and E. C. Pyatt, *Nature (London)*, **205**, 377 (1965).
(26) G. W. Chantry and H. A. Gebbie, *Nature (London)*, **208**, 378 (1965).
(27) Y. Leroy and E. Constant, C. R., *Acad. Sci.*, ***262***, 1391 (1966).
(28) G. W. Chantry, H. A. Gebbie, B. Lassier, and G. Wyllie, *Nature (London)*, **214**, 163 (1967).
(29) J. E. Chamberlain, E. B. C. Werner, H. A. Gebbie, and W. Slough, *Trans. Faraday Soc.*, **63**, 2605 (1967).
(30) M. Davies, G. W. F. Pardoe, J. E. Chamberlain, and H. A. Gebbie, *Trans. Faraday Soc.*, **64**, 847 (1968).
(31) G. E. Glass and R. S. Tobias, *J. Amer. Chem. Soc.*, **89**, 6371 (1967).
(32) G. E. Glass and R. S. Tobias, *J. Organometal. Chem.*, **15**, 481 (1968).
(33) J. P. Fackler, *Progr. Inorg. Chem.*, **7**, 361 (1966).
(34) L. Wolf, E. Butter, and H. Weinett, *Z. Anorg. Allg. Chem.*, **306**, 87 (1960).
(35) G. Schwarzenbach, *Angew. Chem.*, **70**, 451 (1958).
(36) Absorption bands due to metal–ligand bending modes have not been observed for the Cr(II), Fe(III), and Th(IV) acetylacetonates in the vapor phase from 100 to 30 cm^{-1} (see ref 10).

Vibration Relaxation in Carbon Dioxide with Selected Collision Partners. II. Methane, Tetradeuteriomethane, and Fluoromethane

P. M. Walsh and S. H. Bauer*

Department of Chemistry, Cornell University, Ithaca, New York 14850 *(Received November 27, 1972)*

The vibration–translation relaxation times of the ($01^{1}0$) state of CO_2 in mixtures with CH_4, CD_4, and CH_3F were measured over the temperature range 400–1200°K by monitoring the deflection of a narrow parallel beam of monochromatic light by the density gradient behind incident shock waves in the gas mixtures. The reduced relaxation times (infinite dilution) of CO_2 in CD_4 and CH_3F are one tenth as large as those in pure CO_2, and decrease with increasing temperature. The relaxation time for CO_2 in CH_4 is ten to twenty times smaller than in pure CO_2 and is practically constant over the temperature range investigated. Vibrational relaxation times of pure CH_3F in the vicinity of 500°K were also measured.

Introduction

This report is a sequel to that of Buchwald and Bauer[1] who studied the relaxation of CO_2 ($01^{1}0$) by H_2O and D_2O over the temperature range 350–1200°K. The purpose of these investigations is to uncover the molecular parameters of catalyst species that control their efficiencies for vibration–translation energy transfer, and thus to provide critical data for checking theories of V–T relaxation times. Conceivably one could then discover a rationale for selecting additives which increase the efficiency of CO_2 laser operation.

Experimental Section

The technique used was essentially that described previously[1] with several modifications and improvements, as noted below. The diaphragms were circles of polyester film 21 cm in diameter and 0.19 mm thick (Mylar-750A); they were scored across two diagonals by the edge of a rotating end-mill to a depth of about one-half of the film thickness. The electronic system was triggered by a piezoelectric transducer and shock speeds were determined from arrival times at three platinum film resistance gauges mounted downstream from the diaphragm at 7.62, 7.87, and 8.13 m, respectively. The light beam used to measure the density gradients crossed the driven section at 8.11 m from the diaphragm.

The gas mixing and storage tank consisted of a glass-lined 50-gal hot water heater; it was thoroughly degassed by many hours of evacuation with a diffusion pump. The combined leak and degassing rates of the shock tube and storage tank were measured periodically. The leak plus degassing rate of the storage tank was never greater than 1.1×10^{-5} Torr/min and that of the driven section never greater than 2.4×10^{-5} Torr/min. Mixtures were prepared by introducing the desired pressures of the components into the tank, and mixing was promoted by blowing hot air into the flue of the water tank for at least 6 hr. The mixture is then allowed to stand for at least 14 hr before using.

Optical and Electronic Systems. The light source was a Spectra-Physics Model 123 with Model 253A exciter, or a Model 132 helium–neon laser, which was mounted on a table close to the driven section, with its beam perpendicular to the shock tube. After passing through the diagnostic section the beam was deflected through 90° by a small front surface mirror mounted on the shaft of a rigidly supported 1800-rpm motor. Rotation was required for the calibration procedure, which is described below. The photomultiplier housing had an aperture of about 1 cm diameter, one-half of which was covered with a razor blade. On the inside the aperture was covered with a sintered glass plate to diffuse the light, and a neutral density filter to reduce its intensity. An EMI Electronic Ltd. Type 9558B photomultiplier was used (six dynodes only). The tube potential was 750 V and the dynode current was 3.2 mA. An emitter follower was built into the base of the photomultiplier, and the output was recorded with a Tektronix type 535 oscilloscope, type H or L plug-in preamplifier. The overall time constant of this system was 0.20 μsec. The phototube output was recorded photographically and the amplitudes were later read directly from the photographs. The outputs of the platinum film resistance gauges were mixed, differentiated, and amplified and the resulting signal superposed on a raster. Markers (1 and 10 μsec) from a Tektronix type 181 time-mark generator were also superposed on the raster. The sweep speed of the raster was about 10 μsec/cm and the positions of the signals from the resistance gauges could be determined to well within ±0.5 μsec.

Gases. The helium and nitrogen driver gases were supplied by the Air Reduction Co. Helium was Grade 4.5 (Purified) of specified minimum purity 99.995%; nitrogen was Grade 4 (Prepurified) with minimum purity 99.99%. The carbon dioxide, methane, and fluoromethane were supplied by Matheson Gas Products. The carbon dioxide was Coleman Instrument grade of minimum purity 99.99 mol %. The methane was Research grade, minimum purity 99.99 mol %; the specified impurities were nitrogen, carbon dioxide, propane, ethane, and oxygen. The fluoromethane had a minimum purity of 99.0%; the impurities were silicon tetrafluoride and dimethyl ether. Tetradeuteriomethane was supplied by Merck Sharp and Dohme of Canada, Ltd. Its composition was 96.29 mol % CD_4 and 3.71 mol % CHD_3.

Procedure. Prior to our filling the driven section, the driver section was evacuated to 0.2 Torr and the driv-

(1) M. I. Buchwald and S. H. Bauer, *J. Phys. Chem.*, **76**, 3108 (1972).

en section to 4×10^{-5} Torr. The sample was admitted and its pressure recorded. The shock tube wall temperature was measured at two places after an interval of about 3 min, and the average was taken as the initial gas temperature. The total elapsed time between closing the valve separating the driven section from the diffusion pump and shock initiation was less than 5 min except when the sample pressure was measured with the Hg manometer (over 50 Torr), in which case it was somewhat longer. The diaphragm was burst by overpressuring with helium or nitrogen. After each shock the driven section was blown out with nitrogen to remove Mylar dust and chips, and the interferometer windows were wiped clean with dry tissue.

The photomultiplier output *vs.* laser beam deflection was calibrated by rotating the motor-mounted mirror. For each calibration the angular speed of the motor, the distance from the spinning mirror to the razor blade, and the signal from the photomultiplier were measured. The photomultiplier signal showed a linear region when the peak of the Gaussian distribution of the laser beam intensity swept past the edge of the razor blade. The slope of this linear region, the angular speed, and the distance from mirror to the razor provide the calibration constant between the photomultiplier output and small deflections at the center of the laser beam.

Analysis and Results

In the first step of the analysis an iterative procedure was used to calculate the final equilibrium density, ρ_2, from the initial conditions, based on the shock conservation relations and the equation of state. An analysis of the measurement of density gradients by laser beam deflection was given by Kiefer and Lutz.[2] For small deflections of the center of the beam with respect to the knife edge the change in photomultiplier output (ΔV) is directly proportional to density gradient [$d\rho/dx = K\Delta V$], where K is the apparatus constant obtained in the calibration procedure described above. The equation $d\rho/dt = (d\rho/dx)(dx/dt) = Ku_1\Delta V$, where u_1 is the shock speed in laboratory coordinates, may be rewritten in the form

$$\rho(t) - \rho_2 = Ku_1 \int_{\infty}^{t} \Delta V \, dt \qquad (1)$$

Operationally, this implies that the photographic trace of the photomultiplier output can be integrated point by point (starting at the final deflection level), giving a sequence of density values, $\rho(t)$. The relation between the local gas density and its vibrational energy content was obtained from the conservation equations for mass, momentum, and energy for a normal shock in a constant area channel by a method outlined by Simpson, *et al.*[3] Write for the specific enthalpy

$$h = \epsilon_{vib} + AT$$

where A is the heat capacity (at constant pressure) of the rapidly equilibrating degrees of freedom. Then integration along the trace gives

$$\epsilon_{vib}(t) = h_0 - \frac{1}{2}\frac{m^2}{\rho^2} - \frac{A}{R}\frac{p_0}{\rho} - \frac{m^2}{\rho^2}\Big] \qquad (2)$$

where h_0 and p_0 refer to preshock conditions in the gas. If the gas consists of more than one component it is necessary to introduce one of several assumptions regarding the relative rates of vibrational relaxation to permit solution of the coupled rate equations; for example, (1) the added gas relaxes much more slowly than CO_2, (2) the added gas relaxes at the same rate as CO_2, (3) the added gas relaxes much faster than does CO_2. If assumption 1 or 2 is made, then A in eq 2 is the sum of the heat capacities of translation and rotation of both gases. If assumption 3 is made, then A is the sum of the heat capacities of translation and rotation of both gases and of vibration of the added gas. After selecting a suitable assumption, substitution of the integrated densities $\rho(t)$ in eq 2 provides a sequence of vibration energies $\epsilon_{vib}(t)$. In the two-component mixtures of CO_2 with CH_4, CD_4, and CH_3F we assumed that each of the following processes has a single characteristic vibration-translation relaxation time.

$CO_2^v + M = CO_2 + M$	$\tau(CO_2\text{-}M)$
$CO_2^v + CO_2 = CO_2 + CO_2$	$\tau(CO_2\text{-}CO_2)$
$M^v + CO_2 = M + CO_2$	$\tau(M\text{-}CO_2)$
$M^v + M = M + M$	$\tau(M\text{-}M)$
$M^v + CO_2 = M + CO_2^v$	$\tau^v(CO_2\text{-}M)$

It is $\tau(CO_2\text{-}M)$ which we seek to determine for M = CH_4, CD_4, and CH_3F.

Sato, Tsuchiya, and Kuratani[4] solved the coupled differential equations describing this system, subject to the additional assumption that the translational temperature is lower than the characteristic vibrational temperatures of both molecules. The time dependence of the vibrational energy for the two gases is given by

$$-\frac{\epsilon_{vib,CO_2} - \epsilon_{vib,CO_2}^{eq}}{\epsilon_{vib,CO_2}^{eq}} = C_1 e^{\lambda_1 t} + C_2 e^{\lambda_2 t} \qquad (3)$$

$$-\frac{\epsilon_{vib,M} - \epsilon_{vib,M}^{eq}}{\epsilon_{vib,M}^{eq}} = C_1' e^{\lambda_1 t} + C_2' e^{\lambda_2 t} \qquad (4)$$

where λ_1 and λ_2 are the *system* relaxation times and the C's are constants of integration. In this experiment the sum of the vibrational energies of both gases was measured; its time dependence is given by

$$-[\epsilon_{vib} - \epsilon_{vib}^{eq}] = [C_1\epsilon_{vib,CO_2}^{eq} + C_1'\epsilon_{vib,M}^{eq}]e^{\lambda_1 t} + [C_2\epsilon_{vib,CO_2}^{eq} + C_2'\epsilon_{vib,M}^{eq}]e^{\lambda_2 t} \qquad (5)$$

Semilog plots of photomultiplier output were very nearly linear. We concluded that we recorded the slower component of the vibrational relaxation profile with eigenvalue λ_1. This allowed us to make the following approximation

$$-[\epsilon_{vib} - \epsilon_{vib}^{eq}] \cong [C_1\epsilon_{vib,CO_2} + C_1'\epsilon_{vib,M}^{eq}]e^{\lambda_1 t} \qquad (6)$$

$$-\frac{d\epsilon_{vib}}{dt} \cong \lambda_1[C_1\epsilon_{vib,CO_2}^{eq} + C_1'\epsilon_{vib,M}^{eq}]e^{\lambda_1 t} \qquad (7)$$

where ϵ^{eq}_{vib,CO_2} and $\epsilon^{eq}_{vib,M}$ are assumed to be constant. On combining these two relations one obtains

$$d\epsilon_{vib/dt} \cong \lambda_1[\epsilon_{vib} - \epsilon_{vib}^{eq}] \qquad (8)$$

ϵ_{vib} is obtained from the experimental trace *via* eq 2, and is dependent on the assumed magnitude of the heat capacity. $(d\epsilon_{vib}/dt)$ is calculated from the expression obtained by differentiating eq 2. From ϵ_{vib} and $(d\epsilon_{vib}/dt)$ we then obtain λ_1 using eq 8. The ΔV's read from the photomultiplier output trace and integrated according to eq 1

(2) J. H. Kiefer and R. W. Lutz, *J. Chem. Phys.*, **44**, 658 (1966).
(3) C. J. S. M. Simpson, T. R. D. Chandler, and A. C. Strawson, *J. Chem. Phys.*, **51**, 2214 (1969).
(4) Y. Sato, S. Tsuchiya, and K. Kuratani, *J. Chem. Phys.*, **50**, 1911 (1969).

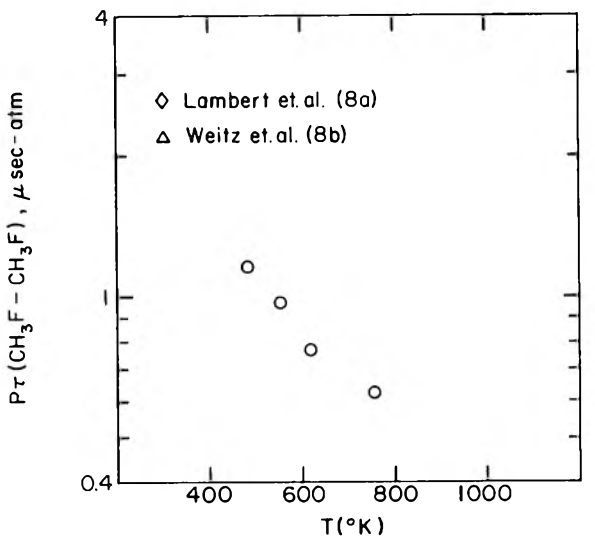

Figure 1. Temperature dependence of reduced vibration–relaxation times in 100% CH_3F. The room temperature points are from ref 8a,b.

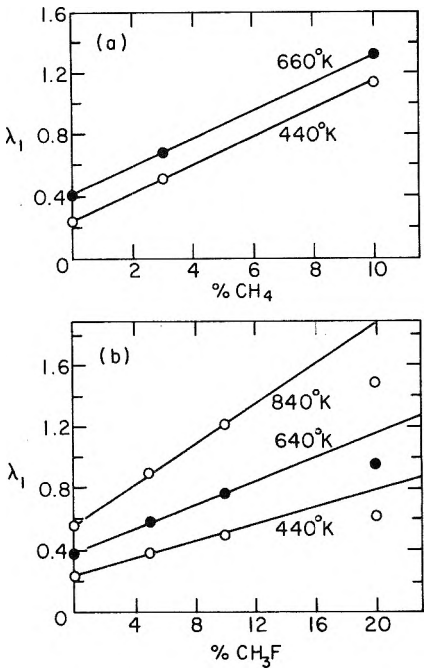

Figure 2. Linearity test for λ_1 in CO_2–M mixtures: (a) CO_2 + CH_4; (b) CO_2 + CH_3F.

to any specified t yield a distinct value for λ_1 on the basis of eq 2 and 8.

Assumption 1 can be rejected since the self-relaxation times of CH_4, CD_4, and CH_3F are shorter than the self-relaxation time of CO_2. $\tau(CH_4\text{–}CH_4)$ has been measured over a wide range of temperature;[5] it is about $0.1\tau(CO_2\text{–}CO_2)$.[6] The relaxation time of pure CD_4 has been measured near room temperature[5a,7] only; if one assumes that it has the same temperature dependence as that for CH_4, then $\tau(CD_4\text{–}CD_4) \cong 0.3\tau(CO_2\text{–}CO_2)$. A room temperature value for the relaxation time of pure CH_3F is available.[8] We measured its τ_{vib} at about 500°K; the results are shown in Figure 1; they extrapolate to the room temperature sound dispersion value; $\tau(CH_3F\text{–}CH_3F) \cong 0.3\tau(CO_2\text{–}CO_2)$.

Assumption 2 can be rejected when λ_1 is demonstrated to be a linear function of the composition of the gas mixture at a given temperature. λ_1 is plotted as a function of composition for CO_2–CH_4 and CO_2–CH_3F mixtures in Figure 2a and 2b, respectively. Up to 10% the dependence is linear for both CO_2–CH_4 and CO_2–CH_3F; for the latter, a slower rise is noted for CH_3F concentrations greater than about 12%. Hence we are justified in assuming that for these mixtures the effect of v–v coupling is not too important, and the added gas is at v–T equilibrium while the CO_2 is vibrationally relaxing. Although we do not have sufficient data to demonstrate a similar relation for CO_2–CD_4 mixtures, we will assume that these follow the same form.

It is now possible to determine the relaxation times of the several gas mixtures. According to assumption 3

$$\tau_{sys} = -1/\lambda_1 \tag{9}$$

τ_{sys} is shown as a function of temperature for mixtures CO_2–CH_4, CO_2–CD_4, and CO_2–CH_3F in Figure 3. In principle, the τ_{sys} for a given shock should show a small uniform variation with time, as the translational temperature attains its equilibrium value behind the shock. However, these temperature changes are so small that only a random variation of τ_{sys} is noted. For each shock values were averaged and assigned to the *average* translational temperature for the interval.

When the added gas relaxes faster than CO_2, and in the absence of a significant contribution from v–v coupling, $\tau(CO_2\text{–M})$ can be obtained from the relation

$$\frac{1}{\tau_{sys}} = \frac{\chi(CO_2)}{\tau(CO_2\text{–}CO_2)} + \frac{\chi(M)}{\tau(CO_2\text{–M})} \tag{10}$$

where $\chi(M)$ is the mole fraction of component M. The average of the derived $\tau(CO_2\text{–M})$ values was assigned to the average temperature for the corresponding shock; the temperature dependence of $\tau(CO_2\text{–}CH_4)$, $\tau(CO_2\text{–}CD_4)$, and $\tau(CO_2\text{–}CH_3F)$ are shown in Figure 4. For comparison, values at lower temperatures derived from two sets of sound dispersion measurements[9] have also been plotted.

Discussion

A. Theories of Vibrational Relaxation in CO_2 Mixtures. There are several theoretical descriptions of vibration–translation and vibration–rotation energy transfer that can be conveniently applied to collisions between CO_2 and CH_4, CD_4, or CH_3F. Estimates of collisional efficiencies for the exchange of translational and vibrational energy induced by short-range repulsive forces have been made on the basis of a semiclassical approximation by Schwartz, Slawsky, and Herzfeld.[10] The application of this theory to CO_2 was given by Herzfeld.[11] The relaxa-

(5) (a) T. L. Cottrell and A. J. Matheson, *Trans. Faraday Soc.*, **58**, 2336 (1962); (b) J. T. Yardley and C. B. Moore, *J. Chem. Phys.*, **49**, 1111 (1968); **52**, 1450 (1970); (c) P. D. Edmonds and J. Lamb, *Proc. Phys. Soc.*, **72**, 940 (1958); (d) A. Eucken and S. Aybar, *Z. Phys. Chem.*, **B46**, 195 (1940); (e) L. W. Richards and D. H. Sigafoos, *J. Chem. Phys.*, **43**, 492 (1965).
(6) C. J. S. M. Simpson and T. R. D. Chandler, *Proc. Roy. Soc., Ser. A*, **317**, 265 (1970).
(7) J. C. Gravitt, C. N. Whetstone, and R. T. Lagemann, *J. Chem. Phys.*, **44**, 70 (1966).
(8) (a) P. G. Corran, J. D. Lambert, R. Salter, and B. Warburton, *Proc. Roy. Soc., Ser. A*, **244**, 212 (1958); (b) E. Weitz, G. Flynn, and A. M. Ronn, *J. Chem. Phys.*, **56**, 6060 (1972); (c) G. Flynn, *et al.*, *Chem. Phys. Lett.*, **17**, 189, 347 (1972).
(9) (a) A. Van Itterbeck and P. Mariens, *Physica*, **7**, 909 (1940); (b) H. J. Bauer and R. Schotter, *J. Chem. Phys.*, **51**, 3261 (1969).
(10) R. N. Schwartz, Z. I. Slawsky, and K. F. Herzfeld, *J. Chem. Phys.*, **20**, 1591 (1952).
(11) K. F. Herzfeld, *J. Chem. Phys.*, **47**, 743 (1967).

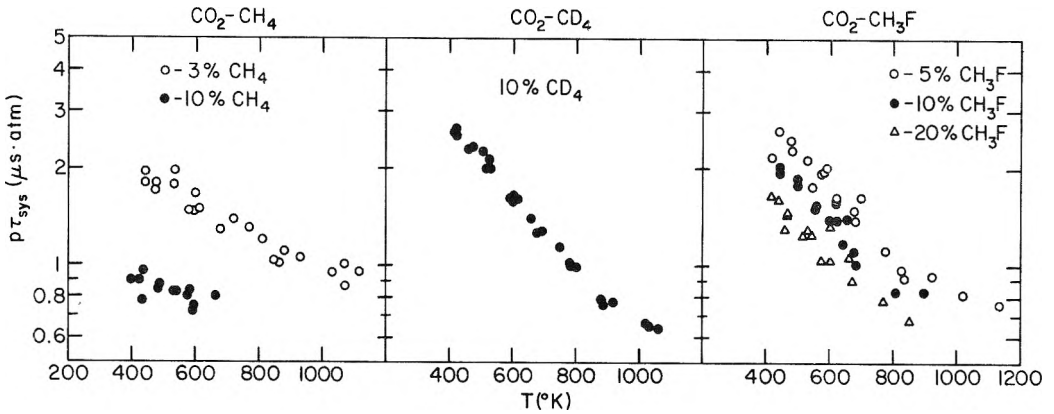

Figure 3. Temperature dependence of $P\tau_{sys}$ for CO_2–M mixtures: (a) CO_2 + CH_4 (3 and 10%); (b) CO_2 + CD_4 (10%); (c) CO_2 + CH_3F (5, 10, and 20%).

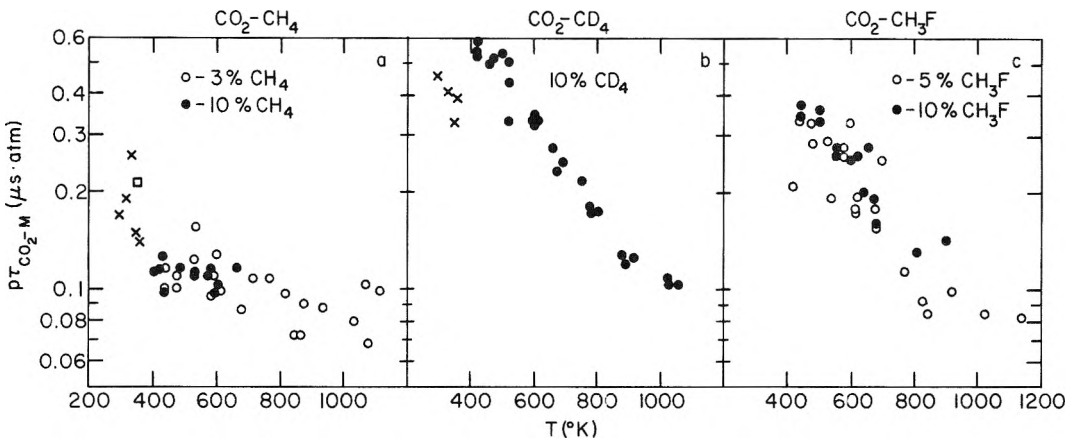

Figure 4. Temperature dependence of reduced vibrational relaxation times, equivalent to infinite dilution of CO_2 in the catalyst gas. Values derived from sound dispersion measurement are plotted as × (ref 9a) and ⊡ (ref 9b): (a) CO_2 in CH_4; (b) CO_2 in CD_4; (c) CO_2 in CH_3F. In this plot values derived from the 20% mixtures were deleted because the analysis of these runs suggested that the temperature estimates were questionable.

tion times $\tau(CO_2\text{–}CH_4)$, $\tau(CO_2\text{–}CD_4)$, and $\tau(CO_2\text{–}CH_3F)$ were calculated according to the methods outlined in ref 10 and by Herzfeld and Litovitz.[12] The interaction parameter l was set equal to $(\sigma_{12}/18.5)$, where σ_{12} is the average molecular diameter for the collision partners as defined by a Lennard-Jones (6–12) potential. The relaxation time was calculated from the averaged transition probability (P_{10})

$$\tau^{-1} = P_{10}Z\frac{C_{010}}{C_{vib}}[1 - e^{-h\nu/kT}] \qquad (11)$$

where ν is the characteristic frequency of the relaxing oscillators; C_{vib} is the total vibrational heat capacity and C_{010} the heat capacity of the doubly degenerate bending mode; and Z is the kinetic theory collision number, $Z \equiv \pi N\sigma_{12}^2(8kT/\pi\mu)^{1/2}$. Collision diameters were obtained from Hirchfelder, Curtiss, and Bird[13a] and Miller and Bernstein;[13b] CD_4 was assumed to be the same size as CH_4. The results of these calculations are shown in Figure 5. Whereas the temperature dependence of $\tau(CO_2\text{–}CD_4)$ and $\tau(CO_2\text{–}CH_3F)$ are in satisfactory agreement with the theory, that of $\tau(CO_2\text{–}CH_4)$ is not.

Estimates of rotation–vibration energy exchange probabilities, induced by short-range repulsive forces, were made by Moore[14] on the basis of a proposal by Cottrell. The latter started with the classical expression for the probability for translation–vibration energy exchange as derived by Landau and Teller, but replaced the relative translational velocity of vibrator and collider with the tangential velocity of the peripheral atoms of the rotating collider. It was thus possible to account for the comparatively short relaxation times observed for molecules with small moments of inertia, and to predict correctly the relative τ's for isotopically substituted pairs (CH_4 *vs.* CD_4, etc.). For application to the present cases, Moore's eq 4 was used with those values of α and Z_0 that gave the best fit to collision numbers for the largest number of the hydrogen compounds for which he could obtain relaxation data. Then, the relaxation times were calculated from the P_{10} values by means of eq 11. These results are also shown in Figure 5. These curves are essentially parallel to the Schwartz-Slawsky-Herzfeld (SSH) curves, but with magnitudes for τ that are ¼–1/10 as large. Moore's theory evidently overestimates the effectiveness of the tangential velocity of the outer atoms of the catalyst molecules for deexciting $CO_2(010)$.

Shields and Burks[15] discussed the translation–rotation–vibration energy exchange problem by *postulating* a time-

(12) K. F. Herzfeld and T. A. Litovitz, "Absorption and Dispersion of Ultrasonic Waves," Academic Press, New York, N. Y., 1959.
(13) (a) J. O. Hirschfelder, C. F. Curtiss, and R. B. Bird, "Molecular Theory of Gases and Liquids," 2nd corrected printing, Wiley, New York, N. Y., 1964, p 1110; (b) G. A. Miller and R. B. Bernstein, *J. Phys. Chem.*, **63**, 710 (1959).
(14) C. B. Moore, *J. Chem. Phys.*, **43**, 2979 (1965).
(15) (a) F. D. Shields and J. A. Burks, *J. Acoust. Soc. Amer.*, **43**, 510 (1968); (b) F. D. Shields, *ibid.*, **45**, 481 (1969); (c) F. D. Shields and G. P. Carney, *ibid.*, **47**, 1269 (1970).

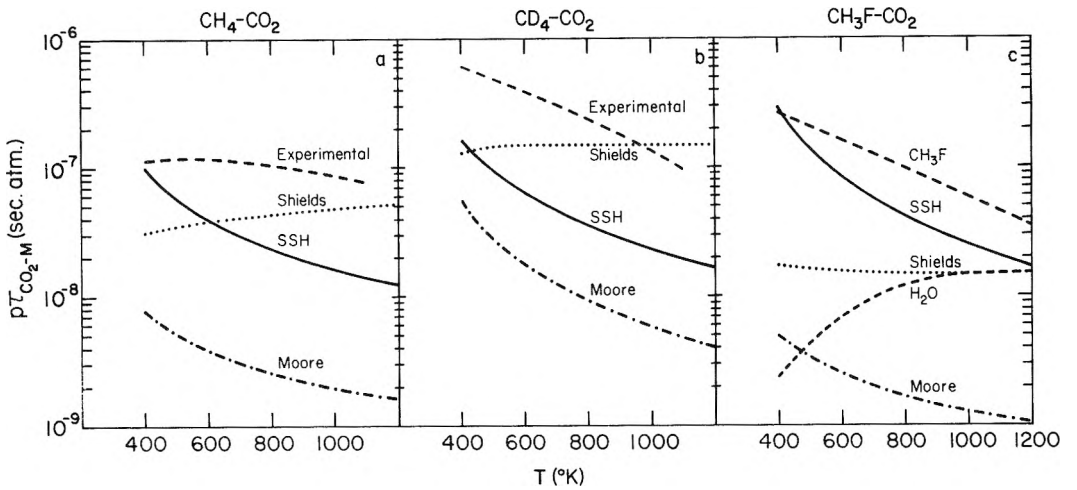

Figure 5. Comparison of reduced relaxation times for CO_2, when CD_4, CH_3F, and CH_4 serve as collision partners, with predictions based on three theories. In c the experimental curve for CO_2–H_2O is included for comparison. Note that the permanent dipole moment of CH_3F is 1.81 D; that of H_2O is 1.842 D.

dependent perturbing force, imposed by the collider on the relaxing molecule, of the form

$$F(t) = F_0 \exp(-\alpha^2 t^2) \cos(2\omega t + \varphi) \qquad (12)$$

In their calculations of CO_2 relaxation by water and hydrogen sulfide the frequency of the perturbing force was set equal to twice the rotational frequency (ω) of the catalyst species. For CH_4, CD_4, and CH_3F, the frequency of the perturbing force was set equal to three times the rotational frequency. In Shield's equation, $\alpha = \alpha_0 \mu^{-1/2}$, where $\alpha_0 = 11.84 \times 10^{13}$ sec^{-1} g$^{1/2}$ mol$^{1/2}$ and μ is the reduced mass of the colliding pair. F_0 is determined from $F_0 = 24\epsilon/\sigma$, where ϵ and σ are the Lennard-Jones parameters for the colliding pair. The results of these estimates are also included in Figure 5. Shields' theory comes closest to reproducing the magnitudes of the relaxation times of the mixtures investigated. However, the agreement is poor at the higher temperatures. This may be a consequence of the fact that the relative velocity of the collision pair does not appear in the time-dependent force, so that the transition probability is underestimated at the higher temperatures.

Among the recent developments in the theory of vibration relaxation in gas mixtures one should list the work of Shin,[16] who formulated a general classical theory of vibration–rotation–translation energy exchange through short-range repulsive interactions. His treatment was successful in accounting for the observed relaxation times in the hydrogen and deuterium halides. At the upper temperature range his model gives a dependence similar to that of the SSH theory, so that while there is an improvement in predicting the magnitudes, it is questionable whether it can account for the observed temperature dependence for the CO_2–CH_4 pair in the absence of strong attraction between colliding molecules. Sharma[17] investigated the effect of vibration–rotation coupling through long-range attractive forces. He calculated transition probabilities for CO_2–H_2 and CO_2–D_2 collisions using dipole–quadrupole interactions, and for CO_2–H_2O collisions using dipole–dipole interactions. That one must take into account vibration–rotation coupling in collisions involving molecules with small moments of inertia and wide rotational energy level spacing is stressed by Sharma. While CH_4, CD_4, and CH_3F belong to this category the rather involved calculations have not yet to be made.

Acknowledgments. The authors thank Dr. Soji Tsuchiya for advice and many helpful discussions. This work was supported by the Advanced Research Projects Agency of the Department of Defense and monitored by the Office of Naval Research under Contract No. N00014-67-A-0077-0006.

(16) (a) H. K. Shin, *J. Phys. Chem.*, **75**, 1079 (1971); (b) H. K. Shin, *Chem. Phys. Lett.*, **10**, 81 (1971); (c) H. K. Shin, *ibid.*, **11**, 628 (1971).
(17) (a) R. D. Sharma, *J. Chem. Phys.*, **50**, 919 (1969); (b) *ibid.*, **54**, 810 (1071).

From the borders of organic chemistry . . . To the borders of theoretical physics:

Inorganic Chemistry brings you a broad range of authoritative information presenting both experimental and theoretical studies in all phases of inorganic chemistry.

Each month, this rapidly growing journal brings you the data you need on synthesis and properties of new compounds, quantitative studies regarding structure, and thermodynamics of inorganic reactions.

When you've seen the 50 or more papers offered in each issue, you'll also want to look through the Notes and Correspondence sections for their concise exchange of scientific views and ideas.

To order INORGANIC CHEMISTRY today, just complete and return the form below.

. . *another ACS service*

Inorganic Chemistry

Inorganic Chemistry
American Chemical Society
1155 Sixteenth Street, N.W.
Washington, D.C. 20036

Yes, I would like to receive INORGANIC CHEMISTRY at the one-year rate checked below:

	U.S.	*Canada*	*Latin America*	*Other Nations*
ACS Member Personal-Use One-Year Rate	☐ $18.00	☐ $22.00	☐ $22.00	☐ $23.00
Nonmember	☐ $54.00	☐ $58.00	☐ $58.00	☐ $59.00

Bill me ☐ Bill company ☐ Payment enclosed ☐

Name _____

Street _____ Home ☐ Business ☐

City _____ State _____ Zip _____

P-73